Advances in Industrial Control

Wei He
Shuzhi Sam Ge
Bernard Voon Ee How
Yoo Sang Choo

Dynamics and Control of Mechanical Systems in Offshore Engineering

AIC
Springer

Advances in Industrial Control

For further volumes:
www.springer.com/series/1412

Wei He • Shuzhi Sam Ge • Bernard Voon Ee How • Yoo Sang Choo

Dynamics and Control of Mechanical Systems in Offshore Engineering

Springer

Wei He
School of Automation Engineering
University of Electronic Science
and Technology of China (UESTC)
Chengdu, China

Bernard Voon Ee How
Centre for Offshore Research & Engin.
National University of Singapore
Singapore, Singapore

Shuzhi Sam Ge
Dept of Electr. & Computer Engineering
The National University of Singapore
Singapore, Singapore

Yoo Sang Choo
Dept of Civil & Environmental Engin.
National University of Singapore
Singapore, Singapore

ISSN 1430-9491
ISSN 2193-1577 (electronic)
Advances in Industrial Control
ISBN 978-1-4471-5336-8
ISBN 978-1-4471-5337-5 (eBook)
DOI 10.1007/978-1-4471-5337-5
Springer London Heidelberg New York Dordrecht

Library of Congress Control Number: 2013945286

Printed on acid-free paper

Springer is part of Springer Science+Business Media (www.springer.com)

We treasure for the opportunities given.
We value friendship more than anything else,
and we are grateful for the blessings that we
received.

Series Editors' Foreword

The series *Advances in Industrial Control* aims to report and encourage technology transfer in control engineering. The rapid development of control technology has an impact on all areas of the control discipline. New theory, new controllers, actuators, sensors, new industrial processes, computer methods, new applications, new philosophies..., new challenges. Much of this development work resides in industrial reports, feasibility study papers and the reports of advanced collaborative projects. The series offers an opportunity for researchers to present an extended exposition of such new work in all aspects of industrial control for wider and rapid dissemination.

Several monographs on control topics from the marine field have been published in the *Advances in Industrial Control* monograph series, for example:

- *Robust Control of Diesel Ship Propulsion* by Nikolaos Xiros (ISBN 978-1-85233-543-4, 2002);
- *Ship Motion Control* by Tristan Perez (ISBN 978-1-85233-959-3, 2005); and
- *Control of Ships and Underwater Vehicles* by Khac Duc Do and Jie Pan (ISBN 978-1-84882-729-5, 2009).

However, they are all characterised by being monographs about aspects of seagoing-vessel or free-swimming remotely-operated-vehicle (ROV) control. On the other hand, *Dynamics and Control of Mechanical Systems in Offshore Engineering* by Wei He, Shuzhi Sam Ge, Bernard Voon Ee How and Yoo Sang Choo is quite different in that it focuses on the units that make up the offshore oil and gas delivery system. Occasionally, topics such as the riser system appear as an isolated or subsidiary chapter in marine control monographs; hence, a monograph that only looks at the control of the complete offshore oil and gas platform delivery system is a valuable entry to *Advances in Industrial Control*.

In its most basic form, the offshore oil and gas delivery system has three components, a surface vessel, the riser tube, and the seabed installations. It is then possible to start at the surface vessel, categorise the various vessel types and work through the implications for the subsequent selections made for the riser and subsea technologies. The surface platform can be fixed, floating and moored, or free floating.

A riser system is the "delivery tube" between the surface platform and the seabed wellhead or a seabed production collection point. The riser can be flexible or fixed, and the related control problem can also include the dynamics of the surface platform. Furthermore, the riser is subject to two operational scenarios as a drilling riser and a production riser. Even with this simplistic description, it is easy to understand how this composite offshore engineering system begins to become very complex very quickly. Industry solutions to the control problems include a riser management system, an example of which is described in Chap. 9 of the monograph, where much mechanical and physical detail of riser systems can be found.

Technically the monograph presents the modelling and control of distributed parameter systems, and uses robust adaptive control methods. Chapters 1 and 2 contain the background material and mathematical preliminaries, respectively, and Chap. 10 closes the monograph with conclusions and future research issues. In between the opening and closing chapters, the monograph reports on the following control problem areas:

- at the marine surface:
  - control of a crane vessel guiding and positioning a subsea unit—Chap. 4;
  - control of a flexible marine riser incorporating surface platform and subsea payload dynamics—Chap. 5;
  - control of a thrusters-assisted single-point mooring system—Chap. 6;
- the riser system:
  - control of a flexible marine riser—Chap. 7;
  - control of a flexible marine riser system with vessel dynamics—Chap. 8; and
- at subsea levels:
  - control of the thruster-assisted installation of a subsea unit—Chap. 3.

The field of offshore production systems is a topic of great economic importance, especially given the recent trend to exploit resources in deeper offshore fields. This is an important monograph showing how control systems techniques can make a contribution to this endeavour. The problems and the proposed solutions will be of interest to the offshore engineering community and to the academic control community, who may be able to make even further contributions and become directly involved in this field. This monograph certainly fills a gap in the *Advances in Industrial Control* monograph series, being, quite possibly, a seminal control monograph for the field and as such will be of interest to a wide range of industrial and control readers.

Industrial Control Centre, Glasgow, Scotland, UK M.J. Grimble
M.A. Johnson

Preface

Offshore engineering is concerned with the design and operation of systems in harsh marine environmental conditions. It encompasses a whole spectrum of diverse multidisciplinary and complex systems and operations such as offshore installations, structures, foundations, cables and pipelines, moorings, risers, drilling, mining, disposal and salvage operations, etc. The design of mechanical systems to operate in the harsh marine environmental conditions is one of the most challenging tasks in offshore engineering. One part of the challenges is in the modeling and control of such systems. This subject has received increasing attention in recent years with growing energy demands extending oil and gas explorations to deeper and even harsher environments.

The main purpose of the book is to investigate the fundamental issues including dynamical modeling and control design for different mechanical systems in offshore engineering. The book presents theoretical explorations on several fundamental problems for dynamics and control of marine mechanical systems. Motivated by the need to develop a general dynamic modeling and control framework to achieve system performance, concepts from control, mechanical structures, and offshore fields are synthesized via a systematic approach and presented. The basic theoretical framework is formed toward mechanical systems in offshore engineering, which not only extends the theory of mechanical structures, but also applies to realistic problems faced by the industry. A comprehensive study is provided for developing advance strategies for the modeling and control design of the systems with guaranteed stability. By investigating the characteristics of mechanical models, advanced control approaches are presented for marine mechanical systems with specific applications, i.e., installation systems, mooring systems, and riser systems. The control designs are coupled with numerical simulations to illustrate the effectiveness.

Offshore applications are characterized by the time-varying environmental disturbances and the sea conditions. For riser systems, vibration and deformation of the flexible structures due to the ocean current disturbances and the tension exerted at the top can produce premature fatigue problems and failures that require costly repairs. Proper control techniques are desirable for preventing damage and improving

the lifespan of these structures. The chapter on structural analysis and riser operations (contributed by Geoff Lyons and Minoo Patel) describing an on-board riser operation management system that provides a real-time guidance for carrying out connected and disconnected mode drilling riser operations on board a vessel as an industrial case study.

The book contains ten chapters, which exploit several independent yet related topics in detail.

Chapter 1 introduces the system description, background, and motivation of the study and presents several general concepts and fundamental observations.

Chapter 2 presents several lemmas and properties used in the subsequent development and derivations of the dynamical models, and further stability analysis for the marine mechanical structures.

In Chap. 3, positioning control in the horizontal plane is investigated for the installation of subsea systems, with thrusters attached, under time-varying irrotational ocean current, when the payload is near to the seabed. Backstepping in combination with adaptive feedback approximation techniques is employed in the design of the control, with the option of high-gain observer for output feedback control. The stability of the design is demonstrated through Lyapunov analysis where semiglobal uniform boundedness of the closed-loop signals are guaranteed. The proposed adaptive neural control is able to capture the dominant dynamic behaviors without exact information on the hydrodynamic coefficients of the structure and current measurements.

In Chap. 4, the model of the coupled crane-cable-payload with nonuniform parameters is presented. Positioning control is derived for the coupled system with uniform parameters using barrier Lyapunov functions. Through Lyapunov analysis, it is shown that the coupled crane, payload flexible system is stable under the control action, the physical limits from operations planning and safety specifications are not transgressed, and positioning of crane and payload is achieved. A stabilizing boundary control is proposed for the coupled system with nonuniform parameters. Rigorous Lyapunov stability analysis is carried out, and uniform boundedness of the system is shown under the proposed control. Finally, the performance of the proposed control is given through numerical simulations.

In Chap. 5, a robust adaptive boundary control of a marine installation system is developed to position the subsea payload to the desired set-point and suppress the cable's vibration. The flexible cable coupled with vessel and payload dynamics is described by a distributed parameter system with one partial differential equation (PDE) and two ordinary differential equations (ODEs). Boundary control is proposed at the top and bottom boundary of the cable based on the Lyapunov direct method. Considering the system parametric uncertainties and the unknown ocean disturbances, the developed adaptive boundary control schemes achieve the uniform boundedness of the steady-state error between the boundary payload and the desired position. The control performance of the closed-loop system is guaranteed by suitably choosing the design parameters.

Chapter 6 is dedicated on the control problem of a thruster-assisted single-point mooring system, in the presence of uncertainties and unknown backlash-like hysteresis nonlinearities. Using backstepping technique and Lyapunov synthesis, and

employing neural networks (NNs) to approximate the unknown nonlinear functions, robust adaptive backstepping control is developed for the full-state feedback case. Subsequently, in order to overcome the measure difficulty in the vessel velocity vector, a high-order NN-based observer is constructed to estimate the unmeasurable state vector. It is shown that the proposed observer has an excellent estimation performance in spite of the existence of uncertainties and unknown backlash-like hysteresis nonlinearities. Based on this observer, robust adaptive output feedback control is developed via backstepping design. Under the proposed control, the semiglobal uniform boundedness of all the signals in the closed-loop systems is guaranteed for both full-state and output feedback cases.

In Chap. 7, boundary control for a coupled nonlinear flexible marine riser with two actuators in transverse and longitudinal directions is developed to reduce the riser's vibrations. The dynamic behavior of the flexible riser is represented by a distributed parameter system (DPS) model with partial differential equations (PDEs) and the control is applied at the top boundary of the riser based on Lyapunov direct method to suppress the riser's vibrations. With the proposed boundary control, the uniform boundedness under ocean current disturbances and exponential stability under the free vibration condition is achieved. The proposed control is independent of system parameters, which ensures the robustness of the system to variations in parameters.

Chapter 8 studies the modeling and control of a flexible marine riser with the vessel dynamics. Both the dynamics of the vessel and the vibration of the riser are considered in the dynamic analysis, which make the system more difficult to control. Boundary control is proposed at the top boundary of the riser to suppress the riser's vibration. Adaptive control is designed when the system parametric uncertainties exist. Employing the Lyapunov direct method, the states of the system are proven to be uniformly ultimately bounded. The state of the system will converge to a small neighborhood of zero by appropriately choosing the design parameters. The design is based on the PDEs of the system, thus avoiding some drawbacks associated with the traditional truncated-model-based design approaches.

Chapter 9 serves as an industrial case study in this book. This chapter investigates the structural analysis and the riser operations of fixed and floating offshore structures using pipe connections between surface facilities and seabed as well as pipes laying on or below the seabed for transportation of oil and gas. The analysis of vertical marine risers under the influences of both internal and external forces is described. Four configurations of the marine risers are introduced including free handing mode, connected mode, operational mode, and nonoperational but connected mode. A marine riser can be maintained in an operable condition by ensuring that the lower ball joint angle remains below about 4 degrees. Three operating procedures are given to bring the angle down. The marine riser monitoring system provides information on the behaviors of the platform and the marine riser, and comparisons can be made with previous results for evaluating the projected fatigue life of the riser. BPP-RMS, an example of the comprehensive Riser Management System (RMS) for riser maintenance and inspection, is presented. BPP-RMS is an on-board riser operation management system that provides a real-time guidance for carrying out connected and disconnected mode drilling riser operations on board a vessel.

Chapter 10, the last chapter, makes conclusions on this book.

In summary, this book covers the dynamical analysis and control design for marine mechanical systems. The book is primarily intended for researchers and engineers in the control system and offshore engineering community. It can also serve as a complementary reading on modeling and control of marine mechanical systems at the post-graduate level.

Acknowledgements

For this book, we have had the great fortune of working with brilliant people who are generous with their time and friendship, through many discussions filled with creativity and inspiration. First of all, we would like to express our gratitude to our co-workers who have contributed to the collaborative studies of this book.

We would also like to express our sincere appreciation to our colleagues who have contributed to the collaborative research. In particular, we would like to thank Keum-Shik Hong, from the Pusan National University, Korea, Frank Lewis, from the University of Texas at Arlington, US, Franz S. Hover, from the Massachusetts Institute of Technology, US, Miroslav Krstic, from the University of California, San Diego, US, Tong Heng Lee and Chang Chieh Hang, from the National University of Singapore, Singapore and their research groups for their excellent research works, and helpful advice on our research. Special thanks go to Oliver Jackson for his assistance and efforts on the process of publishing this book.

Appreciations must be made to Geoff Lyons, Minoo Patel, Keng Peng Tee, Lianfei Zhai, Mou Chen, Beibei Ren, Rongxin Cui, Zhen Wang, Ker Wei Yeoh, Yi Feng Wah, Kim Thow Yap, Hai Lin, and Abdullah Al Mamun for the constructive discussions and sharing of ideas. We would also like to thank Yanan Li, Hoang Minh Vu, Xinxin Yang and Qian Zhao for proofreading and providing numerous useful comments to improve the quality of the book.

Last but not the least, we are deeply gratitude to our families for their invaluable loves, supports and sacrifices over the years.

This work is supported by (i) “Intelligent Deepwater Mooring System”, funded by Agency for Science Technology and Research (A*STAR), Singapore; (ii) “Modelling and Control of Subsea Installation”, funded by The Lloyd’s Register Educational Trust (The LRET), United Kingdom; and (iii) “Design and Research on Boundary Control of a Flexible Marine Riser”, funded by the National Natural Science Foundation of China (NSFC) under the Grant 61203057, China.

Clear River, Chengdu — Wei He
Kent Ridge Crescent, Singapore/Clear River, Chengdu — Shuzhi Sam Ge
Kent Ridge Crescent, Singapore — Bernard Voon Ee How
Kent Ridge Crescent, Singapore — Yoo Sang Choo
January 2013

Contents

Chapter 1
Introduction

1.1 Background and Motivation

Accurate positioning for the installation of the subsea systems onto the seabed is identified as one of the problems in subsea installation operations [1]. Subsea templates, Christmas trees, and manifolds have to be installed accurately in a specified spatial position and compass heading within tight limits, including rotational, vertical, and lateral measurements. The tolerances for a typical subsea installation are within 2.5 m of design location and within 2.5 degrees of design heading for large templates [2] and are more stringent for the installation of manifolds into the templates. With the push for using smaller installation vessels to reduce costs, the operators are concerned with the transmission of motions from the surface vessel, which are more susceptible to influences from the wave forces by virtue of their smaller build. Remote Operated Vehicles (ROVs) are also used to aid structure positioning. This can be feasible for small structures but not for large templates as a result of limited thrust available from the propulsion system. The entanglement of the umbilical of the ROV with the lifting cable and other factors such as long path lengths for round trip communication with the surface, noise, reaction delays, and poor visibility may result in errors during placement [1].

The marine riser is used as a fluid-conveyed curved pipe drilling crude oil, natural gas, hydrocarbon, petroleum materials, mud, and other undersea economic resources, and then transporting those resources in the ocean floor to the production vessel or platform in the ocean surface [3]. A drilling riser is used for drilling pipe protection and transportation of the drilling mud, while a production riser is a pipe used for oil transportation [4]. The stiffness of a flexible marine riser depends on its tension and length; thus, a riser that spans a long distance can produce large vibrations under relatively small disturbances. In marine environment, vibrations excited by vortices can degrade the performance of the flexible marine riser. If the riser spacing and properties are kept constant, the risk of collision will increase with increasing water depth since the static deflection due to the uniform current drag is proportional to the square of the length [5, 6]. Vibrations of the riser due to the ocean current disturbances and the tension exerted at the top can produce premature

W. He et al., *Dynamics and Control of Mechanical Systems in Offshore Engineering*, Advances in Industrial Control, DOI 10.1007/978-1-4471-5337-5_1,

fatigue problems, which require inspections and costly repairs, and as a worst case, environmental pollution due to leakage from damaged areas. Vibration suppression by proper control techniques is desirable for preventing damage and improving the lifespan of the riser.

Marine installation system is used as an accurate position control for marine installation operation in offshore engineering. Accurate position control for marine installation operations has gained increasing attention in recent years [7–9]. Due to the requirements for high accuracy and efficiency arising from the modern ocean industry, improving reliability and efficiency of installation operations during oil and gas production in the ocean environment is an active research topic that has received much attention in offshore engineering. A typical marine installation system consists of an ocean surface vessel, a flexible string-type cable, and a subsea payload to be positioned for installation on the ocean floor. The surface vessel, to which the top boundary of the cable is connected, is equipped with a dynamic positioning system with an active thruster. The bottom boundary of the cable is a payload with an end-point thruster attached. This thruster is used for dynamic positioning of the payload. The total marine installation system is subjected to the environmental disturbances including the ocean current, wave, and wind. Taking into account the unknown time-varying ocean disturbances of the cable leads to the appearance of oscillations, which make the control problem of the marine installation system relatively difficult. Vibration suppression and position control by proper control technique are desirable and feasible for the marine installation system.

In comparison with the dynamic positioning system, the thruster assisted position mooring system for the anchored vessel is an economical solution in deep waters due to the long operational period in harsh environmental conditions. Floating concepts such as the use of Floating Production Storage and Offloading (FPSO) vessels in combination with subsea systems and shuttle tankers have become possible with the use of sophisticated positioning systems for precise and safe positioning. The two main types of positioning systems are the dynamic positioning (DP) systems for free floating vessels and the thruster-assisted position mooring (PM) system for anchored vessels. Many results are obtained for control of dynamic positioning systems in recent years by using the model-based approaches [10, 11] and backstepping-based approaches [12, 13]. In [14], the problem of tracking a desired trajectory is discussed for a fully actuated ocean vessel with dynamic positioning system in the presence of parametric uncertainties and the unknown disturbances. In [15], a hybrid controller is developed to extend the operability and performance of the dynamic positioning system. Station keeping means maintaining the vessel within a desired position in the horizontal plane, which has been identified as one of the typical problems in offshore engineering. A typical thruster-assisted position mooring system consists of an ocean surface vessel and several flexible mooring lines. The surface vessel, to which the top boundary of the mooring lines is connected, is equipped with a dynamic positioning system with active thrusters. The bottom boundary of the mooring lines is fixed in the ocean floor by the anchors. Station keeping for the mooring system is hard to achieve due to the complicated system model and the unknown time-varying ocean disturbances including the ocean current, wave, and wind. The

mooring lines spanning a long distance can produce large vibrations under the ocean disturbances, which can degrade the performance of the system and result in a larger offset from the target position of the vessel.

The remainder of this chapter is organized as follows. In Sect. 1.2, control methods for marine systems are briefly reviewed, where the researches on control of installation systems, mooring systems, and riser systems are discussed. In Sect. 1.3, a brief introduction of the control techniques for flexible mechanical systems, especially for flexible string and beam systems, is presented. Background knowledge of flexible systems is given first, and then the recent researches on boundary control of flexible systems are discussed. Some research problems to be studied in this book are highlighted, such as boundary control and robust adaptive control, which are both theoretically challenging and practically meaningful. In Sect. 1.4, the literature reviews of the adaptive and approximation-based control for rigid mechanical systems are presented. Especially, some research works on neural network control are introduced. The outline of the book is given in Sect. 1.5.

1.2 Mechanical Systems in Offshore Engineering

Dynamics and control of marine mechanical systems under the time-varying ocean disturbances have received increasing attention in recent years with growing energy demands involving oil and gas development in deeper and harsher environments. The three most common marine flexible systems, installation systems, riser systems, and mooring systems, are consisted by different flexible mechanical systems such as beam and string.

The trend in the offshore industry is toward increased use of installation systems and floating platforms such as anchored Floating Production Storage and Offloading (FPSO) vessels in deep water. Traditional marine installation systems consist of the vessel dynamic positioning and crane manipulation to obtain the desired position and heading for the payload [1, 2]. Such methods become difficult in deeper waters due to the longer cable between the surface vessel and payload. The longer cable increases the natural period of the cable and payload system, which in turn increase the effects of oscillations. One solution to alleviate the precision installation problem is the addition of thrusters attached the payload for the installation operation [7, 16, 17]. Such marine installation system consists of an ocean surface vessel, a flexible string-type cable, and a subsea payload to be positioned for installation on the ocean floor. The control for the dynamic positioning of the payload is challenging due to the unpredictable exogenous disturbances such as fluctuating currents and transmission of motions from the surface vessel through the lift cable. The unknown time-varying ocean disturbances along the cable lead to the appearance of oscillations. The paper [7] about the control of the marine installation systems focuses on the dynamics of the payload, where the dynamics of the cable is considered as an external force term to the payload. In [8, 18], the coupled crane-payload flexible installation system with nonuniform parameters is presented, where a barrier Lyapunov function is employed for control design and stability analysis. In [9, 19, 20],

the flexible marine installation system with cable, vessel, and payload dynamics is represented by a set of infinite-dimensional equations, (i.e., PDEs describing the dynamics of the flexible cable) coupled with a set of finite-dimensional equations (i.e., ODEs describing the lumped vessel and payload dynamics). Robust adaptive boundary control of a marine installation system is developed to position the subsea payload to the desired set-point and suppress the cable's vibration.

With the development of offshore industry, the control problems of positioning systems for marine vessels are received increasing attention. During the past decades, the research interests mainly focused on the DP systems, and several excellent control methods are proposed for DP systems; see [11, 14, 15, 21–29] and references therein. Many good results [30–34] for control design of the mooring system in the literatures rely on the ODE model with neglecting the dynamics of the mooring lines. These works on the control of the thruster-assisted position mooring systems mainly focus on the dynamics of the vessel, and the dynamics of the mooring lines are usually ignored for the convenience of the control design. In earlier research [30], a nonlinear passive observer for thruster-assisted position moored ships is developed, where the force from the mooring lines are regarded as external forces, and mooring system is modeled as an ODE system. A finite element model of a single mooring line is derived in [35], but the control is not proposed for the system. More recently, by using a structural reliability measure for the mooring lines, the paper [31] proposes the control to maintain the probability of the mooring line failure below an acceptable level regardless of changing weather conditions. In [32], the switching control is designed for a positioning mooring system that allows the thrusters to assist the mooring system in the varying environmental conditions. In [34], the modeling and control of a positioning mooring system with a drilling riser is investigated. In these works, the dynamics of the mooring lines is considered as an external force term to the vessel dynamics. These kinds of model can influence the dynamic response of the whole mooring system due to the neglect of the coupling between the vessel and the mooring lines. To overcome this shortcoming, in some papers, the mooring system is represented by two PDEs describing the dynamics of the mooring lines coupled with four ODEs describing the lumped vessel dynamics. The paper [36] investigates the station keeping and tension problem in order to avoid line tensions rising for the multicable mooring systems in which the dynamics of the mooring lines are modeled as PDEs. But the paper does not provide the detailed discussion for the control design.

In [11, 21, 22], Kalman filtering and optimal control methods are proposed for linearized vessel models. Based on Lyapunov's direct method, backstepping control methods are proposed in [23, 24], where a passive nonlinear observer is used to estimate the vessel velocities. In [25], the problem of weather optimal dynamic positioning is investigated by using the basic principle of pendulum, where the optimal control minimizes the load of the constant environmental disturbances on the vessel. In [26], the ship dynamics are firstly transformed into a system affine in the ship velocities by using global nonlinear coordinate changes, observers are accordingly designed to globally exponentially estimate unmeasured velocities, and then the control is designed for underactuated ships by using Lyapunov's direct

method and backstepping technique, where the passive property of ship dynamics and their interconnected structure are utilized. This method is extended in [27] by adding integral actions to the control to compensate for a constant bias of environmental disturbances. Alternatively, a reliability-based control algorithm for dynamic positioning of floating vessels is proposed in [29], a hybrid controller is developed in [15] to extend the operational weather window for marine operations to harsh environments, and fuzzy neural network control is designed in [14] for the case where the dynamic model of ship is unknown. An elegant learning control design technique is proposed in [37] for a marine surface ship in uncertain dynamical environments, where the proposed learning control can effectively exploit the learned knowledge without readapting to the unknown system dynamics for another similar control task to achieve a closed-loop stability and improved control performance. In [38], leader-follower formation control is proposed for underactuated autonomous underwater vehicles without the need for leader's velocity and dynamics.

Comparing with DP systems, there are relatively few results on PM systems. Since the late of last century, the PM systems are proved to be a cost-effective solution for offshore drilling rigs and floating oil production, and the control problem of PM systems is investigated. Several excellent research results can be found in [31–33, 39, 40]. In [31], an adaptive controller is designed such that the probability of mooring line failure could be kept below a predefined acceptable level. By using a structural reliability measure for the mooring lines, the control protected the mooring system whenever needed as a result of severe weather conditions and high environmental loads. In [33], a three-level control strategy is presented for PM systems, where a nonlinear passive observer is employed to estimate the low-frequency motion of moored vessel, and nonlinear output PID control law is used to keep the vessel's position and heading based on the measured states. For the PM systems investigated in [32], several controllers are designed for heading, damping, restoring, and mean force, respectively, and the authors integrated these controllers into a switching control system that also included a set of models to track the existing operational conditions and the switching logics. In [31], a model of a futuristic fish farming structure is established, and problems related to interconnected marine structures and strategies for configuration control are studied. The control system is designed such that the loading of the mooring system is limited and the strain in the connectors between the modules is positive.

The physical structure of a marine riser system is shown in Fig. 1.1. In earlier works of marine flexible risers [41–43], the modeling of the riser systems is investigated, and the simulations with different numerical methods are provided to verify the effectiveness of the models. In [44, 45], distributed parameter models with PDEs are used to analyze and investigate the dynamic response of the flexible marine riser under the ocean current disturbances. But the stability and control design are not mentioned in these works. The Timoshenko model also can provide an accurate beam model, which takes into account the rotary inertial energy and the deformation owing to shear. Compared with the Euler–Bernoulli model, the Timoshenko model is more accurate at predicting the beam's response. However, the Timoshenko model is more difficult to implement for control design due

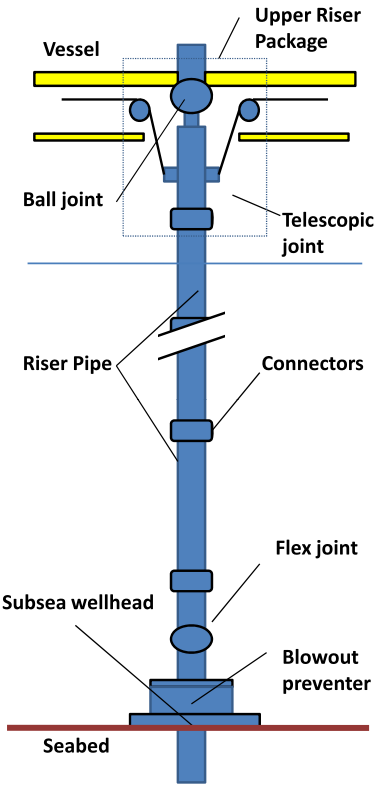

Fig. 1.1 The structure of a marine riser system

to its higher order. For this reason, most of the flexible marine risers with boundary control are based on the Euler–Bernoulli model [46]. In [47], boundary control for the flexible marine riser with actuator dynamics is designed based on the Lyapunov direct method and the backstepping technique. In [48], the boundary control problem of a three-dimensional nonlinear inextensible riser system is considered via the same method as in [47]. In [4], a torque actuator is introduced at the top boundary of the riser to reduce the angle and transverse vibration of the riser with guaranteed a closed-loop stability. In [49], boundary control for a coupled nonlinear flexible marine riser with two actuators in transverse and longitudinal directions is designed to suppress the riser's vibration. In [50, 51], adaptive boundary control is proposed for a flexible marine riser with vessel dynamics, where the coupling between the riser and the vessel is handseled. In these works, the riser is modeled as an Euler–Bernoulli beam structure with PDEs for the purpose of dynamic analysis, since the diameter-to-length ratio of the riser is small. Based on the distributed parameter model, various kinds of control methods integrating computer software and hardware with sensors and actuators are investigated to design control to suppress the riser's vibration.

1.3 Control of Flexible Mechanical Systems

In recent decades, dealing with the vibration problem of flexible systems has become an important research topic, driven by practical needs and theoretical challenges. Lightweight mechanical flexible systems possess many advantages over conventional rigid ones, such as lower cost, better energy efficiency, higher operation speed, and improved mobility. These advantages greatly motivate the applications of the mechanical flexible systems in industry. A large number of systems can be modeled as mechanical flexible systems such as telephone wires, conveyor belts, crane cables, helicopter blades, robotic arms, mooring lines, marine risers, and so on. However, unwanted vibrations due to the flexibility property and the time-varying disturbances restrict the utility of these flexible systems in different engineering applications.

Many physical processes cannot be modeled by ODEs since the state of the system depends on more than one independent variable [52]. The state of a given physical system, such as flexible structure, fluid dynamics, and heat transfer, may depend on the time t and the location x. The flexible mechanical systems are dependent on the spatial and temporal variables, which can be modeled as the distributed parameter systems. The model is represented by a set of infinite-dimensional equations (i.e., PDEs describing the dynamics of the flexible bodies) coupled with a set of finite-dimensional equations (i.e., ODEs describing the boundary conditions). The model of the flexible mechanical system represented by a set of PDEs is difficult to control due to the infinite dimensionality of the system, and many control strategies for the conventional rigid-body system cannot be directly applied to solve the control problem of the flexible system.

The most popular control approaches for the distributed parameter systems are modal control based on the truncated discredited system model, distributed control by using distributed sensors and actuators, and boundary control. Modal control for the distributed parameter systems is based on truncated finite-dimensional modes of the system, which are derived from finite element method, Galerkin's method, or assumed-modes method [53–61]. For these finite-dimensional models, many control techniques developed for ODE systems in [62–66] can be applied. The truncated models are obtained via the model analysis or spatial discretization, in which the flexibility is represented by a finite number of modes by neglecting the higher-frequency modes. The problems arising from the truncation procedure in the modeling need to be carefully treated in practical applications. A potential drawback in the above control design approaches is that the control can cause the actual system to become unstable due to excitation of the unmodeled, high-frequency vibration modes (i.e., spillover effects) [67]. Spillover effects that result in instability of the system are investigated in [68, 69] when the control of the truncated system is restricted to a few critical modes. The control order needs to be increased with the number of flexible modes considered to achieve high accuracy of performance, and the control may also be difficult to implement from the engineering point of view since full state measurements or observers are often required. In an attempt to overcome the above shortcomings of the truncated model-based modal control, boundary control

where the actuation and sensing are applied only through the boundary of the system utilizes the distributed parameter model with PDEs to avoid control spillover instabilities. Boundary control combined with other control methodologies, such as variable structure control [70], sliding-mode control [71], energy-based robust control [72, 73], model-free control [74], the averaging method [75–79], and robust adaptive control [80–82], is developed. In these approaches, system dynamics analysis and control design are carried out directly based on the PDEs of the system.

Distributed control [83–87] requires relatively more actuators and sensors, which makes the distributed control relatively difficult to implement. Compared with the distributed control, boundary control is an economical method to control the distributed parameter system without decomposing the system into a finite-dimensional space. Boundary control is considered to be more practical in a number of research fields, including the vibration control of flexible structures, fluid dynamics, and heat transfer, which requires few sensors and actuators. In addition, the kinetic energy, the potential energy, and the work done by the nonconservative forces in the process of modeling can be directly used to design the Lyapunov function of the closed-loop system.

The relevant applications for boundary control approaches in mechanical flexible structures consist of second-order structures (strings and cables) and fourth-order structures (beams and plates) [88]. The Lyapunov direct method is widely used since the Lyapunov functionals for control design closely relate to kinetic, potential, and work energies of the distributed parameter systems. Based on the Lyapunov direct method, the authors in [47, 48, 61, 67, 70–74, 80, 81, 89–126] have presented results for the boundary control of the flexible mechanical systems. In [80], robust adaptive boundary control is investigated to reduce the vibration for a moving string with spatiotemporally varying tension. In [98], robust and adaptive boundary control is developed to stabilize the vibration of a stretched string on a moving transporter. In [101], a boundary controller for a linear gantry crane model with a flexible string-type cable is developed and experimentally implemented. An active boundary control system is introduced in [102] to damp undesirable vibrations in a cable. In [105], the asymptotic and exponential stability of an axially moving string is proved by using a linear and nonlinear state feedback. In [127], a flexible rotor with boundary control is illustrated, and the experimental implementation of the flexible rotor controller is also presented. Boundary control is applied to beams in [128], where boundary feedback is used to stabilize the wave equations and design active constrained layer damping. Active boundary control of an Euler–Bernoulli beam, which enables the generation of a desired boundary condition at any designators position of a beam structure, is investigated in [129]. In [107], a nonlinear control law is constructed to exponentially stabilize a free transversely vibrating beam via boundary control. In [47, 48], a boundary controller for the flexible marine riser with actuator dynamics is designed based on the Lyapunov direct method and the backstepping technique. In [116], a linear boundary velocity feedback control is designed to ensure exponential stabilization of the vibration of a nonlinear moving string. In [103], boundary control of a nonlinear string is investigated where feedback from the velocity at the boundary of a string is proposed to stabilize the vibrations. It is notable

that robust and adaptive control schemes have been applied to the boundary control design in [9, 49, 50, 80, 81, 98, 130–132]. By using the Laplace transform to derive the exact solution of the wave equation, boundary impedance control for a string system is investigated in [104]. Recently, by combining the backstepping method with adaptive control design, a novel boundary controller and observer are designed to stabilize the string and beam model and tracking the target system. Many remarkable results in this area are obtained in [114, 133–145]. However, this boundary control method is hard to be applied to the marine flexible systems due to difficulties in finding a proper gain kernel. For example, it is hard to find a gain kernel for the model of the marine riser system subjected to the unknown ocean disturbances. Employing the iterative learning control (ILC) scheme, the authors in [99, 100, 146] propose the boundary control for a class of distributed parameter systems. In their research, the external disturbance is assumed to be periodical so that the iterative learning boundary control can be designed. However, the external disturbance is not periodical in the ocean environment, which leads to that the ILC-based boundary control may not be applied in the marine flexible systems.

In the literature of boundary control for the distributed parameter systems, functional analysis and the semigroup theory are usually used for the stability analysis and for the proof of the existence and uniqueness of PDEs; see, for example, [147–155]. Such distributed parameter systems are described by operator equations on an infinite-dimensional Hilbert or Banach space [156–158]. The stability analysis and the solution existence are based on the theory of semigroups on infinite-dimensional state spaces. In [48], the proof of the existence and uniqueness of the control system is carried out by using an infinite-dimensional state space. In [80], the asymptotic stability of the system with proposed control is proved by using semigroup theory. In [147], stability of different infinite-dimensional systems is studied based on the semigroup theory. In [145], the semigroup theory is utilized to prove the strong stability of a one-dimensional wave equation with proposed boundary control. In [152], stabilization of a second-order PDE system under noncollocated control and observations is investigated in Hilbert spaces. In [159], a noncollocated boundary control is developed to stabilize two connected strings with the joint anti-damping, and the exponentially stability is proved by using the semigroup theory. With control at one end and noncollocated observation at the other end, the exponential stability of the closed-loop system is proved in [153]. In [154, 155], a uniformly exponentially stable observer is designed for a class of second-order distributed parameter systems, and the uniqueness and stability of the system are proved based on the semigroup theory.

Compared with the functional-analysis-based methods, the Lyapunov direct method for the distributed parameter systems requires little background beyond calculus for users to understand the control design and the stability analysis. In addition, the Lyapunov direct method provides a convenient technique for PDEs by using well-understood mathematical tools such as algebraic and integral inequalities and integration by parts.

1.4 Adaptive and Approximation-Based Control for Marine Systems

An intuitive solution to alleviate the precision placement problem is the addition of thrusters for localized positioning when the payload is near the target site [160, 161]. The positioning control is challenging due to unpredictable exogenous disturbances such as fluctuating currents and transmission of motions from the surface vessel through the lift cable. In [162], experiments are carried for dynamic positioning of a towed pipe. The nonlinear dynamics associated with the fluid phenomenon on the payloads, represented by a continuous infinite-dimensional Navier–Stokes equation, need to be reduced to a finite-dimensional approximate model that is normally experimentally determined. Due to the size, costs, and the variations in design and construction, full-scale experiments may not be possible in all structures. In most cases, the best way to determine the coefficients required are by means of model testing, where uncertainties attributed to the materials, measurement, and scale effect exist.

Traditionally, such hydrodynamic loads are treated as bounded disturbances, and the standard proportional-integral-derivative (PID) algorithm is applied in motion control. The PID control is shown to exhibit good steady-state performance. However, its transient performance is less satisfactory, since the linear control action tends to produce large overshoots. Although the PID control does not explicitly contain any terms from the dynamic model, the tuning of the PID gains by advanced techniques such as LQR requires knowledge of the model. Without the use of such techniques, PID tuning for the MIMO systems is generally nontrivial and may require full-scale experiments.

In the dynamic control of offshore structures for installation, an important concern is how to deal with unknown perturbations to the nominal model, in the form of parametric and functional uncertainties, unmodeled dynamics, and disturbances from the environment. Marine control applications are characterized by time-varying environmental disturbances and widely changing sea conditions. In this context, the stand-alone model-based control may not be the proper ideal since it generally works best when the dynamic model is known exactly. The presence of uncertainties and disturbances could disrupt the function of the feedback control and lead to degradation of performance. We propose to overcome this problem for the installation of subsea structures by adopting an intelligent control strategy in the form of adaptive neural techniques to compensate for functional uncertainties in the dynamic model and unknown disturbances from the environment. According to the Stone–Weierstrass theorem, a universal approximator, such as a neural network, can approximate any real continuous function on a compact set to an arbitrary degree of accuracy. Such approximators can utilize a standard regressor function whose structure is independent of the dynamic characteristics, thus increasing the portability of the same control algorithm on different marine systems. For systems in which the dynamic models are well established and accurate, existing model-based schemes can be augmented by intelligent control "modules" easily and flexibly to handle disturbances from varying weather conditions and sea states.

Direct compensation of the hydrodynamic loads is desirable but difficult to realize in practice due to the difficulty in obtaining accurate parametric coefficients. For control design, the parametric model should be simple enough for analysis and yet be complex enough to capture the main dynamics of the system. The approximation abilities of artificial NNs have been proven in many research works [163–167]. The major advantages of parallel structure, learning ability, nonlinear function approximation, fault tolerance, and efficient analog VLSI implementation for real-time applications motivate the usage of NNs in nonlinear system control and identification. NNs, combined backstepping designs, are reported in [168], using NN to construct observes can be found in [169, 170], NN control in robot manipulators is reported in [64, 171–173]. Adaptive neural control can overcome some limitations of model-based control that requires exact knowledge of the system parameters [174, 175]. NNs can also be used as an alternative to parameterize the nonlinear hydrodynamic loads when coupled with adaptive control for online tuning. NNs are embedded in the overall control strategy for modeling and compensation purposes in [166, 176–178]. In-depth developments in NNs for modeling and control purposes are made in [175, 178–192].

1.5 Outline of the Book

The general objectives of the book are to develop constructive and systematic methods of designing control for marine mechanical systems with guaranteed stability. By investigating the characteristics of several different marine models, control strategies are proposed to achieve the performance for the concerned systems. The book starts with a brief introduction of control techniques for a classes of marine mechanical systems in Chap. 1.

Chapter 2 presents several lemmas and properties for the subsequent development for the convenience of derives of the dynamical models and further stability analysis for the marine mechanical structures.

In Chap. 3, positioning control in the horizontal plane is investigated for the installation of subsea systems, with thrusters attached, under time-varying irrigational ocean current, when the payload is near to the seabed. Backstepping in combination with adaptive feedback approximation techniques is employed in the design of the control, with the option of high-gain observer for output feedback control. The stability of the design is demonstrated through Lyapunov analysis when the semiglobal uniform boundedness of the closed-loop signals is guaranteed. The proposed adaptive neural control is able to capture the dominant dynamic behaviors without exact information on the hydrodynamic coefficients of the structure and current measurements.

In Chap. 4, the model of the coupled vessel, crane, cable, and payload with nonuniform parameters is presented. Positioning control is derived for the coupled system with uniform parameters using barrier Lyapunov functions. Through Lyapunov analysis, it is shown that the coupled crane, payload flexible system is

stable under the control action, the physical limits from operations planning and safety specifications are not transgressed, and positioning of crane and payload is achieved. A stabilizing boundary control is proposed for the coupled system with nonuniform parameters. Rigorous Lyapunov stability analysis is carried out and the uniform boundedness of the system is shown under the proposed control. Finally, the performance of the proposed control is given through numerical simulations.

In Chap. 5, robust adaptive boundary control of a marine installation system is developed to position the subsea payload to the desired set-point and suppress the cable's vibration. The flexible cable coupled with vessel and payload dynamics is described by a distributed parameter system with one partial differential equation (PDE) and two ordinary differential equations (ODEs). Boundary control is proposed at the top and bottom boundaries of the cable based on the Lyapunov direct method. Considering the system parametric uncertainties and the unknown ocean disturbances, the developed adaptive boundary control schemes achieve the uniform boundedness of the steady-state error between the boundary payload and the desired position. The control performance of the closed-loop system is guaranteed by suitably choosing the design parameters.

Chapter 6 is dedicated to the control problem of a thruster-assisted single-point mooring system in the presence of uncertainties and unknown backlash-like hysteresis nonlinearities. Using backstepping technique and Lyapunov synthesis and employing neural networks (NNs) to approximate the unknown nonlinear functions, robust adaptive backstepping control is developed for the full-state feedback case. Subsequently, in order to overcome the measure difficulty in the vessel velocity vector, a high-order NN-based observer is constructed to estimate the unmeasurable state vector. It is shown that the proposed observer has an excellent estimation performance in spite of the existence of uncertainties and unknown backlash-like hysteresis nonlinearities. Based on this observer, robust adaptive output feedback control is developed via backstepping design. Under the proposed control, the semiglobal uniform boundedness of all the signals in the closed-loop systems is guaranteed for both full-state and output feedback cases.

In Chap. 7, boundary control for a coupled nonlinear flexible marine riser with two actuators in transverse and longitudinal directions is developed to reduce the riser's vibrations. The dynamic behavior of the flexible riser is represented by a distributed parameter system (DPS) model with partial differential equations (PDEs), and the control is applied at the top boundary of the riser based on Lyapunov's direct method to suppress the riser's vibrations. With the proposed boundary control, the uniform boundedness under ocean current disturbance and exponential stability under free vibration condition are achieved. The proposed control is independent of system parameters, which ensures the robustness of the system to variations in parameters.

Chapter 8 studies the modeling and control of a flexible marine riser with the vessel dynamics. Both the dynamics of the vessel and the vibration of the riser are considered in the dynamic analysis, which make the system more difficult to control. Boundary control is proposed at the top boundary of the riser to suppress the riser's vibration. Adaptive control is designed when the system parametric uncertainties

exist. Employing the Lyapunov direct method, the states of the system are proven to be uniformly ultimately bounded. The state of the system will converge to a small neighborhood of zero by appropriately choosing the design parameters. The design is based on the PDEs of the system, thus avoiding some drawbacks associated with the traditional truncated-model-based design approaches.

Chapter 9 investigates the riser operations of fixed and floating offshore structures using pipe connections between surface facilities and seabed as well as pipes laying on or below the seabed for transportation of oil and gas. The analysis of vertical marine risers under the influences of both internal and external forces are described. Four configurations of the marine risers are introduced including free handing mode, connected mode, operational mode, and nonoperational but connected mode. A marine riser can be maintained in an operable condition by ensuring that the lower ball joint angle remains below about 4 degrees. Three operating procedures are given to bring the angle down. The marine riser monitoring system provides information on the behaviors of the platform and the marine riser, and comparisons can be made with previous results for evaluating the projected fatigue life of the riser. BPP-RMS, an example of the comprehensive Riser Management System (RMS) for riser maintenance and inspection, is presented. BPP-RMS is an on-board riser operation management system that provides real-time guidance for carrying out connected and disconnected mode drilling riser operations on board a vessel.

The last chapter, Chap. 10, makes conclusions on this book and recommendations on the future research works.

Chapter 2
Preliminaries

In this chapter, we provide some mathematical preliminaries, useful technical lemmas, and properties of the ocean disturbance, which will be extensively used throughout this book. The chapter is organized as follows. Firstly, the Hamilton principle is introduced in Sect. 2.1. Then, a brief introduction of the ocean disturbance on marine flexible structures is given in Sect. 2.2. Subsequently, the function approximation using NNs is presented in Sect. 2.3, followed by Sect. 2.4 about some useful technical lemmas for completeness.

2.1 The Hamilton Principle

As opposed to lumped mechanical systems, flexible mechanical systems have an infinite number of degrees of freedom, and the model of the system is described by using continuous functions of space and time. The Hamilton principle permits the derivation of equations of motion from energy quantities in a variational form and generates the motion equations of the flexible mechanical systems. The Hamilton principle [193, 194] is represented by

$$\int_{t_1}^{t_2} \delta(E_k - E_p + W)\, dt = 0, \tag{2.1}$$

where t_1 and t_2 are two time instants, $t_1 < t < t_2$ is the operating interval, δ denotes the variational operator, E_k and E_p are the kinetic and potential energies of the system, respectively, and W denotes the work done by the nonconservative forces acting on the system, including internal tension, transverse load, linear structural damping, and external disturbance. The principle states that the variation of the kinetic and potential energies plus the variation of work done by loads during any time interval $[t_1, t_2]$ must equal zero.

There are some advantages using the Hamilton principle to derive the mathematical model of the flexible mechanical systems. Firstly, this approach is independent of the coordinates, and the boundary conditions can be automatically generated by

W. He et al., *Dynamics and Control of Mechanical Systems in Offshore Engineering*, Advances in Industrial Control, DOI 10.1007/978-1-4471-5337-5_2,

this approach [88]. In addition, the kinetic energy, the potential energy, and the work done by the nonconservative forces in the Hamilton principle can be directly used to design the Lyapunov function of the closed-loop system.

2.2 The Ocean Disturbance on Marine Mechanical Structures

Vortex-induced vibration (VIV) is a direct consequence of lift and drag oscillations due to the vortex shedding formation behind bluff bodies [195]. The marine flexible structures used in offshore production system may get out of control when the structural natural frequency of the risers and cables equals frequency of vortex shedding. The effects of a time-varying ocean current, $U(x,t)$, on a riser or a cable can be modeled as a vortex excitation force [196, 197]. The current profile $U(x,t)$ is a function that relates the depth to the ocean surface current velocity $U(t)$. The distributed load on a marine flexible structure, $f(x,t)$, can be expressed as a combination of the inline drag force, $f_D(x,t)$, consisting of a mean drag and an oscillating drag about the mean modeled as

$$f_D(x,t) = \frac{1}{2}\rho_s C_D(x,t)U(x,t)^2 D + A_D \cos\big(4\pi f_v(x,t)t + \theta\big), \tag{2.2}$$

and an oscillating lift force $f_L(x,t)$, perpendicular to $f_D(x,t)$, about a mean deflected profile,

$$f_L(x,t) = \frac{1}{2}\rho_s C_L(x,t)U(x,t)^2 D \cos\big(2\pi f_v(x,t)t + \vartheta\big), \tag{2.3}$$

where ρ_s is the sea water density, $C_D(x,t)$ and $C_L(x,t)$ are the time and spatially varying drag and lift coefficients, respectively, D is the outer diameter of the flexible structures, $f_v(x,t)$ is the shedding frequency, θ and ϑ are the phase angles, and A_D is the amplitude of the oscillatory part of the drag force, typically 20 % of the first term in $f_D(x,t)$ [197]. The nondimensional vortex shedding frequency [4] can be expressed as

$$f_v(x,t) = \frac{S_t U(x,t)}{D}, \tag{2.4}$$

where S_t is the Strouhal number.

In this book, we consider the deflection of the marine flexible structures in transverse and longitudinal directions. Hence, the distributed load can be expressed as

$$f(x,t) = f_D(x,t)\frac{1}{2}\rho_s C_D(x,t)U(x,t)^2 D + A_D \cos\big(4\pi f_v(x,t)t + \theta\big). \tag{2.5}$$

The transverse vortex-induced vibration (VIV) from the lift component is not considered in this book, but the proposed method can be similarly applied without any loss of generality if only the lift component is considered.

2.3 Function Approximation

In this book, a class of linearly parameterized NNs with radial basis functions (RBF) is used to approximate the continuous function $f_j(Z) : \mathbb{R}^q \to \mathbb{R}$,

$$f_{nn,j}(Z) = W_j^T S_j(Z), \tag{2.6}$$

where the input vector $Z = [Z_1, Z_2, \ldots, Z_q]^T \in \Omega_Z \subset \mathbb{R}^q$, the weight vector $W_j \in \mathbb{R}^l$, the NN node number $l > 1$, and $S_j(Z) = [s_1, s_2, \ldots, s_l]^T \in \mathbb{R}^l$. Universal approximation results indicate that, if l is chosen sufficiently large, $W_j^T S_j(Z)$ can approximate any continuous function, $f_j(Z)$, over a compact set $\Omega_Z \subset \mathbb{R}^q$ to any desired accuracy. This is achieved as

$$f_j(Z) = W_j^{*T} S_j(Z) + \epsilon_j(Z) \quad \forall Z \in \Omega_z \in \mathbb{R}^q, \tag{2.7}$$

where W_j^* is the ideal constant weight vector, and $\epsilon_j(Z)$ is the approximation error, which is bounded over the compact set, i.e., $|\epsilon_j(Z)| \leq \epsilon_j^*$ for all $Z \in \Omega_Z$ with $\epsilon_j^* > 0$ is an unknown constant. The ideal weight vector W_j^* is an "artificial" quantity required for analytical purposes. W_j^* is defined as the value of W_j that minimizes $|\epsilon_j|$ for all $Z \in \Omega_Z \subset \mathbb{R}^q$, i.e.,

$$W_j^* = \arg \min_{W_j \in R^l} \left\{ \sup_{Z \in \Omega_Z} \left| f_j(Z) - W_j^T S_j(Z) \right| \right\}. \tag{2.8}$$

Typical choices for $s_k(Z)$ include the sigmoid function, hyperbolic tangent function, and RBF. The RBF NN is a particular network architecture that uses l Gaussian functions of the form

$$s_k(Z) = \exp\left[\frac{-(Z - \mu_k)^T (Z - \mu_k)}{\eta_k^2} \right], \quad k = 1, 2, \ldots, l, \tag{2.9}$$

where $\mu_k = [\mu_{k1}, \mu_{k2}, \ldots, \mu_{kq}]^T$ is the center of the receptive field, and η_k is the width of the Gaussian function [198].

2.4 Lemmas

Lemma 2.1 [199] *Let $\phi_1(x,t) \in \mathbb{R}$ and $\phi_2(x,t) \in \mathbb{R}$ be functions defined for $x \in [0, L]$ and $t \in [0, \infty)$. The Cauchy–Schwarz inequality is*

$$\int_0^L \phi_1 \phi_2 \, dx \leq \left(\int_0^L \phi_1^2 \, dx \right)^{\frac{1}{2}} \left(\int_0^L \phi_2^2 \, dx \right)^{\frac{1}{2}}. \tag{2.10}$$

Lemma 2.2 [88] *The following inequalities hold*:

$$\phi_1 \phi_2 \leq |\phi_1 \phi_2| \leq \phi_1^2 + \phi_2^2 \quad \forall \phi_1, \phi_2 \in \mathbb{R}. \tag{2.11}$$

Lemma 2.3 [88] *The following inequalities hold*:

$$|\phi_1\phi_2| = \left|\left(\frac{1}{\sqrt{\delta}}\phi_1\right)(\sqrt{\delta}\phi_2)\right| \le \frac{1}{\delta}\phi_1^2 + \delta\phi_2^2 \quad \forall \phi_1, \phi_2 \in \mathbb{R} \text{ and } \delta > 0. \tag{2.12}$$

Lemma 2.4 [200] *Let* $\phi(x,t) \in \mathbb{R}$ *be a function defined for* $x \in [0, L]$ *and* $t \in [0, \infty)$ *and satisfying the boundary condition*

$$\phi(0,t) = 0 \quad \forall t \in [0, \infty). \tag{2.13}$$

Then the following inequalities hold:

$$\int_0^L \phi^2\, dx \le L^2 \int_0^L \left[\phi'\right]^2 dx, \tag{2.14}$$

$$\phi^2 \le L \int_0^L \left[\phi'\right]^2 dx. \tag{2.15}$$

If in addition to Eq. (2.13), *the function* $\phi(x,t)$ *satisfies the boundary condition*

$$\phi'(0,t) = 0 \quad \forall t \in [0, \infty), \tag{2.16}$$

then the following inequality also holds:

$$\left[\phi'\right]^2 \le L \int_0^L \left[\phi''\right]^2 dx. \tag{2.17}$$

Proof Define the inner product

$$(\phi_1, \phi_2) = \frac{1}{2}\int_0^L \phi_1\phi_2\, dx + \frac{1}{2\alpha}\phi_1(L)\phi_2(L)$$

and the operator $\mathcal{A}_0\phi = [-\phi'', \alpha\phi'(L,t)]^T$, $\alpha > 0$. Then we have

$$\begin{aligned}(\mathcal{A}_0\phi, \phi) &= \frac{1}{2}\int_0^L -\phi''\phi\, dx + \frac{1}{2}\phi'(L)\phi(L) \\ &= \frac{1}{2}\int_0^L \left[\phi'\right]^2 dx.\end{aligned}$$

Since the operator $\mathcal{A}_0$ is positive and symmetric, we have

$$\begin{aligned}(\mathcal{A}_0\phi, \phi) &\ge \lambda_{\min}(\mathcal{A}_0)\|\phi\|^2 \\ &= \lambda_{\min}(\mathcal{A}_0)\left(\frac{1}{2}\int_0^L [\phi]^2\, dx + \frac{1}{2\alpha}\left[\phi(L)\right]^2\right),\end{aligned}$$

where $\lambda_{\min}(\mathcal{A}_0)$ is the minimum eigenvalue of $\mathcal{A}_0$ given by the solutions of $(\lambda I - \mathcal{A}_0)\phi = 0$. Therefore, we obtain

$$\int_0^L \left[\phi'\right]^2 dx \geq \lambda_{\min}(\mathcal{A}_0)\left(\int_0^L [\phi]^2 dx + \frac{1}{\alpha}\left[\phi(L)\right]^2\right)$$
$$\geq \lambda_{\min}(\mathcal{A}_0)\int_0^L [\phi]^2 dx.$$

The eigenfunctions of $\mathcal{A}_0$ have the following form:

$$W(x) = \sin \beta x,$$

where the pinned boundary condition at $x = 0$ has been used, and $\lambda = \beta^2$. The frequency equation is

$$\beta \sin \beta L - \alpha \cos \beta L = 0.$$

We are free to choose $\alpha = \frac{\sin(1)}{L\cos(1)}$, so the minimum solution of the above equation is $\beta = \frac{1}{L}$ and $\lambda_{\min}(\mathcal{A}_0) = \frac{1}{L^2}$, and we obtain

$$L^2 \int_0^L \left[\phi'\right]^2 dx \geq \int_0^L [\phi]^2 dx.$$

Define $\phi_1(x,t) = \phi'(x,t)$ and $\phi_2(x,t) = \chi(s-x) = \begin{cases} 1, & x \leq s, \\ 0, & x > s, \end{cases}$ where $s \in [0,\ L)$ is a constant. Using the Cauchy–Schwarz inequality, we have

$$\int_0^L \phi_1\phi_2\, dx = \int_0^L \phi'(x,t)\chi(s-x)\, dx = \phi(s,t) \leq s^{\frac{1}{2}}\left(\int_0^L \left[\phi'\right]^2 dx\right)^{\frac{1}{2}}$$
$$\leq L^{\frac{1}{2}}\left(\int_0^L \left[\phi'\right]^2 dx\right)^{\frac{1}{2}}.$$

Therefore, we have

$$\phi^2 \leq L\int_0^L \left[\phi'\right]^2 dx.$$

Similarly, we have

$$\left[\phi'\right]^2 \leq L\int_0^L \left[\phi''\right]^2 dx. \qquad \square$$

Lemma 2.5 *Let $\phi(x,t) \in \mathbb{R}$ be a function defined for $x \in [0, L]$ and $t \in [0, \infty)$ and satisfying the boundary condition*

$$\phi(0,t) = C \quad \forall t \in [0,\infty), \tag{2.18}$$

where C is a constant. Then the following inequality holds:

$$(\phi - C)^2 \leq L \int_0^L \left[\phi'\right]^2 dx \quad \forall (x,t) \in [0,L] \times [0,\infty). \tag{2.19}$$

Proof Define $\phi_1(x,t) = \phi'(x,t)$ and $\phi_2(x,t) = \chi(s-x) = \begin{cases} 1, & x \leq s, \\ 0, & x > s, \end{cases}$ where $s \in [0,\ L)$ is a constant. Using the Cauchy–Schwarz inequality, we have

$$\begin{aligned} \int_0^L \phi_1 \phi_2 \, dx &= \int_0^L \phi'(x,t)\chi(s-x)\, dx \\ &= \phi(s,t) - C \\ &\leq s^{\frac{1}{2}} \left(\int_0^L \left[\phi'\right]^2 dx \right)^{\frac{1}{2}} \\ &\leq L^{\frac{1}{2}} \left(\int_0^L \left[\phi'\right]^2 dx \right)^{\frac{1}{2}}. \end{aligned} \tag{2.20}$$

Therefore, we have

$$(\phi - C)^2 \leq L \int_0^L \left[\phi'\right]^2 dx, \quad \forall (x,t) \in [0,L] \times [0,\infty). \quad \square \tag{2.21}$$

Lemma 2.6 [201] *Rayleigh–Ritz theorem*: *Let $A \in \mathbb{R}^{n \times n}$ be a real, symmetric, positive-definite matrix*; *therefore, all the eigenvalues of A are real and positive. Let $\lambda_{\min}$ and $\lambda_{\max}$ denote the minimum and maximum eigenvalues of A, respectively. Then for all $x \in \mathbb{R}^n$, we have*

$$\lambda_{\min} \|x\|^2 \leq x^T A x \leq \lambda_{\max} \|x\|^2, \tag{2.22}$$

where $\|\cdot\|$ denotes the standard Euclidean norm.

Lemma 2.7 [202, 203] *For bounded initial conditions, $\forall x$ and $\forall t \geq 0$, if there exists a C^1 continuous and positive-definite Lyapunov function $V(x,t) : \Re^n \times \Re_+ \longrightarrow \Re$ satisfying $\kappa_1(\|x\|) \leq V(x,t) \leq \kappa_2(\|x\|)$ and such that $\dot{V}(x,t) \leq -\lambda V(x,t) + c$, where $\kappa_1, \kappa_2 : \mathbb{R}^n \to \mathbb{R}$ are class K functions, and c is a positive constant, then the equilibrium point $x = 0$ of the system $\dot{x} = f(x,t)$ is uniformly bounded.*

Lemma 2.8 [204] *For any real-valued continuous function $f(x,y,z)$, $x \in \mathbb{R}^m$, $y \in \mathbb{R}^n$, $z \in \mathbb{R}^p$, there are smooth scalar functions $\alpha(x,y) \geq 0$ and $\beta(z) \geq 0$ such that*

$$\left| f(x,y,z) \right| \leq \alpha(x,y) + \beta(z). \tag{2.23}$$

Lemma 2.9 [205] *Consider the basis functions of Gaussian RBF NN (2.9) with $\hat{Z}$ being the input vector. If $\hat{Z} = Z - \epsilon\bar{\psi}$, where $\bar{\psi}$ is a bounded vector, and $\epsilon > 0$ is a*

constant, then we have

$$\begin{aligned} s_i(\hat{Z}) &= \exp\left[\frac{-(\hat{Z}-\mu_j)^T(\hat{Z}-\mu_j)}{\eta_j^2}\right], \quad j=1,2,\ldots,l, \\ S(\hat{Z}) &= S(Z)+\epsilon S_t, \end{aligned} \tag{2.24}$$

where S_t is a bounded vector function.

Lemma 2.10 [206] *Suppose that a system output $y(t)$ and its first n derivatives are bounded and such that $|y^{(k)}| < Y_K$ with positive constants Y_K. Consider the following linear system*:

$$\begin{aligned} \varepsilon\dot{\pi}_i &= \pi_{i+1}, \quad i=1,\ldots,n-1, \\ \varepsilon\dot{\pi}_n &= -\bar{\lambda}_1\pi_n - \bar{\lambda}_2\pi_{n-1} - \cdots - \bar{\lambda}_{n-1}\pi_2 - \pi_1 + \eta(t), \end{aligned} \tag{2.25}$$

where ε is any small positive constant, and the parameters $\bar{\lambda}_1$ to $\bar{\lambda}_{n-1}$ are chosen such that the polynomial $s^n + \bar{\lambda}_1 s^{n-1} + \cdots + \bar{\lambda}_{n-1}s + 1$ is Hurwitz. Then, the follow property holds:

$$\xi_k = \frac{\pi_k}{\varepsilon^{k-1}} - \eta^{(k-1)} = -\varepsilon\psi^{(k)}, \quad k=1,\ldots,n-1, \tag{2.26}$$

where $\psi = \pi_n + \bar{\lambda}_1\pi_{n-1} + \cdots + \bar{\lambda}_{n-1}\pi_1$ with $\psi^{(k)}$ denoting the kth derivative of ψ. Also, there exist positive constants t^* and h_k such that for all $t > t^*$, we have $\|\xi_k\| \le \varepsilon h_k$, $k = 1, 2, 3, \ldots, n$.

Lemma 2.11 [207] *For any positive constants k_b, let $\mathcal{Z}_1 := \{z_3 \in \mathbb{R} : -k_b < z_3 < k_b\} \subset R$ and $\mathcal{N} := \mathcal{R}^l \times \mathcal{Z}_1 \subset R^{l+1}$ be open sets. Consider the system*

$$\dot{\eta} = h(t,\eta), \tag{2.27}$$

where $\eta = [w, z_1]^T \in \mathcal{N}$, and $h : \mathbb{R}_+ \times \mathcal{N} \to \mathbb{R}^{l+1}$ is piecewise continuous in t and locally Lipschitz in z, uniformly in t, on $\mathbb{R}_+ \times \mathcal{N}$. Suppose that there exist functions $U : \mathbb{R}^l \to \mathbb{R}_+$ and $V_3 : \mathcal{Z}_1 \to \mathbb{R}_+$, continuously differentiable and positive definite in their respective domains, such that

$$V_3(z_3) \to \infty \quad \text{as } z_3 \to -k_b \text{ or } z_3 \to k_b, \tag{2.28}$$

$$\gamma_1\big(\|w\|\big) \le U(w) \le \gamma_2\big(\|w\|\big) \tag{2.29}$$

where γ_1 and γ_2 are class K_∞ functions. Let $V(\eta) := V_1(z_3) + U(w)$, and let $z_3(0)$ belong to the set $z_3 \in (-k_b, k_b)$. If

$$\dot{V} = \frac{\partial V}{\partial \eta}h \le 0, \tag{2.30}$$

then $z_3(t)$ remains in the open set $z_3 \in (-k_b, k_b)$ for all $t \in [0.\infty)$.

Definition 2.12 (Barrier Lyapunov Function [207]) A BLF is a scalar function $V(x)$, defined with respect to the system $\dot{x} = f(x)$ on an open region $\mathcal{D}$ containing the origin, that is continuous, positive definite, has continuous first-order partial derivatives at every point of $\mathcal{D}$, has the property $V(x) \to \infty$ as x approaches the boundary of $\mathcal{D}$, and satisfies $V(x(t)) \leq b,\ t \geq 0$, along the solution of $\dot{x} = f(x)$ for $x(0) \in \mathcal{D}$ and some constant b.

As discussed in [207], there are many functions $V_1(z_1)$ satisfying Definition 2.12, which may be symmetric or asymmetric. Asymmetric barrier functions are more general than their counterparts and thus can offer more flexibility for control design to obtain better performance. However, they are considerably more difficult to construct analytically and to employ for control design. For clarity, the following symmetric *BLF* candidate considered in [207] is used in this book:

$$V_1 = \frac{1}{2} \log \frac{k_{b1}^2}{k_{b1}^2 - z_1^3}, \tag{2.31}$$

where $\log(\cdot)$ denotes the natural logarithm of $(\cdot)$, and k_b is the constraint on z_1. The *BLF* escapes to infinity at $z_1 = k_b$. It can be shown that V_1 is positive definite and C^1 continuous in the set $z_1 < k_{b1}$. The control design and results in this book can be extended to the asymmetric *BLF* case.

Definition 2.13 (SGUUB [65]) The solution $X(t)$ of a system is semi-globally uniformly ultimately bounded (SGUUB) if, for any compact set Ω_0 and all $X(t_0) \in \Omega_0$, there exist $\mu > 0$ and $T(\mu, X(t_0))$ such that $\|X(t)\| \leq \mu$ for all $t \geq t_0 + T$.

Chapter 3
Dynamic Load Positioning

With the increased focus on subsea installation tasks to tap deep water fields, 21 companies, including five oil and gas operators and six major contractors, have come together for a joint industry project named Deepwater Installation of Subsea Hardware (DISH) [208]. The objective is to investigate and develop solutions for the technical problems associated with installing subsea facilities such as templates and manifolds in very deep water ($\geq$3000 m). To carry out the installation operation, active, passive, or hybrid heave compensation systems have been developed for offshore cranes or module handling systems for the installation operations. One of the most critical phases of such operations is the water entry of the hardware through the splash zone where it experiences hydrodynamic loads including slamming forces. A smooth transition through the splash zone is desirable to prevent damage to the payload.

Near the seabed, the subsea templates, Christmas trees, and manifolds have to be installed accurately in a specified spatial position and compass heading within tight limits, including rotational, vertical, and lateral measurements. The tolerances for a typical subsea installation are within 2.5 m of design location and within 2.5 degrees of design heading for large templates [2] and are more stringent for the installation of manifolds into the templates. Accurate positioning on the seabed has been identified as one of the problems in subsea installation operations.

An intuitive solution to alleviate the precision placement problem is the addition of thrusters for localized positioning when the payload is near the target site [160, 161]. The positioning control is challenging due to the unpredictable exogenous disturbances such as fluctuating currents and transmission of motions from the surface vessel through the lift cable. The nonlinear dynamics associated with the fluid phenomenon on the payloads, represented by a continuous infinite-dimensional Navier–Stokes equation, need to be reduced to a finite-dimensional approximate model that is normally experimentally determined. Due to the size, costs, and variations in design and construction, full-scale experiments may be not possible for all structures. In most cases, the best way to determine the coefficients required is by means of model testing, where uncertainties attributed to the materials, measurement, and scale effect exist. To overcome the limitations of model-based adaptive

W. He et al., *Dynamics and Control of Mechanical Systems in Offshore Engineering*, Advances in Industrial Control, DOI 10.1007/978-1-4471-5337-5_3,

controllers, we adopt adaptive neural control techniques to compensate functional uncertainties and unknown disturbances from the environment through online tuning of the NN weights [209].

In this chapter, positioning control is investigated for the installation of subsea systems, with thrusters attached, under time-varying irrotational ocean current. The dynamic model and the effects of the current disturbance are presented in Sect. 3.1. In Sect. 3.2, backstepping in combination with adaptive feedback approximation techniques is employed in the design of the control, with the option of high-gain observer for output feedback control. The stability of the design is demonstrated through Lyapunov analysis where the semiglobal uniform boundedness of the closed-loop signals is guaranteed. The proposed adaptive neural control is able to capture the dominant dynamic behaviors without exact information on the hydrodynamic coefficients of the structure and current measurements. Comparative simulations with linear PD, PD with adaptive term, and model-based controls are carried out in Sect. 3.4.

3.1 Problem Formulation and Preliminaries

3.1.1 Dynamic Modeling

We consider the horizontal planar dynamics for surge, sway, and yaw motions of the subsea payload. The geographic reference frame, North-East-Down (n-frame) is chosen, defined relative to the Earth's reference ellipsoid, with the x_n, y_n, and z_n axes directed toward the North, East, and Downward normals to the Earth's surface, respectively, and chosen such that the target installation location is at the origin. The configuration in the n-frame is $\eta = [x_n, y_n, \psi_n]^T$, where x_n and y_n describe the distance from the target location, and ψ_n denotes the rotation about the z_n axis. The body-fixed reference frame (b-frame) is a moving coordinate frame with the origin attached to the center of gravity and axes corresponding to the principle axis of inertia. The frames assigned are represented in Fig. 3.1 with the payload velocity defined in the b-frame as $\nu = [u_b, v_b, r_b]^T$, where u_b and $v_b \in \mathbb{R}$ are the components of the absolute velocity in the x_b and y_b directions, $r_b \in \mathbb{R}$ describes the angular velocity about the z_b axis, and the vectors η and ν are related by the transformation

$$\dot{\eta} = J(\eta)\nu, \tag{3.1}$$

where

$$J(\eta) = \begin{bmatrix} \cos\psi_n & -\sin\psi_n & 0 \\ \sin\psi_n & \cos\psi_n & 0 \\ 0 & 0 & 1 \end{bmatrix}. \tag{3.2}$$

Taking into account the inertial generalized forces, the hydrodynamic effects, the gravity and buoyancy contribution, and the thrusters, the dynamics for low-speed

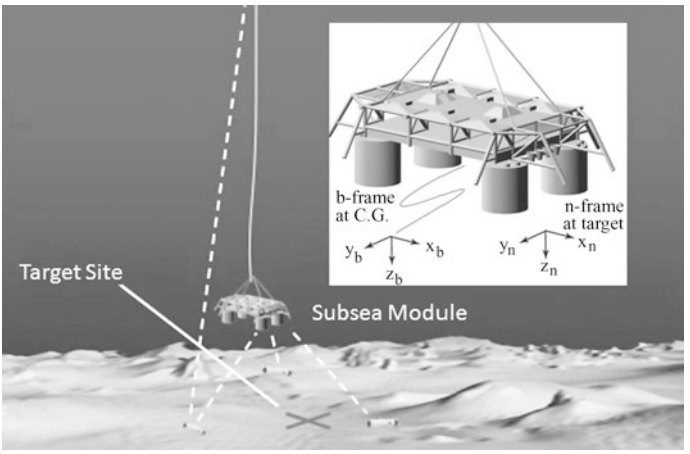

Fig. 3.1 Subsea template with relevant frames

underwater positioning of the structure can be expressed in the canonical form for robotics [210],

$$M\dot{\nu} + C(\nu)\nu + D(\nu)\nu + g(\eta) = \tau, \tag{3.3}$$

where $M \in \mathbb{R}^{3\times3}$ is the system inertia matrix, $C(\nu) \in \mathbb{R}^{3\times3}$ is the Coriolis-centripetal matrix, $D(\nu) \in \mathbb{R}^{3\times3}$ is the damping matrix, $g(\eta) \in \mathbb{R}^3$ is the vector of gravitational and buoyancy forces, and $\tau \in \mathbb{R}^3$ is the control input.

3.1.2 Effects of Time-Varying Current and Disturbances

The effects of ocean current on positioning control of underwater structures are significant. The current is normally assumed to be constant and irrotational for subsea operations planning or control systems design [211]. That is, the current velocity is $v_c = [v_{c,x}, v_{c,y}, 0]^T$ m s^{-1} with $\dot{v}_c = 0$. However, this assumption is not strictly true and can adversely affect the performance of the control.

In this chapter, we extend the investigation to include the effects of a time-varying irrotational current, $v_c(t) = [v_{c,x}(t), v_{c,y}(t), 0]^T$. The magnitude $V_c(t)$ is treated as a first-order Gauss–Markov process,

$$\dot{V}_c(t) + \mu V_c(t) = \omega, \tag{3.4}$$

$$V_{\min} \leq V_c(t) \leq V_{\max}, \tag{3.5}$$

where ω is a Gaussian white noise, $\mu \geq 0$ is a constant, and $V_{\min}$ and $V_{\max}$ are minimum and maximum magnitudes of the current speed, respectively, projected based on hydrographic surveys done on site. In the horizontal plane, the current

velocity can be decomposed to the b-frame via $v_{c,x}(t) = V_c(t)\cos\beta_c$ and $v_{c,y}(t) = V_c(t)\sin\beta_c$, where β_c is the sideslip angle. The disturbance from the ocean current, $\tau_c(\eta, \nu, t)$, is obtained by applying Morrison's equation for cylindrical members or other appropriate empirical formulas depending on the geometry of the module [212]. From (3.3) we obtain

$$M\dot{\nu} + C(\nu)\nu + D(\nu)\nu + g(\eta) = \tau + \tau_d(\eta, \nu, t), \tag{3.6}$$

where $\tau_d(\eta, \nu, t) = \tau_c(\eta, \nu, t) + \tau_l(\eta, \nu, t)$, $\tau_d \in \mathbb{R}^3$ represents the lumped disturbance resulting from the ocean current and unknown disturbance, τ_l, from the lift cable.

Assumption 3.1 For time-dependent functions $\tau_{d,i}(t)$, $i = 1, 2, 3$, there exist constants $\bar{\tau}_{d,i} \in \mathbb{R}^+$ such that $\|\tau_{d,i}(t)\| \leq \bar{\tau}_{d,i}$.

Remark 3.2 The subsea payloads are rigged according to rules and regulations set by the classification societies. The dynamics in the roll and pitch are assumed to be accounted for in the rigging configuration, and the heave motion due to the wave, structure weight, and the upward tension of the cable is to be controlled by a separate heave-compensated system.

Remark 3.3 Assumption 3.1 is reasonable as the effects of the disturbances are largely attributed to the exogenous effects from the environment, which are finite and bounded. The knowledge of exact values for $\bar{\tau}_{d,i}$ are not required. The surface vessel is responsible for global positioning, while the thrusters on the payload are responsible for local positioning and activated close to the target site. To improve the performance further, the effects of the lift cable and coupling with the surface vessel will be investigated in future work.

Assumption 3.4 The reference trajectory for the positioning of the payload, η_r, is a bounded C^2 function, sufficiently smooth to avoid sudden jumps of tracking error.

3.2 Adaptive Neural Control Design

The control objective is to position and orientate the payload for accurate placement via attached thrusters. Tracking control is necessary when the installation is carried out in proximity to other critical equipment on the seabed via a reference trajectory $\eta_r(t) = [x_{nr}(t), y_{nr}(t), \psi_{nr}(t)]^T$. We first consider the case where the full-state information ν and η are available. Dependency of the signals, where obvious, will be omitted.

3.3 Full-State Feedback

We define the generalized tracking error as $z_1(t) = \eta(t) - \eta_r(t)$ and obtain $\dot{z}_1 = J(\eta)\nu - \dot{\eta}_r$. We introduce a virtual control α_1 and define the second error variable as $z_2(t) = \nu(t) - \alpha_1(t)$. From (3.2) we have $J(\eta)J^T(\eta) = I$ and choose

$$\alpha_1(\eta, \dot{\eta}_r, z_2) = J^T(\eta)(\dot{\eta}_r - K_1 z_1), \tag{3.7}$$

where the gain matrix $K_1 = K_1^T > 0$, and obtain

$$\dot{z}_1 = J(\eta)(z_2 + \alpha_1) - \dot{\eta}_r. \tag{3.8}$$

Choosing a Lyapunov function candidate with quadratic z_1,

$$V_1 = \frac{1}{2} z_1^T z_1, \tag{3.9}$$

and taking its time derivative along (3.8), we have

$$\dot{V}_1 = -z_1^T K_1 z_1 + z_1^T J(\eta) z_2. \tag{3.10}$$

Differentiating z_2 with respect to time, we have

$$\dot{z}_2 = M^{-1}\big[h(\nu, \eta) + \tau + \tau_d(\nu, \eta, t)\big] - \dot{\alpha_1}, \tag{3.11}$$

where

$$h(\nu, \eta) = -C(\nu)\nu - D(\nu)\nu - g(\eta), \tag{3.12}$$

$$\dot{\alpha_1} = \frac{\partial \alpha_1}{\partial \eta}\dot{\eta} + \frac{\partial \alpha_1}{\partial \dot{\eta}_r}\ddot{\eta}_r + \frac{\partial \alpha_1}{\partial z_1}\dot{z}_1. \tag{3.13}$$

By Lemma 2.8 and Assumption 3.1, we are able to separate the disturbance term, $\tau_{d,i}(\eta, \nu, t)$, into bounding functions $a_i(\eta, \nu)$ and $b_i(t)$,

$$\big|\tau_{d,i}(\eta, \nu, t)\big| \le a_i(\eta, \nu) + b_i(t), \quad i = 1, 2, 3, \tag{3.14}$$

and there exist some constants $\bar{b}_i$ such that the time-dependent function $|b_i(t)| \le \bar{b}_i$ for all $t \ge t_0$, where $t_0 \ge 0$ is the initial time. Next, consider the Lyapunov function candidate and its time derivative

$$V_2^* = V_1 + \frac{1}{2} z_2^T M z_2, \tag{3.15}$$

$$\begin{aligned}\dot{V}_2^* = &-z_1^T K_1 z_1 + z_1^T J(\eta) z_2 \\ &+ z_2^T\big(h(\nu, \eta) + \tau - M\dot{\alpha_1}\big) + z_2^T \tau_d(\eta, \nu, t).\end{aligned} \tag{3.16}$$

From (3.14) we have

$$\dot{V}_2^* \leq -z_1^T K_1 z_1 + z_1^T J(\eta) z_2 + z_2^T \big(h(\nu,\eta) - M\dot{\alpha_1} + \tau\big) + \sum_{i=1}^{3} |z_{2,i}| \big(a_i(\eta,\nu) + b_i(t)\big), \tag{3.17}$$

where $z_{2,i} \in \mathbb{R}$ for $i = 1, 2, 3$ are the elements of z_2. Consider the model-based control law

$$\tau_{\text{mb}} = -J^T(\eta) z_1 - K_2 z_2 - h(\nu,\eta) + M\dot{\alpha_1} - K\,\text{sgn}(z_2)\big(a_i(\eta,\nu) + \bar{b_i}\big), \tag{3.18}$$

where $\text{sgn}(z_2) = \text{diag}[\text{sgn}(z_{2,i})]$ is a robust sliding term for $i = 1, 2, 3$, $\text{sgn}(\cdot)$ is the signum function, and $K_2 = K_2^T > 0$ and $K = \text{diag}(k_{ii}) \in \mathbb{R}^{3\times 3}$, $k_{ii} > 1$, $i = 1, 2, 3$, are gain matrices. By substituting (3.18) into (3.17) we can rewrite (3.17) as $\dot{V}_2^* \leq -z_1^T K_1 z_1 - z_2^T K_2 z_2$, which is negative semidefinite. Since uncertainties exist in the parameters M, $C(\nu)$, $D(\nu)$, $g(\eta)$, $a_i(\eta,\nu)$, and $b(t)$, or they are unknown, the model-based control law (3.18) may not be realizable. To overcome this challenge, we use NNs to approximate the uncertainties and propose the following control and adaptation laws:

$$\tau = -J^T(\eta) z_1 - K_2 z_2 + \hat{W}^T S(Z), \tag{3.19}$$

$$\dot{\hat{W}}_i = -\Gamma_i \big(S_i(Z) z_{2i} + \sigma_i \hat{W}_i\big), \tag{3.20}$$

where $\hat{W} = \text{blockdiag}[\hat{W}_1^T, \hat{W}_2^T, \hat{W}_3^T]$ are the NN weights, $S(Z) = [S_1^T(Z), S_2^T(Z), S_3^T(Z)]^T$ are the basis functions, Γ_i are constant gain matrices, and $\sigma_i > 0$, $i = i, 2, 3$, are sigma modification constants that impose growth conditions on the weight vectors to improve the stability of $\hat{W}$ when the system is subjected to bounded disturbances [213]. The NN $\hat{W}^T S(Z)$ approximates $W^{*T} S(Z)$ defined by

$$W^{*T} S(Z) = -h(\eta,\nu) + M\dot{\alpha_1} - K\,\text{sgn}(z_2)\big(a_i(\eta,\nu) + \bar{b_i}\big) - \epsilon(Z), \tag{3.21}$$

where $Z = [\eta^T, \nu^T, \alpha_1^T, \dot{\alpha_1}^T]^T$ are the input variables to the adaptive NN, and $\epsilon(Z) \in \mathbb{R}^3$ is the approximation error.

Remark 3.5 In this chapter, we address a more challenging problem by treating the values of M, $C(\nu)$, $D(\nu)$, $g(\eta)$, $a_i(\eta,\nu)$, and $b(t)$ as completely unknown. If individual terms are known exactly, the terms can be excluded from the approximation in Eq. (3.21) and incorporated explicitly as part of the adaptive neural control law (3.19), similar to the model-based control (3.18).

Theorem 3.6 *Consider the dynamic model* (3.6)*, with control law* (3.19) *and adaptation law* (3.20)*. Given that the full-state information is available, for each compact*

set Ω_0 where $(\eta(0), \nu(0), \hat{W}_1(0), \hat{W}_2(0), \hat{W}_3(0)) \in \Omega_0$, i.e., the initial conditions are bounded, the trajectories of the closed-loop system are semiglobally uniformly bounded. The closed-loop error signals z_1, z_2, and $\tilde{W}$ will remain within the compact sets Ω_{z_1}, Ω_{z_2}, and Ω_W, respectively, defined by

$$\Omega_{z_1} := \left\{ z_1 \in R^3 \;\middle|\; \|z_1\| \leq \sqrt{D} \right\}, \tag{3.22}$$

$$\Omega_{z_2} := \left\{ z_2 \in R^3 \;\middle|\; \|z_2\| \leq \sqrt{\frac{D}{\lambda_{\min}(M)}} \right\}, \tag{3.23}$$

$$\Omega_W := \left\{ \tilde{W} \in R^{l\times 3} \;\middle|\; \|\tilde{W}\| \leq \sqrt{\frac{D}{\lambda_{\min}(\Gamma^{-1})}} \right\}, \tag{3.24}$$

where $D = 2(V_2(0) + C/\rho)$ with ρ and C defined in (3.31) and (3.32), respectively.

Proof Consider the augmented Lyapunov function candidate

$$V_2 = V_1 + \frac{1}{2} z_2^T M z_2 + \frac{1}{2} \sum_{i=1}^{3} \tilde{W}_i^T \Gamma_i^{-1} \tilde{W}_i, \tag{3.25}$$

where $\tilde{W}_i = \hat{W}_i - W_i^*$, and $\tilde{W}_i$, $\hat{W}_i$, W_i^* are the NN weight error, estimate, and actual value, respectively. Differentiating (3.25), we obtain

$$\begin{aligned} \dot{V}_2 \leq & -z_1^T K_1 z_1 + z_1^T J(\eta) z_2 + z_2^T \left[h(\nu, \eta) - M\dot{\alpha}_1 + \tau \right] \\ & + \sum_{i=1}^{3} |z_{2,i}| \left(a_i(\eta, \nu) + b_i(t) \right) + \sum_{i=1}^{3} \tilde{W}_i^T \Gamma_i^{-1} \dot{\hat{W}}_i. \end{aligned} \tag{3.26}$$

Using the approximation (3.21), we obtain

$$\begin{aligned} \dot{V}_2 \leq & -z_1^T K_1 z_1 + z_1^T J(\eta) z_2 \\ & + z_2^T \left[-W^{*T} S(Z) - \epsilon(Z) + \tau \right] + \sum_{i=1}^{3} \tilde{W}_i^T \Gamma_i^{-1} \dot{\hat{W}}_i. \end{aligned} \tag{3.27}$$

Substituting the control (3.19) and adaptation law (3.19) into (3.27) yields

$$\dot{V}_2 \leq -z_1^T K_1 z_1 - z_2^T K_2 z_2 - \sum_{i=1}^{3} \left[\sigma_i \tilde{W}_i^T \hat{W}_i \right] + \frac{1}{2} \|\bar{\epsilon}(Z)\| + \frac{1}{2} z_2^T z_2, \tag{3.28}$$

From the property

$$-\sigma_i \tilde{W}_i^T \hat{W}_i \leq -\frac{\sigma_i}{2} \|\tilde{W}_i\|^2 + \frac{\sigma_i}{2} \|W_i^*\|^2 \tag{3.29}$$

we obtain $\dot{V}_2$ and the bounds ρ and C as

$$\dot{V}_2 \leq -\rho V_2 + C, \tag{3.30}$$

$$\rho = \min\left(2\lambda_{\min}(K_1), \frac{2\lambda_{\min}(K_2 - \frac{1}{2}I_{3\times 3})}{\lambda_{\max}(M)}, \min_{i=1,2,3}\left(\frac{\sigma_i}{\lambda_{\max}(\Gamma_i^{-1})}\right)\right), \tag{3.31}$$

$$C = \sum_{i=1}^{3} \frac{\sigma_i}{2}\left\|W_i^*\right\|^2 + \frac{1}{2}\|\bar{\epsilon}\|^2, \tag{3.32}$$

where $\lambda_{\min}(A)$ and $\lambda_{\max}(A)$ denote the minimum and maximum real eigenvalues of a matrix A, respectively. To ensure $\rho > 0$, the control gains K_1 and K_2 are chosen to satisfy the following conditions:

$$\lambda_{\min}(K_1) > 0, \qquad \lambda_{\min}\left(K_2 - \frac{1}{2}I_{3\times 3}\right) > 0. \tag{3.33}$$

From (3.30) and Lemma 2.7 it is straightforward to show that the signals $z_1, z_2, \tilde{W}_1$, $\tilde{W}_2$, and $\tilde{W}_3$ are semiglobally uniformly bounded. From the boundedness of η_r in Assumption 3.1 we know that η is bounded. Since $\dot{\eta}_r$ is also bounded, it follows that α_1 is bounded, and, in turn, ν is also bounded. With W_i^* as slow time varying, we know that $\hat{W}_i$ is also bounded for $i = 1, 2, 3$. For completeness, the details of the proof, similar to [203], are provided here. Multiplying (3.30) by $e^{\rho t}$ yields

$$\frac{d}{dt}\left(V_2 e^{\rho t}\right) \leq C e^{\rho t}. \tag{3.34}$$

Integrating the above inequality, we obtain

$$V_2 \leq \left(V_2(0) - \frac{C}{\rho}\right)e^{-\rho t} + \frac{C}{\rho} \leq V_2(0) + \frac{C}{\rho}. \tag{3.35}$$

Substituting (3.25) into (3.35), we have

$$\frac{1}{2}\|z_1\|^2 \leq V_2(0) + \frac{C}{\rho}. \tag{3.36}$$

Hence, z_1 converges to the compact set Ω_{zs}. The bounds of z_2 and $\tilde{W}_i$ can be similarly shown, and this concludes the proof. □

Remark 3.7 The stability result proposed is semiglobal in the sense that if the number of NN nodes l is chosen large enough such that the approximation holds on Ω_z, then the closed-loop stability can be guaranteed for bounded initial states and NN weights. The exact sizes of the compact sets Ω_{z1}, Ω_{z2}, and Ω_W are not available as they depend on the unknown parameters W^* and ϵ.

Remark 3.8 The control design and stability analysis in this chapter assume that the thrusters are able to provide the force and torque as required. The effects of thruster dynamics such as thruster saturation are explored in [214–216]. It is found that the thruster saturation can cause a severe degradation in the tracking performance. This problem can be alleviated through an appropriate choice of trajectory if the task and disturbances are within the operational range of the propulsion system.

3.3.1 Output Feedback with the High-Gain Observer

The proposed control (3.19) requires full-state feedback $\eta(t)$ and $\nu(t)$ to be implemented. In the absence of velocity sensors such as the Doppler velocity log, we introduce a high-gain observer design to estimate $\nu(t)$ through the certainty equivalence property and separation principle.

By Lemma 2.10, $\frac{\pi_{k+1}}{\varepsilon^k}$ converges asymptotically to $\eta^{(k)}$, the kth-order derivative of η, i.e., ξ_k converges to zero with a small time constant (due to the high-gain $1/\varepsilon$), provided that η and its k derivatives are bounded. Hence, π_{k+1}/ε^k is suitable as an observer to estimate the output derivatives up to the nth order. The observer for system (3.6) is designed with $n = 2$, and the estimate of the unmeasurable state vector z_2 can be defined as

$$\hat{z}_2 = J^T(\eta)(\pi_2/\varepsilon) - \alpha_1. \tag{3.37}$$

From the full-state feedback case, we modify the control law (3.19) and adaptation law (3.20) to obtain the control and adaptation laws for output feedback control as

$$\tau = -J^T(\eta)z_1 - K_2\hat{z}_2 + \hat{W}^T S(\hat{Z}), \tag{3.38}$$

$$\dot{\hat{W}}_i = -\Gamma_i\big(S_i(\hat{Z}_1)\hat{z}_{2,i} + \sigma_i\hat{W}_i\big). \tag{3.39}$$

The time derivative of the Lyapunov function candidate V_2 in (3.25) along the closed-loop trajectory with (3.38) and (3.39) yields

$$\begin{aligned}\dot{V}_2 \le {} & -z_1^T K_1 z_1 - z_2^T\left(K_2 - \frac{1}{2}I_{3\times 3}\right)z_2 - z_2^T K_2\tilde{z}_2 \\ & + \sum_{i=1}^{3} z_{2,i}\big[\hat{W}_i^T S_i(\hat{Z}_i) - W_i^{*T} S_i(Z_i)\big] \\ & - \sum_{i=1}^{3}\big[\tilde{W}_i^T S_i(\hat{Z}_i)\hat{z}_{2,i} + \sigma_i\tilde{W}_i^T\hat{W}_i\big] + \frac{1}{2}\|\bar{\epsilon}\|^2.\end{aligned} \tag{3.40}$$

From Lemma 2.9, using the properties

$$\sigma_i\tilde{W}_i^T\hat{W}_i \le \frac{\sigma_i}{2}\big(\|W_i^*\|^2 - \|\tilde{W}_i\|^2\big), \tag{3.41}$$

$$\left\| S_i(\hat{Z}_i) \right\|^2 \leq l_i, \tag{3.42}$$

and $\tilde{z}_2 = \hat{z}_2 - z_2 = J^T(\eta)\xi_2$ and denoting $\Lambda = \text{diag}[2l_i/\sigma_i]$ and

$$V_{\text{obs}} = (1/2)\xi_2^T \xi_2, \tag{3.43}$$

we obtain

$$\dot{V}_2 \leq -z_1 K_1 z_1 - z_2^T \left(K_2 - \frac{3}{2} I \right) z_2 + \frac{1}{2}\|\bar{\epsilon}\|^2 - \sum_{i=1}^{3} \frac{\sigma_i}{4} \|\tilde{W}_i\|^2$$

$$+ \lambda_{\max}\left(K_2^T K_2 + \Lambda\right) V_{\text{obs}} + \frac{1}{2} \sum_{i=1}^{3} \left(\epsilon^2 \|S_{ti}\|^2 + \sigma_i\right) \left\| W_i^* \right\|^2, \tag{3.44}$$

which can be expressed in the form of (3.30):

$$\dot{V}_2 \leq -\rho V_2 + C, \tag{3.45}$$

$$\rho = \min\left(2\lambda_{\min}(K_1), \frac{2\lambda_{\min}(K_2 - \frac{3}{2} I_{3\times 3})}{\lambda_{\max}(M)}, \min_{i=1,2,3}\left(\frac{\frac{\sigma_i}{4}\|\tilde{W}_i\|^2}{\lambda_{\max}(\Gamma_i^{-1})} \right) \right), \tag{3.46}$$

$$C = \frac{1}{2} \sum_{i=1}^{3} \left(\epsilon^2 \|S_{ti}\|^2 + \sigma_i\right) \left\| W_i^* \right\|^2 + \lambda_{\max}\left(K_2^T K_2 + \Lambda\right) V_{\text{obs}}$$

$$+ \frac{1}{2}\|\bar{\epsilon}\|^2, \tag{3.47}$$

with the bound $V_{\text{obs}} \leq (1/2)\varepsilon^2(h_1^2 + h_2^2)$. To ensure that $\rho > 0$, the control gains K_1 and K_2 are chosen to satisfy the following conditions:

$$\lambda_{\min}(K_1) > 0, \qquad \lambda_{\min}\left(K_2 - \frac{3}{2} I_{3\times 3} \right) > 0. \tag{3.48}$$

Theorem 3.9 *Consider the dynamic model* (3.6) *with output feedback control* (3.38), *adaptation law* (3.39), *and high-gain observer* (2.25). *For each compact set* Ω_0 *where* $(\eta(0), \nu(0), \hat{W}_1(0), \hat{W}_2(0), \hat{W}_3(0)) \in \Omega_0$, *i.e., if the initial conditions are bounded, the trajectories of the closed-loop system are semiglobally uniformly bounded. The tracking error* z_1 *converges to the compact set*

$$\Omega_{zs} = \left\{ z_1 \in R^3 \;\middle|\; \|z_1\| \leq \sqrt{D_s} \right\}, \tag{3.49}$$

where $D_s = 2(V_2(0) + C/\rho)$ *with* ρ *and* C *defined in* (3.46) *and* (3.47), *respectively.*

Proof The stability proof of Theorem 3.9 along with (3.45), (3.46), and (3.47) follows Theorem 3.6 and is omitted for conciseness. □

Remark 3.10 In this chapter, we assume that the position measurements are perfect and propose a rigorous theoretical treatment of the output feedback problem using high-gain observers corresponding to a non-model-based approach. If the output measurements are contaminated with zero-mean Gaussian white noise within tolerance, careful implementation is necessary by designing ϵ to be sufficiently small. Following [66], a saturation function can be used to overcome the peaking phenomenon of the high-gain observer.

Remark 3.11 The tracking error has been shown to converge and remain within a small neighborhood of the origin. If the residual error is desired to be lower, it can be reduced so that C/ρ in both Theorems 3.6 and 3.9 decreases. The reduction is achieved by increasing k_1 and k_2, the approximation accuracy of the NN, and the high-gain $1/\varepsilon$ of the state observer [205].

3.4 Numerical Simulations

In this section, comparative studies are carried out via numerical methods on the proposed control and three different control methodologies. A wet Christmas tree is modeled as a cylinder with dimensions $r = 1.0$ m, $L = 5.2$ m, and $m = 32240$ kg representing the radius, length, and dry mass, respectively. The parameters in the dynamic equation (6) are $M = M_{RB} + M_A$, $M_{RB} = \text{diag}[32240, 32240, 16120]$, $M_A = \text{diag}[16728, 16728, 0]$, $C(\nu) = [0, 0, c_{13}; 0, 0, c_{23}; -c_{13}, -c_{23}, 0]$, $c_{13} = (M_{A,22} - M_{RB,22})\nu_2$, $c_{23} = -(M_{A,11} - M_{RB,11})\nu_1$, and $D(\nu) = 0.5\rho_w C_D \pi r^2 \nu$, where M_{RB} is the rigid body inertia, M_A is the added mass, C_D is the drag coefficient, and $\rho_w = 1024\ \text{kg m}^3$ is the density of seawater. A cylindrical model is chosen for the analysis of the controls for its well-studied hydrodynamic properties and characteristics in the literature [197]. The simulation step size is 0.001 s with the update rate for controls and observer set as 10 Hz. The sampling period of 0.1 s is used to investigate the effects of long sampling rate. A fourth-order Runge–Kutta–Merson program with adaptive step size is used to numerically solve the equation of motions [64].

The control objective for the payload is to track a reference trajectory from an initial state in the n-frame to the target site designated as the origin for installation. The reference trajectory $\eta_r(t) = [x_{nr}(t), y_{nr}(t), \psi_{nr}(t)]^T$ is generated via a Hermite polynomial of the third degree with the general expression

$$\eta_r(t, t_r) = \eta_0 + \left(-2.0\frac{t^3}{t_r^3} + 3.0\frac{t^2}{t_r^2}\right)(\eta_f - \eta_0), \tag{3.50}$$

where $\eta_0 = [5.0, 2.0, 1.047]^T$ and $\eta_f = [0, 0, 0]^T$ are the payload initial and final positions, respectively, and $t_r = 150$ s represents the time at which the reference trajectory reaches the desired final position. The reference trajectory shown in Fig. 3.2 satisfies Assumption 3.1 and is continuous for all t, with bounded η_r, $\dot{\eta}_r$, and $\ddot{\eta}_r$.

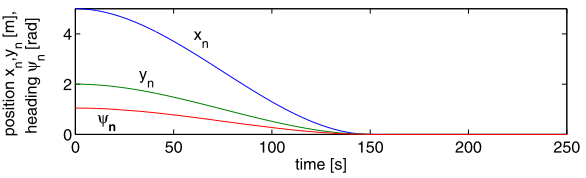

Fig. 3.2 Reference trajectory for position x_n, y_n and orientation ψ_n

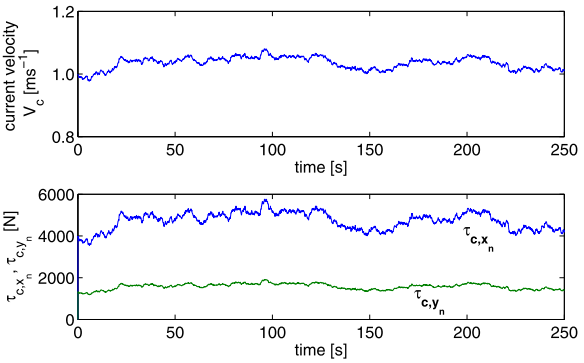

Fig. 3.3 *Top*: irrotational current; *bottom*: disturbance due to current in x_n, y_n direction

From Sect. 3.1.2, the time varying current profile shown in Fig. 3.3 is generated using Eq. (3.4) with bounds $V_{\max} = 1.2\ \mathrm{m\,s^{-1}}$ and $V_{\min} = 0.8\ \mathrm{m\,s^{-1}}$, and $\mu = 0$ is chosen to generate a more random ocean current. The current forces and the motion of a cylinder in fluid are derived from Morison's equations [212],

$$\bar{\tau}_{c,i} = C_D \rho_w \frac{D_c}{2} |v_{c,i}| v_{c,i} + C_m \rho_w \pi \frac{D_c^2}{4} \dot{v}_{c,i}, \quad i = 1, 2, 3, \tag{3.51}$$

where $C_D = 1.0$, $C_m = 1.0$ is the added mass coefficient, D_c is the diameter of the cylindrical member, and $v_{c,i}$ and $\dot{v}_{c,i}$ are the velocity and acceleration of the current in each direction, respectively. The effect of the current is a nonlinear force parallel to the current itself due to the coupling effects of the hydrodynamic terms. However, a reasonable hypothesis is made that the main contribution of the current to the vehicle motion is observed along the current direction [217]. The irrotational current is simulated to be 60° from the North-East, which results in a constant $\beta_c = 30°$ due to the symmetry of the cylindrical payload. Figure 3.3 shows the disturbances due to the current in the x, y direction.

3.4.1 Full-State Feedback

Four different cases are considered. In the first case, we examine the PD (proportional derivative) control. Second, we include an adaptive mechanism to the PD control for current compensation. Third, we evaluate the model-based control developed in (3.18), assuming that the parameters of the subsea structure are completely known. In the fourth case, we investigate the proposed adaptive neural control.

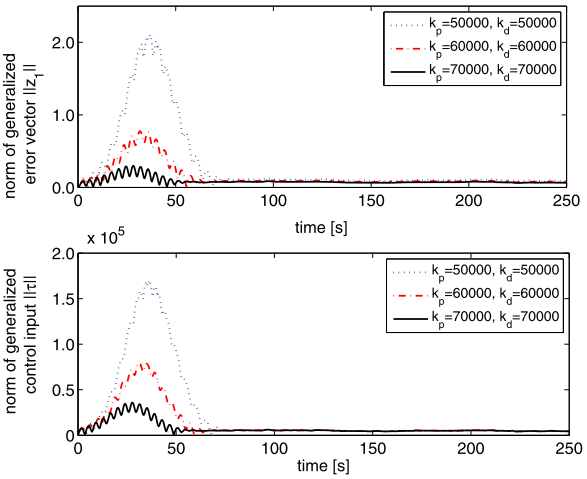

Fig. 3.4 *Top*: the norm of generalized error $\|z_1\|$; *bottom*: the norm of generalized control input $\|\tau\|$ for PD control

Case 1: PD Control. The PD control represents one of the most widely used controls and thus provides a baseline for the comparison of the performance of other controls. In this case, we consider a PD control of the form

$$\tau = -K_P z_1 - K_D \dot{z}_1, \tag{3.52}$$

where K_P and K_D are the proportionate and derivative gain matrices, respectively. The closed-loop analysis of the PD control law applied to underwater dynamics is similar to [216, 218] and not included here. An application of Lasalle's invariance theorem [219] shows that the PD control will perform set point regulation but not trajectory tracking [220]. While the PD control does not perform trajectory tracking, it is included as the control objective is to dynamically position the load at a fixed spatial position. Techniques such as linear quadratic regulator can be used to tune the PD control for better performance but requires exact knowledge of the load model parameters. The following sets of control gains have been implemented in the simulations $\{K_P = 5 \times 10^5 I_{3\times3},\ K_D = 5 \times 10^5 I_{3\times3}\}$, $\{K_P = 6 \times 10^5 I_{3\times3},\ K_D = 6 \times 10^5 I_{3\times3}\}$, and $\{K_P = 7 \times 10^5 I_{3\times3},\ K_D = 7 \times 10^5 I_{3\times3}\}$. Figure 3.4 shows the norm of tracking error and the control input. The control action produces large overshoots in the transient phase, and the norm of the tracking error subsequently reduces to $\|z_1\| \approx 0.1$ during steady state. As the gains of K_P and K_D increase, the tracking errors are reduced. Conversely, the tracking errors increase significantly when the gains are reduced. In practice, large control gains are not recommended as they reduce robustness and cause large overshoots due to noisy measurements.

Case 2: PD Control with Adaptive Mechanism. The control adapted from [217] for an underwater vehicle combines a PD action with an adaptive compensation to provide asymptotic trajectory tracking. The control is given as

$$\tau = K_D s + K\tilde{\eta} + \Phi_T \hat{\lambda}, \tag{3.53}$$

$$\dot{\hat{\lambda}} = K_\lambda^{-1} \Phi_T^T s, \tag{3.54}$$

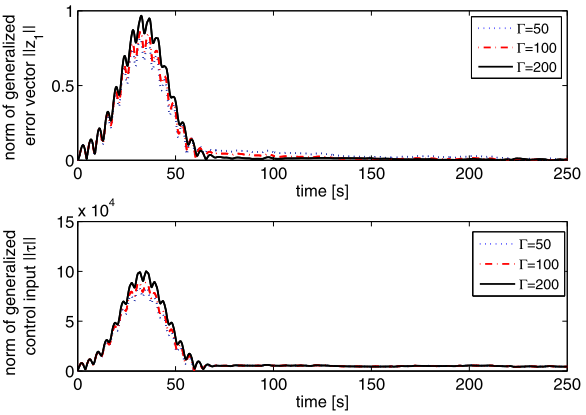

Fig. 3.5 *Top*: the norm of generalized error $\|z_1\|$; *bottom*: the norm of generalized control input $\|\tau\|$ for PD control with adaptive mechanism

where $s = \tilde{\nu} + \Lambda_p \tilde{\eta}$, $\tilde{\nu} = \nu_r - \nu$, $\tilde{\eta} = \eta_r - \eta$, $\nu_r = J^T(\eta)\eta_r$, the matrices K_D, Λ_p, and K are positive gain matrices, $K_\lambda^{-1} = \Gamma > 0$ is the adaptive gain matrix, $\hat{\lambda}$ is the adaptation weight, and $\Phi_T^T s = J^T(\eta)s$ is a regressor. The closed-loop stability analysis can be found in [217] and is not repeated here. The matrices are chosen as $K_D = 6 \times 10^5 I_{3\times3}$, $K = 6 \times 10^5 I_{3\times3}$, and $\Lambda_p = I_{3\times3}$, and three cases with $\Gamma = 50 I_{3\times3}$, $\Gamma = 100 I_{3\times3}$, and $\Gamma = 200 I_{3\times3}$ are simulated. The norm of the tracking error and control input are shown in Fig. 3.5. It is observed that the transient response of the PD control with adaptive mechanism is large due to the inability of the adaptive mechanism to capture the effects of the current. However, when the parameters have converged, the norm of error produced during steady state is lower than that of the PD-type control. The control effort that corroborates the overshoot in the transient region is also observed.

Case 3: Model-Based Backstepping Control. The model-based backstepping control in (3.18) without the robust signum term is investigated here as follows:

$$\tau_{\text{mb}} = -J^T(\eta)z_1 - K_2 z_2 - h(\nu, \eta) + M\dot{\alpha}(\eta_r, \dot{\eta}_r, \ddot{\eta}_r, z_1, z_2), \tag{3.55}$$

assuming that the parameters of the subsea structure are completely known. The effects of the control gains are examined by varying the control gain matrix K_2. Simulations are carried out for $K_1 = k_1 I_{3\times3}$ and $K_2 = k_2 I_{3\times3}$, with $k_1 = 5$ and $k_2 =$ 10000, 20000, and 30000. The tracking errors and control input signals are shown in Fig. 3.6. The norm of the tracking error for the model-based control without the robust term is satisfactory with $\|z_1\| < 0.1$. To achieve low tracking errors, model-based control requires exact knowledge of the system dynamics and parameters. This is difficult to achieve in practice as the geometry of the structure makes the identification of the hydrodynamic effects complex. Inaccurate parameter values can degrade the performance significantly. It is noted that the gains are significantly lower than those of the PD and PD plus earlier adaptive mechanism controls, which is advantageous for robustness toward noisy measurements.

Case 4: Proposed Adaptive Neural Control. Linearly parameterized approximators are used in the control law and update law in (3.7), (3.19), and (3.20).

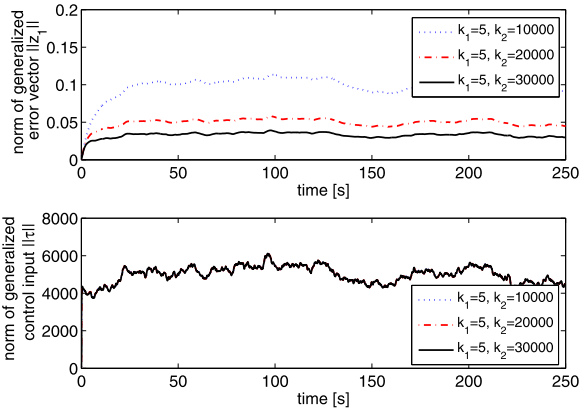

Fig. 3.6 *Top*: the norm of generalized error $\|z_1\|$; *bottom*: the norm of control input $\|\tau\|$ for Model-based control

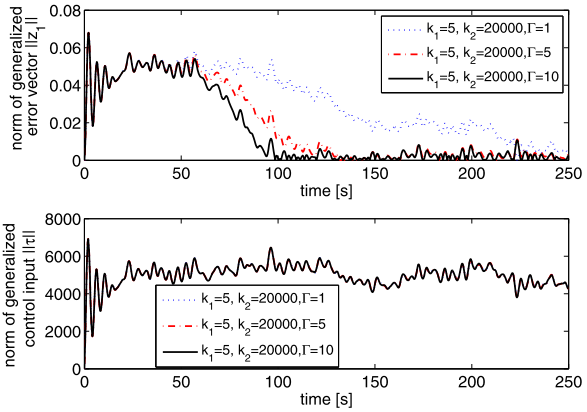

Fig. 3.7 *Top*: the norm of generalized error $\|z_1\|$; *bottom*: the norm of generalized control input $\|\tau\|$ for the proposed control with varying Γ

$\hat{W} = \text{diag}[\hat{W}_1^T, \hat{W}_2^T, \hat{W}_3^T]$ are the approximation weights, $S(Z) = [S_1^T(Z), S_2^T(Z), S_3^T(Z)]^T$ are Gaussian RBF (2.9), and $Z = [\eta^T, \nu^T, \alpha_1^T, \dot{\alpha}_1^T]$ are the input variables. A total of $l = 512$ nodes are employed for each $S_j^T(Z)$ with centers chosen as combinations of $\mu_{k,1} = \mu_{k,2} = \{1.0, -1.0\}$, $\mu_{k,3} = \mu_{k,6} = \mu_{k,9} = \mu_{k,12} = 0$, and $\mu_{k,4} = \mu_{k,5} = \mu_{k,7} = \mu_{k,8} = \mu_{k,10} = \mu_{k,11} = \{0.1, -0.1\}$. The effects of varying the control gains Γ are investigated with $\Gamma = 1.0I_{3\times3}$, $\Gamma = 5.0I_{3\times3}$, and $\Gamma = 10.0I_{3\times3}$, $\sigma_i = 1 \times 10^{-5}$, $\eta_k^2 = 5.0$, $i = 1, 2, 3$, $K_1 = 5I_{3\times3}$, and $K_2 = 20000I_{3\times3}$, which satisfies the conditions in (3.33). From Fig. 3.7 it is observed that tracking performance of the control is satisfactory with the norm of tacking error $\|z_1\| < 0.1$ and low transient overshoots for all three adaptation gains. The tracking error reduces the adaptation gain corresponding to an increase in Γ. Note that care must be taken in the design as a large Γ may result in numerical instability of the system. Figure 3.8 shows the boundedness of the adaptation weights where a larger Γ is shown to improve the convergence rate. Similarly to model-based control, the gains are lower than the PD-type controls, which improves the robustness of the control.

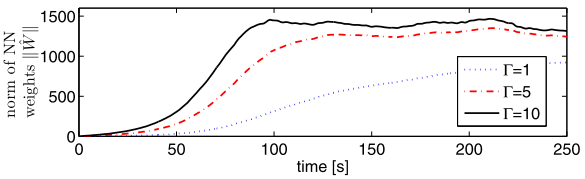

Fig. 3.8 The norm of NN weights $\|\hat{W}\|$ for the proposed control with varying Γ

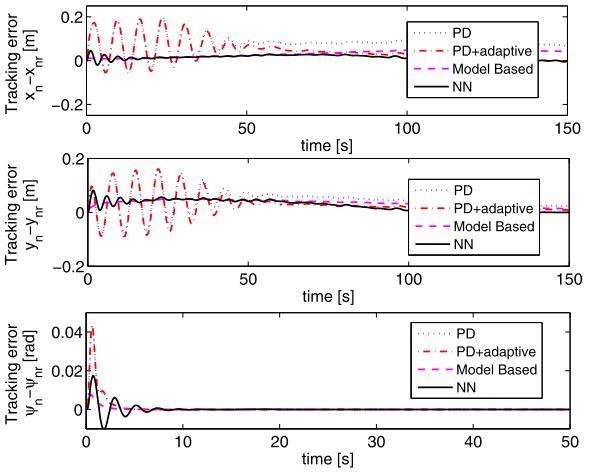

Fig. 3.9 *Top*: tracking error $x_n - x_{nr}$; *center*: tracking error $y_n - y_{nr}$; and *bottom*: tracking error $\psi_n - \psi_{nr}$ for different controls using output feedback

3.4.2 Output Feedback

Using the certainty equivalence approach, the high-gain observer (2.26) has been designed to obtain the velocity estimates $\hat{\nu} = J^T(\eta)(\pi_2/\varepsilon)$ with $n = 2$, $\gamma_1 = 2.0$, and $\varepsilon = 0.1$. The four control types in Sect. 3.4.1 are simulated with the velocity estimate $\hat{\nu}$ and parameters as follows: (i) PD control: $\{K_P = 6 \times 10^5 I_{3\times3},\ K_D = 6 \times 10^5 I_{3\times3}\}$, (ii) PD plus adaptive: $\{\Gamma = 100 I_{3\times3}\}$, (iii) Model-based: $\{K_1 = 5I_{3\times3},\ K_2 = 20000 I_{3\times3}\}$, and (iv) Adaptive Neural: $\{\Gamma = 5I_{3\times3},\ \hat{Z} = [\eta^T, \hat{\nu}^T, \alpha_1^T, \dot{\alpha}_1^T]\}$.

The tracking errors for different controls are shown in Fig. 3.9, while the norm of tracking errors and control inputs are shown in Fig. 3.10. The proposed adaptive neural and model-based controls formulated through backstepping of the system dynamics produce better transient and steady-state response as compared to the PD and PD with adaptive control. The proposed adaptive neural control produces the lowest norm of error. This can be credited to the NN, which is able to capture the system dynamics. From Fig. 3.10 we can see that the low tracking errors of the proposed control are not the results of a larger control effort but are attributed to a proper control action. Due to the large structural mass, the PD-type controls require large control gains for accurate positioning. This is not recommended in practice due to measurement noise, which can result in large overshoots. Figure 3.11 shows the observer error for output feedback control under the adaptive neural control. The

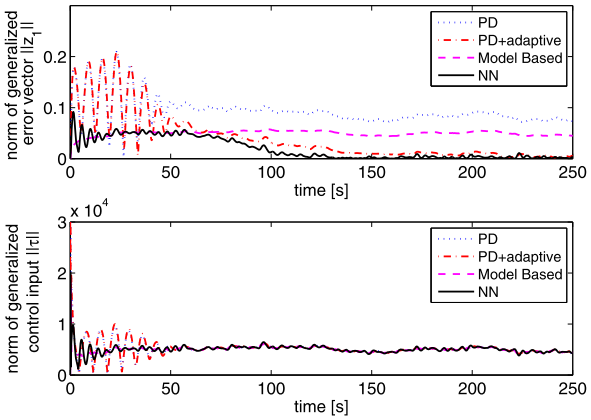

Fig. 3.10 *Top*: the norm of generalized error $\|z_1\|$; *bottom*: the norm of generalized control input $\|\tau\|$ for different controls using output feedback

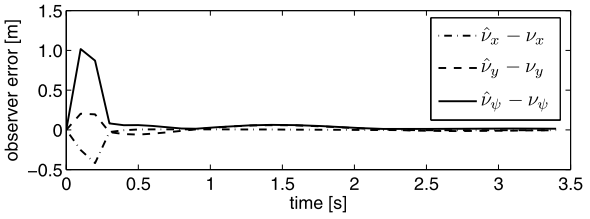

Fig. 3.11 Observer error for output feedback control using the high-gain observer with NN control

convergence of the high-gain observer estimates can be seen as the estimation errors peak around 0.3 s and thereafter converge to a small neighborhood of zero.

3.5 Conclusion

In this chapter, stable adaptive neural-based positioning control has been designed for installation of subsea structure with attached thrusters in the presence of time-varying environmental disturbances and parametric uncertainties. Full-state feedback and output feedback cases have been considered. It has been shown that the closed-loop signals under the proposed control are semiglobally uniformly bounded and converge to a compact set, which can be made arbitrarily small through appropriate choice of design parameters. Simulation results have demonstrated that the adaptive neural control is robust and effective in reducing the tracking error for the subsea installation operation.

Chapter 4
Installation System with Constraints

In the previous chapter, we proposed a tracking control for the payload using an adaptive neural technique to capture the dominant dynamic behaviors through online tuning of the NN weights. This avoided the need for exact information on the hydrodynamic coefficients of the structure and current measurements. With the trend toward installations in deeper waters, the longer cable increases the natural period of the cable and payload system, which in turn increase the effects of pendulum-like oscillations. Time-varying distributed currents may lead to large horizontal offsets between the surface ship and the target installation site. An intuitive solution to alleviate the precision placement problem is the addition of thrusters for localized positioning when the payload is near the target site [160, 161]. The control for the dynamic positioning of the subsea payload is challenging due to unpredictable exogenous disturbances such as fluctuating currents and transmission of motions from the surface vessel through the lift cable.

In this chapter, we investigate the coupled dynamics and control design of the vessel-crane-cable payload system as shown in Fig. 4.1. The flexible lift cable can be modeled by a set of PDEs that possesses an infinite number of dimensions, which makes it difficult to control. To avoid the problems associated with the truncated-model-based design of finite dimensionality, we design the boundary control and perform Lyapunov analysis based on the PDE directly. We tackle the positioning problem for the system with output constraints in the form of safety specifications and operational limits. Existing methods to handle constraints include model predictive control, reference governors, and the use of set invariance.

For the practical system with physical constraints, we employ barrier Lyapunov functions [221–224] in the design of positioning control for the flexible crane-cable-payload subsystem to ensure that the constraints are not violated. The uniform stability of the flexible subsystem is shown, and asymptotic positioning of the boundaries is achieved. Next, we tackle the scenario where the nonuniformity of the cable, uncertainties, and environmental disturbances are considered. Boundary control is formulated using the nonlinear PDE of the cable. Numerical simulations are provided to illustrate the performance of the proposed controls.

W. He et al., *Dynamics and Control of Mechanical Systems in Offshore Engineering*, Advances in Industrial Control, DOI 10.1007/978-1-4471-5337-5_4,

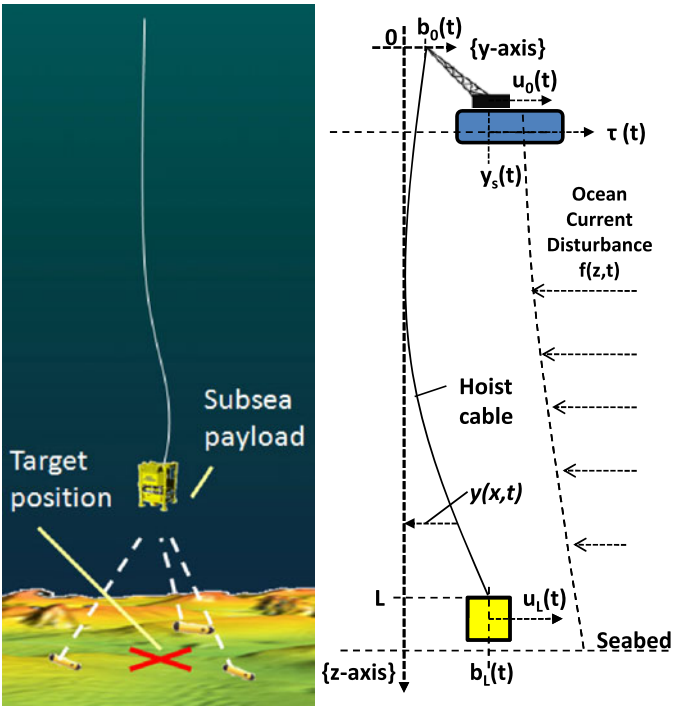

Fig. 4.1 Model of subsea installation operation and cable

The remainder of this chapter is organized as follows. In Sect. 4.1, coupled dynamics of the surface vessel and the crane-cable-payload flexible subsection are presented. Then, in Sect. 4.2, the vessel control is formulated via backstepping. Positioning controls are proposed considering physical systems with practical constraints. Thereafter, a boundary control is derived for the case of a nonuniform cable in Sect. 4.3. The simulation study in Sect. 4.4 demonstrates the effectiveness of the proposed controls under a theoretical worst-case disturbance to stress the controls and a more realistic disturbance to investigate the performance.

4.1 Problem Formulation

4.1.1 Dynamics of Surface Vessel

In the system considered, the top end of the lifting cable is attached to a crane, onboard an ocean surface vessel, and the bottom attached to a subsea module to be positioned for installation on the seafloor. The dynamics of the surface vessel can be modeled as

$$M_s \ddot{y}_s(t) + d_s \dot{y}_s(t) = \tau(t) + f_s(t), \tag{4.1}$$

where $y_s(t)$, $\dot{y}_s(t)$, and $\ddot{y}_s(t)$ are the displacement, velocity, and acceleration of the surface vessel, respectively, M_s is the mass of the surface vessel, d_s is the damping, $\tau(t)$ is the control force from the vessel dynamic positioning thrusters, and $f_s(t)$ is the environmental disturbance. We assume that the motions of the vessel are completely determined by the waves and thruster, which is a reasonable assumption since the vessel mass, wave forces, and thrust on it are much larger than the mass of the crane and coupled forces.

4.1.2 Dynamics of the Crane-Cable-Payload Flexible Subsystem

Dynamic equations that govern the motion of the lifting cable can be derived through the extended Hamilton principle or through discretization such as the finite element method. It has been shown in [225] that, assuming small displacements and employing first-order Taylor series expansion, the equation of motion for the cable can be obtained as

$$\rho(z)\ddot{y}(z,t) + d_c\dot{y}(z,t) = \frac{\partial}{\partial z}\big[T(z,t)y'(z,t)\big] + f(z,t), \tag{4.2}$$

where $y(z,t)$ is the displacement of the cable in the transverse direction, $\rho(z)$ denotes the nonuniform mass per unit length of the cable, $T(z,t)$ is the nonuniform distributed tension, d_c is the damping coefficient for the cable in fluid, and $f(z,t)$ denotes the distributed disturbance along the cable due to ocean currents.

The tension in the cable can be expressed as

$$T(z,t) = T_0(z) + \theta(z)\big[y'(z,t)\big]^2, \tag{4.3}$$

where $T_0(z) > 0$ is the nonuniform tension in the undisturbed string, and $\theta(z) \geq 0$ is a weighting function that accounts for strain in the displaced cable together with $[y'(z,t)]^2$. In the case where the cable is assumed to be uniform, the tension is assumed to be independent of z, with $T_0(z) = T_0$ and $\theta(z,t) = 0.5EA$ as used in [94, 226]. Substituting the tension (4.3) into the dynamical model (4.2) yields the governing equation of the lifting cable

$$\begin{aligned}\rho(z)\ddot{y}(z,t) + d_c\dot{y}(z,t) = \big[T_0(z) + 3\theta(z)\big[y'(z,t)\big]^2\big]y''(z,t)\\ + T_0'(z)y'(z,t) + \theta'(z)\big[y'(z,t)\big]^3 + f(z,t)\end{aligned} \tag{4.4}$$

with initial conditions expressed as

$$y(z,0) = c_1(z) \quad \text{and} \quad \dot{y}(z,0) = c_2(z) \tag{4.5}$$

and boundary conditions

$$y(0,t) = b_0(t) \quad \text{and} \quad y(L,t) = b_L(t), \tag{4.6}$$

where $\{c_1(z), c_2(z)\}$ and $\{b_0(t)b_L(t)\}$ are arbitrary sets of initial conditions and boundary conditions, respectively. The boundary conditions for the cable can be described by the following dynamic equations:

$$M_0\ddot{b}_0(t) = u_0(t) - T(0,t)y'(0,t) - d_0(t)\dot{b}_0(t) - M_0\ddot{y}_s(t), \tag{4.7}$$

$$M_L\ddot{b}_L(t) = u_L(t) + T(L,t)y'(L,t) - d_L(t)\dot{b}_L(t) + f_L(t), \tag{4.8}$$

where $u_0(t)$ and $u_L(t)$ are the control forces, $d_0(t)$ and $d_L(t)$ are the damping coefficients at points $z = 0$ and L, respectively, M_0 is the mass of the crane on the vessel, M_L and $f_L(t)$ are the mass and the environment disturbance on the subsea module attached to the bottom of the cable, respectively. The effects of the vessel motion on the top boundary are coupled into the crane-cable-payload subsystem through $\ddot{y}_s(t)$ in (4.7).

Assumption 4.1 For the distributed disturbance $f(z,t)$ on the cable, we assume that there exists a constant $\bar{f} \in \mathbb{R}^+$ such that $\|f(z,t)\| \leq \bar{f}$ for all $(z,t) \in [0,L] \times [0,\infty)$. This is a reasonable assumption as the effects of the time-varying current, $f(z,t)$, are exogenous, have finite energy, and hence are bounded, i.e., $f(z,t) \in \mathcal{L}_\infty([0,L])$. For similar reasons, the environmental disturbances $f_s(t)$ and $f_L(t)$ are assumed bounded, i.e., there exist positive constants $\overline{f}_s$ and $\overline{f}_L$ such that $|f_s(t)| \leq \overline{f}_s$ and $|f_L(t)| \leq \overline{f}_L$ for all $t \in [0,\infty)$.

Remark 4.2 For control design, only the assertion that there exists an upper bound on the disturbance in Assumption 4.1, $\|f(z,t)\| < \bar{f}$, is necessary. The knowledge of the exact value for $f(z,t)$ is not required for all $(z,t) \in [0,L] \times [0,\infty)$. As such, different disturbance models up to various levels of fidelity, such as those found in [195, 196, 227–229], can be applied without affecting the control design or analysis.

Remark 4.3 The effects of using cables with variation in parameters, uncertainties, disturbances, and the transition between the air and water surface can be incorporated explicitly through $\rho(z)$, $T_0(z)$, $\theta(z)$, and $f(z,t)$.

Assumption 4.4 The values of $\rho(z)$, $T_0(z)$, and $\theta(z)$ are bounded by known constant lower and upper bounds for all $x \in [0,L]$ as follows:

$$0 \leq \underline{\rho} \leq \rho(z) \leq \overline{\rho}, \tag{4.9}$$

$$0 \leq \underline{T} \leq T_0(z) \leq \overline{T}, \tag{4.10}$$

$$0 \leq \underline{\theta} \leq \theta(z) \leq \overline{\theta}. \tag{4.11}$$

The partial derivatives $\rho'(z)$, $T_0'(z)$, and $\theta'(z)$ are within a known range. This is reasonable as general values can be determined in the material selection and operation engineering phase.

4.2 Control Design

As the dynamics of the surface vessel is coupled into the crane-cable-payload system, we first propose a control design for the surface vessel using the backstepping approach [63]. Next, we design positioning controls $u_0(t)$ and $u_L(t)$ for the crane and subsea payload, employing SBLF in view of the constraints on the physical system. In the following subsection, we examine the coupled system with a nonuniform cable and propose a stabilizing boundary control. For conciseness, the dependency of the terms will be omitted where obvious.

4.2.1 DP Control of Surface Vessel

The control design and stability analysis of the vessel with a DP system for global positioning are demonstrated through the backstepping methodology [63]. We define error variables $z_1 = y_s - y_{sd}$ and $z_2 = \dot{y}_s - \alpha_1$, where y_{sd} is the desired position for the surface vessel. Differentiating z_1 with respect to time yields $\dot{z}_1 = z_2 + \alpha_1$. Consider the Lyapunov function candidate $V_1 = (1/2)z_1^2$ and choose the virtual control as $\alpha_1 = -k_1 z_1$. The time derivative of V_1 is

$$\dot{V}_1 = -k_1 z_1^2 + z_1 z_2. \tag{4.12}$$

Differentiating z_2 with respect to time yields $\dot{z}_2 = m_s^{-1}(-d_s \dot{y}_s + \tau + f_s(t)) - \dot{\alpha}_1$, where $\dot{\alpha}_1 = -k_1 \dot{z}_1$. Consider the augmented Lyapunov function candidate $V_2 = V_1 + (1/2)m_s z_2^2$. Taking its time derivative, we have

$$\begin{aligned}\dot{V}_2 \leq {} & -k_1(t)z_1^2(t) + z_1(t)z_2(t) + z_2(t)\big(-d_s \dot{y}_s(t) + \tau(t) - m_s \dot{\alpha}_1(t)\big) \\ & + |z_2(t)|\overline{f}_s.\end{aligned}$$

Designing the model-based vessel control as

$$\tau = -z_1(t) - k_2 z_2(t) + d_s \dot{y}_s(t) + m_s \dot{\alpha}_1(t) - u_{rs}, \tag{4.13}$$

where $u_{rs} = \operatorname{sgn}(z_2(t))\overline{f}_s$, we obtain

$$\dot{V}_2 \leq -k_1 z_1^2(t) - k_2 z_2^2(t). \tag{4.14}$$

Lemma 4.5 *Consider the vessel dynamics* (4.1) *with Assumption* 4.1, *under the action of full-state feedback control law* (4.13). *Then the vessel position in the closed-loop system* y_s *converges to the desired position* y_{sd} *asymptotically.*

Proof With the choice of α_1 and τ as above, the time derivative of the Lyapunov function candidate V_2 is negative semidefinite. The global asymptotic stability of

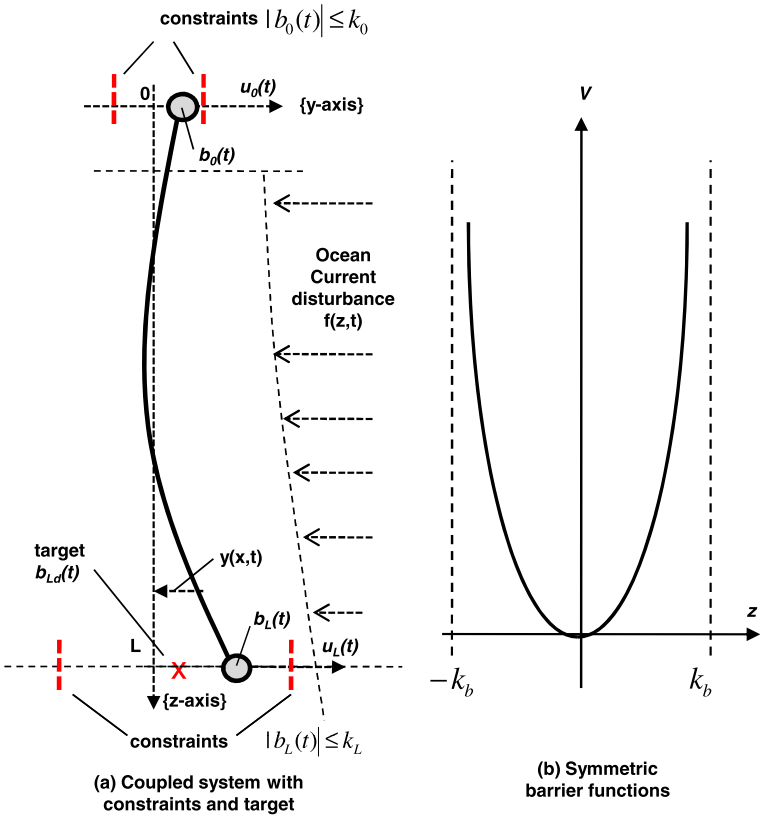

Fig. 4.2 (**a**) Schematic illustration of the coupled system with constraints and target and (**b**) symmetric barrier functions [223]

$z_1(t)$ and $z_2(t)$ can be concluded [63], i.e., $z_1(t)$, $z_2(t) \to 0$, and the vessel position y_s converges to the desired position y_{sd} asymptotically. □

4.2.2 *Boundary Positioning Control Using Barrier Lyapunov Functions*

During subsea installation operations, positioning of the subsea module is desired. As the practical system is subjected to constraints on both the motion of the crane at the top boundary and the maximum offset the payload can deviate at the bottom boundary as shown in Fig. 4.2(a), SBLFs are employed in the position control design for the top crane and bottom payload. By ensuring the boundedness of an SBLF [221–223] in the closed loop coupled with the dynamics of the flexible cable system, we ensure that (i) the coupled crane-cable-payload flexible system is stable, (ii) the

physical limits are not transgressed, and (iii) simultaneous positioning of the crane and payload for installation is achieved.

4.2.2.1 Stability of Flexible System Under Distributed Disturbance

In this subsection, we consider a simplified cable model [88] of (4.4) to illustrate the positioning control design technique using SBLF as follows:

$$\rho \ddot{y}(z,t) + d_c \dot{y}(z,t) = P y''(z,t) + f(z,t), \tag{4.15}$$

where $P = T(z,t) = T(0,t) = T(L,t) > 0$ is the constant tension, with conditions $b_0(t)$ and $b_L(t)$ in (4.6), boundary dynamics (4.7) and (4.8), distributed viscous damping, and disturbance $f(z,t)$ for the positioning of the subsea module. To facilitate the stability analysis, we introduce the transformation

$$w(z,t) = y(z,t) - \frac{z}{L} b_L(t) + \frac{z-L}{L} b_0(t) \tag{4.16}$$

to obtain the modified governing equation as

$$\rho \ddot{w}(z,t) + d_c \dot{w}(z,t) = P w''(z,t) + f^*(z,t), \tag{4.17}$$

where we obtain the distributed disturbance as

$$f^*(z,t) = f(z,t) - \frac{z}{L}\left(\rho \ddot{b}_L(t) + d_c \dot{b}_L\right) + \frac{z-L}{L}\left(\rho \ddot{b}_0(t) + d_c \dot{b}_0\right) \tag{4.18}$$

with pinned conditions at the boundaries and initial conditions

$$w(0,t) = w(L,t) = 0, \tag{4.19}$$

$$w(z,0) = c_3(z), \qquad \dot{w}(z,0) = c_4(z). \tag{4.20}$$

For the stability analysis of the transformed flexible subsystem subjected to the distributed disturbances, we consider the following Lyapunov function candidate:

$$V_p(t) = V_a(t) + V_b(t) \tag{4.21}$$

with

$$V_a(t) = \frac{1}{2}\int_0^L \left\{\rho \dot{w}^2(z,t) + P\left[w'(z,t)\right]^2\right\} dz, \tag{4.22}$$

$$V_b(t) = \int_0^L \rho \beta w(z,t) \dot{w}(z,t)\, dz, \tag{4.23}$$

where $\beta > 0$ is a small positive weighing constant satisfying the inequality

$$\beta < \frac{\min\{\rho,\ P\}}{2\rho \max\{1, L^2\}}. \tag{4.24}$$

Lemma 4.6 *The function $V_b(t)$ in (4.23) with crossing term $w(z,t)\dot{w}(z,t)$ can be upper and lower bounded as*

$$0 \leq \lambda_1 V_a(t) \leq V_b(t) \leq \lambda_2 V_a(t), \tag{4.25}$$

where λ_1 and λ_2 are positive constants.

Proof From Eq. (4.23) and Lemma 2.4, using Young's inequality, we obtain

$$\begin{aligned} \left|V_b(t)\right| &\leq \int_0^L \rho\beta\left\{\dot{w}^2(z,t) + w^2(z,t)\right\} dz \\ &\leq \int_0^L \rho\beta\left\{\dot{w}^2(z,t) + L^2\left[w'(z,t)\right]^2\right\} dz \\ &\leq \frac{2\rho\beta \max\{1, L^2\}}{L \min\{\rho, P, \}} V_a(t), \end{aligned} \tag{4.26}$$

which can be rewritten as

$$-\frac{2\rho\beta \max\{1, L^2\}}{\min\{\rho, P\}} V_a(t) \leq V_b(t) \leq \frac{2\rho\beta \max\{1, L^2\}}{\min\{\rho, P\}} V_a(t). \tag{4.27}$$

Thus, V_b is bounded as

$$\lambda_1 V_a(t) \leq V_b(t) \leq \lambda_2 V_a(t), \tag{4.28}$$

where

$$\lambda_1 = 1 - \frac{2\rho\beta \max\{1, L^2\}}{\min\{\rho, P\}} V_b(t) > 0, \tag{4.29}$$

$$\lambda_2 = 1 + \frac{2\rho\beta \max\{1, L^2\}}{\min\{\rho, P\}} V_b(t) > 1, \tag{4.30}$$

provided that inequality (4.24) is satisfied. □

Lemma 4.7 *The time derivative of the Lyapunov function candidate in (4.21) can be upper bounded with*

$$\dot{V}_p(t) \leq -\lambda_3 V_a(t) + \epsilon_p, \tag{4.31}$$

where λ_3 and ϵ_p are positive constants defined as

$$\lambda_3 = \frac{\min\{\beta(P - d_c\delta_2 L^2 - \delta_3 L^2), d_c - \delta_1 - \beta(\rho + \frac{d_c}{\delta_2})\}}{\max\{\rho, P\}} > 0, \tag{4.32}$$

$$\epsilon_p = \left(\frac{1}{\delta_1} + \frac{\beta}{\delta_3}\right) \max_{t=[0,\infty)} \int_0^L f^{*2}(z,t)\, dz > 0. \tag{4.33}$$

Proof Taking the time derivative of $V_a(t)$ in (4.22), performing integration by parts with boundary conditions (4.19), and using Lemma 2.3 with $\delta_1 > 0$ and disturbance (4.18), we have

$$\begin{aligned}\dot{V}_a(t) &= \int_0^L \left\{\rho\dot{w}(z,t)\ddot{w}(z,t) + Pw'(z,t)\dot{w}(z,t)\right\} dz \\ &\leq \int_0^L \left\{-d_c\dot{w}^2(z,t) + \dot{w}(z,t)f^*(z,t)\right\} dz \\ &\leq \int_0^L \left\{-(d_c-\delta_1)\dot{w}^2(z,t) + \frac{1}{\delta_1}f^{*2}(z,t)\right\} dz. \end{aligned} \tag{4.34}$$

Taking the time derivative of $V_b(t)$ in (4.23) as above with Lemma 2.4 and constants $\delta_2, \delta_3 > 0$ yields

$$\begin{aligned}\dot{V}_b(t) &= \int_0^L \rho\beta w\ddot{w} + \rho\beta\dot{w}^2\, dz \\ &= \beta\int_0^L -d_c w\dot{w} + Pww'' + wf^* + \rho\dot{w}^2\, dz \\ &\leq \beta\int_0^L \left(\rho + \frac{d_c}{\delta_2}\right)\dot{w}^2 - \left(P - d_c\delta_2 L^2 - \delta_3 L^2\right)\left[w'\right]^2 + \frac{1}{\delta_3}f^{*2}\, dz. \end{aligned} \tag{4.35}$$

Combining Eqs. (4.34) and (4.35), we have

$$\begin{aligned}V_p(t) &\leq \int_0^L -\beta\left(P - d_c\delta_2 L^2 - \delta_3 L^2\right)\left[w'\right]^2 - \left[d_c - \delta_1 - \beta\left(\rho + \frac{d_c}{\delta_2}\right)\right]\dot{w}^2 \\ &\quad + \left(\frac{1}{\delta_1} + \frac{\beta}{\delta_3}\right)f^*(z,t)\, dz \\ &\leq -\lambda_3 V_a(t) + \epsilon_p, \end{aligned} \tag{4.36}$$

where λ_3 and ϵ_p are given in (4.32) and (4.33), respectively. □

Remark 4.8 It is observed that under Assumption 4.1 where $f(z,t) \in L_\infty$, if the boundary states b_0, $\dot{b}_0$, $\ddot{b}_0$, b_L, $\dot{b}_L$, and $\ddot{b}_L$ of the original system (4.4) are bounded, we obtain $\epsilon_p < \infty$.

4.2.2.2 Positioning Control Using Barrier Lyapunov Functions

In this subsection, we design positioning controls for the boundary crane and payload using BLF, after which the main result will be formalized.

Top Boundary Consider the crane dynamics at the top boundary for the cable in Eq. (4.4):

$$M_0\ddot{b}_0(t) = u_0(t) - T(0,t)y'(0,t) - d_0(t)\dot{b}_0(t) - M_0\ddot{y}_s(t), \tag{4.37}$$

where the system state $b_0(t)$ at the top boundary is required to satisfy $|b_0(t)| < k_{0c}$ with constraint k_{0c} being a positive constant. We define the error coordinates $z_3 = b_0 - b_{0d}$ and $z_4 = \dot{b}_0 - \alpha_2$, where α_2 is a virtual control to be designed. To design a control that does not drive b_0 out of the interval $(-k_{0c}, k_{0c})$, the following Lyapunov function candidate comprising a barrier function [221] with schematic shown in Fig. 4.2(b) is proposed for the top boundary as

$$V_3 = \frac{\phi_0}{2}\log\frac{k_b^2}{k_b^2 - z_3^2}, \tag{4.38}$$

where ϕ_0 is a positive constant, $\log(*)$ is the natural logarithm of $(*)$, and $k_b = k_{0c} - A_0$ is the constraint on z_3, where $A_0 < k_{0c}$ is a positive constant, that is, we require $|z_3| < k_b$. It can be shown that V_3 is positive definite and C^1 continuous on the set $|z_3| < k_b$ and thus is a valid Lyapunov function candidate. The derivative of V_3 is given by

$$\dot{V}_3 = \frac{\phi_0 z_3 \dot{z}_3}{k_b^2 - z_3^2} = \frac{\phi_0 z_3(z_4 + \alpha_2)}{k_b^2 - z_3^2}, \tag{4.39}$$

for which the design of virtual control

$$\alpha_2 = -\left(k_b^2 - z_3^2\right)\phi_1 z_3, \tag{4.40}$$

where $\phi_1 > 0$ is a constant, yields

$$\dot{V}_3 = -\phi_0\phi_1 z_3^2 + \frac{\phi_0 z_3 z_4}{k_b^2 - z_3^2}. \tag{4.41}$$

In the second step, choose a Lyapunov function candidate as follows:

$$V_4 = V_3 + \frac{1}{2}z_4^2, \tag{4.42}$$

which yields the derivative

$$\dot{V}_4 = -\phi_0\phi_1 z_3^2 + \frac{\phi_0 z_3 z_4}{k_b^2 - z_3^2} + z_4 M_0^{-1}\left(u_0 - T(0,t)y'(0,t) - d_0\dot{b}_0 - M_0\ddot{y}_s - \dot{\alpha}_2\right),$$

where $\dot{\alpha}_2$ is given by

$$\dot{\alpha_2} = \phi_1\left(3z_3^2 - k_b^2\right)\left[z_4 - \left(k_b^2 - z_3^2\right)\phi_1 z_3\right]. \tag{4.43}$$

By designing the control as

$$u_0 = T(0,t)y'(0,t) + d_0\dot{b}_0 + M_0\ddot{y}_s + \dot{\alpha}_2 - M_0\left(\phi_2 z_4 + \frac{\phi_0 z_3}{k_b^2 - z_3^2}\right), \quad (4.44)$$

where $\phi_2 > 0$ is a constant, we have

$$\dot{V}_4 = -\phi_0\phi_1 z_3^2 - \phi_2 z_4^2. \quad (4.45)$$

Bottom Boundary Similar to the methodology as for the top boundary, we consider payload dynamics at the bottom boundary for the crane-cable-payload in Eq. (4.4):

$$M_L\ddot{b}_L(t) = u_L(t) + T(L,t)y'(L,t) - d_L(t)\dot{b}_L(t) + f_L(t), \quad (4.46)$$

where the system state $b_L(t)$ at the bottom boundary is required to satisfy the constraint $|b_L(t)| < k_{Lc}$ with k_{Lc} being a positive constant. We define the error coordinates $z_5 = b_L - b_{Ld}$ and $z_6 = \dot{b}_L - \alpha_3$, where α_3 is a virtual control, and design the Lyapunov function candidate with a barrier function for the payload dynamics as

$$V_5 = \frac{\phi_3}{2}\log\frac{k_c^2}{k_c^2 - z_5^2}, \quad (4.47)$$

where ϕ_3 is a positive constant, and $k_c = k_{Lc} - A_L$ the constraint on z_5, where $A_L < k_{Lc}$ is a positive constant. The derivative of V_5 is given by

$$\dot{V}_5 = \frac{\phi_3 z_5 \dot{z}_3}{k_c^2 - z_5^2} = \frac{\phi_3 z_5(z_6 + \alpha_3)}{k_c^2 - z_5^2}, \quad (4.48)$$

for which the design of virtual control

$$\alpha_3 = -\left(k_c^2 - z_5^2\right)\phi_4 z_5, \quad (4.49)$$

where $\phi_4 > 0$ is a constant, yields

$$\dot{V}_5 = -\phi_3\phi_4 z_5^2 + \frac{\phi_2 z_5 z_6}{k_c^2 - z_5^2}. \quad (4.50)$$

In the second step, choose a Lyapunov function candidate as follows:

$$V_6 = V_5 + \frac{1}{2}z_6^2, \quad (4.51)$$

which yields the derivative

$$\dot{V}_6 \le -\phi_3\phi_4 z_5^2 + \frac{\phi_3 z_5 z_6}{k_c^2 - z_5^2} + z_6 M_L^{-1}\left(u_L + T(L,t)y'(L,t) - d_L\dot{b}_L - \dot{\alpha}_3\right) + M_L^{-1}|z_6|f_L(t), \quad (4.52)$$

where $\dot{\alpha}_3$ is given by

$$\dot{\alpha}_3 = \phi_4\left(3z_5^2 - k_c^2\right)\left[z_6 - \left(k_c^2 - z_5^2\right)\phi_4 z_5\right]. \tag{4.53}$$

By designing the control as

$$u_L = -T(L,t)y'(L,t) + d_L\dot{b}_L + \dot{\alpha}_3 - u_{rblf} - M_L\left(\phi_5 z_6 + \frac{\phi_2 z_5}{k_c^2 - z_5^2}\right), \tag{4.54}$$

where $u_{rblf} = \text{sgn}(z_6)\bar{f}_L$, and $\phi_5 > 0$ is a constant, we have

$$\dot{V}_6 \leq -\phi_3\phi_4 z_5^2 - \phi_5 z_6^2. \tag{4.55}$$

The following theorem presents the result on the positioning control and the stability of the system.

Theorem 4.9 *Consider the flexible cable system* (4.15) *transformed to* (4.17) *with boundary conditions* (4.19), *initial conditions* (4.20), *crane dynamics* (4.37) *at the top boundary, payload dynamics* (4.46) *at the bottom boundary, full-state feedback controls* (4.44) *and* (4.54), *Assumption* 4.1, *and Lemmas* 2.7–4.7. *For the boundary states* b_0, $\dot{b}_0$, $\ddot{b}_0$, b_L, $\dot{b}_L$, *and* $\ddot{b}_L$ *of the original system* (4.15) *with initial conditions in the sets* Ω_0 *and* Ω_L, *where* $(b_0(0), \dot{b}_0(0)) \in \Omega_0 := \{(b_0, \dot{b}_0) \in \mathbb{R}^2 | -k_{0c} < b_0 < k_{0c}\}$ *and* $(b_L(0), \dot{b}_L(0)) \in \Omega_L := \{(b_L, \dot{b}_L) \in R^2 | -k_{Lc} < b_L < k_{Lc}\}$, *the following properties hold*:

(i) *The flexible system* (4.17) *subjected to distributed displacement* $f^*(z,t)$ *under Assumption* 4.1 *is uniformly bounded, i.e.,* $w(z,t) \in \mathcal{L}_\infty$ *for all* $(z,t) \in [0,L] \times [0,\infty)$, *with all closed-loop signals bounded, which implies that the original system* (4.15), $y(z,t) \in \mathcal{L}_\infty$ *for all* $(z,t) \in [0,L] \times [0,\infty)$.

(ii) *The positioning error* z_3 *is asymptotically stable, i.e.,* $b_0(t) \to b_{0d}(t)$ *as* $t \to \infty$ *with all states are bounded, and the constraint* $|z_3(t)| < k_b$ *is never violated.*

(iii) *The positioning error* z_5 *is asymptotically stable, i.e.,* $b_L(t) \to b_{Ld}(t)$ *as* $t \to \infty$ *with all states bounded, and the constraint* $|z_5(t)| < k_c$ *is never violated.*

Proof (i) Since $\dot{V}_4 \leq 0$, it can be shown that $V_4(t)$ is bounded for all $t > 0$, provided that $V_4(0)$ is bounded and $|z_3(0)| < k_b$. From (4.42) it follows that $V_3(t)$ is bounded. According to (4.38), we know that if $V_3(t)$ is bounded, it must be true that $|z_3(t)| \neq k_b$. Therefore, the tracking error z_3 remains in the region $|z_3(t)| < k_b$. Hence, we have $|b_0(t)| < k_{0c}$, and the states $\dot{b}_0$ and $\ddot{b}_0$ at the top boundary are bounded. The boundedness of b_L, $\dot{b}_L$, $\ddot{b}_L$ can be similarly shown. Since the boundary states are bounded, Lemma 4.7 holds, and $V_p(t)$ is upper bounded with Eq. (4.31). From Eqs. (4.25) and (4.31) we have

$$\dot{V}_p(t) \leq -\lambda V_p(t) + \epsilon_p, \tag{4.56}$$

where $\lambda = \lambda_3/\lambda_2$. The uniform boundedness of $w(z,t)$ can be shown by multiplying Eq. (4.56) by $e^{\lambda t}$:

$$\frac{\partial}{\partial t}\left(V_p e^{\lambda t}\right) \leq \epsilon_p e^{\lambda t}. \tag{4.57}$$

Integration of the above and application of Lemma 2.7 with Eqs. (4.25) and (4.22) yield

$$\lambda_1 V_a(t) \leq V_p(t) \leq V_p(0) + \frac{\epsilon_p}{\lambda} \in \mathcal{L}_\infty. \tag{4.58}$$

Since $V_a(t)$ is bounded, $\dot{w}(z,t)$ and $w'(z,t)$ are bounded for all $(z,t) \in [0,L] \times [0,\infty)$. Using Lemma 2.4, we obtain $w(z,t) \in \mathcal{L}_\infty$, and hence $y(z,t), y'(z,t) \in \mathcal{L}_\infty$. At this point, we have shown that all signals in the positioning controls (4.44) and (4.54) are bounded. Finally, using Assumption 4.1 and Eqs. (4.17) to (4.20), we conclude that $\ddot{w}(z,t)$ and hence $\ddot{y}(z,t)$ are bounded for all $(z,t) \in [0,L] \times [0,\infty)$.

(ii) To show that $b_0(t) \to b_{0d}$ as $t \to \infty$, we compute $\ddot{V}_4$ as follows:

$$\ddot{V}_4 = -2\phi_0\phi_1 z_3 \dot{z}_3 - 2\phi_2 z_4 \dot{z}_4. \tag{4.59}$$

From the boundedness of the closed-loop signals, we can show that $\ddot{V}_2$ is bounded and uniformly continuous. Using Barbalat's lemma [62], $z_3(t), z_4(t) \to 0$ as $t \to \infty$. Hence, the state $b_0(t) \to b_{0d}(t)$ as $t \to \infty$.

(iii) The proof is similar to that in (i) and will be omitted for conciseness. □

Remark 4.10 In the control design, a particular choice of SBLF, e.g., $V_5 = (\phi_3/2)\log\left(k_c^2/(k_c^2 - z_5^2)\right)$ was employed. We can extend the result for asymmetric barrier Lyapunov functions (ABLS) or general forms of barrier functions in Lyapunov synthesis satisfying $V_5(z_5) \to \infty$ as $z_5 \to -k_b$ or $z_5 \to k_c$ by following the methodology in [223], where $k_b \neq k_c > 0$ are the barrier constraints.

Remark 4.11 To handle unknown perturbations to the nominal model in the form of parametric uncertainties or modeling errors, adaptive model-based or approximation-based control techniques can be employed following the framework setup in [203, 222, 223].

4.3 Boundary Stabilization of Coupled System with Nonuniform Cable

In this subsection, we consider the nonuniformity of the cable and design boundary controls for stabilization of the crane and payload thruster using the PDE of the flexible subsystem subjected to a distributed disturbance via Lyapunov synthesis.

Consider the following Lyapunov function candidate:

$$V(t) = V_c(t) + V_d(t) + V_e(t), \tag{4.60}$$

where

$$V_c(t) = \frac{1}{2}\int_0^L \left\{\rho(z)\dot{y}^2(z,t) + T_0(z)\left[y'(z,t)\right]^2 + \frac{1}{2}\theta(z)\left[y'(z,t)\right]^4\right\} dz, \tag{4.61}$$

$$V_d(t) = \frac{1}{L}\int_0^L \left\{\rho(z)\gamma(z)z\dot{y}(z,t)y'(z,t)\right\} dz, \tag{4.62}$$

$$V_e(t) = \frac{1}{2}M_0\dot{b}_0^2(t) + \frac{1}{2}M_L\left[\dot{y}(L,t) + \frac{3}{8}\gamma(L)y'(L,t)\right]^2, \tag{4.63}$$

and $\gamma(z)$ is a positive scalar function satisfying the inequality

$$0 < \int_0^L \gamma(z)\, dz < \frac{L\min\{\underline{\rho},\ \underline{T}, \underline{\theta}\}}{2\overline{\rho}}. \tag{4.64}$$

Lemma 4.12 *The function $V_d(t)$ with crossing term $\int_0^L \dot{y}(z,t)y'(z,t)\, dz$ can be upper and lower bounded as*

$$0 \le \lambda_4 V_c(t) \le V_d(t) \le \lambda_5 V_c(t), \tag{4.65}$$

where λ_4 and λ_5 are positive constants.

Proof From Eq. (4.62) by Young's inequality we have

$$\left|V_d(t)\right| \le \int_0^L \rho(z)\gamma(z)\left\{\dot{y}^2(z,t) + \left[y'(z,t)\right]^2\right\} dz. \tag{4.66}$$

Comparing (4.66) with (4.62), we obtain

$$\left|V_d(t)\right| \le \int_0^L \rho(z)\gamma(z)\left\{\dot{y}^2(z,t) + \left[y'(z,t)\right]^2\right\} dz \tag{4.67}$$

$$\le \frac{2\overline{\rho}\int_0^L \gamma(z)\, dz}{L\min\{\underline{\rho},\ \underline{T}, \underline{\theta}\}} V_c(t), \tag{4.68}$$

which can be rewritten as

$$-\frac{2\overline{\rho}\int_0^L \gamma(z)\, dz}{L\min\{\underline{\rho}, \underline{T}, \underline{\theta}\}} V_c(t) \le V_d(t) \le \frac{2\overline{\rho}\int_0^L \gamma(z)\, dz}{L\min\{\underline{\rho}, \underline{T}, \underline{\theta}\}} V_c(t). \tag{4.69}$$

Thus, V_d is bounded as

$$\lambda_4 V_c(t) \le V_d(t) \le \lambda_5 V_c(t), \tag{4.70}$$

where

$$\lambda_4 = 1 - \frac{2\overline{\rho}\int_0^L \gamma(z)\,dz}{L\min\{\underline{\rho},\underline{T},\underline{\theta}\}}V_d(t) > 0, \tag{4.71}$$

$$\lambda_5 = 1 + \frac{2\overline{\rho}\int_0^L \gamma(z)\,dz}{L\min\{\underline{\rho},\underline{T},\underline{\theta}\}}V_d(t) > 1, \tag{4.72}$$

provided that condition (4.64) is satisfied. □

Lemma 4.13 *Designing boundary controls $u_0(t)$ and $u_L(t)$ at $z = 0$ and L, respectively, as*

$$u_0(t) = -k_0\dot{y}(0,t) + 2T(0,t)y'(0,t) + d_0(t)\dot{b}_0(t) + M_0\ddot{y}_s, \tag{4.73}$$

$$u_L(t) = -k_L\left[\dot{y}(L,t) + \frac{3}{4}\gamma(L)y'(L,t)\right] - u_{rbc} + d_L\dot{b}_L(t) - 2T(L,t)y'(L,t) - \frac{3}{4}M_L\gamma(L)\dot{y}'(L,t), \tag{4.74}$$

where $u_{rbc} = \mathrm{sgn}[\dot{y}(L,t) + \frac{3}{4}\gamma(L)y'(L,t)]\overline{f}_L$, the time derivative of the Lyapunov function candidate in (4.60) can be upper bounded with

$$\dot{V}(t) \le -\lambda_6\big[V_c(t) + V_e(t)\big] + \varepsilon, \tag{4.75}$$

where $\lambda_6 > 0$ and $\varepsilon > 0$ are positive constants.

Proof Taking the time derivative of $V_c(t)$, performing integration by parts, using Lemma 2.3 with $\delta_4 > 0$, and substituting the governing equation of the cable (4.4), we have

$$\begin{aligned}\dot{V}_c(t) &= \int_0^L \big\{\rho\dot{y}\ddot{y} + T_0y'\dot{y}' + \theta\big[y'\big]^3\dot{y}'\big\}\,dz \\ &\le T(L,t)\dot{y}(L,t)y'(L,t) - T(0,t)\dot{y}(0,t)y'(0,t) \\ &\quad - (d_c - \delta_4)\int_0^L \dot{y}^2\,dz + \frac{1}{\delta_4}\int_0^L f^2\,dz.\end{aligned} \tag{4.76}$$

A similar treatment of $V_d(t)$ as for $V_c(t)$ above, with $\delta_5 > 0$, yields

$$\begin{aligned}\dot{V}_d(t) &= \frac{1}{L}\int_0^L \gamma z\big\{y'\rho\ddot{y} + \rho\dot{y}\dot{y}'\big\}\,dz \\ &\le \frac{1}{2}\gamma(L)T_0(L)\big[y'(L,t)\big]^2 - \frac{1}{2L}\int_0^L\left(\frac{\partial\{\gamma z\}}{\partial z}T_0 - \gamma zT_0'\right)\big[y'\big]^2\,dz \\ &\quad + \frac{3}{4}\gamma(L)\theta(L)\big[y'(L,t)\big]^4 - \frac{1}{4L}\int_0^L\left(3\frac{\partial\{\gamma z\}}{\partial z}\theta - \gamma z\theta'\right)\big[y'\big]^4\,dx\end{aligned}$$

$$+\frac{1}{2}\gamma(L)\rho(L)\dot{y}^2(L,t)-\frac{1}{2L}\int_0^L\frac{\partial\{\gamma\rho z\}}{\partial z}[\dot{y}]^2\,dz+\frac{\delta_5}{L}\int_0^L\gamma^2z^2\big[y'\big]^2\,dx$$
$$+\frac{1}{\delta_5 L}\int_0^L f^2\,dz. \tag{4.77}$$

For clarity, we separate $V_e(t)$ into $V_{e0}(t)$ and V_{eL} at $z=0$ and $z=L$, respectively, for the boundary control design. Taking the time derivative of $V_{e0}(t)$ along Eq. (4.7) yields

$$\dot{V}_{e0}=\dot{y}(0,t)\big[u_0(t)-T(0,t)y'(0,t)-d_0(t)\dot{b}_0(t)-M_0\ddot{y}_s\big]. \tag{4.78}$$

Substituting the boundary control of the crane (4.73) at $z=0$ into Eq. (4.78), we obtain

$$\begin{aligned}\dot{V}_{e0}&=\dot{y}(0.t)\big[-k_0\dot{y}(0,t)+T(0,t)y'(0,t)\big]\\&=-k_0\dot{y}^2(0,t)+T(0,t)y'(0,t)\dot{y}(0.t).\end{aligned} \tag{4.79}$$

Substituting the designed boundary control (4.74) at $z=L$, we have

$$\begin{aligned}\dot{V}_{eL}(t)\le&-k_L\bigg[\dot{y}(L,t)+\frac{3}{4}\gamma(L)y'(L,t)\bigg]^2-T(L,t)y'(L,t)\dot{y}(L,t)\\&-\frac{3}{4}\gamma(L)T(L,t)\big[y'(L,t)\big]^2.\end{aligned} \tag{4.80}$$

Combining Eqs. (4.76), (4.77), (4.80), and (4.79), we obtain

$$\begin{aligned}\dot{V}(t)\le&\frac{1}{2}\gamma(L)T_0(L)\big[y'(L,t)\big]^2+\frac{3}{4}\gamma(L)\theta(L)\big[y'(L,t)\big]^4+\frac{1}{2}\gamma(L)\rho(L)\dot{y}^2(L,t)\\&-\frac{1}{2L}\int_0^L\bigg(\frac{\partial\{\gamma z\}}{\partial z}T_0-\gamma zT_0'-2\delta_5\gamma^2z^2\bigg)\big[y'\big]^2\,dz\\&-\frac{1}{4L}\int_0^L\bigg(3\frac{\partial\{\gamma z\}}{\partial z}\theta-\gamma z\theta'\bigg)\big[y'\big]^4\,dx\\&-\frac{1}{2L}\int_0^L\bigg(\frac{\partial\{\gamma\rho z\}}{\partial z}+2Ld_c-2L\delta_4\bigg)[\dot{y}]^2\,dz+\bigg(\frac{1}{\delta_4}+\frac{1}{\delta_5 L}\bigg)\int_0^L f^2\,dz\\&-k_0\dot{y}^2(0,t)-k_L\bigg[\dot{y}(L,t)+\frac{3}{8}\gamma(L)y'(L,t)\bigg]^2\\&-\frac{3}{4}T(L,t)\gamma(L)\big[y'(L,t)\big]^2.\end{aligned}$$

Using $\theta(L)[y'(L,t)]^2=T(L,t)-T_0(L)$, we have

$$V(t)\le-\frac{1}{4}\gamma(L)T_0(L)\big[y'(L,t)\big]^2+\frac{1}{2}\gamma(L)\rho(L)\dot{y}^2(L,t)$$

$$
\begin{aligned}
&- k_L\left[\dot{y}(L,t)+\frac{3}{4}\gamma(L)y'(L,t)\right]^2-\frac{1}{4L}\int_0^L\left(3\frac{\partial\{\gamma z\}}{\partial z}\theta-\gamma z\theta'\right)[y']^4\,dx\\
&-\frac{1}{2L}\int_0^L\left(\frac{\partial\{\gamma z\}}{\partial z}T_0-\gamma zT_0'-2\delta_5\gamma^2z^2\right)[y']^2\,dz\\
&-\frac{1}{2L}\int_0^L\left(\frac{\partial\{\gamma\rho z\}}{\partial z}+2Ld_c-2L\delta_4\right)[\dot{y}]^2\,dz-k_0\dot{y}^2(0,t)\\
&+\left(\frac{1}{\delta_4}+\frac{1}{\delta_5L}\right)\int_0^L f^2\,dz. \qquad (4.81)
\end{aligned}
$$

From the first three terms in (4.81) we have

$$
\begin{aligned}
&-\frac{1}{4}\gamma(L)T_0(L)\big[y'(L,t)\big]^2+\frac{1}{2}\gamma(L)\rho(L)\dot{y}^2(L,t)\\
&\quad-\frac{1}{2}k_L\left[\dot{y}(L,t)+\frac{3}{4}\gamma(L)y'(L,t)\right]^2\\
&\le-\left[-k_L\frac{9}{32}\gamma(L)^2+\frac{1}{4}\gamma(L)T_0(L)\right]\big[y'(L,t)\big]^2\\
&\quad-\frac{1}{2}\left[\frac{k_L}{2}-\gamma(L)\rho(L)\right]\dot{y}^2(L,t). \qquad (4.82)
\end{aligned}
$$

From Eqs. (4.81), (4.82), and (4.60) we can show that

$$
\dot{V}(t)\le-\lambda_6\big[V_c(t)+V_e(t)\big]+\varepsilon \qquad (4.83)
$$

where

$$
\begin{aligned}
\lambda_6=\min\Bigg\{&\int_0^L\left(\frac{\partial\{\gamma(z)\rho(z)z\}}{L\rho(z)\partial z}+\frac{2d_c}{\rho(z)}-\frac{2\delta_4}{\rho(z)}\right)dz\\
&\int_0^L\frac{1}{LT_0(z)}\left(\frac{\partial\{\gamma z\}}{\partial z}T_0-\gamma zT_0'-2\delta_5\gamma^2z^2\right)dz,\\
&\int_0^L\frac{1}{2L\theta(z)}\left(3\frac{\partial\{\gamma z\}}{\partial z}\theta-\gamma z\theta'\right)dz,\ \frac{2k_0}{M_0},\ \frac{2k_L}{M_L}\Bigg\}>0, \qquad (4.84)
\end{aligned}
$$

$$
\varepsilon=\left(\frac{1}{\delta_4}+\frac{1}{\delta_5L}\right)\max_{t=[0,\infty)}\int_0^L f^2\,dz\le\infty \qquad (4.85)
$$

with admissible values of control gain k_L bounded as

$$
2\gamma(L)\rho(L)<k_L<\frac{8}{9}\frac{T_0(L)}{\gamma(L)}. \quad \square \qquad (4.86)
$$

By Eqs. (4.65) and (4.75) we can rewrite the time derivative of the Lyapunov function candidate in the form of Lemma 2.7 as

$$\dot{V}(t) \leq -\lambda V(t) + \varepsilon, \tag{4.87}$$

where $\lambda = \lambda_6/\lambda_5$. The following theorem presents the results for the boundary for the coupled system.

Theorem 4.14 *Consider the coupled system* (4.1), (4.4), (4.7), *and* (4.8), *with initial conditions* (4.5), *boundary conditions* (4.6), *scalar function* $\gamma(z)$ *satisfying inequalities* (4.64) *and* (4.32), *Assumptions* 4.1 *and* 4.4, *full-state feedback from the vessel, crane, and payload, vessel control* (4.13), *and boundary controls* (4.73) *and* (4.74). *Then the closed-loop system subjected to the distributed disturbance* $f(z,t)$ *is uniformly bounded.*

Proof The uniform boundedness of the deflection $y(z,t)$ can be shown by multiplying Eq. (4.87) by $e^{\lambda t}$:

$$\frac{\partial}{\partial t}\left(V e^{\lambda t}\right) \leq \varepsilon e^{\lambda t}. \tag{4.88}$$

Integration of the above and application of Lemma 2.7 yield

$$V(t) \leq \left(V(0) - \frac{\varepsilon}{\lambda}\right)e^{\lambda t} + \frac{\varepsilon}{\lambda} \leq V(0) + \frac{\varepsilon}{\lambda} \in \mathcal{L}_\infty. \tag{4.89}$$

Utilizing Eqs. (4.61) and (4.65), we have

$$V_c(t) \leq \frac{1}{\lambda_4} V(t) \in \mathcal{L}_\infty. \tag{4.90}$$

Since $V_c(t)$ is bounded, $\dot{y}(z,t)$ and $y'(z,t)$ are bounded for all $(z,t) \in [0,L] \times [0,\infty)$. By Lemma 4.5, since $\dot{y}(z,t)$ and $y'(z,t)$ are bounded, the boundary controls (4.73) and (4.74) are bounded. From the above statements and Eqs. (4.4)–(4.8) we can conclude that $\ddot{y}(z,t)$ and $y(z,t) \in \mathcal{L}_\infty$. □

Remark 4.15 The challenge in addressing nonuniformities when working with boundary control lies in the determining an appropriate (nonuniform) cross term in the Lyapunov function [88]. In [98], the increasing nonuniform term in the form of $\gamma(z) = \gamma_1 e^{\gamma_2 z}$ with $\gamma_1 > 0$ sufficiently small and γ_2 large was proposed. When $T_0(z)$ and $\theta(z)$ are constants, $\gamma(z)$ and $\gamma(z)\rho(z)$ can be chosen to be nondecreasing.

Remark 4.16 The robust signum control terms in control (4.13), (4.54), and (4.74) may induce chattering due to the discontinuous property which results in mechanical wear and tear. To solve this problem, several nice smooth modifications have been

investigated in the literature, such as boundary layers [230, 231] and the use of a hyperbolic tangent function [232], which has the following nice property:

$$0 \leq |\chi| - \chi \tanh\left(\frac{\chi}{\varepsilon_d}\right) \leq 0.2785\varepsilon_d \quad \forall \chi \in \mathbb{R}, \tag{4.91}$$

where $\varepsilon_d > 0$. For example, let $u_{rs} = k_3 \tanh(z_2/\varepsilon_d)$ in (4.13) where $k_3 \geq \bar{f}_s$. From (4.14) and (4.91), we obtain

$$\dot{V}_2 \leq -k_1 z_1^2 - k_2 z_2^2 + 0.2785 k_3 \varepsilon_d. \tag{4.92}$$

Obviously, $\dot{V}$ is strictly negative whenever the errors z_1 and z_2 are outside the compact set

$$\Omega_{c_s} = \left\{(z_1, z_2) \mid k_1 z_1^2 + k_2 z_2^2 \leq 0.2785 k_3 \varepsilon_d\right\}, \tag{4.93}$$

i.e., z_1 will converge to a small neighborhood of zero, whose size is adjustable by the design parameters k_1 and k_2. By smoothing the signum function, the closed-loop system is stable with a small residual error and a reduction in chattering. Similar smoothing modifications can be applied for u_{rblf} and u_{rbc} in (4.54) and (4.74), and the analysis is omitted for conciseness.

4.4 Numerical Simulations

4.4.1 Worst-Case Harmonic Disturbances

The closed-loop system (4.1) and (4.2) with boundary dynamics (4.7) and (4.8), distributed disturbance (2.5), vessel control (4.13), positioning controls (4.44) and (4.54), and stabilizing boundary controls (4.73) and (4.74) is simulated to investigate the performance of the proposed controls under theoretical worst-case disturbances. A nondimensionalization and finite difference scheme is used to numerically solve the PDE.

The vessel with $M_s = 9.6 \times 10^7$ kg and $d_s = 9.2 \times 10^7$ starts the initial condition $y_s(0) = 10.0$ m with target position $y_{sd} = 0.0$ m at the origin. The crane with $M_0 = 1.0 \times 10^6$ kg, $d_0 = 8.0 \times 10^5$, cable with $T(z,t) = T_0 + 0.5EA[y'(z,t)]^2$, $T_0 = 4.0 \times 10^6$ N, $L = 1000$ m, $E = 4.0 \times 10^9$, $D = 0.2$ m, $\rho = 8.02$ kg m^{-3}, $d_c = 0$, and payload modeled as a cylinder with $M_L = 4 \times 10^5$ kg, $d_L = 2 \times 10^5$, height $h_c = 10.0$ m, and diameter $D_c = 5.0$ m starts initially at rest and is excited by a distributed transverse load. It is noted that the damping of the cable d_c and robust signum terms in all proposed controls are set to zero to demonstrate the robustness of the proposed control.

The ocean surface current velocity $U(t)$ is modeled as a mean flow with worst-case sinusoid components $\omega_i = \{2.2189, 4.4378, 6.6567, 8.8756\}$ for $i = 1$ to 4 that

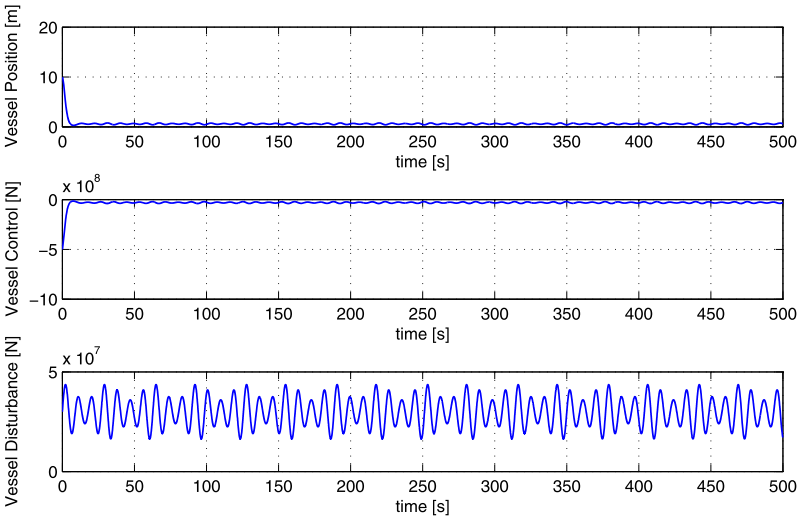

Fig. 4.3 (*Top*) surface vessel position with desired position at the origin, (*center*) vessel control thrust, and (*bottom*) disturbance acting on the vessel

match the first four natural frequencies of the cable. The current $U(t)$ can be expressed as

$$U(t) = \bar{U} + U_m \sum_{i=1}^{N} \sin(\omega_i t), \quad i = 1, 2, \ldots, N, \tag{4.94}$$

where $\bar{U}$ is the mean flow current, and U_m is the amplitude of the oscillating flow. The full current load is applied from $z = 0$ to 300 m and thereafter linearly declines to an oscillating current with mean 1.0 $\mathrm{m\,s^{-1}}$ at $z = 1000$ m to obtain a depth-dependent ocean current profile $U(z, t)$. The distributed disturbance is generated using Eq. (2.5), the disturbance on the vessel is generated as

$$f_s = \left[3 + 0.8\sin(0.7t) + 0.2\sin(0.5t) + 0.2\sin(0.9t)\right] \times 10^6, \tag{4.95}$$

and the disturbance on the subsea payload modeled as a cylinder is derived from Morison's equation

$$f_L = \frac{1}{2} C_D \rho_s h D_c \left|U(L, t)\right| U(L, t), \tag{4.96}$$

where $C_D = 1.0$ is the drag coefficient.

Surface Vessel Control The surface vessel subjected to disturbance (4.95) is simulated under the action of backstepping control (4.13) with control gains $k_1 = 1.0$ and $k_2 = 5.0 \times 10^7$. The position, control, and disturbance on the surface vessel are shown in Fig. 4.3, where it can be observed that the backstepping control is able to position the vessel near its desired position at the origin.

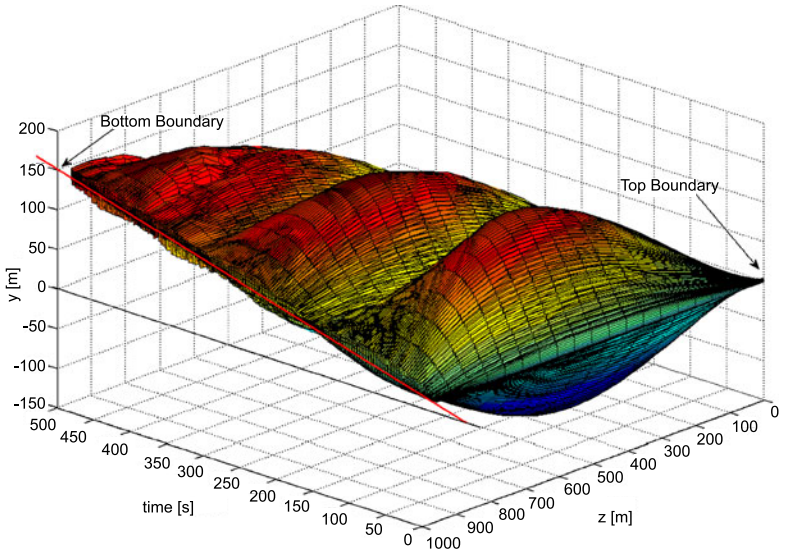

Fig. 4.4 Spatial-time representation of cable motions without control under worst-case disturbances. The top boundary is at the crane, and the bottom boundary at the subsea payload

Crane-Cable-Payload Subsystem Without Controls Under the action of the vessel control, the dynamics of the cable is simulated without control, and the 3D spatial time representation is shown in Fig. 4.4. It can be seen that at $t = 500$ s, the subsea payload has deviated 150 m from the origin under the action of the distributed disturbance on the cable and the disturbance force acting on the payload due to the current.

SBLF Positioning Controls The positioning controls (4.44) and (4.54) developed using SBLF are simulated with crane desired position $b_{0d} = 0$ m, constraints $k_{0c} = 30$ m and $A_0 = 10$ m, control gains $\phi_0 = \phi_1 = \phi_2 = 10$, subsea payload desired position $b_{Ld} = 10$ m, constraints $k_{Lc} = 50$ m and $A_L = 30$ m, and control gains $\phi_3 = \phi_4 = \phi_5 = 5.0$. The 3D spatial time representation is shown in Fig. 4.5, and the position, control, and tension at the top (crane) and bottom (subsea payload) boundaries are shown in Figs. 4.6 and 4.7, respectively. The designed control is able to keep the crane at the desired position, and the subsea payload position converges from the origin to the desired position when the system is subjected to the environmental disturbances.

Stabilizing Boundary Control The boundary controls (4.73) and (4.74) are simulated with $k_0 = k_L = 5 \times 10^8$ and $\gamma = 1 \times 10^{-5}$. The 3D spatial time representation for the boundary control is shown in Fig. 4.8, and the position, control, and tension at the top (crane) and bottom (subsea payload) boundaries are shown in Figs. 4.9 and 4.10, respectively. From the simulations it is observed that the proposed boundary control can stabilize the boundary at the origin under the influence of the disturbances.

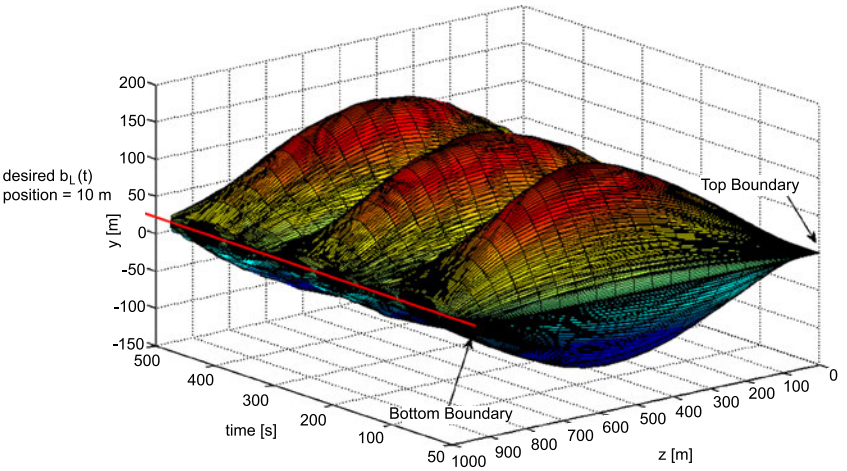

Fig. 4.5 Spatial-time representation of cable motions with positioning control under worst-case disturbances. The top boundary is at the crane, and the bottom boundary is at the subsea payload, maintained at desired position $b_L = 10$ m

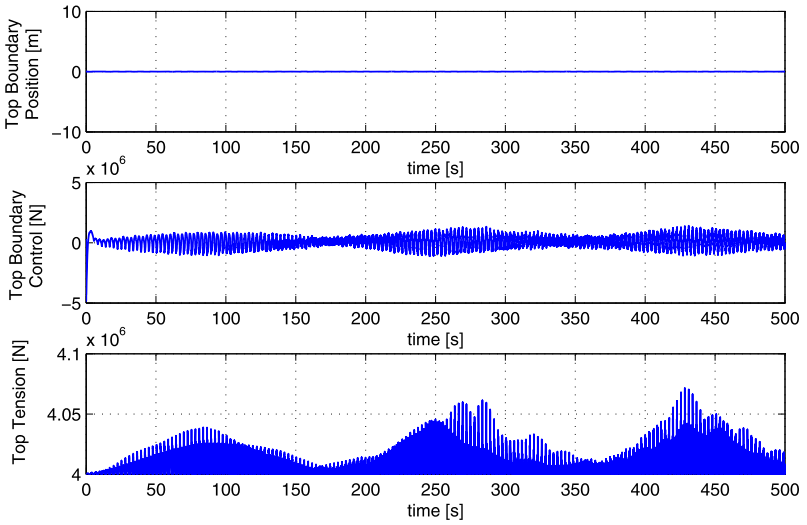

Fig. 4.6 (*Top*) Position of the crane with desired position at origin, (*center*) control force on the crane, and (*bottom*) tension at crane with position control (4.44) under worst-case disturbances

Remark 4.17 To demonstrate the robustness of the proposed control, the damping of the cable and all robust signum terms in all proposed controls are set to zero. The ocean surface current and hence the distributed disturbance are simulated with

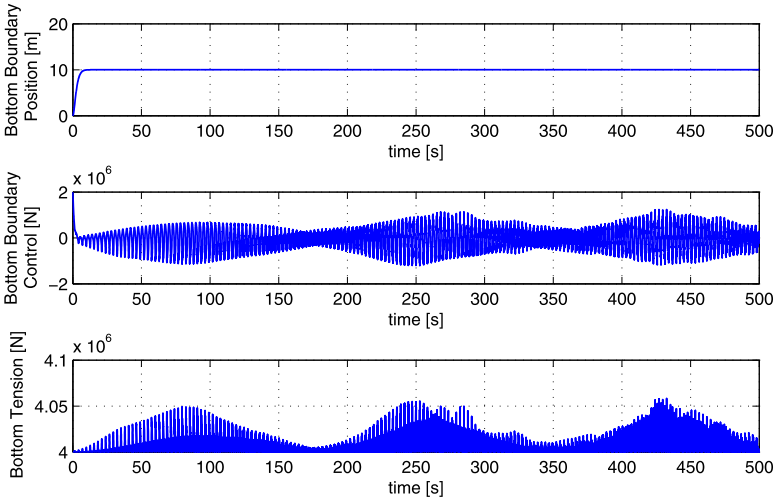

Fig. 4.7 (*Top*) Position of the payload with desired position at $B_{LD} = 10$ m, (*center*) control force, and (*bottom*) cable tension at subsea payload with positioning control (4.54) under worst-case disturbances

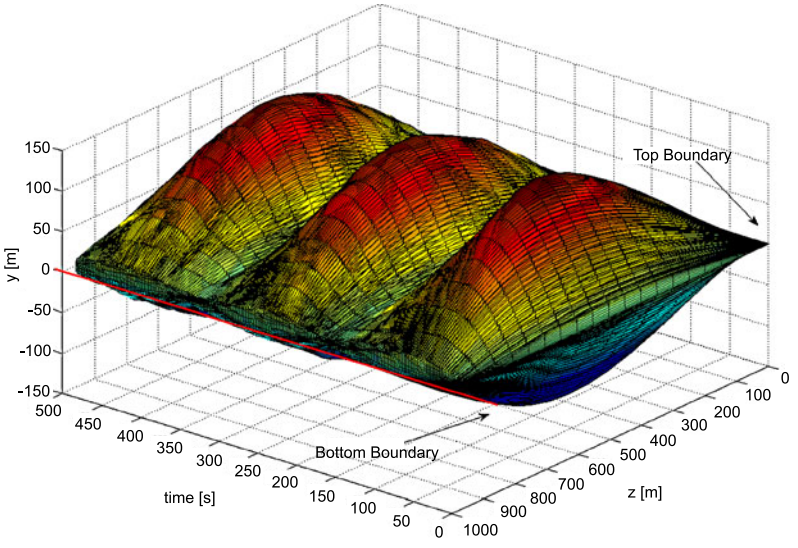

Fig. 4.8 Spatial-time representation of the cable motions control with stabilizing boundary controls (4.73) and (4.74) under worst-case disturbances

worst-case sinusoid components to excite large-amplitude transverse resonance in the cable. As such, a large oscillating control signal is required to keep the payload at the target location.

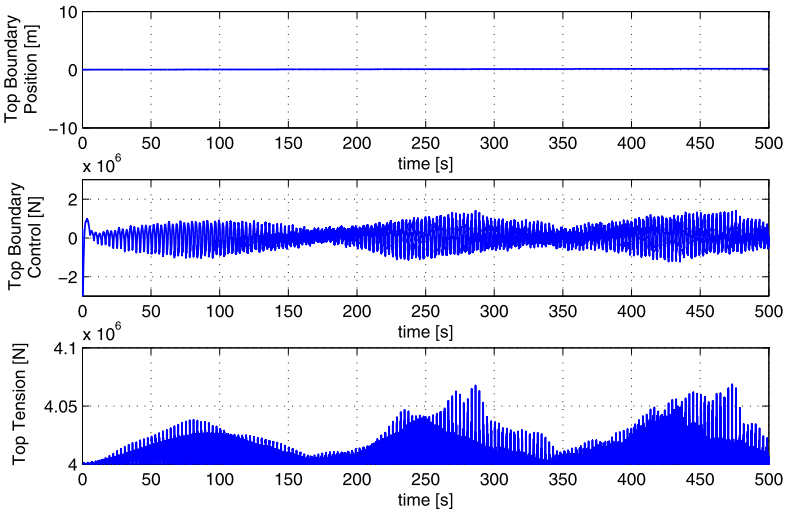

Fig. 4.9 (*Top*) Position of the crane, (*center*) control force on the crane, and (*bottom*) tension at crane with stabilizing boundary control (4.73) under worst-case disturbances

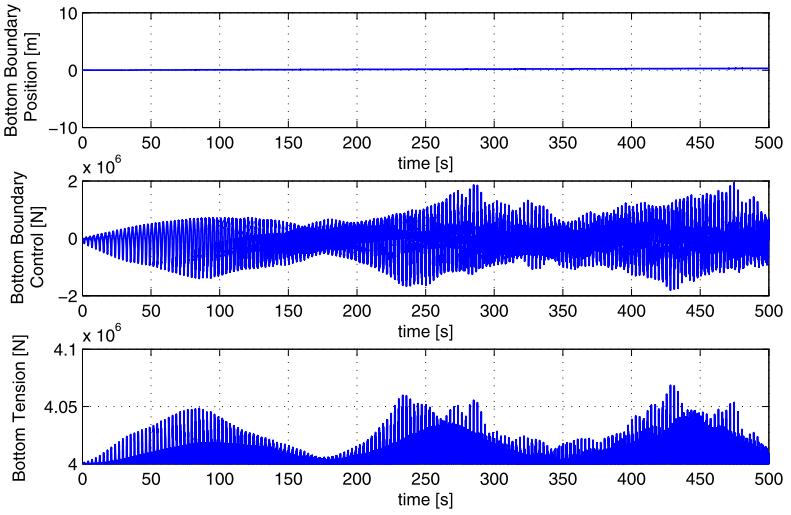

Fig. 4.10 (*Top*) Position of the payload, (*center*) control force on the payload, and (*bottom*) tension at payload with stabilizing boundary control (4.74) under worst-case disturbances

4.4.2 Practical Disturbances

To validate the proposed control under practical disturbances, hydrodynamic analysis has been carried out for the vessel to calculate the vessel disturbance f_s. The excitation forces for wave, wind, and current and the Response Amplitude Operations

(RAOs) of the vessel are generated using a hydrodynamic software. The underwater dimensions of the vessel are 355 m length × 57 m breath × 11.8 m maximum drought. Head sea, wind, and current in the same direction are simulated with JONSWAP spectrum of significant wave height, $H_s = 3.0$ m (rough sea), peak period of spectrum = 7.0 s, γ coefficient = 3.30, and Harris wind spectrum with wind velocity = 10.0 m s^{-1}. The second-order drift forces are calculated based on the Lagally approach [233].

The ocean surface current velocity $U(t)$ can be modeled by using a first-order Gauss–Markov process [234]

$$\dot{U}(t) + \mu U(t) = \omega(t), \tag{4.97}$$

$$U_{\min} \leq U(t) \leq U_{\max}, \tag{4.98}$$

where $\omega(t)$ is Gaussian white noise, $\mu \geq 0$ is a constant, $U_{\min} = 1.6$ m s^{-1} and $U_{\max} = 2.4$ m s^{-1} are chosen minimum and maximum magnitudes of the current velocity, respectively, and $\mu = 0$. The full current load is applied from $z = 0$ to 300 m, and thereafter linearly decline to $0.1U$ at $z = 1000$ m to obtain a depth-dependent ocean current profile $U(z, t)$. The hyperbolic tangent function smoothing modification with $\varepsilon_d = 1 \times 10^{-3}$ for the signum terms, $\overline{f}_s = 4 \times 10^6$ N, $\overline{f}_L = 1500$ N, and a rate limiter with time constant $\tau_c = 0.2$ has been applied to the following proposed controls.

Surface Vessel Control The surface vessel subjected to disturbance f_s is simulated under the action of backstepping control (4.13) with $u_{rs} = \tanh(z_2(t)/\varepsilon_d)\overline{f}_s$ and control gains $k_1 = 10.0$ and $k_2 = 5.0 \times 10^6$. The position, control, and disturbance on the surface vessel are shown in Fig. 4.11, where it can be observed that the backstepping control is able to position the vessel near its desired position at the origin.

Crane-Cable-Payload Subsystem Without Controls Under the action of the vessel control, the dynamics of the cable is simulated without control, and the spatial time representation is shown in Fig. 4.12. It can be seen that at $t = 200$ s, the subsea payload has deviated more than 30 m from the origin under the action of the distributed disturbance on the cable and the disturbance force acting on the payload due to the current.

SBLF Positioning Controls The positioning controls (4.44) and (4.54) developed using SBLF are simulated with crane desired position $b_{0d} = 0$ m, constraints $k_{0c} = 30$ m and $A_0 = 10$ m, control gains $\phi_0 = \phi_2 = \phi_3 = \phi_5 = 0.5$, $\phi_1 = \phi_4 = 5.0$, $u_{rblf} = \tanh(z_6/\varepsilon_d)\bar{f}_L$, subsea payload desired position $b_{Ld} = 10$ m, and constraints $k_{Lc} = 50$ m and $A_L = 30$ m. The spatial time representation is shown in Fig. 4.13, and the position, control, and tension at the top (crane) and bottom (subsea payload) boundaries are shown in Figs. 4.14 and 4.15, respectively. The designed

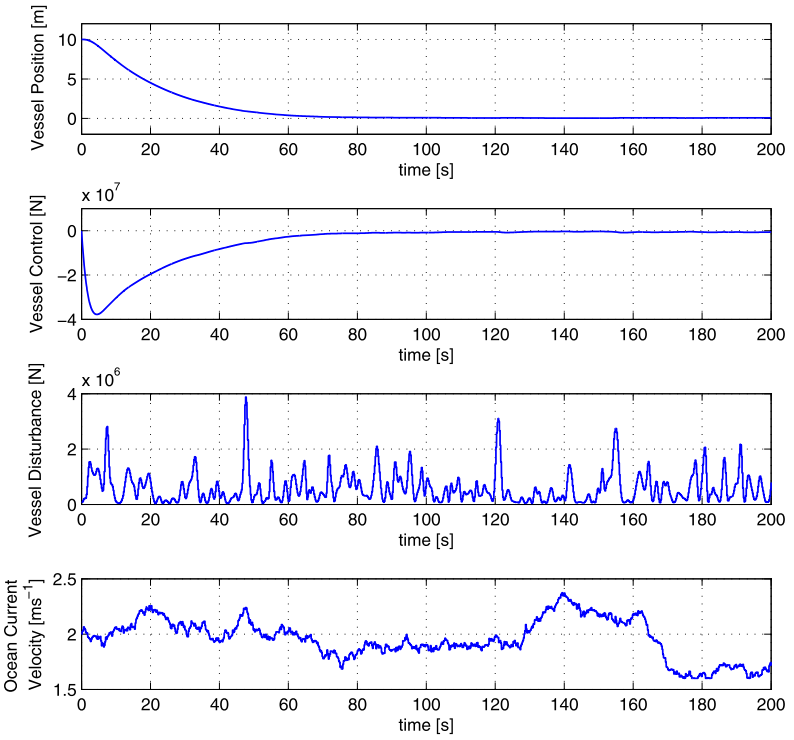

Fig. 4.11 (*Top*) Surface vessel position with desired position at the origin, (*center*) vessel control thrust, and (*bottom*) disturbance acting on the vessel

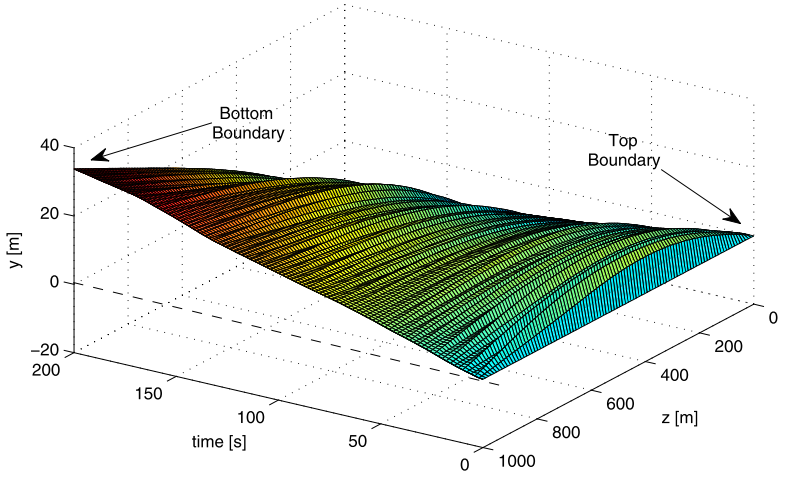

Fig. 4.12 Spatial-time representation of cable motions without control. The top boundary is at the crane, and the bottom boundary at the subsea payload

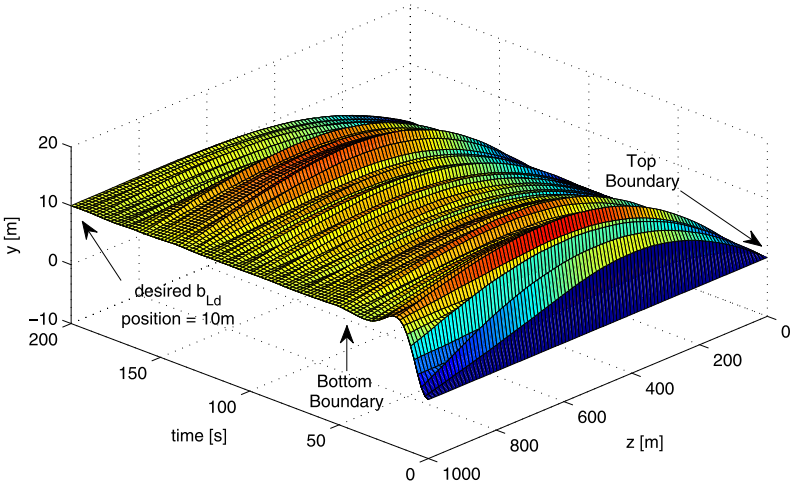

Fig. 4.13 Spatial-time representation of cable motions with positioning control. The top boundary is at the crane, and the bottom boundary is at the subsea payload, maintained at desired position $b_L = 10$ m

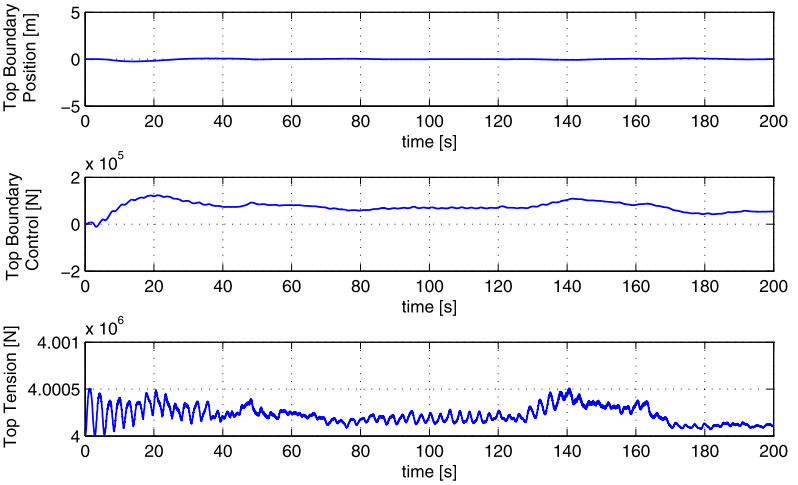

Fig. 4.14 (*Top*) Position of the crane with desired position at origin, (*center*) control force on the crane, and (*bottom*) tension at crane with position control (4.44)

control is able to keep the crane at the desired position, and the subsea payload position converges from the origin to the desired position when the system is subjected to the environmental disturbances.

Stabilizing Boundary Control The boundary controls (4.73) and (4.74) are simulated with $u_{rbc} = \tanh((\dot{y}(L,t) + \frac{3}{4}\gamma(L)y'(L,t))/\varepsilon_d)\overline{f}_L$, $k_0 = k_L = 1 \times 10^9$, and

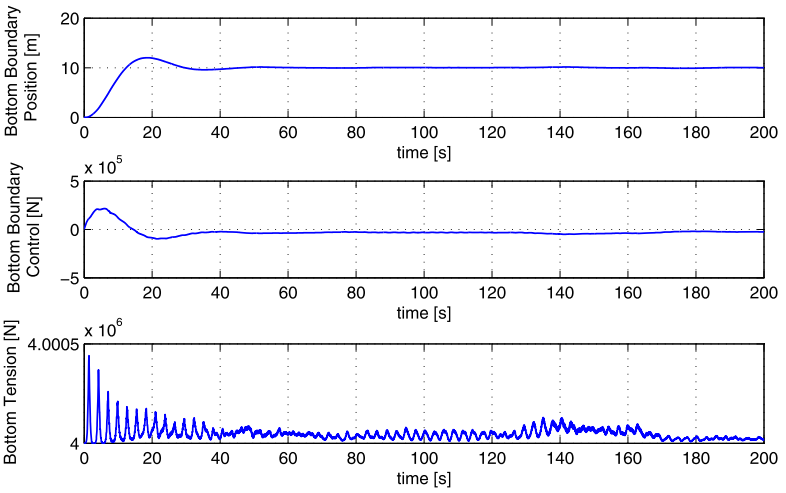

Fig. 4.15 (*Top*) Position of the payload with desired position at $B_{LD} = 10$ m, (*center*) control force, and (*bottom*) cable tension at subsea payload under positioning control (4.54)

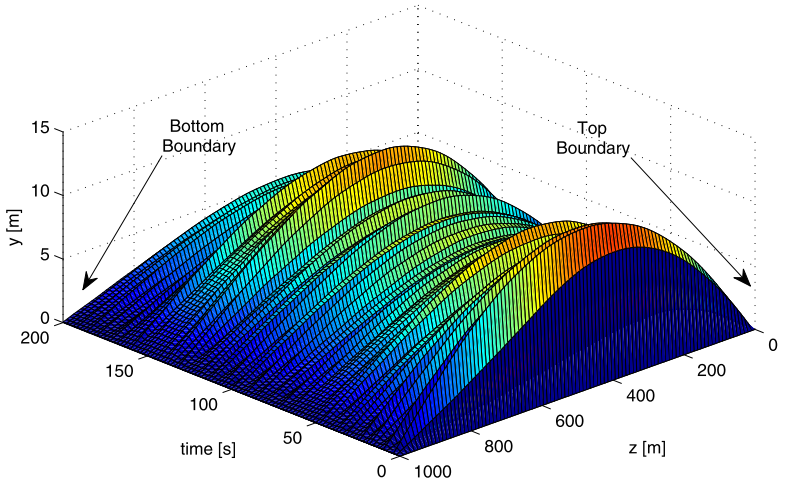

Fig. 4.16 Spatial-time representation of the cable motions control under stabilizing boundary controls (4.73) and (4.74)

$\gamma = 1 \times 10^{-3}$. The spatial time representation for the boundary control is shown in Fig. 4.16, and the position, control, and tension at the top (crane) and bottom (subsea payload) boundaries are shown in Figs. 4.17 and 4.18, respectively. From the simulations it is observed that the proposed boundary controls can stabilize the boundary at the origin under the influence of the disturbances.

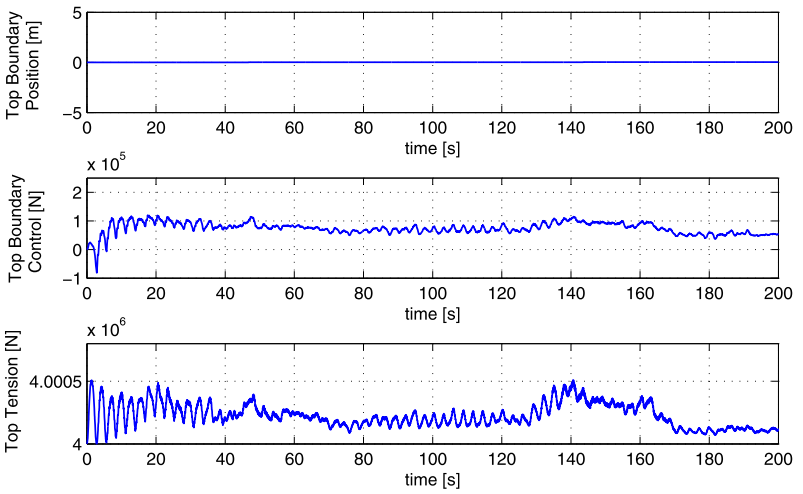

Fig. 4.17 (*Top*) Position of the crane, (*center*) control force on the crane, and (*bottom*) tension at crane with stabilizing boundary control (4.73)

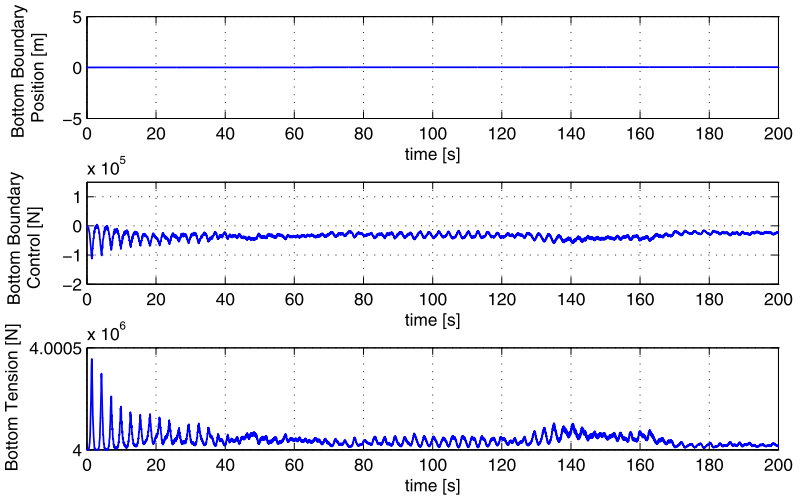

Fig. 4.18 (*Top*) Position of the payload, (*center*) control force on the payload, and (*bottom*) tension at payload with stabilizing boundary control (4.74)

4.5 Conclusion

In this chapter, the model of the coupled vessel, crane, cable, and payload with nonuniform parameters has been presented. Positioning controls have been derived for the coupled system with uniform parameters using barrier Lyapunov functions. Through Lyapunov analysis, it was shown that the coupled crane-payload flexible

system is stable under the control action, the physical limits from operations planning and safety specifications are not transgressed, and positioning of crane and payload is achieved. A stabilizing boundary control is proposed for the coupled system with nonuniform parameters. Rigorous Lyapunov stability analysis is carried out, and the uniform boundedness of the system was shown under the proposed control. Finally, the performance of the proposed controls have been illustrated through numerical simulations.

During the lowering operation on long lines, there can be very significant dynamic effects on the lift cable and load. The excitation caused by the motions of the surface vessel can be amplified with large oscillations and high dynamic tensile loads in the lifting line, which may result in breaking of the lifting cable. Considering the ship motions, control of longitudinal vibrations and tension to reduce the high dynamic tensile loads is desirable in ocean engineering. Due to the coupled effects, the control design and the direct proof for the Lyapunov stability are quite difficult. Boundary control on axially moving systems has been studied in [80, 105, 108, 116, 235], which may inspire the control design for the longitudinal vibrations of the flexible systems. Passive or active heave compensator can be incorporated following [236]. Coupled with the ship motions, heave control in the longitudinal direction to reduce the high dynamic tensile loads is desirable for safe and reliable operations. In the marine environment, the control longitudinal vibrations and tension are challenging due to the unpredictable ocean disturbances such as fluctuating currents and transmission of motions from the surface vessel through the lift cable.

In the simulations, the control is able to generate the adequate response for positioning the payload at the desired location within tight limits. For implementation, thruster performance needs to be included during the operation planning process such as weather window selection and safety considerations to ensure that the environmental forces are within operational limits and the required thrust is available for positioning.

Chapter 5
Marine Installation System

5.1 Introduction

The accurate position control for marine installation operations has gained increasing attention when the trend in the offshore industry is toward the deep water. Due to the requirements for high accuracy and efficiency arising from the modern ocean industry, improving reliability and efficiency of installation operations during oil and gas production in the ocean environment is a challenging research topic in offshore engineering. Traditional marine installation systems consist of the vessel dynamic positioning and crane manipulation to obtain the desired position and heading for the payload [1, 2]. Such methods become difficult in deeper waters due to the longer cable between the surface vessel and payload. The longer cable increases the natural periods of the cable and payload system, which in turn increase the effects of oscillations. One solution to alleviate the precision installation problem is the addition of thrusters attached the payload for the installation operation [7].

Such marine installation system consists of an ocean surface vessel, a flexible string-type cable, and a subsea payload to be positioned for installation on the ocean floor as depicted in Fig. 5.1. The surface vessel, to which the top boundary of the cable is connected, is equipped with a dynamic positioning system with an active thruster. The bottom boundary of the cable is a payload with an end-point thruster attached. This thruster is used for dynamic positioning of the payload. The total marine installation system is subjected to environmental disturbances including ocean current, wave, and wind. A cable that spans a long distance can produce large vibrations under relatively small disturbances, which can degrade the performance of the system and result in a larger offset from the target installation site. The control for the dynamic positioning of the payload is challenging due to the unpredictable exogenous disturbances such as fluctuating currents and transmission of motions from the surface vessel through the lift cable. Taking into account the unknown time-varying ocean disturbances of the cable leads to the appearance of oscillations, which make the control problem of the marine installation system relatively difficult. Current research [7] on the control of the marine installation systems focuses on the dynamics of the payload, where the dynamics of the cable is ignored for the

W. He et al., *Dynamics and Control of Mechanical Systems in Offshore Engineering*, Advances in Industrial Control, DOI 10.1007/978-1-4471-5337-5_5,

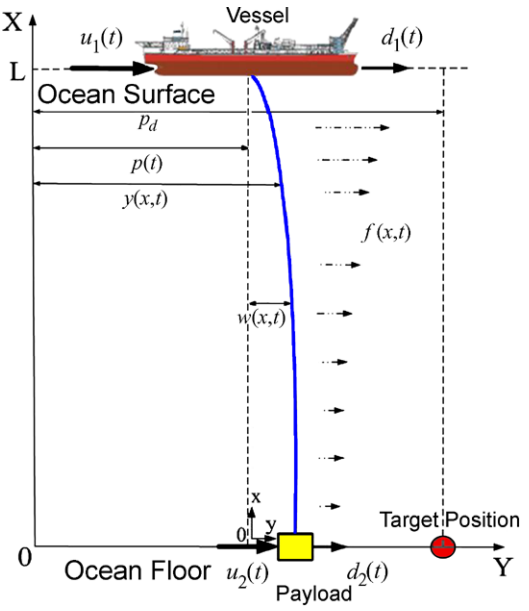

Fig. 5.1 A typical flexible marine installation system

convenience of the control design. The dynamics of the cable is considered as an external force term to the payload. In this chapter, all the dynamics of the vessel, cable, and payload are considered. The flexible marine installation system with cable, vessel, and payload dynamics is represented by a set of infinite-dimensional equations (i.e., PDEs describing the dynamics of the flexible cable) coupled with a set of finite-dimensional equations (i.e., ODEs describing the lumped vessel and payload dynamics).

For the marine installation system, the dynamic position control of the payload is as vital as the vibration suppression of the cable. Therefore, in the control design, it is necessary to consider both vibration suppression and the dynamic positioning. In the framework of boundary control, we are going to investigate the robust adaptive boundary control problem for the string-type model with system parametric uncertainty and under unknown time-varying ocean disturbance. The adaptive control design aims to compensate the effects of both parametric and disturbance uncertainties and achieve the uniform ultimate boundedness. In this chapter, we design the boundary control based on the distributed-parameter model of the flexible marine installation system. The stability analysis of the closed-loop system is based on Lyapunov's direct method without resorting to the semigroup theory or functional analysis. Although a flexible marine installation system is considered in this chapter specifically, the analysis and control design can be extended and applied for position control and vibration suppression for a class of mechanical string-type system exposed to undesirable distributed transverse loads. In this chapter, the dynamics of the vessel, payload, and vibration of the cable are considered in the dynamic analysis. The main contributions of this chapter include:

(i) The dynamic model of a flexible marine installation system subjected to ocean current disturbance is derived based on the Hamilton principle. The governing equation of the system is represented as a nonhomogeneous hyperbolic PDE with unknown disturbance term $f(x,t)$.
(ii) Two implementable boundary controllers at the top and bottom boundaries of the cable are designed to position the subsea payload to the desired set-point and suppress the cable's vibration. Robust adaptive boundary control is designed to compensate for the system parametric uncertainty and the effect of unknown time-varying distributed disturbance $f(x,t)$.
(iii) With the proposed boundary control, the uniform boundedness of the installation system under ocean disturbance is proved via Lyapunov synthesis. The control performance of the system is guaranteed by suitably choosing the design parameters.

The rest of the chapter is organized as follows. The governing equation (PDE) and boundary conditions (ODEs) of the flexible marine installation system are introduced by use of the Hamilton principle in Sect. 5.2. The boundary control design via Lyapunov's direct method is discussed separately for both exact model case and system parametric uncertainty case in Sect. 5.3, where it is shown that the uniform boundedness of the closed-loop system can be achieved by the proposed control. Simulations are carried out to illustrate performance of the proposed control in Sect. 5.4. The conclusion of this chapter is given in Sect. 5.5.

5.2 Problem Formulation

For the marine installation system shown in Fig. 5.1, the frame X–Y is the fixed inertia frame, and the frame x–y is the local reference frame fixed along the vertical direction of the surface vessel. The top boundary of the cable is at the vessel, and the bottom boundary of the cable is at the underwater payload. Forces from thrusters on the vessel and payload are the control inputs of the system, and the boundary position and slope of the cable are used as the feedback signals in the control design. p_d is the desired target position, $p(t)$ is the position of the vessel, $w(x,t)$ is the elastic transverse reflection with respect to frame x–y at the position x for time t, and $y(x,t) := p(t) + w(x,t)$ is the position of the cable with respect to frame X–Y at the position x for time t. Note that $w(L,t) = 0$ due to the connection between the vessel and the top boundary of the cable.

In this chapter, we only consider the transverse degree of freedom. We assume that the original position of the vessel is directly above the subsea payload with no horizontal offset, and the payload is filled with seawater.

The kinetic energy of the installation system E_k can be represented as

$$E_k = \frac{1}{2}M\left[\frac{\partial y(L,t)}{\partial t}\right]^2 + \frac{1}{2}\rho\int_0^L\left[\frac{\partial y(x,t)}{\partial t}\right]^2 dx + \frac{1}{2}m\left[\frac{\partial y(0,t)}{\partial t}\right]^2, \quad (5.1)$$

where x and t represent the independent spatial and time variables, respectively, M denotes the mass of the surface vessel, m denotes the mass of bottom payload, $y(L,t) = p(t)$, $\frac{\partial y(L,t)}{\partial t} = \frac{\partial p(t)}{\partial t}$, and $\frac{\partial^2 y(L,t)}{\partial t^2} = \frac{\partial^2 p(t)}{\partial t^2}$ are the position, velocity, and acceleration of the vessel, respectively, $\rho > 0$ is the uniform mass per unit length of the cable, and L is the length of the cable.

The potential energy E_p due to the strain energy of the cable can be obtained from

$$E_p = \frac{1}{2} T \int_0^L \left[\frac{\partial w(x,t)}{\partial x} \right]^2 dx, \tag{5.2}$$

where T is the tension of the cable. The definition of $y(x,t)$ yields $\frac{\partial y(x,t)}{\partial x} = \frac{\partial w(x,t)}{\partial x}$. Then we have

$$E_p = \frac{1}{2} T \int_0^L \left[\frac{\partial y(x,t)}{\partial x} \right]^2 dx. \tag{5.3}$$

The virtual work done by ocean current disturbance on the vessel, cable, and payload is given by

$$\delta W_f = \int_0^L f(x,t)\delta y(x,t)\, dx + d_1(t)\delta y(L,t) + d_2(t)\delta y(0,t), \tag{5.4}$$

where $f(x,t)$ is the distributed transverse load on the cable due to the hydrodynamic effects of the ocean current, wave, and wind, $d_1(t)$ denotes the environmental disturbances on the vessel, and $d_2(t)$ denotes the environmental disturbances on the paylaod. The virtual work done by damping on the vessel, cable, and payload is represented by

$$\begin{aligned} \delta W_d = &- \int_0^L c \frac{\partial y(x,t)}{\partial t} \delta y(x,t)\, dx - c_1 \frac{\partial y(L,t)}{\partial t} \delta y(L,t) \\ &- c_2 \frac{\partial y(0,t)}{\partial t} \delta y(0,t), \end{aligned} \tag{5.5}$$

where c is the distributed viscous damping coefficient of the cable, c_1 denotes the damping coefficient of the vessel, and c_2 denotes the damping coefficient for the payload. We introduce the control u_1 applied to the top boundary of the cable from the thruster attached in the vessel and the control u_2 applied to the bottom boundary of the cable from the thruster attached in the payload. The virtual work done by the boundary control is written as

$$\delta W_m = u_1(t)\delta w(L,t) + u_2(t)\delta w(0,t). \tag{5.6}$$

Then, we have the total virtual work done on the system as

$$\begin{aligned}\delta W &= \delta W_f + \delta W_d + \delta W_m \\ &= \int_0^L \left[f(x,t) - c\frac{\partial y(x,t)}{\partial t} \right] \delta y(x,t)\, dx \\ &\quad + \left[u_1(t) + d_1(t) - c_1 \frac{\partial y(L,t)}{\partial t} \right] \delta y(L,t) \\ &\quad + \left[u_2(t) + d_2(t) - c_2 \frac{\partial y(0,t)}{\partial t} \right] \delta y(0,t). \end{aligned} \tag{5.7}$$

Applying the Hamilton principle [193], we obtain the governing equation of the system as

$$\rho \ddot{y}(x,t) - T y''(x,t) + c\dot{y}(x,t) = f(x,t) \tag{5.8}$$

for $(x,t) \in (0,L) \times [0,\infty)$ and the boundary conditions of the system as

$$u_1(t) + d_1(t) - c_1 \dot{y}(L,t) - M\ddot{y}(L,t) - T y'(L,t) = 0, \tag{5.9}$$

$$u_2(t) + d_2(t) - c_2 \dot{y}(0,t) - m\ddot{y}(0,t) + T y'(0,t) = 0, \tag{5.10}$$

for $t \in [0,\infty)$.

Remark 5.1 With consideration of the distributed transverse load $f(x,t)$, the governing equation of the installation system, Eq. (5.8), is represented by a nonhomogeneous hyperbolic PDE. This model differs from the string system governed by a homogeneous PDE in [80, 98, 101–103, 105, 108, 110, 114, 116].

Assumption 5.2 For the distributed load $f(x,t)$ on the cable, the disturbance $d_1(t)$ on the vessel, and the disturbance $d_2(t)$ on the payload, we assume that there exist constants $\bar{f} \in \mathbb{R}^+$, $\bar{d}_1 \in \mathbb{R}^+$, and $\bar{d}_2 \in \mathbb{R}^+$, such that $|f(x,t)| \leq \bar{f}$ for all $(x,t) \in [0,L] \times [0,\infty)$, $|d_1(t)| \leq \bar{d}_1$ for all $t \in [0,\infty)$, and $|d_2(t)| \leq \bar{d}_2$ for all $t \in [0,\infty)$. This is a reasonable assumption as the time-varying disturbances $f(x,t)$, $d_1(t)$, and $d_2(t)$ have finite energy and hence are bounded, i.e., $f(x,t) \in \mathcal{L}_\infty([0,L])$, $d_1(t) \in \mathcal{L}_\infty$, and $d_2(t) \in \mathcal{L}_\infty$.

Remark 5.3 For control design in Sect. 5.3, only the assertion that there exist upper bounds on the disturbance in Assumption 5.2, $|f(x,t)| < \bar{f}$, $|d_1(t)| \leq \bar{d}_1$, and $|d_2(t)| \leq \bar{d}_2$, is necessary. The knowledge of the exact values for $f(x,t)$, $d_1(t)$, and $d_2(t)$ is not required. As such, different distributed load models up to various levels of fidelity, such as those found in [195, 196, 227–229], can be applied without affecting the control design or analysis.

Property 5.4 [237] If the kinetic energy of system (5.8)–(5.10), given by Eq. (5.1), is bounded for all $t \in [0,\infty)$, then $\dot{y}(x,t)$, $\dot{y}'(x,t)$, and $\dot{y}''(x,t)$ are bounded for all $(x,t) \in [0,L] \times [0,\infty)$.

Property 5.5 [237] If the potential energy of system (5.8)–(5.10), given by Eq. (5.3), is bounded for all $t \in [0, \infty)$, then $y'(x,t)$ and $y''(x,t)$ are bounded for all $(x,t) \in [0, L] \times [0, \infty)$.

5.3 Control Design

The control objective is to design boundary control to position the subsea payload to the desired set-point p_d and simultaneously suppress the vibrations of the cable in the presence of the time-varying ocean disturbance. The control forces $u_1(t)$ and $u_2(t)$ are from the thruster in the vessel and the thruster attached in the subsea payload, respectively. In this section, the Lyapunov direct method is used to construct boundary control $u_1(t)$ and $u_2(t)$ at the top and bottom boundaries of the cable and to analyze the stability of the closed-loop system.

In this chapter, we analyze two cases for the flexible marine installation system: (i) exact model-based control, i.e., T, m, and c_2 are all known; and (ii) adaptive control for the system parametric uncertainty, i.e., T, m, and c_2 are unknown. For the first case, robust boundary control is introduced for the exact model of the installation system subjected to ocean disturbance. For the second case where the system parameters cannot be directly measured, the adaptive control is designed to compensate the system parametric uncertainty.

5.3.1 Exact Model-Based Boundary Control of the Installation System

To stabilize the system given by governing Eq. (5.8) and boundary conditions, Eqs. (5.9) and (5.10), we propose the following boundary control:

$$u_1(t) = -k_q y(L,t) - k_v \dot{y}(L,t) - \operatorname{sgn}\big[\dot{y}(L,t)\big]\bar{d}_1, \tag{5.11}$$

$$u_2(t) = -k_p\big(y(0,t) - p_d\big) - k_s u_a(t) - T y'(0,t) + m\dot{y}'(0,t) + c_2\dot{y}(0,t) - \operatorname{sgn}(u_a)\bar{d}_2, \tag{5.12}$$

where $\operatorname{sgn}(\cdot)$ denotes the signum function, k_q, k_v, k_p, and k_s are the positive control gains, and the auxiliary signal u_a is defined as

$$u_a(t) = \dot{y}(0,t) - y'(0,t). \tag{5.13}$$

After differentiating the auxiliary signal, Eq. (5.13), multiplying the resulting equation by m, and substituting Eq. (5.10), we obtain

$$m\dot{u}_a(t) = T y'(0,t) + d_2(t) - m\dot{y}'(0,t) - c_2\dot{y}(0,t) + u_2(t). \tag{5.14}$$

Substituting Eq. (5.12) into Eq. (5.14), we have

$$m\dot{u}_a(t) = -k_s u_a(t) - k_p\big(y(0,t) - p_d\big) + d_2(t) - \mathrm{sgn}(u_a)\bar{d}_2. \tag{5.15}$$

Remark 5.6 The proposed boundary control does not require distributed sensing, and all the signals in the boundary control can be measured by sensors or obtained by a backward difference algorithm. $y(L,t)$ and $y(0,t)$ can be sensed by two the global positioning systems (GPS) located in the vessel and the end-point thruster, respectively. $y'(0,t)$ can be measured by an inclinometer at the bottom boundary of the cable. For the exact model-based boundary control (5.12), the tension of the cable can be measured via a force sensor. In practice, the effect of measurement noise from sensors is unavoidable, which will affect the controller implementation, especially when the high-order differentiating terms with respect to time exist. In our proposed controller (5.11) and (5.12), $\dot{y}(L,t)$, $\dot{y}(0,t)$, and $\dot{y}'(0,t)$ with only one time differentiation with respect to time can be calculated with a backward difference algorithm.

Remark 5.7 The control design is based on the distributed-parameter model, Eqs. (5.8) to (5.10), and the spillover problems associated with traditional truncated model-based approaches caused by ignoring high-frequency modes in controller and observer design are avoided.

Consider the Lyapunov function candidate

$$V = V_1 + V_2 + \Delta, \tag{5.16}$$

where the energy term V_1, auxiliary term V_2, and small crossing term Δ are defined as

$$V_1 = \frac{\beta}{2}\rho\int_0^L [\dot{y}]^2\,dx + \frac{\beta}{2}T\int_0^L \big[y'\big]^2\,dx + \frac{\beta}{2}M\big[\dot{y}(L,t)\big]^2 + \frac{\beta k_p}{2}\big[y(0,t) - p_d\big]^2 + \frac{\beta k_q}{2}\big[y(L,t)\big]^2, \tag{5.17}$$

$$V_2 = \frac{1}{2}mu_a^2, \tag{5.18}$$

$$\Delta = \alpha\rho\int_0^L (x-L)\dot{y}y'\,dx, \tag{5.19}$$

where α and β are two positive weighting constants.

Lemma 5.8 *The Lyapunov function candidate given by* (5.16)*, can be upper and lower bounded as*

$$0 \le \lambda_1(V_1 + V_2) \le V \le \lambda_2(V_1 + V_2), \tag{5.20}$$

where λ_1 *and* λ_2 *are two positive constants defined as*

$$\lambda_1 = 1 - \frac{2\alpha\rho L}{\min(\beta\rho, \beta T)} > 0, \tag{5.21}$$

$$\lambda_2 = 1 + \frac{2\alpha\rho L}{\min(\beta\rho, \beta T)} > 1, \tag{5.22}$$

provided that

$$\alpha < \frac{\min(\beta\rho, \beta T)}{2\rho L}. \tag{5.23}$$

Proof Substituting inequality (2.11) into Eq. (5.19) yields

$$\begin{aligned} |\Delta| &\le \alpha\rho L \int_0^L \left([y']^2 + [\dot{y}]^2 \right) dx \\ &\le \alpha_1 V_1, \end{aligned} \tag{5.24}$$

where

$$\alpha_1 = \frac{2\alpha\rho L}{\min(\beta\rho, \beta T)}. \tag{5.25}$$

Then, we obtain

$$-\alpha_1 V_1 \le \Delta \le \alpha_1 V_1. \tag{5.26}$$

If α is a small positive weighting constant satisfying $0 < \alpha < \frac{\min(\beta\rho, \beta T)}{2\rho L}$, then we obtain

$$\alpha_2 = 1 - \alpha_1 = 1 - \frac{2\alpha\rho L}{\min(\beta\rho, \beta T)} > 0, \tag{5.27}$$

$$\alpha_3 = 1 + \alpha_1 = 1 + \frac{2\alpha\rho L}{\min(\beta\rho, \beta T)} > 1. \tag{5.28}$$

Then, we further have

$$0 \le \alpha_2 V_1 \le V_1 + \Delta \le \alpha_3 V_1. \tag{5.29}$$

Given the Lyapunov function candidate in Eq. (5.16), we obtain

$$0 \le \lambda_1 (V_1 + V_2) \le V \le \lambda_2 (V_1 + V_2), \tag{5.30}$$

where $\lambda_1 = \min(\alpha_2, 1) = \alpha_2$ and $\lambda_2 = \max(\alpha_3, 1) = \alpha_3$ are positive constants. □

Lemma 5.9 *The time derivative of the Lyapunov function in* (5.16) *can be upper bounded with*

$$\dot{V} \leq -\lambda V + \varepsilon, \tag{5.31}$$

where λ *and* ε *are two positive constants.*

Proof Differentiating Eq. (5.16) with respect to time leads to

$$\dot{V} = \dot{V}_1 + \dot{V}_2 + \dot{\Delta}. \tag{5.32}$$

The first term of Eq. (5.32)

$$\dot{V}_1 = A_1 + A_2 + \beta M \ddot{y}(L,t)\dot{y}(L,t) + \beta k_p\big(y(0,t) - p_d\big)\dot{y}(0,t), \tag{5.33}$$

where

$$A_1 = \beta\rho \int_0^L \dot{y}\ddot{y}\, dx, \tag{5.34}$$

$$A_2 = \beta T \int_0^L y'\dot{y}'\, dx. \tag{5.35}$$

Substituting the governing equation (5.8) into A_1, we obtain

$$A_1 = \beta \int_0^L \dot{y}\big(Ty'' + f - c\dot{y}\big)\, dx. \tag{5.36}$$

Using the boundary conditions and integrating Eq. (5.35) by parts, we obtain

$$\begin{aligned} A_2 &= \beta T \int_0^L y' d(\dot{y}) \\ &= \beta T y'(L,t)\dot{y}(L,t) - \beta T y'(0,t)\dot{y}(0,t) - \beta T \int_0^L \dot{y}y''\, dx. \end{aligned} \tag{5.37}$$

Substituting Eqs. (5.36) and (5.37) into Eq. (5.33), we have

$$\begin{aligned} \dot{V}_1 = {} & \beta T y'(L,t)\dot{y}(L,t) - \beta T y'(0,t)\dot{y}(0,t) - \beta c \int_0^L [\dot{y}]^2\, dx + \beta \int_0^L f\dot{y}\, dx \\ & + \beta M \ddot{y}(L,t)\dot{y}(L,t) + \beta k_p\big[y(0,t) - p_d\big]\dot{y}(0,t) \\ & + \beta k_q y(L,t)\dot{y}(L,t). \end{aligned} \tag{5.38}$$

Substituting Eqs. (5.9) and (5.13) into Eq. (5.38), we obtain

$$\dot{V}_1 = -\frac{\beta T}{2}\left[\left[\dot{y}(0,t)\right]^2 + \left[y'(0,t)\right]^2\right] + \frac{\beta T}{2}u_a^2 + \beta\left[u_1 + d_1 - c_1\dot{y}(L,t)\right]\dot{y}(L,t)$$
$$- \beta c\int_0^L [\dot{y}]^2\,dx + \beta\int_0^L f\dot{y}\,dx + \beta k_p\big(y(0,t) - p_d\big)\dot{y}(0,t)$$
$$+ \beta k_q y(L,t)\dot{y}(L,t). \tag{5.39}$$

Substituting Eq. (5.11) and using inequality (2.12), we obtain

$$\dot{V}_1 \le -\frac{\beta T}{2}\left[\left[\dot{y}(0,t)\right]^2 + \left[y'(0,t)\right]^2\right] + \frac{\beta T}{2}u_a^2 - \beta(k_v + c_1)\left[\dot{y}(L,t)\right]^2$$
$$- \beta(c - \delta_2)\int_0^L [\dot{y}]^2\,dx + \frac{\beta}{\delta_2}\int_0^L f^2\,dx + \frac{\beta k_p}{2\delta_1}\left[y(0,t) - p_d\right]^2$$
$$+ \frac{\beta k_p\delta_1}{2}\left[\dot{y}(0,t)\right]^2, \tag{5.40}$$

where δ_1 and δ_2 are positive constants.

The second term of Eq. (5.32) can be rewritten as

$$\dot{V}_2 = mu_a\dot{u}_a,$$
$$\le -k_s u_a^2 + k_p u_a^2 - k_p\left[y(0,t) - p_d\right]^2 + 8k_p L\int_0^L \left[y'\right]^2 dx + 8k_p\left[y(L,t)\right]^2$$
$$+ 4k_p p_d^2, \tag{5.41}$$

where inequalities (2.11) and (2.15) are employed. We obtain the third term of Eq. (5.32) as

$$\dot{\Delta} = \alpha\rho\int_0^L \left((x-L)\ddot{y}y' + (x-L)\dot{y}\dot{y}'\right)dx$$
$$= \alpha\int_0^L (x-L)y'\left[Ty'' + f - c\dot{y}\right]dx + \alpha\rho\int_0^L (x-L)\dot{y}\dot{y}'\,dx. \tag{5.42}$$

After integrating Eq. (5.42) by parts and using the boundary conditions, we obtain

$$\dot{\Delta} \le \frac{\alpha TL}{2}\left[y'(0,t)\right]^2 - \frac{\alpha T}{2}\int_0^L \left[y'\right]^2 dx + \frac{\alpha L}{\delta_3}\int_0^L f^2\,dx + \alpha L\delta_3\int_0^L \left[y'\right]^2 dx$$
$$+ \frac{\alpha cL}{\delta_4}\int_0^L [\dot{y}]^2\,dx + \alpha cL\delta_4\int_0^L \left[y'\right]^2 dx + \frac{\alpha\rho L}{2}\left[\dot{y}(0,t)\right]^2$$
$$- \frac{\alpha\rho}{2}\int_0^L [\dot{y}]^2\,dx, \tag{5.43}$$

where δ_3 and δ_4 are positive constants. Substituting Eqs. (5.40), (5.41), and (5.43) into Eq. (5.16), we obtain

$$\begin{aligned}\dot{V} \leq & -\left(\beta c + \frac{\alpha\rho}{2} - \frac{\alpha c L}{\delta_4}\right)\int_0^L [\dot{y}]^2\,dx - \beta\delta_2 - \beta(k_v + c_1)\big[\dot{y}(L,t)\big]^2 \\ & - \left(\frac{\alpha T}{2} - 16k_p L - \alpha L\delta_3 - \alpha c L\delta_4\right)\int_0^L \big[y'\big]^2\,dx \\ & - \left(k_s - k_p - \frac{\beta T}{2}\right)u_a^2 - \left(\frac{\beta T}{2} - \frac{\alpha\rho L}{2} - \frac{\beta k_p\delta_1}{2}\right)\big[\dot{y}(0,t)\big]^2 \\ & - \left(\frac{\beta T}{2} - \frac{\alpha T L}{2}\right)\big[y'(0,t)\big]^2 - k_p\left(1 - \frac{\beta}{2\delta_1}\right)\big[y(0,t) - p_d\big]^2 \\ & + \left(\frac{\beta}{\delta_2} + \frac{\alpha L}{\delta_3}\right)\int_0^L \bar{f}^2\,dx + 4k_p p_d^2 + 8k_p\big[y(L,t)\big]^2 \\ \leq & -\lambda_3(V_1 + V_2) + \varepsilon, \end{aligned} \tag{5.44}$$

where the constants k_s, k_v, k_p, k_q, α, β, δ_1, δ_2, δ_3, and δ_4 are chosen to satisfy the following conditions:

$$\alpha < \frac{\min(\beta\rho, \beta T)}{2\rho L}, \tag{5.45}$$

$$\frac{\beta T}{2} - \frac{\alpha\rho L}{2} - \frac{\beta k_p\delta_1}{2} \geq 0, \tag{5.46}$$

$$\frac{\beta T}{2} - \frac{\alpha T L}{2} \geq 0, \tag{5.47}$$

$$\sigma_1 = \beta c + \frac{\alpha\rho}{2} - \beta\delta_2 - \frac{\alpha c L}{\delta_4} > 0, \tag{5.48}$$

$$\sigma_2 = \frac{\alpha T}{2} - 16k_p L - \alpha L\delta_3 - \alpha c L\delta_4 > 0, \tag{5.49}$$

$$\sigma_3 = \beta(k_v + c_1) > 0, \tag{5.50}$$

$$\sigma_4 = 1 - \frac{\beta}{2\delta_1} > 0, \tag{5.51}$$

$$\sigma_5 = k_s - k_p - \frac{\beta T}{2} > 0, \tag{5.52}$$

$$\sigma_6 = 8k_p > 0, \tag{5.53}$$

$$\lambda_3 = \min\left(\frac{2\sigma_1}{\beta\rho}, \frac{2\sigma_2}{\beta T}, \frac{2\sigma_3}{\beta M}, \frac{2\sigma_4}{\beta}, \frac{2\sigma_5}{m}, \frac{2\sigma_6}{\beta k_q}\right) > 0, \tag{5.54}$$

$$\varepsilon = \left(\frac{\beta}{\delta_2} + \frac{\alpha L}{\delta_3}\right)\int_0^L \bar{f}^2\,dx + 4k_p p_d^2 \in \mathcal{L}_\infty. \tag{5.55}$$

From inequalities (5.30) and (5.44) we have

$$\dot{V} \leq -\lambda V + \varepsilon, \tag{5.56}$$

where $\lambda = \lambda_3/\lambda_2$ and ε are positive constants. □

With the above lemmas, the exact model-based control design for the flexible marine installation system subjected to ocean current disturbance can be summarized in the following theorem.

Theorem 5.10 *For the system dynamics described by* (5.8) *and boundary conditions* (5.9)–(5.10), *under Assumption* 5.2 *and the boundary control* (5.11) *and* (5.12), *given that the initial conditions are bounded, the transverse reflection* $w(x,t)$ *of the closed-loop system is uniformly bounded, and the system boundary error signal* $e(t) = y(0,t) - p_d$ *remains within the compact set* Ω *defined by*

$$\Omega := \big\{ e \in R \mid |e| \leq D \big\}, \tag{5.57}$$

where $D = \sqrt{\frac{2}{\beta k_p \lambda_1}(V(0) + \frac{\varepsilon}{\lambda})}$.

Proof Multiplying Eq. (5.31) by $e^{\lambda t}$ yields

$$\frac{\partial}{\partial t}\big(V e^{\lambda t}\big) \leq \varepsilon e^{\lambda t}. \tag{5.58}$$

Integrating the above inequality, we obtain

$$V \leq \left(V(0) - \frac{\varepsilon}{\lambda}\right)e^{-\lambda t} + \frac{\varepsilon}{\lambda} \leq V(0)e^{-\lambda t} + \frac{\varepsilon}{\lambda} \in \mathcal{L}_\infty, \tag{5.59}$$

which implies that V is bounded. Using inequality (2.15) and Eq. (5.17), we have

$$\begin{aligned} \frac{\beta}{2L} T w^2(x,t) &\leq \frac{\beta}{2} T \int_0^L \big[w'(x,t)\big]^2 dx = \frac{\beta}{2} T \int_0^L \big[y'(x,t)\big]^2 dx \\ &\leq V_1 \leq V_1 + V_2 \leq \frac{1}{\lambda_1} V. \end{aligned} \tag{5.60}$$

Appropriately rearranging the terms of the above inequality (5.60), we obtain that $w(x,t)$ is uniformly bounded as follows:

$$\big|w(x,t)\big| \leq \sqrt{\frac{2L}{\beta T \lambda_1}\left(V(0)e^{-\lambda t} + \frac{\varepsilon}{\lambda}\right)} \quad \forall (x,t) \in [0,L] \times [0,\infty). \tag{5.61}$$

Combining Eq. (5.17) and inequality (5.60) yields

$$\frac{\beta k_p}{2}\big[y(0,t) - p_d\big]^2 \leq V_1 \leq V_1 + V_2 \leq \frac{1}{\lambda_1} V \in \mathcal{L}_\infty, \tag{5.62}$$

$$\left|y(0,t)-p_d\right| \leq \sqrt{\frac{2}{\beta k_p \lambda_1}\left(V(0)e^{-\lambda t}+\frac{\varepsilon}{\lambda}\right)} \quad \forall t \in [0,\infty). \quad \square \quad (5.63)$$

Remark 5.11 In the above analysis, the deflection of the cable $w(x,t)$ can be made smaller, provided that the design control parameters are appropriately selected. By choosing the proper values of α and β, it is shown that the increase in the control gains k_v and k_s will result in larger σ_3 and σ_5, which will lead to a greater λ_3. Then the value of λ will increase, which will reduce the size of Ω and bring a better vibration suppression performance.

Remark 5.12 Even though $y(0,t)$ may be far from the desired position p_d, it is guaranteed that the steady bottom boundary state error $y(0,\infty)-p_d$ can be made smaller, provided that the design parameters are appropriately selected. It is easily seen that the increase in the control gains k_v and k_s will result in a better tracking performance. However, increasing k_v and k_s will lead to a high-gain control scheme. Therefore, in practical applications, the design parameters should be adjusted carefully for achieving suitable transient performance and control action.

Remark 5.13 From Eq. (5.60) we can state that V_1 and V_2 are bounded for all $t \in [0,\infty)$. The boundedness of V_1 and V_2 implies that $\dot{y}(x,t)$, $y'(x,t)$ are bounded for all $(x,t) \in [0,L] \times [0,\infty)$ and u_a is bounded for all $t \in [0,\infty)$. Then, we can obtain that the potential energy, Eq. (5.3), is bounded. Using Property 5.5, we can further obtain that $y''(x,t)$ is bounded for all $t \in [0,\infty)$. From the boundedness of $\dot{y}(x,t)$ we can state that $\dot{y}(0,t)$ and $\dot{y}(L,t)$ are bounded for all $t \in [0,\infty)$. Therefore, we can conclude that the kinetic energy of the system in Eq. (5.1) is also bounded for all $t \in [0,\infty)$. Using Property 5.4, we can obtain that $\dot{y}(x,t)$ and $\dot{y}'(x,t)$ are also bounded for all $(x,t) \in [0,L] \times [0,\infty)$. Applying Assumption 5.2, Eq. (5.8), and the above statements, we can state that $\ddot{y}(x,t)$ is also bounded for all $(x,t) \in [0,L] \times [0,\infty)$. From the above information we see that the proposed controls (5.11) and (5.12) ensure that all internal system signals including $w(x,t)$, $y'(x,t)$, $\dot{y}(x,t)$, $\dot{y}'(x,t)$, and $\ddot{y}(x,t)$ are uniformly bounded. Since $y'(x,t)$, $\dot{y}(x,t)$, and $\dot{y}'(x,t)$ are all bounded for all $(x,t) \in [0,L] \times [0,\infty)$, we can conclude that the boundary controls (5.11) and (5.12) are also bounded for all $t \in [0,\infty)$.

5.3.2 Robust Adaptive Boundary Control for System Parametric Uncertainty

The previous exact model-based boundary control Eq. (5.11) requires the exact knowledge of the marine installation system. Adaptive boundary control is designed to improve the performance of the system via parameter estimation when the system parameters are unknown. The exact model-based boundary control provides a stepping stone toward the adaptive control, which is designed to deal with the system

parametric uncertainty. In this section, the previous boundary control is redesigned by using adaptive control when T, m, and c_2 are all unknown. We rewrite Eq. (5.14) in the following form:

$$m\dot{u}_a = P\Phi + d_2 + u_2, \tag{5.64}$$

where the vectors P and Φ are defined as

$$P = \begin{bmatrix} y'(0,t) & -\dot{y}'(0,t) & -\dot{y}(0,t) \end{bmatrix}, \tag{5.65}$$

$$\Phi = [T \quad m \quad c_2]^T. \tag{5.66}$$

We propose the following adaptive boundary control for the system:

$$u_1 = -k_q y(L,t) - k_v \dot{y}(L,t) - \operatorname{sgn}\big[\dot{y}(L,t)\big]\bar{d}_1, \tag{5.67}$$

$$u_2 = -P\hat{\Phi} - k_s u_a - \operatorname{sgn}(u_a)\bar{d}_2 - k_p\big(y(0,t) - p_d\big), \tag{5.68}$$

where the parameter estimate vector $\hat{\Phi}$ is defined as

$$\hat{\Phi} = [\hat{T} \quad \hat{m} \quad \hat{c}_2]^T. \tag{5.69}$$

The adaptation law is designed as

$$\dot{\hat{\Phi}} = \Gamma P^T u_a - r\Gamma\hat{\Phi}, \tag{5.70}$$

where $\Gamma \in \mathbb{R}^{3\times 3}$ is a diagonal positive-definite matrix, and r is a positive constant. We assume that all the eigenvalues of Γ are real and positive, and denote by $\lambda_{\max}$ and $\lambda_{\min}$ the maximum and minimum eigenvalues of Γ, respectively. The parameter estimate error vector $\tilde{\Phi} \in \mathbb{R}^3$ is defined as

$$\tilde{\Phi} = \Phi - \hat{\Phi}. \tag{5.71}$$

Substituting Eq. (5.68) into Eq. (5.64) and substituting Eq. (5.71) into Eq. (5.70), we have

$$m\dot{u}_a = P\tilde{\Phi} - k_s u_a + d_2 - \operatorname{sgn}(u_a)\bar{d}_2 - k_p\big(y(0,t) - p_d\big), \tag{5.72}$$

$$\dot{\tilde{\Phi}} = -\Gamma P^T u_a + r\Gamma\hat{\Phi}. \tag{5.73}$$

Remark 5.14 For the proposed adaptive control (5.68), the parameter estimation term, signum term, and auxiliary signal term are introduced to compensate the system parametric uncertainty and the effect of unknown time-varying distributed disturbance. The controls (5.67) and (5.68) are independent of system parameters, and the knowledge of the exact values of disturbance $f(x,t)$, $d_1(t)$, and $d_2(t)$ is not required, thus possessing stability robustness to variations in system parameters and unknown disturbance.

Consider the Lyapunov function candidate

$$V_a = V + \frac{1}{2}\tilde{\Phi}^T \Gamma^{-1} \tilde{\Phi}, \tag{5.74}$$

where V is defined in Eq. (5.16).

Lemma 5.15 *The Lyapunov function candidate given by* (5.74) *can be upper and lower bounded as*

$$0 \leq \lambda_{1a}\big(V_1 + V_2 + \|\tilde{\Phi}\|^2\big) \leq V_a \leq \lambda_{2a}\big(V_1 + V_2 + \|\tilde{\Phi}\|^2\big), \tag{5.75}$$

where λ_{1a} *and* λ_{2a} *are two positive constants defined as*

$$\lambda_{1a} = \min\left(1 - \frac{2\alpha\rho L}{\min(\beta\rho, \beta T)}, \frac{1}{2\lambda_{\max}}\right), \tag{5.76}$$

$$\lambda_{2a} = \max\left(1 + \frac{2\alpha\rho L}{\min(\beta\rho, \beta T)}, \frac{1}{2\lambda_{\min}}\right). \tag{5.77}$$

Proof From inequality (5.20) we have

$$\lambda_1(V_1 + V_2) \leq V \leq \lambda_2(V_1 + V_2), \tag{5.78}$$

where λ_1 and λ_2 are positive constants defined in Eqs. (5.21) and (5.22). Using the properties of matrix Γ and Lemma 2.6, we have

$$\frac{1}{2\lambda_{\max}}\|\tilde{\Phi}\|^2 \leq \frac{1}{2}\tilde{\Phi}^T \Gamma^{-1} \tilde{\Phi} \leq \frac{1}{2\lambda_{\min}}\|\tilde{\Phi}\|^2. \tag{5.79}$$

Combining inequalities (5.78) and (5.79), we have

$$0 \leq \lambda_{1a}\big(V_1 + V_2 + \|\tilde{\Phi}\|^2\big) \leq V_a \leq \lambda_{2a}\big(V_1 + V_2 + \|\tilde{\Phi}\|^2\big), \tag{5.80}$$

where $\lambda_{1a} = \min(\alpha_2, \frac{1}{2\lambda_{\max}})$ and $\lambda_{2a} = \max(\alpha_3, \frac{1}{2\lambda_{\min}})$ are positive constants. □

Lemma 5.16 *The time derivative of the Lyapunov function in* (5.74) *can be upper bounded with*

$$\dot{V}_a \leq -\lambda_a V_a + \psi, \tag{5.81}$$

where λ_a *and* ψ *are positive constants.*

Proof We obtain the time derivative of the Lyapunov function candidate in Eq. (5.74) as

$$\dot{V}_a = \dot{V} + \tilde{\Phi}^T \Gamma^{-1} \dot{\tilde{\Phi}}. \tag{5.82}$$

Substituting Eq. (5.72) into the second term of Eq. (5.32), we have

$$\begin{aligned}\dot{V}_2 &= m u_a \dot{u}_a \\ &\le -k_s u_a^2 + k_p u_a^2 - k_p \big[y(0,t) - p_d\big]^2 \\ &\quad + 16 k_p L \int_0^L \big[y'\big]^2 dx + 4 k_p p_d^2 + P\tilde{\Phi} u_a. \end{aligned} \tag{5.83}$$

Applying the results of Lemma 5.9 and substituting Eqs. (5.40), (5.83), and (5.43) into Eq. (5.16), we obtain

$$\dot{V} \le -\lambda_3 (V_1 + V_2) + P\tilde{\Phi} u_a + \varepsilon, \tag{5.84}$$

where λ_3 is defined in Eq. (5.54), and ε is defined in Eq. (5.52). Substituting inequalities (5.84) into Eq. (5.82) yields

$$\dot{V}_a \le -\lambda_3 (V_1 + V_2) + \tilde{\Phi}^T \big(P^T u_a + \Gamma^{-1} \dot{\tilde{\Phi}}\big) + \varepsilon. \tag{5.85}$$

Substituting Eq. (5.73) into Eq. (5.85), we have

$$\begin{aligned}\dot{V}_a &\le -\lambda_3 (V_1 + V_2) + r\tilde{\Phi}^T \hat{\Phi} + \varepsilon \\ &\le -\lambda_3 (V_1 + V_2) - \frac{r}{2} \|\tilde{\Phi}\|^2 + \frac{r}{2} \|\Phi\|^2 + \varepsilon \\ &\le -\lambda_{3a} \big(V_1 + V_2 + \|\tilde{\Phi}\|^2\big) + \frac{r}{2} \|\Phi\|^2 + \varepsilon, \end{aligned} \tag{5.86}$$

where $\lambda_{3a} = \min(\lambda_3, \frac{r}{2})$ is a positive constant. From inequalities (5.80) and (5.86) we have

$$\dot{V}_a \le -\lambda_a V_a + \psi, \tag{5.87}$$

where $\lambda_a = \lambda_{3a}/\lambda_{2a}$ and $\psi = \frac{r}{2} \|\Phi\|^2 + \varepsilon > 0$.

With the above lemmas, the adaptive control design for the marine installation system subjected to ocean current disturbance can be summarized in the following theorem. □

Theorem 5.17 *For the system dynamics described by* (5.8) *and boundary conditions* (5.9)–(5.10), *under Assumption* 5.2, *with the boundary controls* (5.67) *and* (5.68) *and the adaptation law* (5.70), *given that the initial conditions are bounded, the closed-loop system is uniformly bounded, and the system boundary error signal* $e(t) = y(0,t) - p_d$ *remains within the compact set* Ω_a *defined by*

$$\Omega_a := \big\{ e \in R \mid |e| \le D_a \big\}, \tag{5.88}$$

where $D_a = \sqrt{\frac{2}{\beta k_p \lambda_{1a}} (V_a(0) + \frac{\psi}{\lambda_a})}$.

Proof Multiplying Eq. (5.81) by $e^{\lambda_a t}$ yields

$$\frac{\partial}{\partial t}\left(V_a e^{\lambda_a t}\right) \leq \delta e^{\lambda_a t}. \tag{5.89}$$

Integrating the above inequality, we obtain

$$V_a \leq \left(V_a(0) - \frac{\psi}{\lambda_a}\right)e^{-\lambda_a t} + \frac{\psi}{\lambda_a} \leq V_a(0)e^{-\lambda_a t} + \frac{\psi}{\lambda_a} \in \mathcal{L}_\infty, \tag{5.90}$$

which implies that V_a is bounded. Using inequality (2.15) and Eq. (5.17), we have

$$\begin{aligned}\frac{\beta}{2L}Tw^2(x,t) \leq \frac{\beta}{2}T\int_0^L \left[w'(x,t)\right]^2 dx = \frac{\beta}{2}T\int_0^L \left[y'(x,t)\right]^2 dx \leq V_1 \\ \leq V_1 + V_2 \leq \frac{1}{\lambda_{1a}}V_a.\end{aligned} \tag{5.91}$$

Appropriately rearranging the terms of the above inequality, we obtain that $w(x,t)$ is uniformly bounded as follows:

$$\left|w(x,t)\right| \leq \sqrt{\frac{2L}{\beta T\lambda_{1a}}\left(V_a(0)e^{-\lambda_a t} + \frac{\psi}{\lambda_a}\right)} \quad \forall (x,t) \in [0,L]\times[0,\infty). \tag{5.92}$$

Combining Eq. (5.17) and inequality (5.56) yields

$$\frac{\beta k_p}{2}\left[y(0,t) - p_d\right]^2 \leq V_1 \leq V_1 + V_2 \leq \frac{1}{\lambda_{1a}}V_a \in \mathcal{L}_\infty, \tag{5.93}$$

$$\left|y(0,t) - p_d\right| \leq \sqrt{\frac{2}{\beta k_p \lambda_{1a}}\left(V_a(0)e^{-\lambda_a t} + \frac{\psi}{\lambda_a}\right)}, \quad \forall t \in [0,\infty). \quad \square \tag{5.94}$$

Remark 5.18 From the similar analysis of Remarks 5.11 and 5.12 we can conclude that both steady bottom boundary state error $y(0,\infty) - p_d$ and the deflection of the cable $w(x,t)$ can be made smaller by appropriately choosing the control gains k_p, k_q, k_v, and k_s.

Remark 5.19 From Eq. (5.90) we can obtain that the parameter estimate error $\tilde{\Phi}$ is bounded for all $t \in [0,\infty)$. Using the derivation similar to that employed in Remark 5.13, we can state that the proposed controls, Eqs. (5.67) and (5.68), ensure that all internal system signals including $y(x,t)$, $y'(x,t)$, $\dot{y}(x,t)$, $\dot{y}'(x,t)$, and $\ddot{y}(x,t)$ are uniformly bounded. Since $\hat{\Phi}$, $y'(x,t)$, and $\dot{y}(x,t)$ are all bounded for all $(x,t) \in [0,L]\times[0,\infty)$, we can conclude that the robust adaptive boundary controls, Eqs. (5.67) and (5.68), are also bounded for all $t \in [0,\infty)$.

Table 5.1 Parameters of the flexible marine installation system

Parameter	Description	Value
L	Length of the cable	1000.00 m
D	Diameter of the cable	0.05 m
M	Mass of the vessel	9.60×10^7 kg
m	Mass of the payload	4×10^5 kg
c_1	Damping coefficient of the vessel	9.00×10^7 N s m^{-1}
c_2	Damping coefficient of the payload	2.00×10^5 N s m^{-1}
T	Tension	4.00×10^6 N
ρ	Mass per unit length of the cable	8.02 kg m^{-1}
ρ_s	Sea water density	1024.00 kg m^{-3}
c	Distributed damping coefficient of the cable	1.00 N s m^{-1}
p_d	Desired set-point	50.00 m

5.4 Numerical Simulations

Simulations for a marine installation system under ocean disturbance are carried out to demonstrate the effectiveness of the proposed boundary controls Eqs. (5.11) and (5.12). Numerical methods are applied to obtain the approximate solution of system (5.8)–(5.10) when there is no obtainable analytical solution. In this chapter, we select the finite difference method to simulate the system performance with boundary control.

The cable, initially at rest, is excited by a distributed transverse disturbance due to ocean current. The corresponding initial conditions of the marine installation system are given as

$$y(x,0) = 0, \tag{5.95}$$

$$\frac{\partial y(x,0)}{\partial t} = 0. \tag{5.96}$$

The system parameters are given in Table 5.1.

In the simulation, the ocean surface current velocity $U(t)$ is given by Eq. (4.94). We assume that the full current load is applied from $x = 1000$ m to $x = 0$ m and thereafter linearly declines to zero at the ocean floor, $x = 0$, to obtain a depth-dependent ocean current profile $U(x,t)$ as in Chap. 3. The distributed load $f(x,t)$ is generated by Eq. (2.5) with $C_D = 1$, $\theta = 0$, $S_t = 0.2$, and $f_v = 2.625$. The distributed load at the top boundary of the cable is shown in Fig. 5.2. The disturbance $d_1(t)$ on the vessel is generated by the equation

$$d_1(t) = \left[3 + 0.8\sin(0.7t) + 0.2\sin(0.5t) + 0.2\sin(0.9t)\right] \times 10^6. \tag{5.97}$$

The disturbance $d_2(t)$ on the payload is given by the equation

$$d_2(t) = \left[3 + 0.8\sin(0.7t) + 0.2\sin(0.5t) + 0.2\sin(0.9t)\right] \times 10^4. \tag{5.98}$$

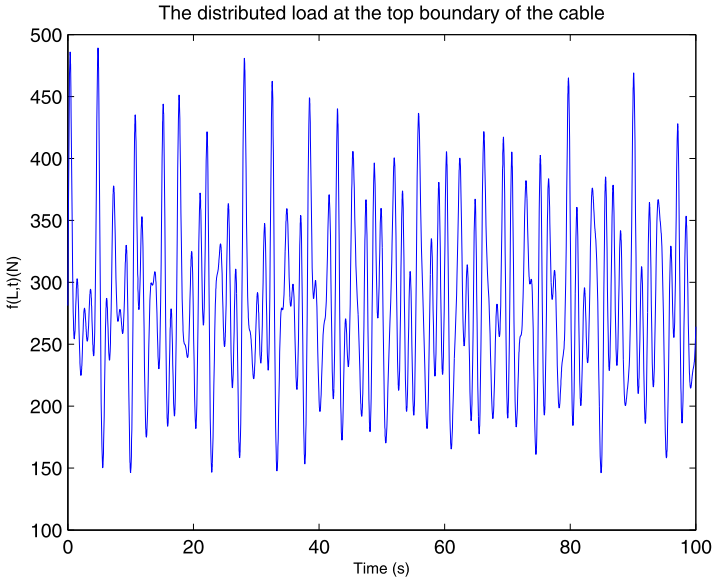

Fig. 5.2 The distributed load at the top boundary of the cable $f(L,t)$

The position of the cable for free vibration, i.e., $u_1(t) = u_2(t) = 0$, exposed to ocean disturbance is shown in Fig. 5.3. The boundary position of the cable is given in Fig. 5.4. It is clear that the system is unstable and the vibration of the cable is quite large.

The position of the cable with the active PD controls $u_1(t) = -K_1(y(L,t) - y_d) - K_2\dot{y}(L,t)$ and $u_2(t) = -K_3(y(L,t) - y_d) - K_4\dot{y}(L,t)$, by choosing $K_1 = 1 \times 10^6$, $K_2 = 1 \times 10^6$, $K_3 = 1 \times 10^4$, and $K_4 = 1 \times 10^4$, is presented in Fig. 5.5. The corresponding boundary position of the cable and boundary control input are shown in Figs. 5.6 and 5.7. The position of the cable with exact model-based controls, Eqs. (5.11) and (5.12), by choosing $k_v = 2 \times 10^7$, $k_p = 4 \times 10^2$, and $k_s = 2 \times 10^{10}$, under ocean disturbance is shown in Fig. 5.8. The corresponding boundary position of the cable and boundary control input are shown in Figs. 5.9 and 5.10. When the system parameters T, m, and c_2 are unknown, the position of the cable with adaptive controls, Eqs. (5.67) and (5.68), by choosing $k_v = 2 \times 10^7$, $k_p = 4 \times 10^2$, $k_s = 2 \times 10^{10}$, $r = 0.001$, and $\Gamma = \text{diag}\{5 \times 10^6, 1 \times 10^4, 5 \times 10^6\}$, under ocean disturbance is shown in Fig. 5.11. The parameter estimators, $\hat{T}$, $\hat{m}$, and $\hat{c}_2$ for the adaptive boundary control are presented in Fig. 5.12. The corresponding boundary position of the cable and boundary control input are shown in Figs. 5.13 and 5.14.

Figures 5.5, 5.8, and 5.11 illustrate that the PD control, model-based boundary control, and adaptive boundary control are all able to bring the subsea payload to the desired position $p_d = 50\,\text{m}$ and stabilize the cable at the small neighborhood of its equilibrium position. In comparison with the control, the installation system with

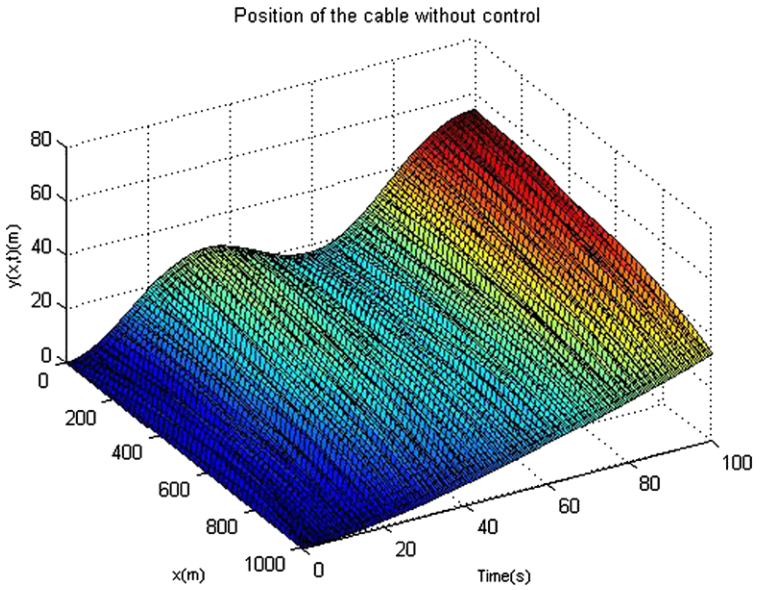

Fig. 5.3 Position of the cable without control

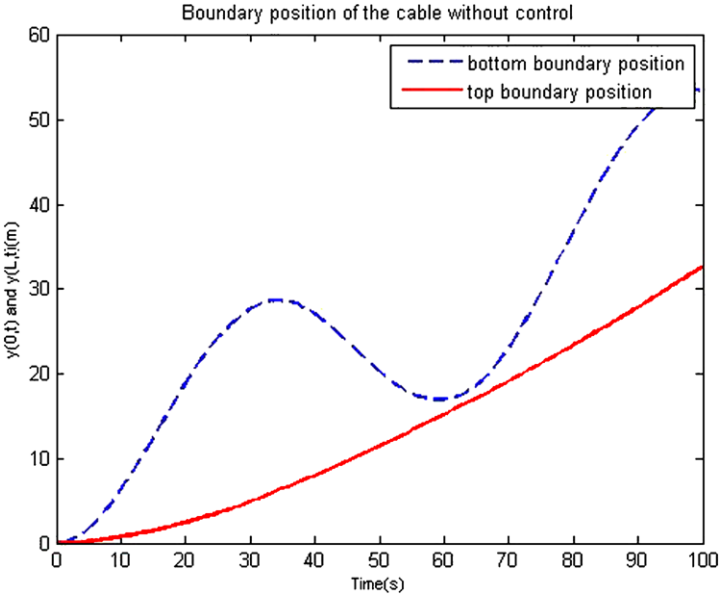

Fig. 5.4 Boundary position of the cable without control

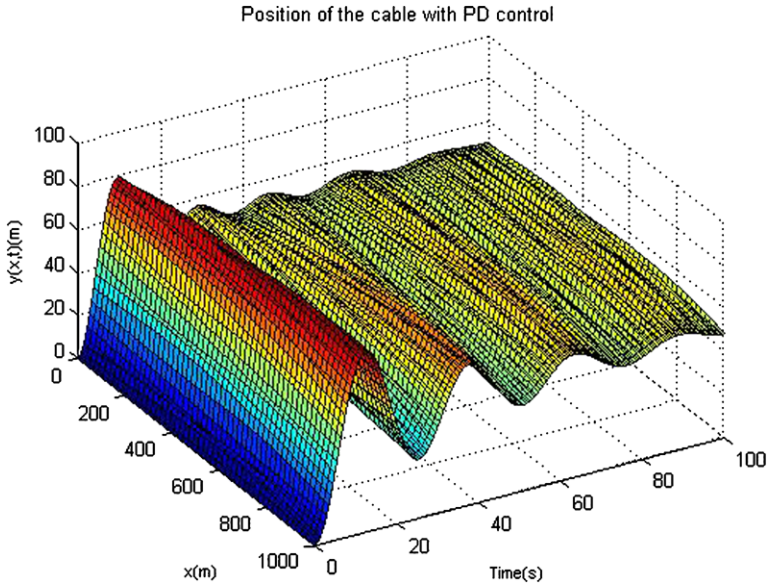

Fig. 5.5 Position of the cable with PD control

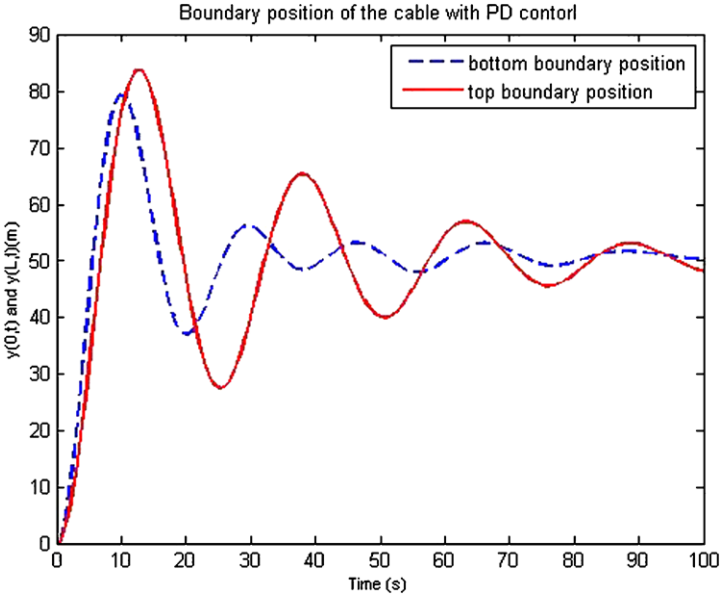

Fig. 5.6 Boundary position of the cable with PD control

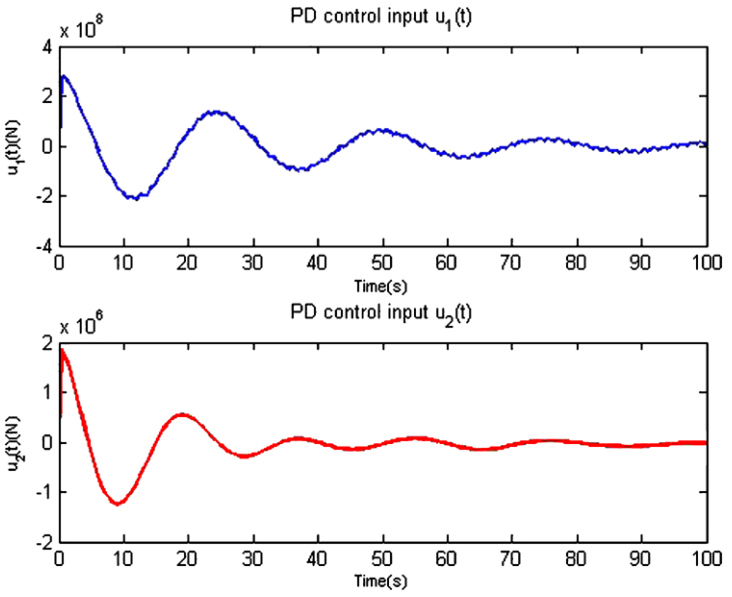

Fig. 5.7 PD control inputs $u_1(t)$ and $u_2(t)$

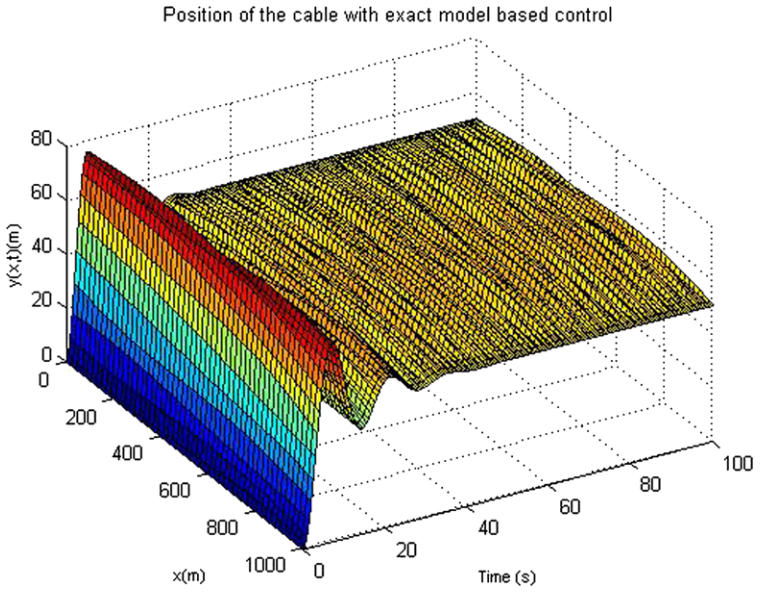

Fig. 5.8 Position of the cable with model-based boundary control

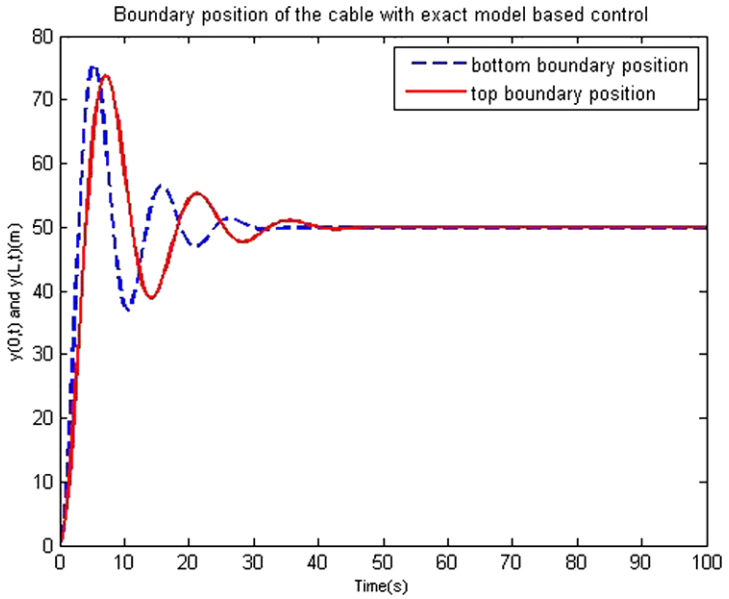

Fig. 5.9 Boundary position of the cable with model-based control

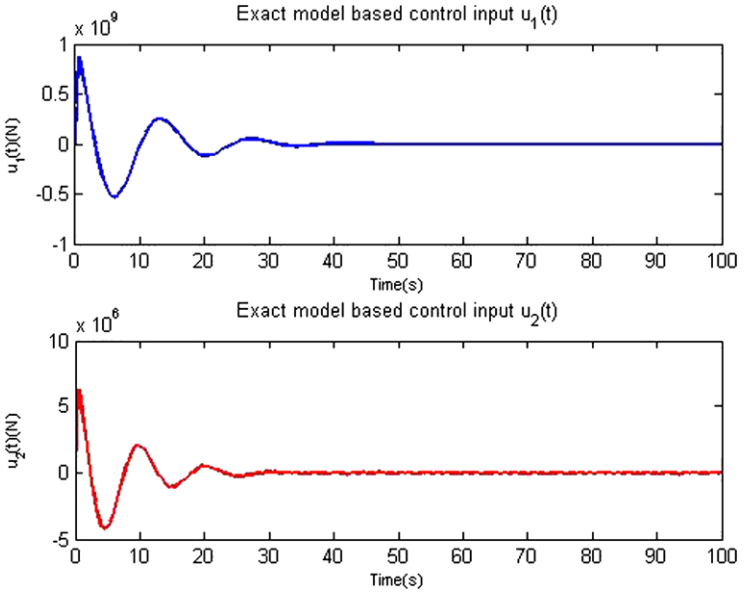

Fig. 5.10 Model-based control inputs $u_1(t)$ and $u_2(t)$

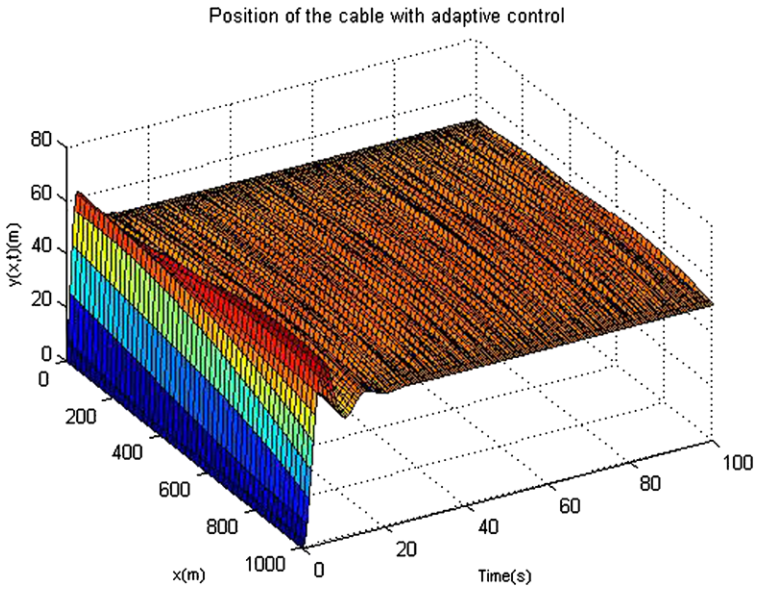

Fig. 5.11 Position of the cable with robust adaptive boundary control

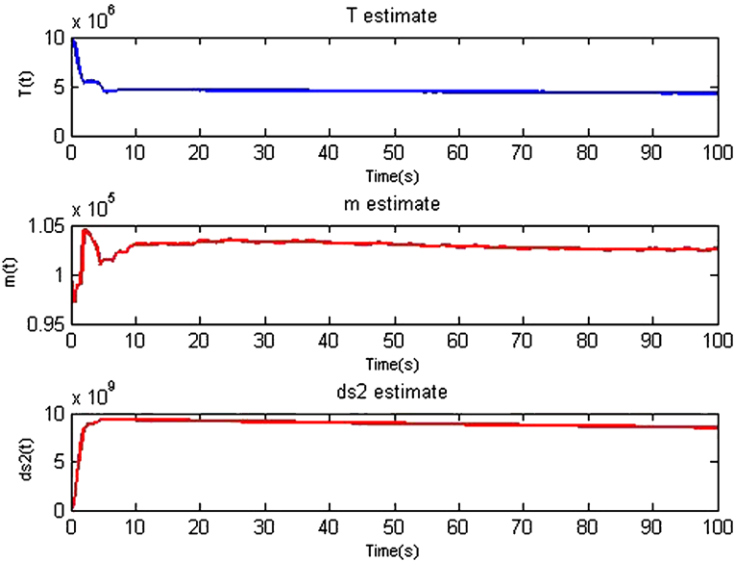

Fig. 5.12 Parameter estimation

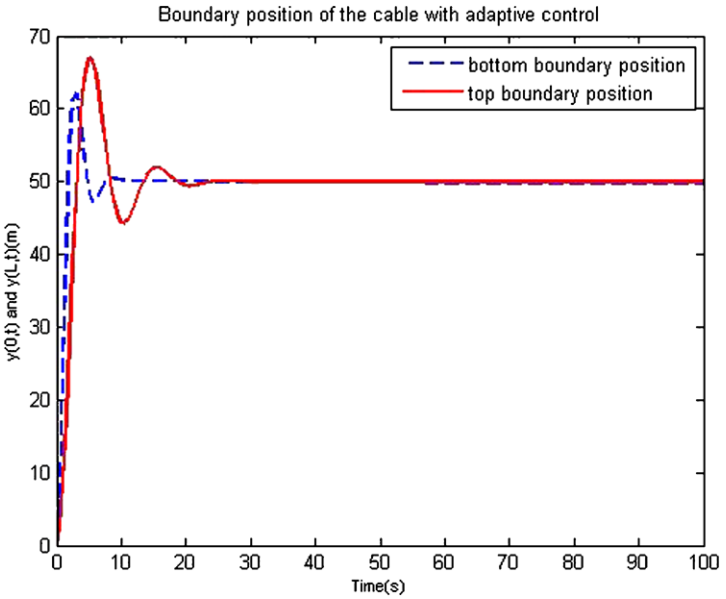

Fig. 5.13 Boundary position of the cable with robust adaptive control

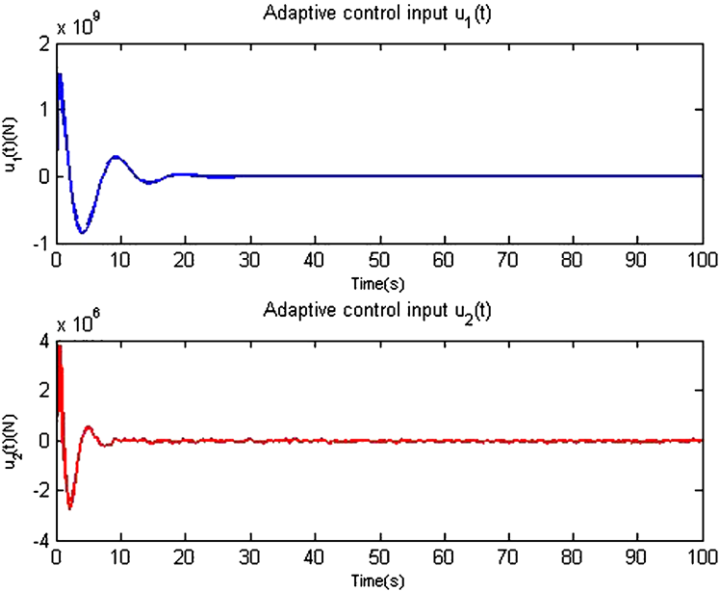

Fig. 5.14 Adaptive control inputs $u_1(t)$ and $u_2(t)$

the model-based boundary control and the robust adaptive control in this chapter converges quite quickly and has a better performance.

5.5 Conclusion

In this chapter, both position control and vibration suppression have been investigated for a flexible marine installation system subjected to the ocean disturbance. Two cases for the flexible marine installation system have been studied: (i) exact model-based control and (ii) adaptive control for the system parametric uncertainty. For the first case, a boundary controller has been introduced for the exact model of the installation system. For the second case where the system parameters cannot be directly measured, to fully compensate the effect of unknown system parameters, a signum term and an auxiliary signal term have been introduced to develop a robust adaptive boundary control law. Both types of boundary control have been designed based on the original infinite-dimensional model (PDE), and thus the spillover instability phenomenon has been eliminated. All the signals of the closed-loop system have been proved to be uniformly bounded by using the Lyapunov direct method. The exact model-based boundary controls (5.11) and (5.12) require the measurement of the tension, top position, and slope of the cable, while the robust adaptive boundary controls (5.67) and (5.68) only require measurements of the top position and slope of the cable. The proposed schemes have offered implementable design procedures for the control of marine installation systems since all the signals in the control can be measured by sensors or calculated by a backward difference algorithm. The simulation results have illustrated that the proposed control is able to position the payload to the desired set-point and suppress the vibration of the cable with a good performance.

Chapter 6
Adaptive Control of Thruster-Assisted Single-Point Mooring Systems

6.1 Introduction

In this chapter, we investigate the control problem of single-point mooring systems, which are often used in offshore loading or offloading gas or fluid products. Also, in this chapter, we consider unknown backlash-like hysteresis, which may exist in thruster dynamics. As we know, hysteresis often occurs in actuators, such as wear and tear gears, while the existence of hysteresis limits both static and dynamic performances of feedback control systems [238]. A fundamental method to deal with hysteresis is the inverse compensation, where the hysteresis effect is canceled out by constructing a proper inverse of the hysteresis operator, see, e.g., [239] and [240]. Alternatively, there are also some approaches for controller synthesis by using the properties of the hysteresis model, and the reader may refer to, for instance, [241–246], etc. In [241], backlash-like hysteresis is first presented as a linear term plus a bounded nonlinear term, and then adaptive control is designed for a class of single-input-single-output (SISO) nonlinear dynamic systems preceded by unknown backlash-like hysteresis nonlinearities. This class of systems is reconsidered in [242], where bounded external disturbances are also taken into account, and robust adaptive backstepping control is developed. Furthermore, using a similar method to deal with hysteresis, the authors in [243] design decentralized adaptive control for unknown interconnected systems with both backlash-like hysteresis and interactions between subsystems. In [244], adaptive variable structure control is designed for a class of affine nonlinear systems by using the stop or play hysteresis operators to define the Prandtl–Ishlinskii hysteresis. Employing this definition, in [245] and [246], adaptive neural network control is proposed for uncertain pure-feedback nonlinear systems with hysteresis input and nonlinear systems with both uncertain hysteresis inputs and time-varying state delays, respectively. All above-mentioned control methods are state feedback control, so output feedback control should be investigated for nonlinear systems with hysteresis input when some system states are hard to be measured.

In this chapter, both state feedback and output feedback control are designed for thruster-assisted single-point mooring systems with unknown backlash-like hys-

W. He et al., *Dynamics and Control of Mechanical Systems in Offshore Engineering*, Advances in Industrial Control, DOI 10.1007/978-1-4471-5337-5_6,

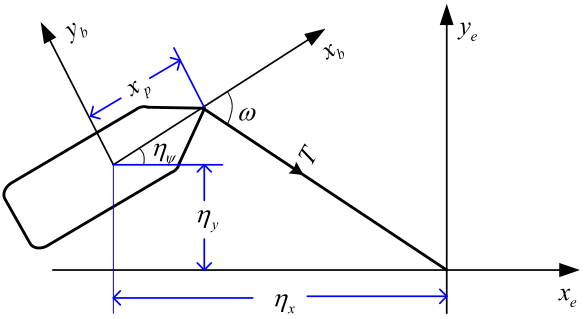

Fig. 6.1 Geometry of single-point mooring system

teresis in thruster dynamics. This chapter is organized as follows. In Sect. 6.2, the dynamic model of a single-point mooring system is given, and preliminaries are presented. In Sect. 6.3, state feedback control is proposed, and then output feedback control is presented by constructing a HONN-based observer to estimate the unmeasurable state vector of the single-point mooring system. The stability of closed-loop systems is analyzed. In Sect. 6.4, simulations of a single-point mooring system are demonstrated to illustrate the effectiveness of the proposed control methods. Finally, in Sect. 6.5, conclusions are obtained.

6.2 System Dynamics and Preliminaries

6.2.1 System Dynamics

The motions and state variables of the single-point mooring system are defined and measured with respect to two principal reference frames: earth-fixed frame and body-fixed frame. As shown in Fig. 6.1, the earth-fixed frame is denoted as (x_e, y_e) with its origin located at the connection of the mooring line and the mooring terminal. The (x_e, y_e) plane lies on the water surface, and the x_e axis points along the desired heading of the vessel. The body-fixed frame, denoted as (x_b, y_b), is fixed to the vessel body, while the origin coincides with the center of gravity of the moored vessel. The x_b axis is directed from aft to fore along the longitudinal axis of the vessel, and the y_b axis is directed to starboard.

6.2.1.1 Vessel Dynamics

The multiple-input-multiple-output (MIMO) dynamics of a three degree-of-freedom (DOF) moored surface vessel can be expressed as

$$\begin{cases} \dot{\eta} = J(\eta)v, \\ M\dot{v} + C(v)v + D(v)v + g(\eta) = \tau_{\text{moor}}(\eta) + \Phi(\tau_c) + \tau_{\text{env}}(\eta), \end{cases} \tag{6.1}$$

where the output $\eta = [\eta_x, \eta_y, \eta_\psi]^T \in \mathbb{R}^3$ consists of the position (η_x, η_y) and heading (η_ψ) of the vessel in the earth-fixed inertial frame, respectively; $v = [v_x, v_y, v_\psi]^T \in \mathbb{R}^3$ shows the vessel-frame surge, sway, and yaw velocities, respectively; $\tau_c = [\tau_u, \tau_v, \tau_r]^T \in \mathbb{R}^3$ represents the generalized force vector in surge, sway, and jaw generated by the propulsion system; $\Phi(\tau_c) = [\phi_1(\tau_{c1}), \phi_2(\tau_{c2}), \phi_3(\tau_{c3})]^T \in \mathbb{R}^3$ is a vector-valued backlash-like hysteresis input nonlinearity; M is the inertia matrix with $M = M^T > 0$, and $C(v)$ and $D(v)$ are the matrix of Coriolis and centripetal terms and the damping matrix, respectively, all of which are unknown; $g(\eta)$ is an unknown vector of restoring forces due to gravitational forces and moments; $\tau_{\text{moor}}(\eta)$ denotes the mooring force vector in surge, sway, and jaw generated by the mooring line tension, which will be defined later; $\tau_{\text{env}}(\eta)$ is an unknown disturbance from environment, which is mainly produced by wind and wave; and $J(\eta)$ is the three DOF rotation matrix,

$$J(\eta) = \begin{bmatrix} \cos\eta_\psi & -\sin\eta_\psi & 0 \\ \sin\eta_\psi & \cos\eta_\psi & 0 \\ 0 & 0 & 1 \end{bmatrix}. \tag{6.2}$$

For the backlash-like hysteresis input nonlinearity, $\Phi(\tau_c) = [\phi_1(\tau_{c1}), \phi_2(\tau_{c2}), \phi_3(\tau_{c3})]^T$, its ith element is defined as follows:

$$\frac{d\phi_i(\tau_{ci})}{dt} = h_{ri}\left|\frac{d\tau_{ci}}{dt}\right|\big(h_{ai}\tau_{ci} - \phi_i(\tau_{ci})\big) + h_{Bi}\frac{d\tau_{ci}}{dt}, \quad i = 1, 2, 3, \tag{6.3}$$

where τ_{ci} denotes the input to backlash-like hysteresis, h_{ri}, h_{ai}, and h_{Bi} are constants, and $h_{ai} > 0$ is the slope of the lines satisfying $h_{ai} > h_{Bi}$. Based on the analysis in [241], Eq. (6.3) can be solved explicitly:

$$\phi_i\big(\tau_{ci}(t)\big) = h_{ai}\tau_{ci}(t) + d_i(\tau_{ci}), \quad i = 1, 2, 3, \tag{6.4}$$

$$\begin{aligned} d_i(\tau_{ci}) = {} & \big[\phi_i(\tau_{ci})(0) - h_{ai}\tau_{ci}(0)\big]e^{-h_{ri}(\tau_{ci}-\tau_{ci}(0))\,\text{sgn}(\dot{\tau}_{ci})} \\ & + e^{-h_{ri}\tau_{ci}\,\text{sgn}(\dot{\tau}_{ci})}\int_{\tau_{ci}(0)}^{\tau_{ci}} [h_{Bi} - h_{ai}]e^{-h_{ri}\varsigma_j\,\text{sgn}(\dot{\tau}_{ci})}\,d\varsigma_j. \end{aligned} \tag{6.5}$$

The solution indicates that dynamic (6.3) can be used to model a class of backlash-like hysteresis. Figure 6.2 shows that model (6.3) generates backlash-like hysteresis curves, where the parameters $h_{ri} = 1$, $h_{ai} = 2.866$, and $h_{Bi} = 0.289$, the input signal $\tau_{ci}(t) = 4.8\sin(3.6t)$, and the initial condition $\tau_{ci}(0) = 0$. As demonstrated in [241], $d_i(\tau_{ci})$ is bounded, i.e., $|d_i(\tau_{ci})| \le d_i^*$. In this chapter, we assume that d_i^* is unknown.

Using the above notation, the vector-valued backlash-like hysteresis input nonlinearity, $\Phi(\tau_c)$, can be written in the following form:

$$\Phi(\tau_c) = H_a\tau_c + D(\tau_c), \tag{6.6}$$

where $H_a = \text{diag}\{h_{a1}, h_{a2}, h_{a3}\} > 0$, and $D(\tau_c) = [d_1(\tau_{c1}), d_2(\tau_{c2}), d_3(\tau_{c3})]^T$ with $\|D(\tau_c)\| \le D^*$, $D^* = \sqrt{d_1^{*2} + d_2^{*2} + d_3^{*2}}$ being an unknown positive constant.

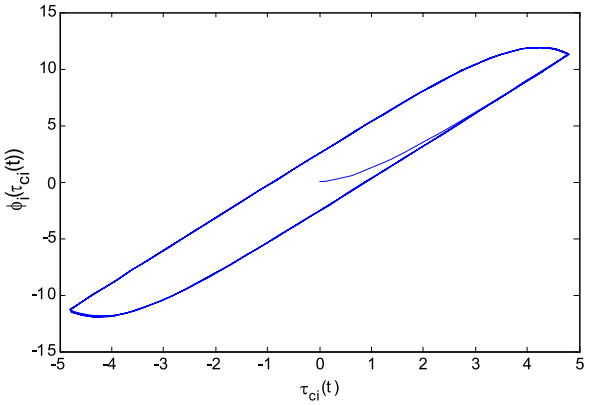

Fig. 6.2 Hysteresis curves

6.2.1.2 Mathematical Model of Mooring Force

For the purpose of slow motion dynamic analysis of mooring system, mooring line is modeled quasi-statically [247, 248]. The geometry of the single-point mooring system is shown in Fig. 6.1. From Fig. 6.1, the mooring force vector in surge, sway, and jaw generated by the mooring line tension, τ_{moor}, can be expressed as

$$\tau_{\text{moor}}(\eta) = \left[T(\eta)\cos\big(\omega(\eta)\big), -T(\eta)\sin\big(\omega(\eta)\big), -x_p T(\eta)\sin\big(\omega(\eta)\big)\right]^T, \quad (6.7)$$

where $T(\eta)$ denotes the actual tension of the mooring line, x_p is the distance from the center of gravity of the moored vessel to the connection of the mooring line and the moored vessel, and $\omega(\eta)$ is the angle between the x_b axis and the mooring line, which can be calculated from

$$\omega(\eta) = \arcsin\left(\frac{\eta_y + x_p \sin\eta_\psi}{l(\eta)}\right) + \eta_\psi. \quad (6.8)$$

The deformed length of the mooring line $l(\eta)$ is a function of η, which can be calculated from

$$l(\eta) = \sqrt{(\eta_x - x_p\cos\eta_\psi)^2 + (\eta_y + x_p\sin\eta_\psi)^2}. \quad (6.9)$$

In this chapter, the mooring line is considered to be a synthetic rope. Following the method of [248] and [249], the actual tension $T(\eta)$ in the mooring line can be described by

$$T(\eta) = p_m\left(\frac{l(\eta) - l_w}{l_w}\right)^{q_m} S_b, \quad (6.10)$$

where S_b is the average breaking strength, p_m and q_m are empirically determined constants, and l_w is the working length of the unstrained rope.

6.2.1.3 Mathematical Models of Wind and Waves

In this chapter, wind and waves are considered as the main environmental disturbance. This means that the environmental disturbance can be expressed as

$$\tau_{\text{env}}(\eta) = \tau_{\text{wind}} + \tau_{\text{wave}}(\eta), \tag{6.11}$$

where τ_{wind} is the force vector in surge, sway, and jaw generated by wind, and $\tau_{\text{wave}}(\eta)$ denotes the force vector produced by waves.

Mathematical models of wind forces and moment are introduced into the single mooring systems to improve the performance and robustness of the system in extreme conditions. The force vector in surge, sway, and jaw generated by wind, τ_{wind}, can be formulated as [234]

$$\tau_{\text{wind}} = \begin{bmatrix} F_{x\text{wind}} \\ F_{y\text{wind}} \\ N_{\text{wind}} \end{bmatrix} = \begin{bmatrix} \frac{1}{2} C_{xd}(\gamma_r) \rho_a V_r^2 A_T \\ \frac{1}{2} C_{yd}(\gamma_r) \rho_a V_r^2 A_L \\ \frac{1}{2} C_{Nd}(\gamma_r) \rho_a V_r^2 A_L L_v \end{bmatrix}, \tag{6.12}$$

where $F_{x\text{wind}}$, $F_{y\text{wind}}$, and N_{wind} denote the wind forces and moment in the horizontal plane, respectively; V_r and γ_r are the relative wind speed and angle with respect to the vessel bow, respectively; $C_{xd}(\gamma_r)$ and $C_{yd}(\gamma_r)$ are the empirical force coefficients; $C_{Nd}(\gamma_r)$ is a moment coefficient; ρ_a is the density of air; A_T and A_L are the transverse and lateral projected areas; and L_v is the overall length of the vessel.

The force vector in surge, sway, and jaw produced by waves, $\tau_{\text{wave}}(\eta)$, can be presented by [250]

$$\tau_{\text{wave}}(\eta) = \begin{bmatrix} F_{x\text{wave}}(\eta) \\ F_{y\text{wave}}(\eta) \\ N_{\text{wave}}(\eta) \end{bmatrix} = \begin{bmatrix} \rho_w g L_v C_{xv} \cos^3(\theta_0 - \eta_\psi) \\ \rho_w g L_v C_{yv} \sin^3(\theta_0 - \eta_\psi) \\ \rho_w g L_v^2 C_{Nv} \sin 2(\theta_0 - \eta_\psi) \end{bmatrix}, \tag{6.13}$$

where $F_{x\text{wave}}(\eta)$, $F_{y\text{wave}}(\eta)$, and $N_{\text{wave}}(\eta)$ denote the wave forces and moment in the horizontal plane, respectively; ρ_w is the density of water; θ_0 is the absolute angle of attack; g is the gravitational constant; and C_{xv}, C_{yv}, and C_{Nv} are the wave excitation coefficients in surge, sway, and yaw, respectively.

6.2.2 *Control Objective and Assumptions*

As mentioned in [251], the position mooring system can be controlled in both setpoint control mode and tracking control mode, where the setpoint control objective is to keep the vessel at the specified setpoint position or heading, and the tracking control make the vessel track a reference trajectory that is computed from the old to the new position or heading setpoint. Therefore, given a desired position or a desired trajectory, η_d, the control objective is to design a stable control law to ensure

that the tracking error converges to a very small neighborhood of the origin in finite time, while all signals of the closed-loop system are bounded.

Before the control design, the following assumptions are made for the system, while a useful lemma is presented.

Assumption 6.1 The desired trajectory vector η_d is continuous, differentiable, and twice differentiable, while η_d, $\dot{\eta}_d$, and $\ddot{\eta}_d$ are all bounded.

Assumption 6.2 The inertia matrix M and the slopes of the hysteresis H_a are unknown, but there exist positive constants m^*, $\bar{h}_a^*$, and h_a^* such that $\|M\| \leq m^*$ and $h_a^* \leq \|H_a\| \leq \bar{h}_a^*$.

6.2.3 Nonlinear Function Approximation Using HONN

In control engineering, NNs are usually used as a tool for modeling nonlinear functions because of their good capabilities in function approximation. In this chapter, the following high-order neural networks (HONNs) are used to approximate the continuous function $Q(Z): \mathbb{R}^q \to \mathbb{R}^n$ [252],

$$
\begin{aligned}
Q(Z) &= W^T S(Z), \quad W \in \mathbb{R}^{l\times n} \text{ and } S(Z) \in \mathbb{R}^l, \\
S(Z) &= \left[s_1(Z), s_2(Z), \ldots, s_l(Z)\right]^T, \\
s_i(Z) &= \prod_{j\in I_i}\left[s(Z_j)\right]^{\kappa_j(i)}, \quad i = 1, 2, \ldots, l,
\end{aligned}
$$

where $Z = [Z_1, Z_2, \ldots, Z_q]^T \in \Omega_Z \subset \mathbb{R}^q$ is the input vector, positive integer l denotes the neural network node number, and n is the dimension of the function vector, $\{I_1, I_2, \ldots, I_l\}$ is a collection of l nonordered subsets of $\{1, 2, \ldots, q\}$, and $\kappa_j(i)$ are nonnegative integers, W is an adjustable synaptic weight matrix, $s(Z_j)$ is chosen as the hyperbolic tangent function $s(Z_j) = (e^{Z_j} - e^{-Z_j})/(e^{Z_j} + e^{-Z_j})$.

For a desired function $Q^*(Z)$, there exists an ideal weight matrix W^* such that the smooth function $Q^*(Z)$ can be approximated by an ideal NN on a compact set $\Omega_Z \subset \mathbb{R}^q$

$$
Q^* = W^{*T} S(Z) + \varepsilon_Z, \tag{6.14}
$$

where ε_Z is the bounded NN approximation error satisfying $\|\varepsilon_Z\| \leq \varepsilon_0$ on the compact set, which can be reduced by increasing the number of the adjustable weights. The ideal weight matrix W^* is an "artificial" quantity required for analytical purpose and is defined as that minimizing $\|\varepsilon_Z\|$ for all $Z \in \Omega_Z \subset \mathbb{R}^q$ in a compact region, i.e.,

$$
\begin{aligned}
W^* \triangleq \arg\min_{W\in\mathbb{R}^{l\times p}}\left\{\sup_{Z\in\Omega_Z}\left\|Q^* - W^T S(Z)\right\|\right\}, \quad \Omega_Z \subset \mathbb{R}^q, \\
\text{and compact set } \Omega_w \subset \mathbb{R}^{l\times p}.
\end{aligned} \tag{6.15}
$$

In general, the ideal NN weight matrix W^* is an unknown constant. Its estimate $\hat{W}$, should be used for controller design, which will be discussed later.

6.3 Control Design

To control the single-point mooring system (6.1), we will first investigate full-state feedback control under the assumption that all states of the vessel can be obtained. And then, output feedback control will be proposed for the case where only the system output can be obtained. Both the full-state feedback control and output feedback control will be designed via backstepping method.

6.3.1 Full-State Feedback Control

Step 1: Consider the first equation of the single-point mooring system (6.1). Define error variables $z_1 = \eta - \eta_d$ and $z_2 = v - \alpha_1$, and consider the Lyapunov function candidate $V_1 = \frac{1}{2} z_1^T z_1$. Differentiating z_1 with respect to time yields

$$\dot{z}_1 = J(\eta)(z_2 + \alpha_1) - \dot{\eta}_d. \tag{6.16}$$

Noting the property $J^T(\eta)J(\eta) = I$ and choosing the virtual control as

$$\alpha_1 = J^T(\eta)(\dot{\eta}_d - K_1 z_1), \tag{6.17}$$

where $K_1 = K_1^T > 0$, the time derivative of V_1 along the trajectories of (6.16) is given by

$$\dot{V}_1 = -z_1^T K_1 z_1 + z_1^T J(\eta) z_2. \tag{6.18}$$

The first term on the right-hand side (RHS) is stabilizing, and the second term will be handled in the next step.

Step 2: Differentiating z_2 with respect to time yields

$$\dot{z}_2 = M^{-1}\big[-C(v)v - D(v)v - g(\eta) + \tau_{\text{moor}}(\eta) + \Phi(\tau_c) + \tau_{\text{env}}(\eta)\big] - \dot{\alpha}_1, \tag{6.19}$$

where $\dot{\alpha}_1 = (\partial\alpha_1/\partial\eta)\dot{\eta} + (\partial\alpha_1/\partial\dot{\eta}_d)\ddot{\eta}_d + (\partial\alpha_1/\partial z_1)\dot{z}_1$. Substituting (6.6) into (6.19), we have

$$\dot{z}_2 = M^{-1}\big[-C(v)v - D(v)v - g(\eta) + \tau_{\text{moor}}(\eta) + H_a\tau_c + D(\tau_c) + \tau_{\text{env}}(\eta)\big] - \dot{\alpha}_1. \tag{6.20}$$

Consider the Lyapunov function candidate $V_2^* = V_1 + \frac{1}{2} z_2^T H_a^{-1} M z_2$. Its derivative along (6.20) is

$$\dot{V}_2^* = -z_1^T K_1 z_1 + z_1^T J(\eta) z_2 + z_2^T \big[Q(Z) + \tau_c + H_a^{-1} D(\tau_c) \big], \tag{6.21}$$

where $Q(Z) = H_a^{-1}[-C(v)v - D(v)v - g(\eta) + \tau_{\text{moor}}(\eta) + \tau_{\text{env}}(\eta) - M\dot{\alpha}_1]$ with $Z = [\eta^T, v^T, \alpha_1^T, \dot{\alpha}_1^T]^T$. The matrices M, $C(v)$, $D(v)$, and $g(\eta)$ are unknown, while $\tau_{\text{moor}}(\eta)$ and $\tau_{\text{env}}(\eta)$ are difficult to be calculated since some coefficients of a real mooring system are hard to obtain, for example, the average breaking strength S_b, the constants p_m and q_m in (6.10), the empirical force coefficients $C_{xd}(\gamma_r)$ and $C_{yd}(\gamma_r)$, the moment coefficient $C_{Nd}(\gamma_r)$, and the wave excitation coefficients C_{xv}, C_{xv}, and C_{xv}. Therefore, in this chapter, we handle $\tau_{\text{moor}}(\eta)$ and $\tau_{\text{env}}(\eta)$ as unknown functions. To compensate for the unknown function $Q(Z)$, we can employ HONN to approximate $Q(Z)$, which can be expressed as

$$Q(Z) = W^{*T} S(Z) + \varepsilon_Z, \tag{6.22}$$

where $W^* \in \mathbb{R}^{l\times 3}$ denotes the ideal constant weight matrix, $S(Z) \in \mathbb{R}^l$, l is the neural network node number, and $\varepsilon_Z \in \mathbb{R}^3$ is the approximation error with $\|\varepsilon_Z\| \le \varepsilon_Z^*$ and constant $\varepsilon_Z^* > 0$.

Since W^* is unknown, we can use its estimate $\hat{W}$ to construct the adaptive control τ_c and the NN weight adaptation law as follows:

$$\tau_c = -J^T(\eta) z_1 - K_2 z_2 - \hat{W}^T S(Z) - \hat{\beta}\,\text{Tanh}\left(\frac{z_2}{b}\right), \tag{6.23}$$

$$\dot{\hat{W}} = \Gamma_w \big[S(Z) z_2^T - \sigma_w \hat{W} \big], \tag{6.24}$$

$$\dot{\hat{\beta}} = \Gamma_\beta \left[\text{Tanh}\left(\frac{z_2}{b}\right) z_2^T - \sigma_\beta \hat{\beta} \right], \tag{6.25}$$

where $K_2 \in \mathbb{R}^{3\times 3}$ is a diagonal positive matrix; $\hat{\beta} \in \mathbb{R}^{3\times 3}$ is the estimate of the positive matrix $\beta^* = \lambda_{\beta m} I$ with $\lambda_{\beta m} = \varepsilon_Z^* + \|H_a^{-1}\| D^*$; $b > 0$ is a positive constant; $\text{Tanh}(\frac{z_2}{b}) = [\tanh(\frac{z_{21}}{b}), \tanh(\frac{z_{22}}{b}), \tanh(\frac{z_{23}}{b})]^T$ with z_{2i} $(i = 1, 2, 3)$ being the ith element of z_2; $\Gamma_w = \Gamma_w^T \in \mathbb{R}^{l\times l} > 0$ and $\Gamma_\beta = \Gamma_\beta^T \in \mathbb{R}^{3\times 3} > 0$ are design constant matrices; and $\sigma_w > 0$ and $\sigma_\beta > 0$ are design constants.

Remark 6.3 The positive constant matrix β^* and the positive constant $\lambda_{\beta m}$ are introduced only for analysis of the stability of the closed-loop system, and we do not need to know their true values in the whole procedure of control design.

Denote $\tilde{W} = \hat{W} - W^*$ and $\tilde{\beta} = \hat{\beta} - \beta^*$ and consider the augmented Lyapunov function candidate

$$V_2 = V_1 + \frac{1}{2} z_2^T H_a^{-1} M z_2 + \text{tr}\left\{ \frac{1}{2} \tilde{W}^T \Gamma_w^{-1} \tilde{W} \right\} + \text{tr}\left\{ \frac{1}{2} \tilde{\beta}^T \Gamma_\beta^{-1} \tilde{\beta} \right\}. \tag{6.26}$$

The time derivative of V_2 along the trajectories of (6.20), (6.23), (6.24), and (6.25) is given by

$$\begin{aligned}\dot{V}_2 &= \dot{V}_1 + z_2^T H_a^{-1} M \dot{z}_2 + \operatorname{tr}\{\tilde{W}^T \Gamma_w^{-1} \dot{\tilde{W}}\} + \operatorname{tr}\{\tilde{\beta}^T \Gamma_\beta^{-1} \dot{\tilde{\beta}}\} \\ &= -z_1^T K_1 z_1 + z_1^T J(\eta) z_2 + z_2^T \left[(\hat{W}^T - \tilde{W}^T) S(Z) + \varepsilon_Z + \tau_c + H_a^{-1} D(\tau_c)\right] \\ &\quad + \operatorname{tr}\{\tilde{W}^T [S(Z) z_2^T - \sigma_w \hat{W}]\} + \operatorname{tr}\left\{\tilde{\beta}^T \left[\operatorname{Tanh}\left(\frac{z_2}{b}\right) z_2^T - \sigma_\beta \hat{\beta}\right]\right\} \\ &= -z_1^T K_1 z_1 - z_2^T K_2 z_2 + z_2^T \left[\varepsilon_Z + H_a^{-1} D(\tau_c)\right] \\ &\quad - z_2^T \beta^* \operatorname{Tanh}\left(\frac{z_2}{b}\right) - \sigma_w \operatorname{tr}\{\tilde{W}^T \hat{W}\} - \sigma_\beta \operatorname{tr}\{\tilde{\beta}^T \hat{\beta}\}. \end{aligned} \tag{6.27}$$

Denote $\beta = \varepsilon_Z + H_a^{-1} D(\tau_c) \triangleq [\beta_1, \beta_2, \beta_3]^T$. The following property is always established: $|\beta_i| \leq \|\beta\| \leq \|\varepsilon_Z\| + \|H_a^{-1}\| \|D(\tau_c)\| \leq \lambda_{\beta m}$ for all $i = 1, 2, 3$, which implies that

$$z_2^T \left[\varepsilon_Z + H_a^{-1} D(\tau_c)\right] = \sum_{i=1}^{3} z_{2i} \beta_i \leq \lambda_{\beta m} \sum_{i=1}^{3} |z_{2i}|. \tag{6.28}$$

Considering (6.28) and using the facts that

$$-\sigma_w \operatorname{tr}\{\tilde{W}^T \hat{W}\} \leq -\frac{\sigma_w}{2} \|\tilde{W}\|_F^2 + \frac{\sigma_w}{2} \|W^*\|_F^2, \tag{6.29}$$

$$-\sigma_\beta \operatorname{tr}\{\tilde{\beta}^T \hat{\beta}\} \leq -\frac{\sigma_\beta}{2} \|\tilde{\beta}\|_F^2 + \frac{\sigma_\beta}{2} \|\beta^*\|_F^2, \tag{6.30}$$

we have

$$\begin{aligned}\dot{V}_2 \leq\ & -z_1^T K_1 z_1 - z_2^T K_2 z_2 + \lambda_{\beta m} \sum_{i=1}^{3} |z_{2i}| \\ & - \lambda_{\beta m} z_2^T \operatorname{Tanh}\left(\frac{z_2}{b}\right) - \frac{\sigma_w}{2} \|\tilde{W}\|_F^2 + \frac{\sigma_w}{2} \|W^*\|_F^2 \\ & - \frac{\sigma_\beta}{2} \|\tilde{\beta}\|_F^2 + \frac{\sigma_\beta}{2} \|\beta^*\|_F^2. \end{aligned} \tag{6.31}$$

Using the equality $-\lambda_{\beta m} z_2^T \operatorname{Tanh}(\frac{z_2}{b}) = -\lambda_{\beta m} \sum_{i=1}^{3} [z_{2i} \tanh(\frac{z_{2i}}{b})]$ and the property of the function $\tanh(\cdot)$ [253] that

$$0 \leq |x| - x \tanh\left(\frac{x}{b}\right) \leq 0.2785 b \quad \text{for } b > 0,\ x \in \mathbb{R}, \tag{6.32}$$

we obtain

$$\begin{aligned}\dot{V}_2 \leq & -z_1^T K_1 z_1 - z_2^T K_2 z_2 + \lambda_{\beta m} \sum_{i=1}^{3} \left[|z_{2i}| - z_{2i} \tanh\left(\frac{z_{2i}}{b}\right) \right] \\ & - \frac{\sigma_w}{2} \|\tilde{W}\|_F^2 + \frac{\sigma_w}{2} \|W^*\|_F^2 - \frac{\sigma_\beta}{2} \|\tilde{\beta}\|_F^2 + \frac{\sigma_\beta}{2} \|\beta^*\|_F^2 \\ \leq & -z_1^T K_1 z_1 - z_2^T K_2 z_2 - \frac{\sigma_w}{2} \|\tilde{W}\|_F^2 - \frac{\sigma_\beta}{2} \|\tilde{\beta}\|_F^2 + \mu_1^*, \end{aligned} \tag{6.33}$$

where

$$\mu_1^* = 0.8355 b \lambda_{\beta m} + \frac{\sigma_\beta}{2} \|\beta^*\|_F^2 + \frac{\sigma_w}{2} \|W^*\|_F^2. \tag{6.34}$$

The following theorem shows the stability and control performance of the closed-loop system.

Theorem 6.4 *Consider the single-point mooring system* (6.1) *with Assumptions* 6.1 *and* 6.2, *the full-state feedback control law* (6.23), *and the adaptation laws* (6.24) *and* (6.25). *For bounded initial conditions, there exist constant matrices* $K_1 > 0$, $K_2 > 0$, $\Gamma_w > 0$, $\Gamma_\beta > 0$, $\sigma_w > 0$, *and* $\sigma_\beta > 0$ *such that the overall closed-loop control system is semiglobally stable in the sense that all signals in the closed-loop system are bounded and the tracking error is smaller than a prescribed error bound.*

Proof Denote by $\lambda_{\min}(\bullet)$ and $\lambda_{\max}(\bullet)$ the minimum and maximum eigenvalues of $\bullet$, respectively, and let

$$\rho_1 = \min\left\{ 2\lambda_{\min}(K_1), \frac{2h_a^* \lambda_{\min}(K_2)}{m^*}, \frac{\sigma_w}{\lambda_{\max}(\Gamma_w^{-1})}, \frac{\sigma_\beta}{\lambda_{\max}(\Gamma_\beta^{-1})} \right\}. \tag{6.35}$$

From (6.33) and (6.35) we can obtain that

$$\dot{V}_2 \leq -\rho_1 V_2 + \mu_1^*. \tag{6.36}$$

Multiplying (6.36) by $e^{\rho_1 t}$ yields

$$\frac{d(V_2(t))e^{\rho_1 t}}{dt} \leq e^{\rho_1 t} \mu_1^*. \tag{6.37}$$

Integrating over $[0, t]$ leads to

$$0 \leq V_2(t) \leq \frac{\mu_1^*}{\rho_1} + \left[V(0) - \frac{\mu_1^*}{\rho_1} \right] e^{-\rho_1 t}. \tag{6.38}$$

The above inequality implies that all signals of the closed-loop system, i.e., z_1, z_2, $\tilde{W}$, and $\tilde{\beta}$, are uniformly ultimately bounded. Furthermore, $\hat{W}$, $\hat{\beta}$, η, v, α_1, and τ_c are also uniformly ultimately bounded. From (6.34) and (6.35) we know that for

any given constants b, σ_w, and σ_β, the value of $\frac{\mu_1^*}{\rho_1}$ can be made arbitrarily small by increasing $\lambda_{\min}(K_1)$ and $\lambda_{\min}(K_2)$ and decreasing $\lambda_{\max}(\Gamma_w^{-1})$ and $\lambda_{\max}(\Gamma_\beta^{-1})$. Therefore, the tracking error z_1 can become arbitrarily small. This completes the proof. □

6.3.2 Output Feedback Control

In the previous subsection, we have designed a full-state feedback adaptive control of the single-point mooring system for the case where all states can be obtained. However, in practice, it is hard to measure the velocity vector v. To deal with this problem, output feedback control is considered in this subsection for the single-point mooring system by using HONN observer to estimate the velocity vector.

6.3.2.1 HONN-Based Observer

Adding and subtracting $K_v v$ on the RHS of the second equation of the single-point mooring system (6.1) and substituting (6.6) into (6.1) yield

$$\begin{cases} \dot{\eta} = J(\eta)v, \\ \dot{v} = -K_v v + M^{-1}[MK_v v + \tau_{\text{moor}}(\eta) + \tau_{\text{env}}(\eta) \\ \qquad + H_a\tau_c - C(v)v - D(v)v - g(\eta)] + M^{-1}D(\tau_c), \end{cases} \tag{6.39}$$

where $K_v = k_v I > 0$ is a positive constant matrix with constant $k_v > 0$. If we denote

$$Q_o(Z_o) = M^{-1}\big[MK_v v + \tau_{\text{moor}}(\eta) + \tau_{\text{env}}(\eta) + H_a\tau_c - C(v)v - D(v)v - g(\eta)\big],$$

the continuous function $Q_o(Z_o)$ can be estimated by HONN as

$$Q_o(Z_o) = W_o^{*T} S(Z_o) + \varepsilon_{Z_o}, \tag{6.40}$$

where $W_o^* \in \mathbb{R}^{l_o \times 3}$ is the ideal weight matrix, $Z_o = [\eta^T, v^T, \tau_c^T]^T$, $\varepsilon_{Z_o} \in \mathbb{R}^3$ is the approximation error with $\|\varepsilon_{Z_o}\| \le \varepsilon_{Z_o}^*$ and constant $\varepsilon_{Z_o}^* > 0$, and l_o is the neural network node number. Thus, the HONN observer can be designed as follows:

$$\begin{cases} \dot{\hat{\eta}} = J(\eta)\hat{v} - K_\eta(\hat{\eta} - \eta), \\ \dot{\hat{v}} = -J(\eta)(\hat{\eta} - \eta) - K_v\hat{v} + \hat{W}_o^T S(\hat{Z}_o), \\ \dot{\hat{W}}_o = \Gamma_o[S(\hat{Z}_o)(\hat{\eta}^T - \eta^T) - \sigma_o\hat{W}_o], \end{cases} \tag{6.41}$$

where $K_\eta = k_\eta I > 0$ is a positive constant matrix with constant $k_\eta > 0$, $\hat{Z}_o = [\hat{\eta}^T, \hat{v}^T, \tau_c^T]^T$, $\hat{W}_o \in \mathbb{R}^{l_o \times 3}$ denotes the estimation of the ideal weight matrix W_o^*, $\Gamma_o \in \mathbb{R}^{l_o \times l_o} > 0$ is a design constant matrix, and $\sigma_o > 0$ is a design constant.

Lemma 6.5 *For bounded system output η and control input τ_c, consider the NN observer (6.41). There exist an instant t^* and small constants ϵ_η and ϵ_v such that, for all $t > t^*$, the following inequalities hold*: $\|\hat{\eta} - \eta\| \leq \epsilon_\eta$ *and* $\|\hat{v} - v\| \leq \epsilon_v$.

Proof Denote $\tilde{\eta} = \hat{\eta} - \eta$, $\tilde{v} = \hat{v} - v$, and $\tilde{W}_o = \hat{W}_o - W_o^*$. Subtracting Eq. (6.39) from Eq. (6.41) and subtracting W_o^* on both sides of the last equation in (6.41), the state space error description of the observer is

$$\begin{cases} \dot{\tilde{\eta}} = J(\eta)\tilde{v} - K_\eta \tilde{\eta}, \\ \dot{\tilde{v}} = -J(\eta)\tilde{\eta} - K_v \tilde{v} + \hat{W}_o^T S(\hat{Z}_o) - W_o^{*T} S(Z_o) - \varepsilon_{Z_o} - M^{-1} D(\tau_c), \\ \dot{\tilde{W}}_o = \Gamma_o [S(\hat{Z}_o)\tilde{\eta}^T - \sigma_o \hat{W}_o]. \end{cases} \tag{6.42}$$

Choosing the Lyapunov function candidate

$$V_o = \frac{1}{2}\tilde{\eta}^T \tilde{\eta} + \frac{1}{2}\tilde{v}^T \tilde{v} + \frac{1}{2}\operatorname{tr}\{\tilde{W}_o^T \Gamma_o^{-1} \tilde{W}_o\}, \tag{6.43}$$

the time derivative of V_o along (6.42) is given by

$$\begin{aligned} \dot{V}_o &= \tilde{\eta}^T \dot{\tilde{\eta}} + \tilde{v}^T \dot{\tilde{v}} + \operatorname{tr}\{\tilde{W}_o^T \Gamma_o^{-1} \dot{\tilde{W}}_o\} \\ &= -\tilde{\eta}^T K_\eta \tilde{\eta} + \tilde{v}^T \left[-K_v \tilde{v} + \hat{W}_o^T S(\hat{Z}_o) - W_o^{*T} S(Z_o) - \varepsilon_{Z_o} - M^{-1} D(\tau_c)\right] \\ &\quad + \operatorname{tr}\{\tilde{W}_o^T \left[S(\hat{Z}_o)\tilde{\eta}^T - \sigma_o \hat{W}_o\right]\} \\ &= -\tilde{\eta}^T K_\eta \tilde{\eta} - \tilde{v}^T K_v \tilde{v} + \tilde{v}^T \tilde{W}_o^T S(\hat{Z}_o) + \tilde{v}^T \varrho + \tilde{\eta}^T \tilde{W}_o^T S(\hat{Z}_o) \\ &\quad - \sigma_o \operatorname{tr}\{\tilde{W}_o^T \hat{W}_o\}, \end{aligned} \tag{6.44}$$

where $\varrho = W_o^{*T} S(\hat{Z}_o) - W_o^{*T} S(Z_o) - \varepsilon_{Z_o} - M^{-1} D(\tau_c)$. Since the hyperbolic tangent function $s_i(\bullet)$ is bounded, both $S(\hat{Z}_o)$ and $S(Z_o)$ are bounded. Furthermore, ϱ is bounded due to the boundedness of W^*, ε_{Z_o}, and $D(\tau_c)$, which implies that $\|\varrho\| \leq \varrho^*$ with constant $\varrho^* > 0$. Using the inequalities

$$\begin{aligned} \tilde{v}^T \tilde{W}_o^T S(\hat{Z}_o) &\leq \frac{1}{2\gamma}\tilde{v}^T \tilde{v} + \frac{\gamma l_o}{2}\|\tilde{W}_o\|_F^2, \\ \tilde{\eta}^T \tilde{W}_o^T S(\hat{Z}_o) &\leq \frac{1}{2\gamma}\tilde{\eta}^T \tilde{\eta} + \frac{\gamma l_o}{2}\|\tilde{W}_o\|_F^2, \\ \tilde{v}^T \varrho &\leq \frac{1}{2\gamma}\tilde{v}^T \tilde{v} + \frac{\gamma}{2}\varrho^{*2}, \\ -\sigma_o \operatorname{tr}\{\tilde{W}_o^T \hat{W}_o\} &\leq -\frac{\sigma_o}{2}\|\tilde{W}_o\|_F^2 + \frac{\sigma_o}{2}\|W_o^*\|_F^2, \end{aligned}$$

we have

$$\dot{V}_o \leq -\left(k_\eta - \frac{1}{2\gamma}\right)\tilde{\eta}^T \tilde{\eta} - \left(k_v - \frac{1}{\gamma}\right)\tilde{v}^T \tilde{v} - \left(\frac{\sigma_o}{2} - \gamma l_o\right)\|\tilde{W}_o\|_F^2 + \mu_o^*, \tag{6.45}$$

where γ is a positive constant, and $\mu_o^* = \frac{\gamma}{2}\varrho^{*2} + \frac{\sigma_o}{2}\|W_o^*\|_F^2$. Choosing the parameters as

$$k_\eta > \frac{1}{2\gamma}, \qquad k_v > \frac{1}{\gamma}, \qquad \sigma_o > 2\gamma l_o \tag{6.46}$$

and denoting

$$\rho_o = \min\left\{2\left(k_\eta - \frac{1}{2\gamma}\right), 2\left(k_v - \frac{1}{\gamma}\right), \frac{\sigma_o - 2\gamma l_o}{\lambda_{\max}(\Gamma_o^{-1})}\right\}, \tag{6.47}$$

we can obtain that

$$\dot{V}_o \leq -\rho_o V_o + \mu_o^*. \tag{6.48}$$

The above equation implies that the state estimation errors $\tilde{\eta}$ and $\tilde{v}$ converge to the compact set $\Omega_{so} := \{\tilde{\eta} \in \mathbb{R}^3, \tilde{v} \in \mathbb{R}^3 | \ \|\tilde{\eta}\| \leq \sqrt{2\mu_o^*/\rho_o}$ and $\|\tilde{v}\| \leq \sqrt{2\mu_o^*/\rho_o}\}$ asymptotically. Since ρ_o is adjustable, μ_o^*/ρ_o can be made arbitrarily small. Therefore, for any given small constants ϵ_η and ϵ_v, there exists an instant t^* such that, for all $t > t^*$, the following inequalities hold: $\|\hat{\eta} - \eta\| \leq \epsilon_\eta$ and $\|\hat{v} - v\| \leq \epsilon_v$. This completes the proof. □

6.3.2.2 Output Feedback Control Design

Based on the above observer, output feedback robust adaptive control for the single-point mooring systems (6.1) can be constructed as follows.

Step 1: Consider the first equation of (6.1). Define the error variables $z_1 = \eta - \eta_d$ and $\hat{z}_2 = \hat{v} - \alpha_1$ and consider the Lyapunov function candidate $V_1 = \frac{1}{2}z_1^T z_1$. Differentiating z_1 with respect to time yields

$$\dot{z}_1 = J(\eta)(-\tilde{v} + \hat{z}_2 + \alpha_1) - \dot{\eta}_d. \tag{6.49}$$

Noting that $J^T(\eta)J(\eta) = I$ and choosing the virtual control as

$$\alpha_1 = J^T(\eta)(\dot{\eta}_d - K_1 z_1), \tag{6.50}$$

where $K_1 = K_1^T > 0$, the time derivative of V_1 along the trajectories of (6.49) is given by

$$\dot{V}_1 = -z_1^T K_1 z_1 - z_1^T J(\eta)\tilde{v} + z_1^T J(\eta)\hat{z}_2. \tag{6.51}$$

The first term on the RHS is stabilizing, and the last two terms will be handled in the next step.

Step 2: Differentiating $\hat{z}_2$ with respect to time yields

$$\dot{\hat{z}}_2 = \dot{\hat{v}} - \dot{\alpha}_1, \tag{6.52}$$

where $\dot{\alpha}_1 = (\partial\alpha_1/\partial\eta)\dot{\eta} + (\partial\alpha_1/\partial\dot{\eta}_d)\ddot{\eta}_d + (\partial\alpha_1/\partial z_1)\dot{z}_1$. From $\tilde{v} = \hat{v} - v$ we know that $\dot{\tilde{v}} = \dot{v} + \dot{\tilde{v}}$. Substituting $\dot{\hat{v}}$ into (6.52) and considering the second equation of the system (6.1), we have

$$\dot{\hat{z}}_2 = M^{-1}\big[\tau_{\text{moor}}(\eta) + \tau_{\text{env}}(\eta) + H_a\tau_c - C(v)v - D(v)v - g(\eta)\big] + M^{-1}D(\tau_c) - \dot{\alpha}_1 + \dot{\tilde{v}}. \tag{6.53}$$

Consider the Lyapunov function candidate $V_2^* = V_1 + \frac{1}{2}\hat{z}_2^T H_a^{-1} M\hat{z}_2$. Its time derivative along (6.53) is

$$\dot{V}_2^* = -z_1^T K_1 z_1 - z_1^T J(\eta)\tilde{v} + z_1^T J(\eta)\hat{z}_2 + \hat{z}_2^T\big[Q(Z) + \tau_c + H_a^{-1}D(\tau_c)\big] + \hat{z}_2^T H_a^{-1} M\dot{\tilde{v}}, \tag{6.54}$$

where $Q(Z) = H_a^{-1}[\tau_{\text{moor}}(\eta) + \tau_{\text{env}}(\eta) - C(v)v - D(v)v - g(\eta) - M\dot{\alpha}_1]$ with $Z = [\eta^T, v^T, \alpha_1^T, \dot{\alpha}_1^T]^T$. The unknown function $Q(Z)$ can be approximated by using HONN, which can be represented by

$$Q(Z) = W^{*T}S(Z) + \varepsilon_Z, \tag{6.55}$$

where $W^* \in \mathbb{R}^{l\times 3}$ denotes the ideal constant weight matrix, $S(Z) \in \mathbb{R}^l$, l is the neural network node number, and $\varepsilon_Z \in \mathbb{R}^3$ is the approximation error with $\|\varepsilon_Z\| \le \varepsilon_Z^*$ and constant $\varepsilon_Z^* > 0$. However, since the velocity vector v is not available, we can use its estimation to substitute it. Then, we construct the adaptive control τ_c and the NN weight adaptation law as

$$\tau_c = -J^T(\eta)z_1 - K_2\hat{z}_2 - \hat{W}^T S(\hat{Z}) - \hat{\beta}\,\text{Tanh}\left(\frac{\hat{z}_2}{b}\right), \tag{6.56}$$

$$\dot{\hat{W}} = \Gamma_w\big[S(\hat{Z})\hat{z}_2^T - \sigma_w\hat{W}\big], \tag{6.57}$$

$$\dot{\hat{\beta}} = \Gamma_\beta\left[\text{Tanh}\left(\frac{\hat{z}_2}{b}\right)\hat{z}_2^T - \sigma_\beta\hat{\beta}\right], \tag{6.58}$$

where $\hat{W} \in \mathbb{R}^{l\times 3}$ denotes the NN weight matrix, $S(\hat{Z}) \in \mathbb{R}^l$ with $\hat{Z} = [\eta^T, \hat{v}^T, \alpha_1^T, \dot{\alpha}_1^T]^T$, l is the neural network node number, and $\text{Tanh}(\frac{\hat{z}_2}{b}) = [\tanh(\frac{\hat{z}_{21}}{b}), \tanh(\frac{\hat{z}_{22}}{b}), \tanh(\frac{\hat{z}_{23}}{b})]^T$ with $\hat{z}_{2i}$ $(i = 1, 2, 3)$ being the ith element of the vector $\hat{z}_2$, $K_2 \in \mathbb{R}^{3\times 3}$ is a diagonal positive matrix; $\hat{\beta} \in \mathbb{R}^{3\times 3}$ is the estimate of the positive matrix $\beta^* = \lambda_{\beta m} I$ with $\lambda_{\beta m} = \frac{2l_o m^*}{h_a^*}\|W_o^*\| + 2l\|W^*\| + \varepsilon_Z^* + \frac{m^*\varepsilon_{Z_o}^*}{h_a^*}$; $b > 0$ is a positive constant; $\Gamma_w = \Gamma_w^T \in \mathbb{R}^{l\times l} > 0$ and $\Gamma_\beta = \Gamma_\beta^T \in \mathbb{R}^{3\times 3} > 0$ are design constant matrices; and $\sigma_w > 0$ and $\sigma_\beta > 0$ are design constants.

Theorem 6.6 *Consider the single-point mooring system* (6.1) *with Assumptions* 6.1 *and* 6.2, *the output feedback control law* (6.56), *the observer* (6.41), *and the adaptation laws* (6.57) *and* (6.58). *For any given positive constant* $\gamma > 0$ *and bounded*

initial conditions, if the parameters satisfy

$$K_1 > \frac{1}{2}I, \qquad K_2 > \frac{m^{*2}}{2h_a^{*2}}\left(1 + k_v + \frac{1}{\gamma}\right)I,$$
$$k_\eta > \frac{1}{2\gamma} + \frac{1}{2}, \qquad k_v > 1 + \frac{2}{\gamma}, \qquad \sigma_o > \gamma l_o,$$

then the overall closed-loop control system is semiglobally stable in the sense that all signals in the closed-loop system are bounded and the tracking error is smaller than a prescribed error bound.

Proof Denoting $\tilde{W} = \hat{W} - W^*$ and $\tilde{\beta} = \hat{\beta} - \beta^*$ and considering the augmented Lyapunov function candidate

$$V_2 = V_o + V_1 + \frac{1}{2}\hat{z}_2^T H_a^{-1} M \hat{z}_2 + \mathrm{tr}\left\{\frac{1}{2}\tilde{W}^T \Gamma_w^{-1} \tilde{W}\right\} + \mathrm{tr}\left\{\frac{1}{2}\tilde{\beta}^T \Gamma_\beta^{-1} \tilde{\beta}\right\}, \quad (6.59)$$

the time derivative of V_2 along the trajectories of (6.54), (6.56), (6.57), and (6.58) is given by

$$\begin{aligned}
\dot{V}_2 &= \dot{V}_o + \dot{V}_1 + \hat{z}_2^T H_a^{-1} M \dot{\hat{z}}_2 + \mathrm{tr}\{\tilde{W}^T \Gamma_w^{-1} \dot{\tilde{W}}\} + \mathrm{tr}\{\tilde{\beta}^T \Gamma_\beta^{-1} \dot{\tilde{\beta}}\} \\
&= \dot{V}_o - z_1^T K_1 z_1 - z_1^T J(\eta)\tilde{v} + z_1^T J(\eta)\hat{z}_2 + \hat{z}_2^T H_a^{-1} M \dot{\tilde{v}} \\
&\quad + \hat{z}_2^T \left[W^{*T} S(Z) + \varepsilon_Z - J^T(\eta) z_1 - K_2 \hat{z}_2 - \hat{W}^T S(\hat{Z}) - \hat{\beta}\,\mathrm{Tanh}\left(\frac{\hat{z}_2}{b}\right) \right. \\
&\quad \left. + H_a^{-1} D(\tau_c) \right] + \mathrm{tr}\{\tilde{W}^T [S(\hat{Z})\hat{z}_2^T - \sigma_w \hat{W}]\} \\
&\quad + \mathrm{tr}\left\{\tilde{\beta}^T \left[\mathrm{Tanh}\left(\frac{\hat{z}_2}{b}\right)\hat{z}_2^T - \sigma_\beta \hat{\beta}\right]\right\}. \qquad (6.60)
\end{aligned}$$

Adding and subtracting $\hat{z}_2^T W^{*T} S(\hat{Z})$ on the RHS of (6.60) and substituting the second equation of (6.42) into (6.60) yield

$$\begin{aligned}
\dot{V}_2 &= -z_1^T K_1 z_1 - \hat{z}_2^T K_2 \hat{z}_2 - z_1^T J(\eta)\tilde{v} \\
&\quad - \hat{z}_2^T H_a^{-1} M J(\eta)\tilde{\eta} - \hat{z}_2^T H_a^{-1} M K_v \tilde{v} + \hat{z}_2^T H_a^{-1} M \tilde{W}_o^T S(\hat{Z}_o) \\
&\quad - \hat{z}_2^T \beta - \hat{z}_2^T \beta^* \mathrm{Tanh}\left(\frac{\hat{z}_2}{b}\right) - \sigma_w \mathrm{tr}\{\tilde{W}^T \hat{W}\} - \sigma_\beta \mathrm{tr}\{\tilde{\beta}^T \hat{\beta}\} + \dot{V}_o, \quad (6.61)
\end{aligned}$$

where

$$\beta = H_a^{-1} M W_o^{*T} [S(\hat{Z}_o) - S(Z_o)] + W^{*T} [S(Z) - S(\hat{Z})] - H_a^{-1} M \varepsilon_{Z_o} + \varepsilon_Z.$$

If we denote $\beta := [\beta_1, \beta_2, \beta_3]^T$, the following property is always established for $i = 1, 2, 3$:

$$\begin{aligned}\beta_i| \le \|\beta\| &\le \frac{m^*}{h_a^*}\|W_o^*\|\|S(\hat{Z}_o) - S(Z_o)\| + \|W^*\|\|S(Z) - S(\hat{Z})\| + \|\varepsilon_Z\| \\ &\le + \frac{m^*}{h_a^*}\|\varepsilon_{Z_o}\|\lambda_{\beta m},\end{aligned} \tag{6.62}$$

which implies that

$$-\hat{z}_2^T\beta = -\sum_{i=1}^{3}\hat{z}_{2i}\beta_i \le \lambda_{\beta m}\sum_{i=1}^{3}|\hat{z}_{2i}|. \tag{6.63}$$

Considering Eq. (6.63) and property (6.32) and using the inequalities

$$\begin{aligned}-z_1^T J(\eta)\tilde{v} &\le \frac{1}{2}z_1^T z_1 + \frac{1}{2}\tilde{v}^T\tilde{v}, \\ -\hat{z}_2^T H_a^{-1} M J(\eta)\tilde{\eta} &\le \frac{m^{*2}}{2h_a^{*2}}\hat{z}_2^T\hat{z}_2 + \frac{1}{2}\tilde{\eta}^T\tilde{\eta}, \\ -\hat{z}_2^T H_a^{-1} M K_v\tilde{v} &\le \frac{k_v m^{*2}}{2h_a^{*2}}\hat{z}_2^T\hat{z}_2 + \frac{k_v}{2}\tilde{v}^T\tilde{v}, \\ \hat{z}_2^T H_a^{-1} M\tilde{W}_o^T S(\hat{Z}_o) &\le \frac{m^{*2}}{2\gamma h_a^{*2}}\hat{z}_2^T\hat{z}_2 + \frac{\gamma l_o}{2}\|\tilde{W}_o\|_F^2, \\ -\sigma_w \operatorname{tr}\{\tilde{W}^T\hat{W}\} &\le -\frac{\sigma_w}{2}\|\tilde{W}\|_F^2 + \frac{\sigma_w}{2}\|W^*\|_F^2, \\ -\sigma_\beta \operatorname{tr}\{\tilde{\beta}^T\hat{\beta}\} &\le -\frac{\sigma_\beta}{2}\|\tilde{\beta}\|_F^2 + \frac{\sigma_\beta}{2}\|\beta^*\|_F^2,\end{aligned}$$

we have

$$\begin{aligned}\dot{V}_2 \le &-z_1^T\left(K_1 - \frac{1}{2}I\right)z_1 - \hat{z}_2^T\left[K_2 - \frac{m^{*2}}{2h_a^{*2}}\left(1 + k_v + \frac{1}{\gamma}\right)I\right]\hat{z}_2 \\ &- \frac{\sigma_w}{2}\|\tilde{W}\|_F^2 c\gamma l_o 2\|\tilde{W}_o\|_F^2 - \frac{\sigma_\beta}{2}\|\tilde{\beta}\|_F^2 + 0.8355b\lambda_{\beta m} + \frac{\sigma_w}{2}\|W^*\|_F^2 \\ &+ \frac{\sigma_\beta}{2}\|\beta^*\|_F^2 + \frac{(1+k_v)}{2}\tilde{v}^T\tilde{v} + \frac{1}{2}\tilde{\eta}^T\tilde{\eta} + \dot{V}_o.\end{aligned} \tag{6.64}$$

Substituting (6.45) into (6.64) leads to

$$\begin{aligned}\dot{V}_2 \le &-z_1^T\left(K_1 - \frac{1}{2}I\right)z_1 - \hat{z}_2^T\left[K_2 - \frac{m^{*2}}{2h_a^{*2}}\left(1 + k_v + \frac{1}{\gamma}\right)I\right]\hat{z}_2 - \frac{\sigma_w}{2}\|\tilde{W}\|_F^2 \\ &- \frac{\sigma_\beta}{2}\|\tilde{\beta}\|_F^2 - \left(k_\eta - \frac{1}{2\gamma} - \frac{1}{2}\right)\tilde{\eta}^T\tilde{\eta} - \left(\frac{k_v}{2} - \frac{1}{2} - \frac{1}{\gamma}\right)\tilde{v}^T\tilde{v}\end{aligned}$$

$$-\frac{(\sigma_o-\gamma l_o)}{2}\|\tilde{W}_o\|_F^2+\mu_1^*, \tag{6.65}$$

where $\mu_1^*=0.8355b\lambda_{\beta m}+\frac{\sigma_w}{2}\|W^*\|_F^2+\frac{\sigma_\beta}{2}\|\beta^*\|_F^2+\mu_o^*$. Furthermore, choosing the parameters such that

$$\begin{aligned} &K_1>\frac{1}{2}I, \qquad K_2>\frac{m^{*2}}{2h_a^{*2}}\left(1+k_v+\frac{1}{\gamma}\right)I,\\ &k_\eta>\frac{1}{2\gamma}+\frac{1}{2}, \qquad k_v>1+\frac{2}{\gamma}, \qquad \sigma_o>\gamma l_o \end{aligned} \tag{6.66}$$

and denoting

$$\begin{aligned} \rho_1=\min\Bigg\{&2\lambda_{\min}\left(K_1-\frac{1}{2}I\right),\frac{2h_a^*\lambda_{\min}(K_2-\frac{m^{*2}}{2h_a^{*2}}(1+k_v+\frac{1}{\gamma})I)}{m^*},\frac{\sigma_w}{\lambda_{\max}(\Gamma_w^{-1})},\\ &\frac{\sigma_\beta}{\lambda_{\max}(\Gamma_\beta^{-1})},2\left(k_\eta-\frac{1}{2\gamma}-\frac{1}{2}\right),\left(k_v-1-\frac{2}{\gamma}\right),\frac{(\sigma_o-\gamma l_o)}{\lambda_{\max}(\Gamma_o^{-1})}\Bigg\}, \end{aligned} \tag{6.67}$$

we can obtain that

$$\dot{V}_2\le-\rho_1V_2+\mu_1^*. \tag{6.68}$$

Similarly as in the proof of Theorem 6.4, we can conclude from (6.68) that all signals of the closed-loop system are uniformly ultimately bounded. Furthermore, for any given constants b, σ_w, σ_β, γ, and σ_o, the value of $\frac{\mu_1^*}{\rho_1}$ can be made arbitrarily small by adjusting the parameters K_1, K_2, k_η, k_v, Γ_w, Γ_β, and Γ_o. Therefore, the tracking error z_1 can become arbitrarily small. This completes the proof. □

6.4 Simulations

In our simulation study, we consider the model of Cybership II [254, 255], a 1:70 scale supply vessel replica built in a marine control laboratory in the Norwegian University of Science and Technology, which can be represented by (6.1). For clarity and completeness, its parameters are first given in this section.

The system inertia matrix M, the matrix of Coriolis and centripetal terms $C(v)$ and the damping matrix $D(v)$ are given as

$$M=\begin{bmatrix}25.8 & 0 & 0\\ 0 & 33.8 & 1.0115\\ 0 & 1.0115 & 2.76\end{bmatrix},$$

$$C(v)=\begin{bmatrix}0 & 0 & -33.8v_y-1.0115v_\psi\\ 0 & 0 & 25.8v_x\\ 33.8v_y+1.0115v_\psi & -25.8v_x & 0\end{bmatrix},$$

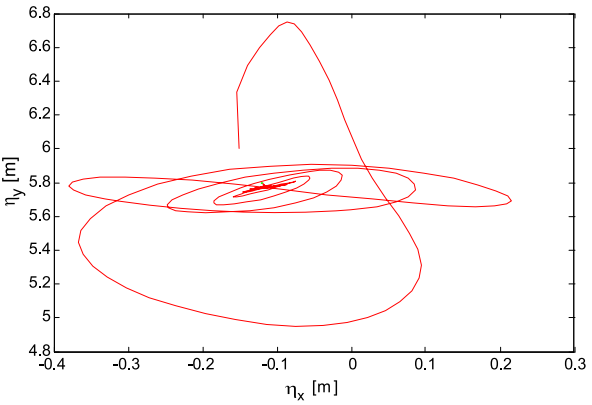

Fig. 6.3 Control performance

$$D(v) = \begin{bmatrix} -X_u - X_{uuu}v_x^2 & 0 & 0 \\ 0 & -Y_v - Y_{vvv}v_y^2 & -d_{23}(v) \\ 0 & -d_{32}(v) & -N_r - N_{rrr}v_\psi^2 \end{bmatrix},$$

where $d_{23}(v) = Y_r + Y_{rrr}v_\psi^2 + Y_{vvr}v_y^2 + Y_{vrr}v_y v_\psi$ and $d_{32}(v) = N_v + N_{vvv}v_y^2 + N_{vrr}v_\psi^2 + N_{vvr}v_\psi v_y$. This nonlinear damping matrix $D(v)$ is valid for all feasible velocities [255]. In this chapter, the parameters are chosen as $X_u = -0.7225$, $X_{uuu} = -5.8664$, $Y_v = -0.8612$, $Y_{vvv} = -36.42$, $N_r = -1.9$, $N_{rrr} = -0.75$, $Y_r = 0.1079$, $Y_{rrr} = -3.45$, $Y_{vvr} = -0.425$, $Y_{vrr} = -0.425$, $N_v = 0.1052$, $N_{vvv} = -0.75$, $N_{vrr} = 0.04$, and $N_{vvr} = 0.04$. The matrix $g(\eta)$ is specified as

$$g(\eta) = [0.2\cos\eta_\psi - 0.36\sin\eta_\psi, 0.2\sin\eta_\psi + 0.36\cos\eta_\psi, 0.18].$$

The hysteresis parameters are chosen as $h_{r1} = 1$, $h_{a1} = 1$, $h_{B1} = 0.2$, $h_{r2} = 1$, $h_{a2} = 1$, $h_{B2} = 0.2$, $h_{r3} = 1$, $h_{a3} = 2$, and $h_{B3} = 0.3$. The mooring line is considered as the nylon vetted rope, where $p_m = 0.14$, $q_m = 1.93$, $l_w = 1$ m, $x_p = 0.6$, and $S_b = 6.80625$ lbf. The initial states of ship dynamics are $\eta(0) = [-0.15, 6, 0.0837]^T$ and $v(0) = [0.2, 9, 0.1]^T$, where all units are SI.

The parameters of state feedback controller are listed as follows. The number of neurons used is $l = 102$, and the initial neural network estimate $\hat{W}(0) = 0$. The design parameters are chosen as $K_1 = \text{diag}\{0.1, 0.1, 0.1\}$ and $K_2 = \text{diag}\{0.4, 0.4, 0.4\}$.

First, keep the vessel at a desired position with $\eta_{xd} = -0.12$ and $\eta_{yd} = 0.58$ and a desired heading $\eta_{xd} = 0$ by using the proposed state feedback control. Simulation results are shown in Figs. 6.3, 6.4, 6.5 and 6.6. Figure 6.3 shows the position of the surface vessel, which demonstrates control performance. Figure 6.4 exhibits the system outputs following the desired trajectory, while Figs. 6.5 and 6.6 display the bounded control inputs and the norm of NN weighting matrix, respectively. From the above simulation results we can clearly see that there are large errors between the desired outputs and real outputs at the initial simulation time. After several seconds vibration, the vessel surge, sway, and yaw can be maintained in a small neighborhood of their desired values. Under the proposed control, the surface vessel can be

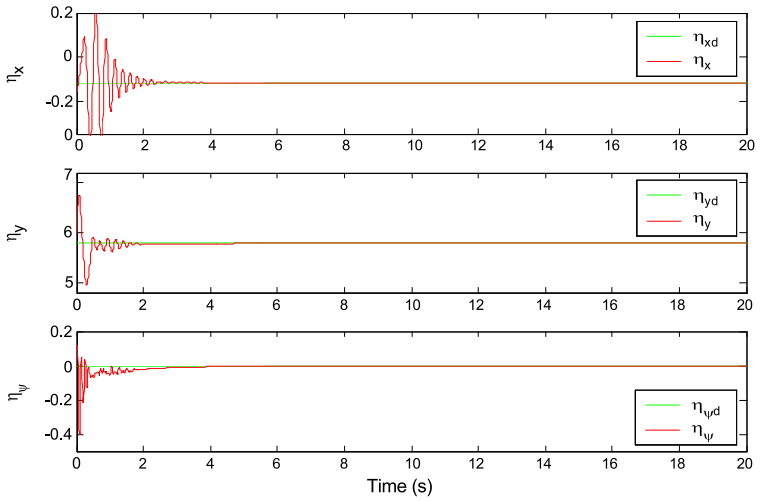

Fig. 6.4 States of surface vessel

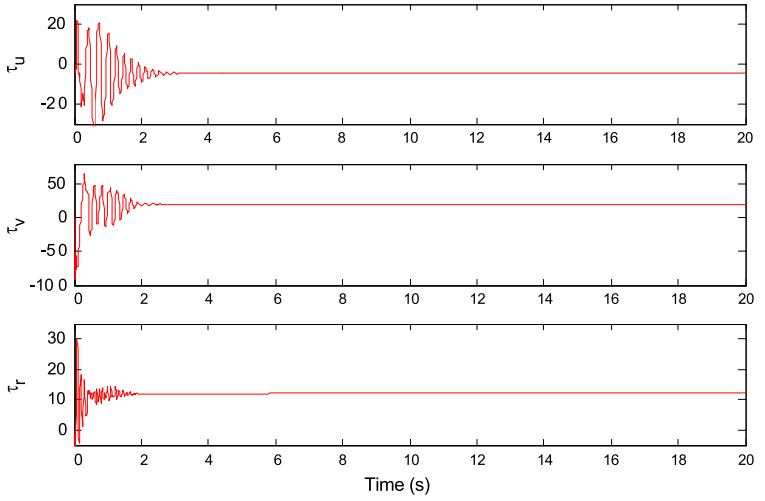

Fig. 6.5 Control inputs

maintained at a fixed position and heading after several seconds adaptation, while the control inputs and NN weighting matrix are all bounded.

Next, let the vessel track a desired trajectory, $\eta_d(t) = [\eta_{xd}(t), \eta_{yd}(t), \eta_{\psi d}(t)]^T$ by using the previous control, where $\eta_{xd} = \sqrt{0.02}t$, $\eta_{yd} = 10\cos(0.1\eta_{xd}(t))$, and $\eta_{\psi d}(t) = \tan^{-1}(d\eta_{yd}/d\eta_{xd})$. This gives a maximum desired speed of 0.2 $\mathrm{m\,s^{-1}}$, which corresponds to 3.1 knots in the full-scale vessel. The simulation results are shown in Figs. 6.7, 6.8 and 6.9. It can be observed that the tracking performance of the ship is satisfactory, while Fig. 6.7 shows that the ship remains within a small

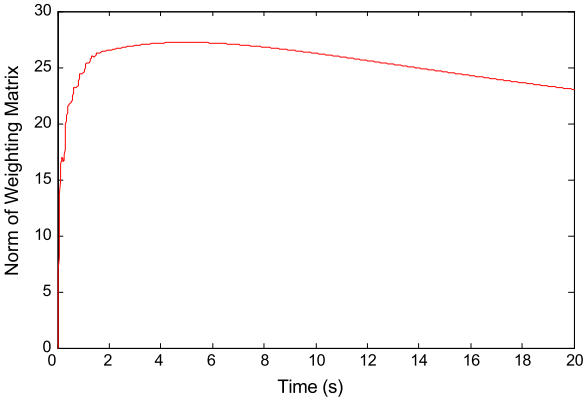

Fig. 6.6 Norm of NN weighting matrix, $\|\hat{W}\|$

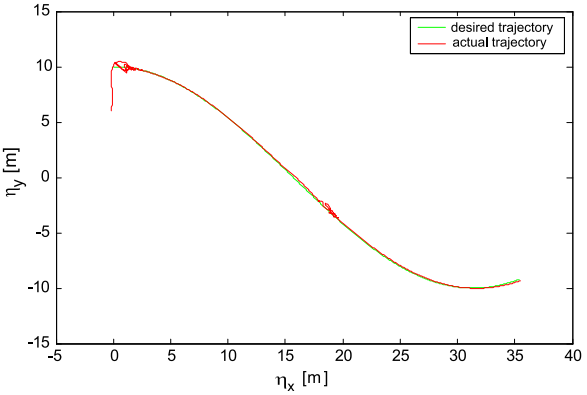

Fig. 6.7 Tracking performance

neighborhood of the desired path. Figure 6.8 demonstrates the system outputs following the desired trajectory, and Fig. 6.9 displays the bounded control inputs, respectively. From the above simulation results it can be seen that the vessel surge, sway, and yaw can track their desired trajectories, although there are large tracking errors at the initial simulation time. At the same time, the control inputs are all bounded.

6.5 Conclusion

In this chapter, both full-state and output feedback adaptive neural network controls are investigated for single-point mooring system with unknown backlash-like hysteresis in truster dynamics. The backlash-like hysteresis is transformed into a liner term plus a bounded nonlinear term, and then an effective full-state feedback control is proposed via backstepping design. To overcome the measure difficulty in the velocity vector, a HONN-based observer is constructed to estimate the unmeasurable states, and then an output feedback adaptive neural network control is developed. The closed-loop systems for both control schemes are proved to be semiglobally

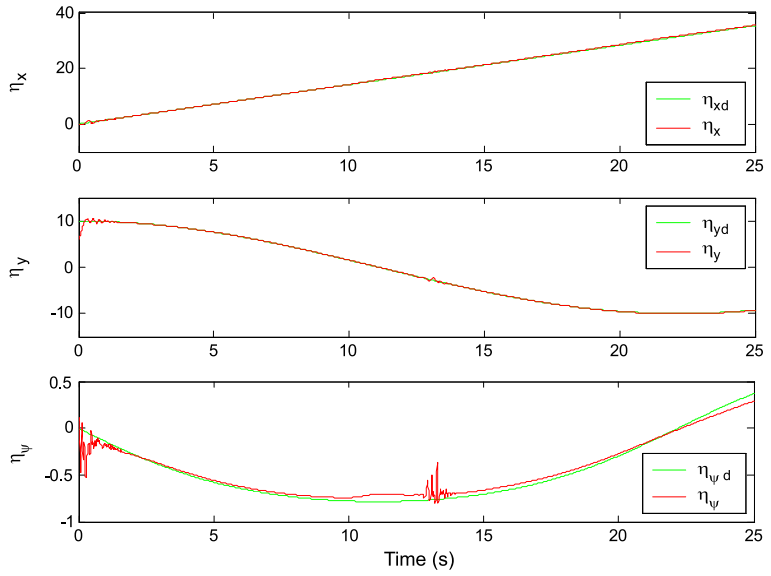

Fig. 6.8 States of surface vessel

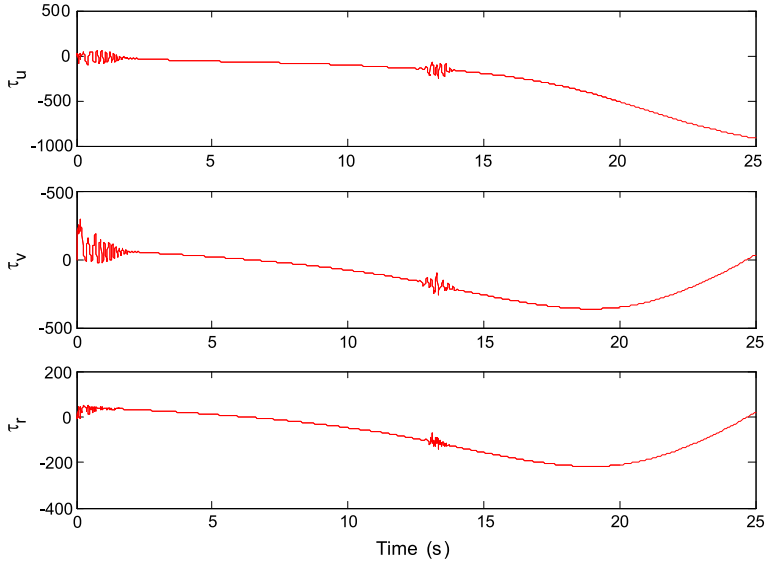

Fig. 6.9 Control inputs

uniformly ultimately bounded. Simulations of a ship model have demonstrated that the single-point mooring system is able to both keep the vessel at the specified set-point position and heading and track the desired trajectory under the proposed controls.

Chapter 7
Coupled Nonlinear Flexible Marine Riser

7.1 Introduction

Vibration problems of slender bodies in ocean engineering such as oil drilling and gas exploration have received increasing attention. Improving reliability and efficiency of operations during oil and gas production in the ocean environment is a challenging research topic in offshore engineering. With the trends toward exploiting resources in deep waters and harsher environments, the vibration problem of riser becomes more and more significant [256]. A typical marine riser system depicted in Fig. 7.1 is the connection between a vessel on the ocean surface and a well head on the ocean floor. A drilling riser is used for drilling pipe protection and transportation of the drilling mud, while a production riser is a pipe used for oil transportation. The stiffness of a flexible marine riser depends on its tension and length, and thus a riser that spans a long distance can produce large vibrations under relatively small disturbances. In marine environment, vibrations excited by vortices can degrade the performance of the flexible marine riser. Vibrations of the riser due to the ocean current disturbance and tension exerted at the top can produce premature fatigue problems, which require inspections and costly repairs, and as a worst case, environmental pollution due to leakage from damaged areas. Vibration reduction to minimize the bending stresses is desirable for preventing damage and improving lifespan.

For purpose of dynamic analysis, the flexible riser is regarded as a distributed parameter system which is infinite-dimensional and mathematically represented by PDEs with various boundary conditions involving functions of space and time. The riser system can be modeled as an Euler–Bernoulli beam structure since the diameter-to-length ratio of the riser is small from the ocean surface to the ocean floor. In practice, dynamics of flexible risers are usually represented by a set of PDEs with appropriate boundary equations or approximated by ordinary differential equations (ODEs). In [3, 44, 45], PDEs based on the Euler–Bernoulli beam model have been used to analyze the dynamic response of the flexible marine riser system under the ocean current disturbance. In [48], a boundary controller for the flexible marine riser with actuator dynamics is designed based on Lyapunov's direct method

W. He et al., *Dynamics and Control of Mechanical Systems in Offshore Engineering*, Advances in Industrial Control, DOI 10.1007/978-1-4471-5337-5_7,

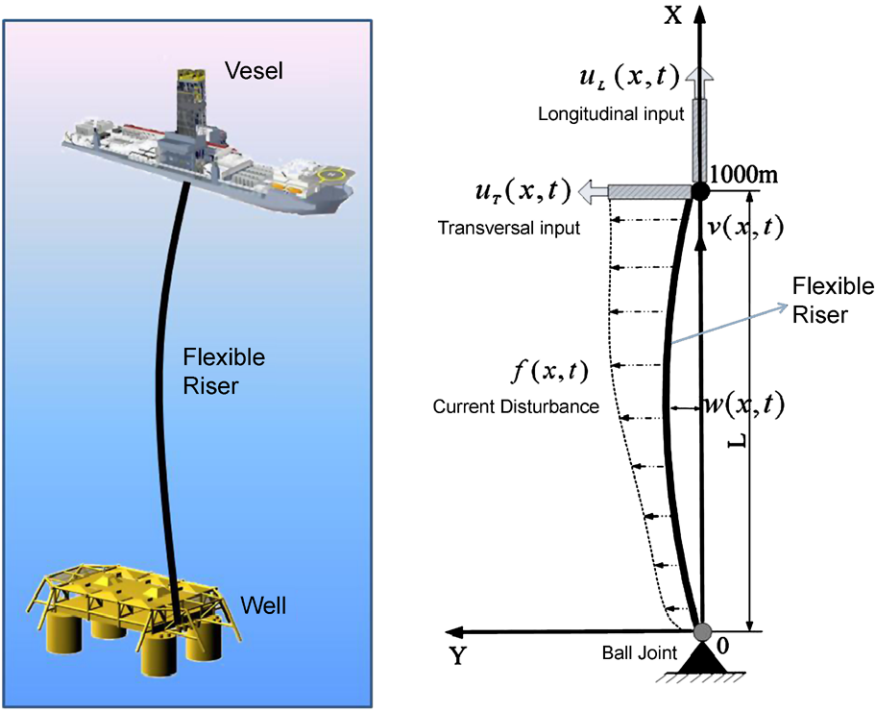

Fig. 7.1 A typical marine riser system

and the backstepping technique. In [4], a boundary control law is designed to generate the required signal for riser angle control and transverse vibration reduction with guaranteed closed-loop stability, and the exponential stability of the system is proved under the free vibration conditions. The dynamics of the flexible mechanical system is modeled by a set of PDEs with infinite number of dimensions, which makes it difficult to control.

In this chapter, we design the boundary control law based on the distributed parameter system model of the flexible riser system. As shown in Fig. 7.1, the control is implemented at the top of the riser through two actuators in transverse and longitudinal directions. The control objective is to design a controller to reduce both transverse and longitudinal vibrations of the riser. The control inputs from the two actuators in the vessel are designed via Lyapunov's direct method, and the required measurements for feedback are the displacement in the transverse and longitudinal directions at the top of the riser. Although a flexible riser is considered in this chapter specifically, the analysis and control design can be extended and applied for vibration control for a class of tensioned beams exposed to undesirable distributed transverse loads. Other examples of practical application in the marine environment include free hanging underwater pipelines or drill strings.

In former marine flexible riser research, the axial deformation of the riser is usually ignored for the convenience of dynamic analysis. Only the transverse dynamics

of the riser is considered, and the coupling between transverse and longitudinal displacements is neglected, which can influence the dynamic response of the riser system and lead to an imprecise model. In this chapter, both the axial deformation and transverse displacement of the riser are considered in the dynamic analysis. To the best of our knowledge, this is the first application of boundary control to a flexible marine riser for reduction of transverse and longitudinal vibrations through two actuators. The main contributions of this chapter include:

(i) A coupled nonlinear dynamic model of the marine flexible riser for reduction of transverse and longitudinal vibrations is derived under the distributed ocean current disturbance.
(ii) An implementable boundary control with two actuators in transverse and longitudinal directions is designed to reduce both transverse and longitudinal vibrations of the marine flexible riser.
(iii) The uniform boundedness under ocean current disturbance and exponential stability under free vibration condition is proved via Lyapunov's direct method.
(iv) Numerical simulations via finite difference method are used to verify the effectiveness and performance of the proposed controller.

The rest of the chapter is organized as follows. Section 7.2 illustrates the dynamic equations (PDEs) of the flexible riser and boundary conditions by analyzing the dynamics of this flexible structure with fluctuant environmental disturbances. In Sect. 7.3, the boundary control design via Lyapunov's direct method is discussed for this coupled nonlinear flexible beam, where it is shown that the uniform boundedness of the closed-loop system can be guaranteed under the distributed ocean current disturbance and the exponential stability can be achieved under free vibration condition. The numerical simulation with the finite difference method is presented in Sect. 7.4 to verify the performance of the proposed controller. The conclusion of this chapter is given in Sect. 7.5.

7.2 Problem Formulation

In this chapter, we assume that the vessel is directly above the subsea well head with no horizontal offset and the riser is filled with seawater. The flexible marine riser with uniform density and flexural rigidity is modeled as the Euler–Bernoulli beam structure since the diameter-to-length ration of the riser is small.

The kinetic energy of the riser system E_k can be represented as

$$E_k = \frac{1}{2}\rho \int_0^L \left[\left(\frac{\partial w(x,t)}{\partial t} \right)^2 + \left(\frac{\partial v(x,t)}{\partial t} \right)^2 \right] dx, \tag{7.1}$$

where x and t represent the independent spatial and time variables, respectively, $w(x,t)$ and $v(x,t)$ are the displacements in the transverse and longitudinal directions of the riser at the position x for time t, $\rho > 0$ is the uniform mass per unit length of the riser, and L is the length of the beam.

The potential energy E_p due to the bending and the axial deformation [59] can be obtained from

$$E_p = \frac{1}{2}EI\int_0^L \left[\frac{\partial^2 w(x,t)}{\partial x^2}\right]^2 dx + \frac{1}{2}T\int_0^L \left[\frac{\partial w(x,t)}{\partial x}\right]^2 dx + \frac{1}{2}EA\int_0^L \left\{\frac{\partial v(x,t)}{\partial x} + \frac{1}{2}\left[\frac{\partial w(x,t)}{\partial x}\right]^2\right\}^2 dx, \tag{7.2}$$

where T is the tension of the riser, EI is the bending stiffness, and EA is the axial stiffness. The first term of Eq. (7.2) is due to the bending, the second term is due to axial force, and the third term is due to the strain energy of the beam.

The work done by ocean current disturbance on the riser is given by

$$W_f = \int_0^L f(x,t)w(x,t)\,dx, \tag{7.3}$$

where $f(x,t)$ is the distributed transverse load due to the hydrodynamic effects of the ocean current. The work done by linear structure damping is represented by

$$W_d = -\int_0^L c_1\left[\frac{\partial w(x,t)}{\partial t}\right]w(x,t)\,dx - \int_0^L c_2\left[\frac{\partial v(x,t)}{\partial t}\right]v(x,t)\,dx, \tag{7.4}$$

where $c_1, c_2 > 0$ are the structural distributed transverse and longitudinal damping coefficients, respectively. Both c_1 and c_2 are assumed to be constant in this chapter. We introduce the boundary control at the top boundary of the riser to produce a transverse motion u_T and a longitudinal motion u_L for vibration reduction. The work done by the two actuators can be written as

$$W_m = u_T w(L,t) + u_L v(L,t), \tag{7.5}$$

and the total work W done on the system is given by

$$\begin{aligned} W &= W_f + W_d + W_m \\ &= \int_0^L \left\{\left[f(x,t) - c_1\frac{\partial w(x,t)}{\partial t}\right]w(x,t) - c_2\left[\frac{\partial v(x,t)}{\partial t}\right]v(x,t)\right\}dx \\ &\quad + u_T w(L,t) + u_L v(L,t). \end{aligned} \tag{7.6}$$

Applying the Hamilton principle, Eq. (2.1), we obtain the governing equations of the system as

$$\rho\ddot{w} + EIw'''' - Tw'' - f + c_1\dot{w} - EAv''w' - EAv'w'' - \frac{3}{2}EA\left(w'\right)^2 w'' = 0, \tag{7.7}$$

$$\rho\ddot{v} + c_2\dot{v} - EAv'' - EAw'w'' = 0 \quad \forall (x,t) \in (0,L) \times [0,\infty). \tag{7.8}$$

Setting the terms with single integrals in the Hamilton principle equation equal to zero, we obtain the boundary conditions of the system as

$$w''(0,t) = w''(L,t) = w(0,t) = v(0,t) = 0, \tag{7.9}$$

$$-EIw'''(L,t) + Tw'(L,t) + EAv'(L,t)w'(L,t) + \frac{1}{2}EA\big[w'(L,t)\big]^3 = u_T(t), \tag{7.10}$$

$$\frac{1}{2}EA\big[w'(L,t)\big]^2 + EAv'(L,t) = u_L(t) \quad \forall t \in [0,\infty). \tag{7.11}$$

Property 7.1 [4, 237] If the kinetic energy of system (7.7)–(7.11), given by Eq. (7.1), is bounded for all $(x,t) \in [0,L] \times [0,\infty)$, then $\dot{w}'(x,t)$, $\dot{w}''(x,t)$, $\dot{v}'(x,t)$, and $\dot{v}''(x,t)$ are bounded for all $(x,t) \in [0,L] \times [0,\infty)$.

Property 7.2 [4, 237] If the potential energy of the system (7.7)–(7.11), given by Eq. (7.2), is bounded for all $(x,t) \in [0,L] \times [0,\infty)$, then $w''(x,t)$, $w'''(x,t)$, $w''''(x,t)$, and $v''(x,t)$ are bounded for all $(x,t) \in [0,L] \times [0,\infty)$.

Assumption 7.3 For the distributed disturbance $f(x,t)$, we assume that there exists a constant $\bar{f} \in \mathbb{R}^+$ such that $\|f(x,t)\| \leq \bar{f}$ for all $(x,t) \in [0,L] \times [0,\infty)$. This is a reasonable assumption as the effects of the time-varying current $f(x,t)$ have finite energy and hence are bounded, i.e., $f(x,t) \in \mathcal{L}_\infty([0,L])$.

Remark 7.4 For control design in Sect. 7.3, only the assertion that there exists an upper bound on the disturbance in Assumption 7.3, $\|f(x,t)\| < \bar{f}$, is necessary. The knowledge of the exact value for $f(x,t)$ is not required for all $(x,t) \in [0,L] \times [0,\infty)$. As such, different VIV models up to various levels of fidelity, such as those found in [195, 196, 227–229], can be applied without affecting the control design or analysis.

Remark 7.5 The VIV problem can be separated into the drag and the lift components, perpendicular to each other. The vector sum results in a force with oscillating magnitude and direction, thereby producing the figure of "8" response in the riser. Under Assumption 7.3, it is possible that control applied to these two cases in separate axes may be sufficient for vibration reduction of the VIV problem. The combination of drag and oscillating lift will be treated in future analysis using a 3D riser model.

7.3 Control Design

The control objective is to reduce the vibrations of the riser, i.e., $w(x,t)$ and $v(x,t)$, under the time-varying distributed transverse load $f(x,t)$ from the ocean current.

In this section, Lyapunov's direct method is used to construct boundary control laws $u_T(t)$ and $u_L(t)$ at the top boundary of the flexible marine riser and to analyze the close-loop stability of the system.

To stabilize the system given by Eqs. (7.7) and (7.8), we propose the following control laws:

$$u_T = -k_1\dot{w}(L,t) - k_2 w(L,t), \tag{7.12}$$

$$u_L = -k_3\dot{v}(L,t) - k_4 v(L,t), \tag{7.13}$$

where k_i, $i = 1, 2, 3, 4$, are positive constants.

Remark 7.6 The control is independent of system parameters, thus possessing stability robustness to variations in system parameters. The control design is based on the distributed parameter system model given by Eqs. (7.7) and (7.8), and the spillover problems associated with traditional truncated model-based approaches caused by ignoring high-frequency modes in controller and observer design are avoided. For recent results on model-based control of distributed system, which are helpful in avoiding spillover effects, the readers can refer to [57, 58].

Remark 7.7 In the proposed controller (7.12) and (7.13), $w(L,t)$ and $v(L,t)$ can be measured through position sensors at the top boundary of the riser. In practice, the effect of measurement noise from sensors is unavoidable, which will affect the controller implementation, especially when the high-order differentiating terms with respect to time exist. In our proposed controller (7.12) and (7.13), $\dot{w}(L,t)$ and $\dot{v}(L,t)$ with only one time differentiating with respect to time can be obtained through a backward difference algorithm of the values of $w(L,t)$ and $v(L,t)$. It is noted that differentiating twice and three times positions $w(L,t)$ and $v(L,t)$ with respect to time to get $\ddot{w}(L,t)$, $\dddot{w}(L,t)$, $\ddot{v}(L,t)$, and $\dddot{v}(L,t)$, respectively, is undesirable in practice due to noise amplification. For these cases, observers are needed to design the estimates of the state values according to the boundary conditions.

7.3.1 Uniformly Stable Control Under Ocean Current Disturbance

Consider the Lyapunov function candidate

$$V(t) = E_b(t) + E_c(t) + E_d(t). \tag{7.14}$$

The energy term $E_b(t)$, an auxiliary term $E_c(t)$, and a small crossing term $E_d(t)$ are defined as

$$E_b = \frac{1}{2}\rho\int_0^L \left(\dot{w}^2 + \dot{v}^2\right) dx + \frac{1}{2}EI\int_0^L \left[w''\right]^2 dx + \frac{1}{2}EA\int_0^L \left(v' + \frac{1}{2}\left[w'\right]^2\right)^2 dx$$

$$+\frac{1}{2}T\int_0^L \left[w'\right]^2 dx, \tag{7.15}$$

$$E_c = \frac{k_2+\beta_1 k_1}{2}w^2(L,t) + \frac{k_4+\beta_2 k_3}{2}v^2(L,t), \tag{7.16}$$

$$E_d = \beta_1\rho\int_0^L w\dot{w}\,dx + \beta_2\rho\int_0^L v\dot{v}\,dx, \tag{7.17}$$

where k_i, $i = 1, 2, 3, 4$, are positive control parameters, and β_j, $j = 1, 2$, are small positive weighting constants.

Lemma 7.8 *The Lyapunov function candidate given by (7.14) can be upper and lower bounded as*

$$0 \le \lambda_1\big(E_b(t) + E_c(t)\big) \le V(t) \le \lambda_2\big(E_b(t) + E_c(t)\big), \tag{7.18}$$

where λ_1 and λ_2 are positive constants.

Proof Using inequality (2.12) and the inequality $2[v'(x,t)]^2 \le [w'(x,t)]^2$ [257], we have

$$|E_b| \ge \frac{1}{2}\min\left[\rho, T - \frac{EA}{2\delta}, EA, EA\left(\frac{1}{4}-\delta\right)\right] \times \int_0^L \left\{\dot{w}^2 + \dot{v}^2 + \left[w'\right]^2 + \left[v'\right]^2 + \left[w'\right]^4\right\} dx,$$

where δ is a positive constant.

Substituting inequalities (2.11) and (2.14) into Eq. (7.17) yields

$$\begin{aligned} |E_d| &\le \beta_1\rho\int_0^L \dot{w}^2\,dx + \beta_1\rho L^2\int_0^L \left[w'\right]^2 dx + \beta_2\rho\int_0^L \dot{v}^2\,dx \\ &\quad + \beta_2\rho L^2\int_0^L \left[v'\right]^2 dx \\ &\le \alpha E_b, \end{aligned} \tag{7.19}$$

where

$$\alpha = 2\rho\frac{\max(\beta_1, \beta_1 L^2, \beta_2, \beta_2 L^2)}{\min[\rho, T - \frac{EA}{2\delta}, EA, EA(\frac{1}{4}-\delta)]}. \tag{7.20}$$

Then, we obtain

$$-\alpha E_b \le E_d \le \alpha E_b. \tag{7.21}$$

Considering β_1 and β_2 as two small positive weighting constants and choosing them properly, we can obtain

$$\alpha_1 = 1 - \alpha = 1 - 2\rho \frac{\max(\beta_1, \beta_1 L^2, \beta_2, \beta_2 L^2)}{\min(\rho, T, EI, EA)} > 0, \tag{7.22}$$

$$\alpha_2 = 1 + \alpha = 1 + 2\rho \frac{\max(\beta_1, \beta_1 L^2, \beta_2, \beta_2 L^2)}{\min(\rho, T, EI, EA)} > 1. \tag{7.23}$$

Then, we further have

$$0 \le \alpha_1 E_b \le E_b + E_d \le \alpha_2 E_b. \tag{7.24}$$

Given the Lyapunov function candidate in Eq. (7.14), we obtain

$$0 \le \lambda_1 \big(E_b(t) + E_c(t)\big) \le V(t) \le \lambda_2 \big(E_b(t) + E_c(t)\big), \tag{7.25}$$

where $\lambda_1 = \min(\alpha_1, 0.5(k_2 + \beta_1 k_1), 0.5(k_4 + \beta_2 k_3))$ and $\lambda_2 = \max(\alpha_1, 0.5(k_2 + \beta_1 k_1), 0.5(k_4 + \beta_2 k_3))$ are positive constants. □

Lemma 7.9 *The time derivative of the Lyapunov function in* (7.14) *can be upper bounded with*

$$\dot{V}(t) \le -\lambda V(t) + \varepsilon, \tag{7.26}$$

where λ *and* ε *are positive constants.*

Proof We differentiate Eq. (7.14) with respect to time to obtain

$$\dot{V}(t) = \dot{E}_b + \dot{E}_c + \dot{E}_d. \tag{7.27}$$

The first term of Eq. (7.27)

$$\dot{E}_b = B_1 + B_2 + B_3 + B_4, \tag{7.28}$$

where

$$B_1 = \rho \int_0^L \dot{w}\ddot{w}\, dx + \rho \int_0^L \dot{v}\ddot{v}\, dx, \tag{7.29}$$

$$B_2 = EI \int_0^L w'' \dot{w}''\, dx, \tag{7.30}$$

$$B_3 = EA \int_0^L \left(v' + \frac{1}{2}[w']^2\right)\left(\dot{v}' + w'\dot{w}'\right) dx, \tag{7.31}$$

$$B_4 = T \int_0^L w'\dot{w}'\, dx. \tag{7.32}$$

Using the governing equation in the expression for B_1, we obtain

$$B_1 = \int_0^L \dot{w}\Big(-EIw'''' + Tw'' + \frac{3}{2}EA\big[w'\big]^2 w'' + EAw''v' + EAw'v'' + f - c_1\dot{w}\Big)\,dx + \int_0^L \dot{v}\big(EAv'' + EAw'w'' - c_2\dot{v}\big)\,dx. \tag{7.33}$$

Applying the boundary conditions and integrating Eq. (7.30) by parts, we obtain

$$\begin{aligned} B_2 &= EI\int_0^L w''d\big(\dot{w}'\big) \\ &= -EIw'''(L,t)\dot{w}(L,t) + EI\int_0^L \dot{w}w''''\,dx. \end{aligned} \tag{7.34}$$

Applying the boundary conditions and integrating Eq. (7.31) by parts, we obtain

$$\begin{aligned} B_3 = {} & EAv'(L,t)\dot{v}(L,t) - EA\int_0^L \dot{v}v''\,dx + EAv'(L,t)w'(L,t)\dot{w}(L,t) \\ & - EA\int_0^L \dot{w}\big(v''w' + v'w''\big)\,dx + \frac{1}{2}EA\big[w'(L,t)\big]^2\dot{v}(L,t) - EA\int_0^L \dot{v}w'w''\,dx \\ & + \frac{1}{2}EA\big[w'(L,t)\big]^3\dot{w}(L,t) - \frac{3}{2}EA\int_0^L \dot{w}\big[w'\big]^2 w''\,dx. \end{aligned} \tag{7.35}$$

Using the boundary conditions and integrating Eq. (7.32) by parts, we obtain

$$\begin{aligned} B_4 &= T\int_0^L w'd(\dot{w}) \\ &= Tw'(L,t)\dot{w}(L,t) - T\int_0^L \dot{w}w''\,dx. \end{aligned} \tag{7.36}$$

Substituting Eqs. (7.33), (7.34), (7.35), and (7.36) into Eq. (7.28), we have

$$\begin{aligned} \dot{E}_b = {} & \Big(-EIw'''(L,t) + Tw'(L,t) + EAw'(L,t)v'(L,t) + \frac{1}{2}EA\big[w'(L,t)\big]^3\Big) \\ & \times \dot{w}(L,t) + \Big(\frac{1}{2}EA\big[w'(L,t)\big]^2 + EAv'(L,t)\Big)\dot{v}(L,t) - c_1\int_0^L \dot{w}^2\,dx \\ & - c_2\int_0^L \dot{v}^2\,dx + \int_0^L f\dot{w}\,dx. \end{aligned} \tag{7.37}$$

Using inequality (2.12), we obtain

$$\dot{E}_b \le u_T \dot{w}(L,t) + u_L \dot{v}(L,t) - (c_1 - \delta_1)\int_0^L \dot{w}^2\,dx - c_2\int_0^L \dot{v}^2\,dx + \int_0^L \frac{1}{\delta_1} f^2\,dx, \tag{7.38}$$

where $\delta_1 > 0$ is a positive constant.

The second term of Eq. (7.27)

$$\dot{E}_c = (k_2 + \beta_1 k_1) w(L,t)\dot{w}(L,t) + (k_4 + \beta_2 k_3) v(L,t)\dot{v}(L,t). \tag{7.39}$$

The third term of Eq. (7.27) is rewritten as

$$\begin{aligned}
\dot{E}_d &= \beta_1\rho\int_0^L \left(\dot{w}^2 + w\ddot{w}\right)dx + \beta_2\rho\int_0^L \left(\dot{v}^2 + v\ddot{v}\right)dx \\
&= \beta_1\int_0^L \Big[-EIww'''' + Tww'' + fw - c_1 w\dot{w} + \frac{3}{2}EAww'^2w'' + EAww''v' \\
&\quad + EAww'v'' + \rho\dot{w}^2\Big]dx + \beta_2\int_0^L \left[EAvv'' + EAvw'w'' + \rho\dot{v}^2 - c_2 v\dot{v}\right]dx \\
&= D_1 + D_2 + D_3 + D_4 + D_5 + D_6 + D_7 + D_8 + D_9 + D_{10} + D_{11} + D_{12},
\end{aligned} \tag{7.40}$$

where

$$D_1 = -\beta_1\int_0^L EIww''''\,dx, \tag{7.41}$$

$$D_2 = \beta_1\int_0^L Tww''\,dx, \tag{7.42}$$

$$D_3 = \beta_1\int_0^L fw\,dx, \tag{7.43}$$

$$D_4 = -\beta_1\int_0^L c_1 w\dot{w}\,dx, \tag{7.44}$$

$$D_5 = \beta_1\int_0^L \frac{3}{2}EAww'^2w''\,dx, \tag{7.45}$$

$$D_6 = \beta_1\int_0^L EAww''v'\,dx, \tag{7.46}$$

$$D_7 = \beta_1\int_0^L EAww'v''\,dx, \tag{7.47}$$

$$D_8 = \beta_1 \int_0^L \rho \dot{w}^2 \, dx, \tag{7.48}$$

$$D_9 = \beta_2 \int_0^L EAvv'' \, dx, \tag{7.49}$$

$$D_{10} = \beta_2 \int_0^L EAvw'w'' \, dx, \tag{7.50}$$

$$D_{11} = \beta_2 \int_0^L \rho \dot{v}^2 \, dx, \tag{7.51}$$

$$D_{12} = \beta_2 \int_0^L c_2 v\dot{v} \, dx. \tag{7.52}$$

After integrating Eqs. (7.41) and (7.42) by parts and using the boundary conditions, we obtain

$$D_1 = -\beta_1 EIw(L,t)w'''(L,t) - \beta_1 EI \int_0^L \left[w''\right]^2 dx, \tag{7.53}$$

$$D_2 = \beta_1 Tw(L,t)w'(L,t) - \beta_1 T \int_0^L \left[w'\right]^2 dx. \tag{7.54}$$

Using inequalities (2.12) and (2.14), we obtain

$$\begin{aligned} D_3 &\leq \frac{\beta_1}{\delta_2} \int_0^L f^2 \, dx + \beta_1 \delta_2 \int_0^L w^2 \, dx \\ &\leq \frac{\beta_1}{\delta_2} \int_0^L f^2 \, dx + \beta_1 \delta_2 L^2 \int_0^L \left[w'\right]^2 dx \end{aligned} \tag{7.55}$$

$$D_4 \leq \beta_1 \frac{c_1}{\delta_3} \int_0^L \dot{w}^2 \, dx + \beta_1 c_1 \delta_3 L^2 \int_0^L \left[w'\right]^2 dx, \tag{7.56}$$

where $\delta_2, \delta_3 > 0$. Integrating Eq. (7.45) by parts, we obtain

$$\begin{aligned} D_5 &= \beta_1 \int_0^L \frac{3}{2} EAww'^2 d\left(w'\right) \\ &= \frac{3\beta_1}{2} EAw\left[w'\right]^3 \Big|_0^L - \frac{3\beta_1}{2} EA \int_0^L w'\left(w'\left[w'\right]^2 + 2ww'w''\right) dx. \end{aligned} \tag{7.57}$$

The polynomial of the last term in Eq. (7.57) is the same as D_5. Rewriting Eq. (7.57), we obtain

$$D_5 = \frac{\beta_1}{2} EAw(L,t)\left[w'(L,t)\right]^3 - \frac{\beta_1}{2} EA \int_0^L \left[w'\right]^4 dx. \tag{7.58}$$

After integrating Eqs. (7.46), (7.49), and (7.50) by parts and using the boundary conditions, we obtain

$$D_6 = \beta_1 EAw(L,t)w'(L,t)v'(L,t) - \beta_1 EA\int_0^L \left[w'\right]^2 v'\,dx - D_7, \quad (7.59)$$

$$D_9 = \beta_2 EAv(L,t)v'(L,t) - \beta_2 EA\int_0^L \left[v'\right]^2 dx, \quad (7.60)$$

$$D_{10} = \beta_2 EAv(L,t)\left[w'(L,t)\right]^2 - \beta_2 EA\int_0^L v'\left[w'\right]^2 dx - D_{10}. \quad (7.61)$$

The last term in Eq. (7.61) is the same as D_{10}. Rewriting Eq. (7.61), we obtain

$$D_{10} = \frac{\beta_2}{2} EAv(L,t)\left[w'(L,t)\right]^2 - \frac{\beta_2}{2} EA\int_0^L v'\left[w'\right]^2 dx, \quad (7.62)$$

Using inequality (2.12), we obtain

$$D_{12} \le \beta_2 \frac{c_2}{\delta_4}\int_0^L \dot{v}^2\,dx + \beta_2 c_2 \delta_4 L^2 \int_0^L \left[v'\right]^2 dx, \quad (7.63)$$

where $\delta_4 > 0$. Combining the above expressions D_1–D_{12} and utilizing the boundary conditions (7.10) and (7.11) , we obtain

$$\begin{aligned}
\dot{E}_d(t) \le{}& \beta_1 w(L,t)u_T + \beta_2 v(L,t)u_L - \beta_1 EI\int_0^L \left[w''\right]^2 dx - \beta_1 T\int_0^L \left[w'\right]^2 dx \\
&+ \frac{\beta_1}{\delta_2}\int_0^L f^2\,dx + \beta_1\delta_2 L^2\int_0^L \left[w'\right]^2 dx + \beta_1\frac{c_1}{\delta_3}\int_0^L \dot{w}^2\,dx \\
&+ \beta_1 c_1\delta_3 L^2\int_0^L \left[w'\right]^2 dx - \frac{\beta_1}{2} EA\int_0^L \left[w'\right]^4 dx - \beta_1 EA\int_0^L \left[w'\right]^2 v'\,dx \\
&+ \beta_1\int_0^L \rho\dot{w}^2\,dx - \beta_2 EA\int_0^L \left[v'\right]^2 dx - \frac{\beta_2}{2} EA\int_0^L v'\left[w'\right]^2 dx \\
&+ \beta_2\int_0^L \rho\dot{v}^2\,dx + \beta_2\frac{c_2}{\delta_4}\int_0^L \dot{v}^2\,dx + \beta_2 c_2\delta_4 L^2\int_0^L \left[v'\right]^2 dx. \quad (7.64)
\end{aligned}$$

Substituting Eqs. (7.38), (7.39), and (7.64) into Eq. (7.27), we obtain

$$\begin{aligned}
\dot{V}(t) \le{}& \left[\dot{w}(L,t) + \beta_1 w(L,t)\right]u_T + \left[\dot{v}(L,t) + \beta_2 v(L,t)\right]u_L \\
&- \left(c_1 - \delta_1 - \beta_1\rho - \beta_1\frac{c_1}{\delta_3}\right)\int_0^L \dot{w}^2\,dx - \left(c_2 - \beta_2\rho - \beta_2\frac{c_2}{\delta_4}\right)\int_0^L \dot{v}^2\,dx \\
&- \beta_1 EI\int_0^L \left[w''\right]^2 dx - \frac{\beta_1}{2} EA\int_0^L \left[w'\right]^4 dx
\end{aligned}$$

$$
\begin{aligned}
&- \left(\beta_1 - \frac{\beta_2}{2}\right) EA \int_0^L \left[w'\right]^2 v' \, dx - \left(\beta_2 EA - \beta_2 c_2 \delta_4 L^2\right) \int_0^L \left[v'\right]^2 dx \\
&+ \left(\frac{1}{\delta_1} + \frac{\beta_1}{\delta_2}\right) \int_0^L f^2 \, dx \\
&- \left(\beta_1 T - \beta_1 \delta_2 L^2 - \beta_1 c_1 \delta_3 L^2\right) \int_0^L \left[w'\right]^2 dx + (k_2 + \beta_1 k_1) w(L,t) \dot{w}(L,t) \\
&+ (k_4 + \beta_2 k_3) v(L,t) \dot{v}(L,t). \qquad (7.65)
\end{aligned}
$$

Then substituting the control law given by Eqs. (7.12) and (7.13) into Eq. (7.65), we obtain

$$
\begin{aligned}
\dot{V}(t) \leq & -k_1 \left[\dot{w}(L,t)\right]^2 - k_2 \beta_1 \left[w(L,t)\right]^2 - k_3 \left[\dot{v}(L,t)\right]^2 - k_4 \beta_2 \left[v(L,t)\right]^2 \\
& - \left(c_1 - \delta_1 - \beta_1 \rho - \beta_1 \frac{c_1}{\delta_3}\right) \int_0^L \dot{w}^2 \, dx - \left(c_2 - \beta_2 \rho - \beta_2 \frac{c_2}{\delta_4}\right) \int_0^L \dot{v}^2 \, dx \\
& - \beta_1 EI \int_0^L \left[w''\right]^2 dx - \left(\beta_1 - \frac{\beta_2}{2}\right) EA \int_0^L \left(v' + \frac{1}{2}\left[w'\right]^2\right)^2 dx \\
& - \left(\beta_1 T - \beta_1 \delta_2 L^2 - \beta_1 c_1 \delta_3 L^2\right) \int_0^L \left[w'\right]^2 dx + \left(\frac{1}{\delta_1} + \frac{\beta_1}{\delta_2}\right) \int_0^L f^2 \, dx \\
\leq & -\lambda_3 (E_b + E_c) + \varepsilon, \qquad (7.66)
\end{aligned}
$$

where

$$\lambda_3 = \min\left(\frac{2k_2\beta_1}{k_2 + \beta_1 k_1}, \frac{2k_4\beta_2}{k_4 + \beta_2 k_3}, \frac{2\sigma_1}{m_z}, \frac{2\sigma_2}{m_z}, \frac{2\sigma_3}{EI}, \frac{2\sigma_5}{EA}, \frac{2\sigma_7}{T}\right) > 0, \qquad (7.67)$$

$$\sigma_1 = c_1 - \delta_1 - \beta_1 \rho - \beta_1 \frac{c_1}{\delta_3} > 0, \qquad (7.68)$$

$$\sigma_2 = c_2 - \beta_2 \rho - \beta_2 \frac{c_2}{\delta_4} > 0, \qquad (7.69)$$

$$\sigma_3 = \beta_1 EI > 0, \qquad (7.70)$$

$$\sigma_4 = \frac{\beta_1}{2} EA > 0, \qquad (7.71)$$

$$\sigma_5 = \left(\beta_1 - \frac{\beta_2}{2}\right) EA > 0, \qquad (7.72)$$

$$\sigma_6 = \beta_2 EA - \beta_2 c_2 \delta_4 L^2 > 0, \qquad (7.73)$$

$$\sigma_5 \leq \frac{\min(4\sigma_4, \sigma_6)}{4}, \qquad (7.74)$$

$$\sigma_7 = \beta_1 T - \beta_1 \delta_2 L^2 - \beta_1 c_1 \delta_3 L^2 > 0, \qquad (7.75)$$

$$\varepsilon = \left(\frac{1}{\delta_1} + \frac{\beta_1}{\delta_2}\right)\int_0^L f^2\,dx \le \left(\frac{1}{\delta_1} + \frac{\beta_1}{\delta_2}\right)\int_0^L \bar{f}^2\,dx < \infty. \tag{7.76}$$

From inequalities (7.25) and (7.66) we have

$$\dot{V}(t) \le -\lambda V(t) + \varepsilon, \tag{7.77}$$

where $\lambda = \lambda_3/\lambda_2 > 0$ and $\varepsilon > 0$. □

With the above lemmas, we are ready to present the following stability theorem of the closed-loop riser system subject to ocean current disturbance.

Theorem 7.10 *For the system dynamics described by* (7.7) *and* (7.8) *and boundary conditions* (7.9) *to* (7.11), *under Assumption* 7.3 *and the control laws* (7.12) *and* (7.13), *given that the initial conditions are bounded and that the required state information given by* $w(L,t)$, $v(L,t)$, $\dot{w}(L,t)$, *and* $\dot{v}(L,t)$ *is available, the closed-loop system is uniformly bounded as follows*:

$$\left|w(x,t)\right| \le \sqrt{\frac{2L}{T\lambda_1}\left(V(0)e^{-\lambda t} + \frac{\varepsilon}{\lambda}\right)} \quad \forall (x,t) \in (0,L)\times[0,\infty), \tag{7.78}$$

$$\left|v(x,t)\right| \le \sqrt{\frac{2L}{EA\lambda_1}\left(V(0)e^{-\lambda t} + \frac{\varepsilon}{\lambda}\right)} \quad \forall (x,t) \in (0,L)\times[0,\infty), \tag{7.79}$$

where λ *and* ε *are positive constants*.

Proof Multiplying Eq. (7.26) by $e^{\lambda t}$ yields

$$\frac{\partial}{\partial t}\left(Ve^{\lambda t}\right) \le \varepsilon e^{\lambda t}. \tag{7.80}$$

Integrating the above inequalities, we obtain

$$V(t) \le \left(V(0) - \frac{\varepsilon}{\lambda}\right)e^{-\lambda t} + \frac{\varepsilon}{\lambda} \le V(0)e^{-\lambda t} + \frac{\varepsilon}{\lambda} \in \mathcal{L}_\infty, \tag{7.81}$$

which implies that $V(t)$ is bounded. Utilizing inequality (2.15) and Eq. (7.15), we have

$$\frac{1}{2L}Tw^2(x,t) \le \frac{1}{2}T\int_0^L \left[w'(x,t)\right]^2 dx \le E_b(t) \le \frac{1}{\lambda_1}V(t) \in \mathcal{L}_\infty, \tag{7.82}$$

$$\frac{1}{2L}EAv^2(x,t) \le \frac{1}{2}EA\int_0^L \left[v'(x,t)\right]^2 dx \le E_b(t) \le \frac{1}{\lambda_1}V(t) \in \mathcal{L}_\infty. \tag{7.83}$$

Rearranging the terms of the above two inequalities, we obtain

$$\left|w(x,t)\right| \le \sqrt{\frac{2L}{T\lambda_1}\left(V(0)e^{-\lambda t} + \frac{\varepsilon}{\lambda}\right)} \quad \forall (x,t) \in (0,L)\times[0,\infty), \tag{7.84}$$

$$|v(x,t)| \leq \sqrt{\frac{2L}{EA\lambda_1}\left(V(0)e^{-\lambda t} + \frac{\varepsilon}{\lambda}\right)} \quad \forall (x,t) \in (0,L) \times [0,\infty). \tag{7.85}$$

From Eqs. (7.82) and (7.83) we can state that $E_b(t)$ is bounded for all $t \in [0,\infty)$. Since $E_b(t)$ is bounded, $\dot{w}(x,t)$, $w'(x,t)$, $w''(x,t)$, $\dot{v}(x,t)$, and $v'(x,t)$ are bounded for all $(x,t) \in [0,L] \times [0,\infty)$. From Eq. (7.1), the kinetic energy of the system is bounded, and by Property 7.1, $\dot{w}'(x,t)$ and $\dot{v}'(x,t)$ are bounded for all $(x,t) \in [0,L] \times [0,\infty)$. From the boundedness of the potential energy given by Eq. (7.2), we can use Property 7.2 to conclude that $w''''(x,t)$ and $v''(x,t)$ are bounded for all $(x,t) \in [0,L] \times [0,\infty)$. Finally, using Assumption 7.3, Eqs. (7.7) through (7.11), and the above statements, we can conclude that $\ddot{w}(x,t)$ and $\ddot{v}(x,t)$ are also bounded for all $(x,t) \in [0,L] \times [0,\infty)$. From Lemma 2.7 and the above proof, it is shown that the deflections $w(x,t)$ and $v(x,t)$ are uniformly bounded for all $(x,t) \in [0,L] \times [0,\infty)$. □

Remark 7.11 From the above stability analysis, $\dot{w}(x,t)$, $\dot{v}(x,t)$, $w(x,t)$, and $v(x,t)$ are all bounded for all $(x,t) \in [0,L] \times [0,\infty)$, and we can conclude the control inputs of u_T and u_L are bounded for all $t \in [0,\infty)$.

7.3.2 Exponentially Stable Control Without Disturbance

In this section, by using the same Lyapunov function candidate (7.14) and the control laws (7.12) and (7.13) of Sect. 7.3.1, we analyze the free vibration case of the flexible riser system, i.e., the ocean current disturbance $f(x,t) = 0$, and the exponentially stability is proved.

Lemma 7.12 [203] *For bounded initial conditions and for all x and $t \geq 0$, if there exists a C^1 continuous and positive definite Lyapunov function $V(x,t) : \Re^n \times \Re_+ \longrightarrow \Re$ satisfying $\kappa_1(\|x\|) \leq V(x,t) \leq \kappa_2(\|x\|)$ and such that $\dot{V}(x,t) \leq -\lambda V(x,t)$, where $\kappa_1, \kappa_2 : \mathbb{R}^n \to \mathbb{R}$ are class K functions, then the equilibrium point $x = 0$ of the system $\dot{x} = f(x,t)$ is exponentially stable.*

Theorem 7.13 *For the system dynamics described by (7.7) and (7.8) and boundary conditions (7.9) to (7.11), if the free vibration case is considered, i.e., $f(x,t) = 0$, the exponential stability under the free vibration condition can be achieved with the proposed boundary controllers (7.12) and (7.13) as follows:*

$$|w(x,t)| \leq \sqrt{\frac{2L}{T\lambda_1}V(0)e^{-\lambda t}} \quad \forall (x,t) \in (0,L) \times [0,\infty), \tag{7.86}$$

$$|v(x,t)| \leq \sqrt{\frac{2L}{EA\lambda_1}V(0)e^{-\lambda t}} \quad \forall (x,t) \in (0,L) \times [0,\infty), \tag{7.87}$$

where λ and λ_1 are positive constants.

Proof From inequality (7.26), under the free vibration condition, i.e., $f(x,t)=0$, we obtain the time derivative of the Lyapunov function candidate (7.14) as

$$\dot{V}(t) \leq -\lambda V(t), \tag{7.88}$$

where $\lambda = \lambda_3/\lambda_2$. Multiplying Eq. (7.88) by $e^{\lambda t}$ yields

$$\frac{\partial}{\partial t}\left(Ve^{\lambda t}\right) \leq 0. \tag{7.89}$$

Integrating the above inequality, we obtain

$$V(t) \leq V(0)e^{-\lambda t} \in \mathcal{L}_\infty, \tag{7.90}$$

which implies that $V(t)$ is bounded. Similarly, utilizing inequality (2.15) and Eq. (7.15), we have

$$\frac{1}{2L}Tw^2(x,t) \leq \frac{1}{2}T\int_0^L \left[w'(x,t)\right]^2 dx \leq E_b(t) \leq \frac{1}{\lambda_1}V(t) \in \mathcal{L}_\infty, \tag{7.91}$$

$$\frac{1}{2L}EAv^2(x,t) \leq \frac{1}{2}EA\int_0^L \left[v'(x,t)\right]^2 dx \leq E_b(t) \leq \frac{1}{\lambda_1}V(t) \in \mathcal{L}_\infty. \tag{7.92}$$

Rearranging the terms of the above two inequalities, we obtain

$$\left|w(x,t)\right| \leq \sqrt{\frac{2L}{T\lambda_1}V(0)e^{-\lambda t}} \quad \forall (x,t) \in (0,L)\times[0,\infty), \tag{7.93}$$

$$\left|v(x,t)\right| \leq \sqrt{\frac{2L}{EA\lambda_1}V(0)e^{-\lambda t}} \quad \forall (x,t) \in (0,L)\times[0,\infty). \tag{7.94}$$

From Lemma 7.12 and the above proof, we conclude that the free vibration riser system under the control law is exponentially stable. □

Remark 7.14 For the free vibration case of the flexible riser system, the displacements $w(x,t)$ and $v(x,t)$ exponentially converge to zero at the rate of convergence λ as $t \longrightarrow \infty$.

7.4 Numerical Simulations

Simulations for a 1000 m riser under ocean current disturbance are carried out to demonstrate the effectiveness of the proposed control laws (7.12) and (7.13). The detailed parameters of the riser system are shown in Table 7.1. Numerical methods are applied to get an approximate solution of system (7.7)–(7.11) when there is no obtainable analytical solution. In this chapter, the finite difference (FD) scheme is chosen to simulate the system performance.

Table 7.1 Parameters of the riser system

Parameter	Description	Value
L	Length of riser	1000.00 m
d	Riser inner diameter	76.2 mm
D	Riser external diameter	152.40 mm
EI	Bending stiffness of the riser	1.22×10^5 N m^2
EA	Axial stiffness of the riser	3.92×10^7 N
T	Tension	1.11×10^8 N
ρ	Mass per unit length of the flexible riser	108.00 kg m^{-1}
ρ_s	Sea water density	1024.00 kg m^{-3}
c_1	Structural transverse damping coefficient	5.00 N s m^{-2}
c_2	Structural longitudinal damping coefficient	1.00 N s m^{-2}

The riser, initially at rest, is excited by a distributed transverse disturbance due to the ocean current. The corresponding initial conditions of the riser system are given as

$$w(x,0) = \dot{w}(x,0) = v(x,0) = \dot{v}(x,0) = 0. \tag{7.95}$$

We assume that the full current load is applied from $x = 1000$ m to $x = 0$ m and thereafter linearly declines to zero at the ocean floor, $x = 0$, to obtain a depth-dependent ocean current profile $U(x,t)$ as in Chap. 3. The distributed load $f(x,t)$ is generated by Eq. (2.5) with $C_D = 1$, $\theta = 0$, $S_t = 0.2$, and $f_v = 2.625$. In this chapter, we consider four simulation cases with different control inputs.

(i) The transverse and longitudinal displacements of the riser for free vibration (i.e., without control input, $k_1 = k_2 = k_3 = k_4 = 0$) under ocean current disturbance are shown in Fig. 7.2.
(ii) With only transverse control input, i.e., $k_1 = k_2 = 1 \times 10^6$ and $k_3 = k_4 = 0$, the transverse and longitudinal displacements of the riser are shown in Fig. 7.3.
(iii) With only longitudinal control input, i.e., $k_1 = k_2 = 0$ and $k_3 = k_4 = 1 \times 10^8$, the transverse and longitudinal displacements of the riser are shown in Fig. 7.4.
(iv) With both transverse and longitudinal control inputs, i.e., $k_1 = k_2 = 1 \times 10^6$ and $k_3 = k_4 = 1 \times 10^8$, the transverse and longitudinal displacements of the riser are shown in Fig. 7.5.

From Figs. 7.3, 7.4 and 7.5 it is observed that there is a significant reduction of the riser's transverse displacement when the transverse control is applied. Similarly, when the longitudinal control is applied, a significant reduction of the riser's longitudinal displacement is observed. When control inputs in transverse and longitudinal

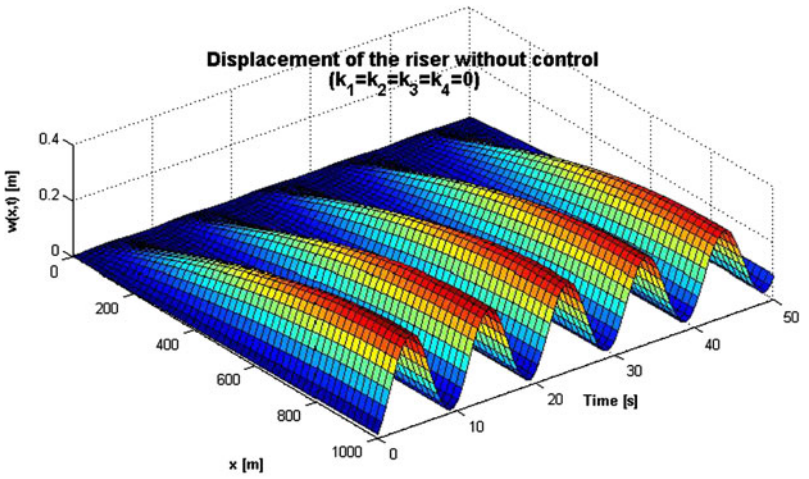

(a)

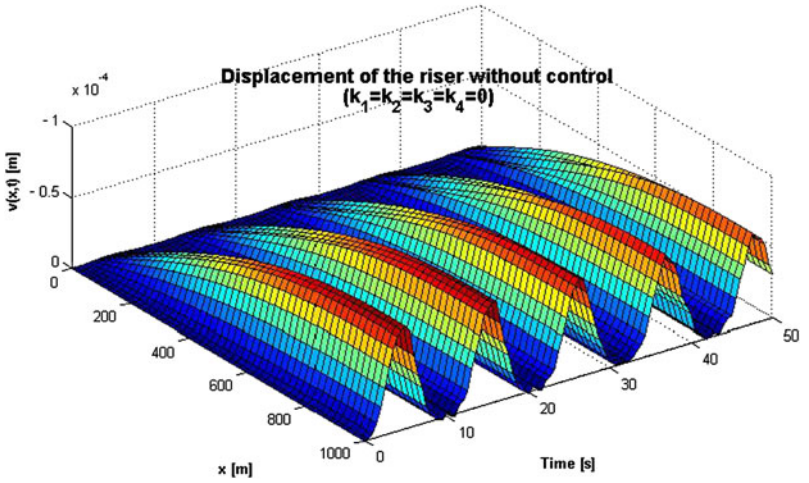

(b)

Fig. 7.2 (**a**) Transverse displacement $w(x,t)$ and (**b**) longitudinal displacement $v(x,t)$

directions are applied, the riser's displacements in both transverse and longitudinal directions are reduced. Peak displacement reduction in the middle and bottom of the riser is observed although the actuators are not located at these positions. The corresponding control inputs $u_T(t)$ and $u_L(t)$ are shown in Figs. 7.6 and 7.7, respectively. It is shown that the transverse control input is of negative value, which means that the actual transverse control input is exerted in the opposite direction of the ocean disturbance $f(x,t)$. The transverse control input varies between 0 and

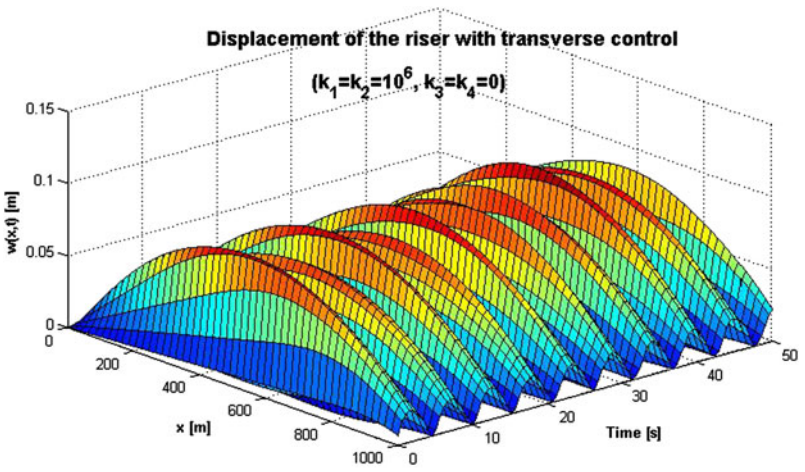

(a)

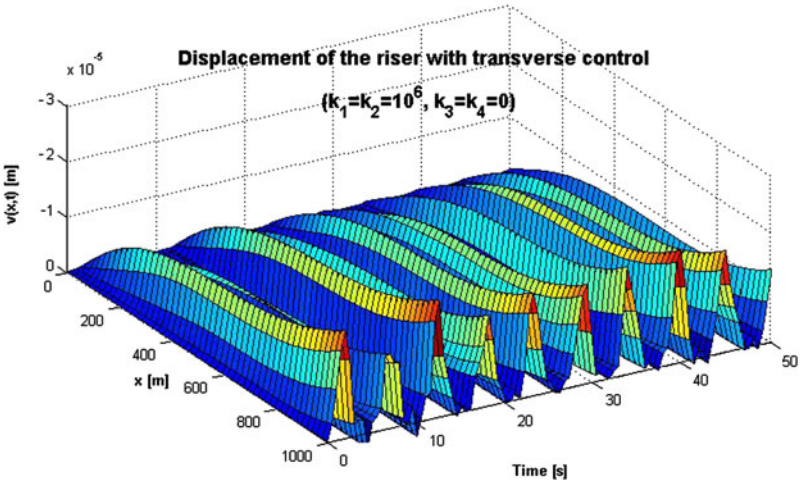

(b)

Fig. 7.3 (**a**) Transverse displacement $w(x,t)$ and (**b**) longitudinal displacement $v(x,t)$

2.5×10^4 N, and the longitudinal control input varies between 0 and 1200 N, which are implementable in practice.

Vibration displacements of the riser are examined at $x = 1000$ m and $x = 500$ m, and the results for controlled and uncontrolled responses are shown in Figs. 7.8 and 7.9 respectively. With the two control inputs, it can be observed that the vibration displacements are reduced at both locations, which brings the top displacements of the riser close to zero.

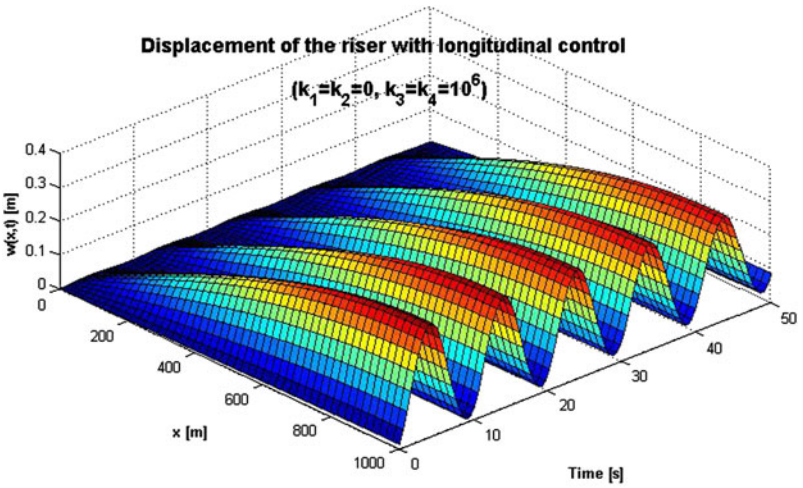

(a)

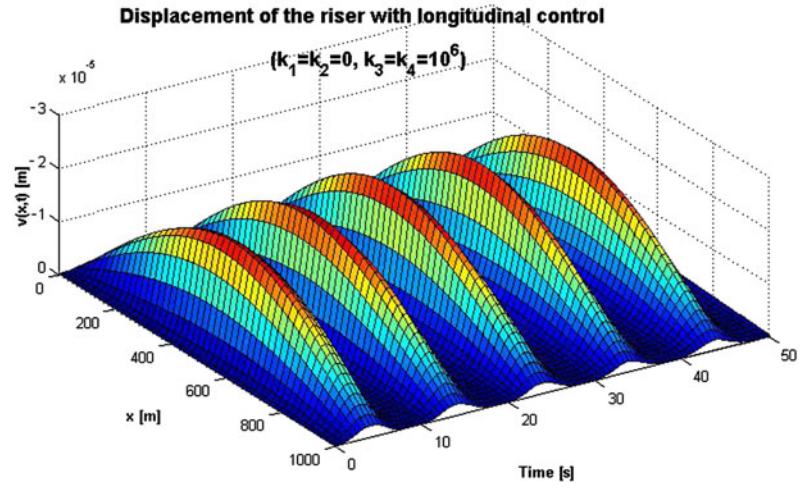

(b)

Fig. 7.4 (**a**) Transverse displacement $w(x,t)$ and (**b**) longitudinal displacement $v(x,t)$

7.5 Conclusion

Vibration regulation of a distributed-parameter marine flexible riser subject to the ocean current disturbance has been investigated in this chapter. The boundary control has been developed with two actuators in transverse and longitudinal directions based on the distributed-parameter system model with PDEs, and the problems associated with traditional truncated-model-based design are overcome. With proposed

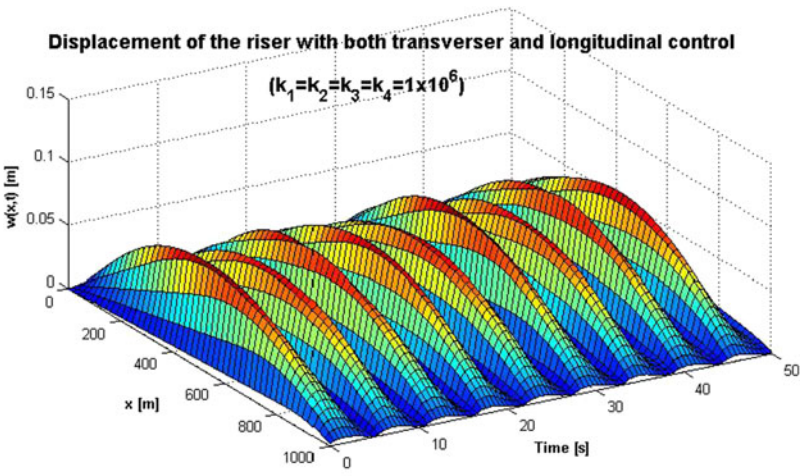

(a)

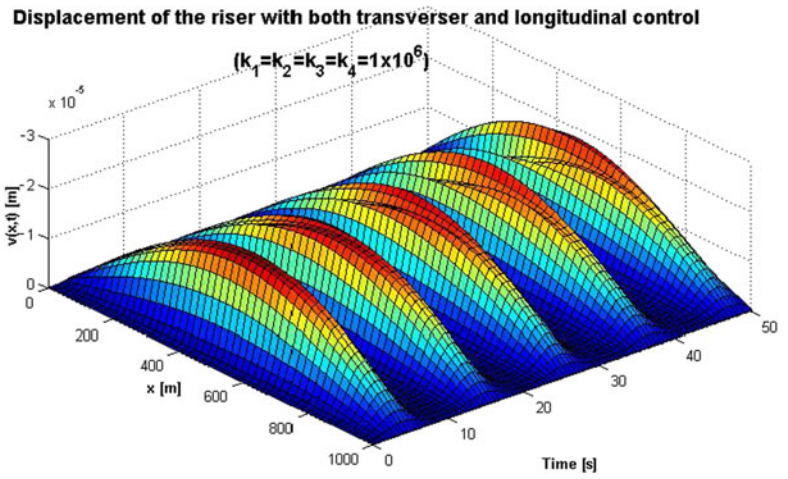

(b)

Fig. 7.5 (**a**) Transverse displacement $w(x,t)$ and (**b**) longitudinal displacement $v(x,t)$

control, closed-looped stability under external disturbance and exponential stability under free vibration condition have been proven based on Lyapunov's direct method. The control is easy to implement since it is independent of the system parameters and only two sensors and actuators are required. Numerical simulations have been provided to verify the effectiveness of the presented boundary control.

In this chapter, we focused on a specific system model in the vertical plane. In practice, all the marine flexible systems are located in the Earth-frame, which is

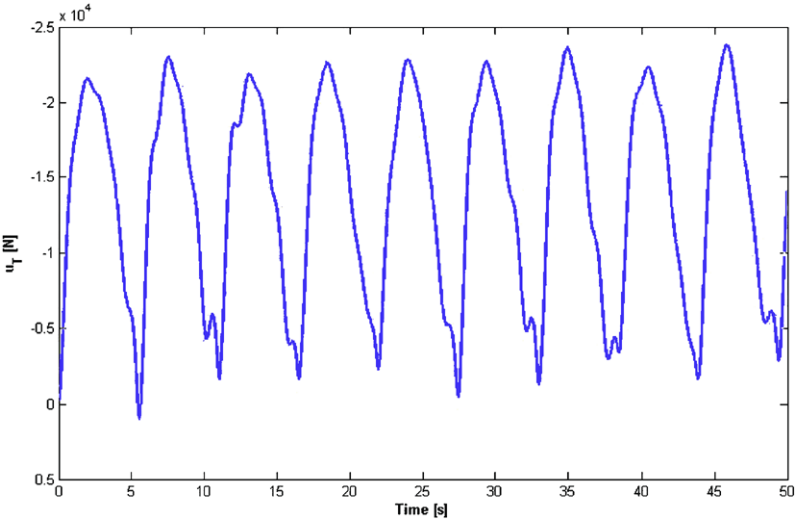

Fig. 7.6 Transverse control input $u_T(t)$

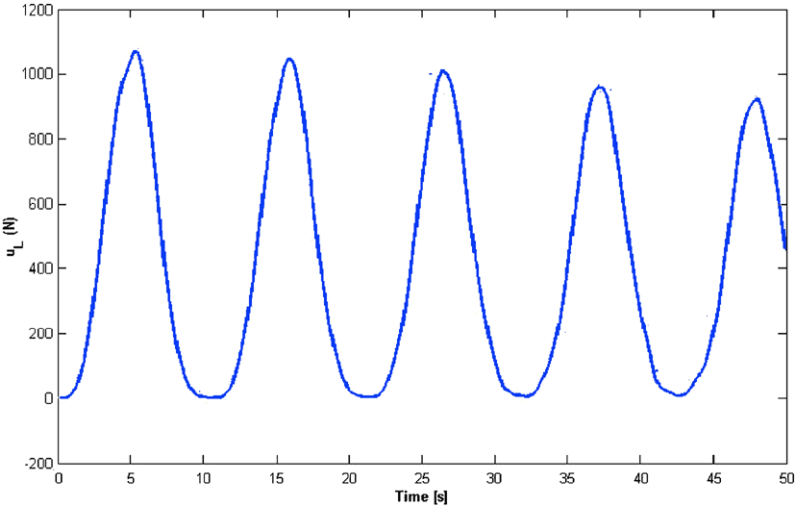

Fig. 7.7 Longitudinal control input $u_L(t)$

a three-dimensional space including X, Y, and Z axes. In the three-dimensional space, there are strong couplings between motions of a flexible marine system along the X, Y, and Z axes. Due to the coupled effects, the modeling and control design for the marine flexible systems in the three-dimensional space is not a straightforward extension. These couplings make the control of a flexible marine system in the three-

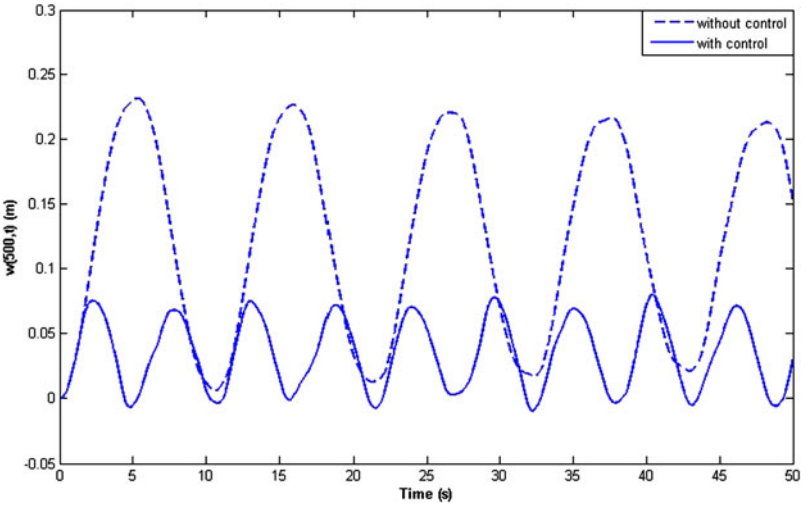

(a)

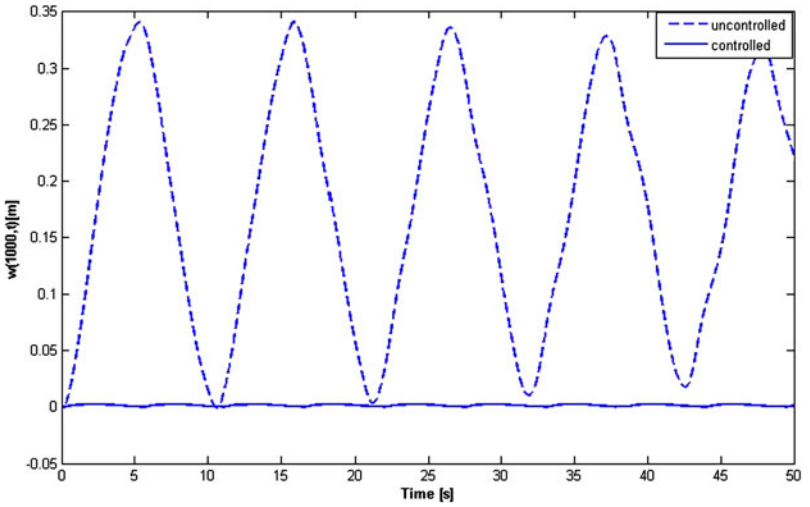

(b)

Fig. 7.8 Transverse displacements: (**a**) transverse displacement at $x = 500$ m, $w(500, t)$ for controlled (*solid*) and uncontrolled (*dashed*) and (**b**) transverse displacement at $x = 1000$ m, $w(1000, t)$ for controlled (*solid*) and uncontrolled (*dashed*)

dimensional space more difficult than the one studied in this book. Therefore, the control problem of a flexible marine system that deforms in the three-dimensional space is an interesting and challenging topic. For example, boundary control of a three-dimensional flexible marine riser has been investigated in [47]. More investi-

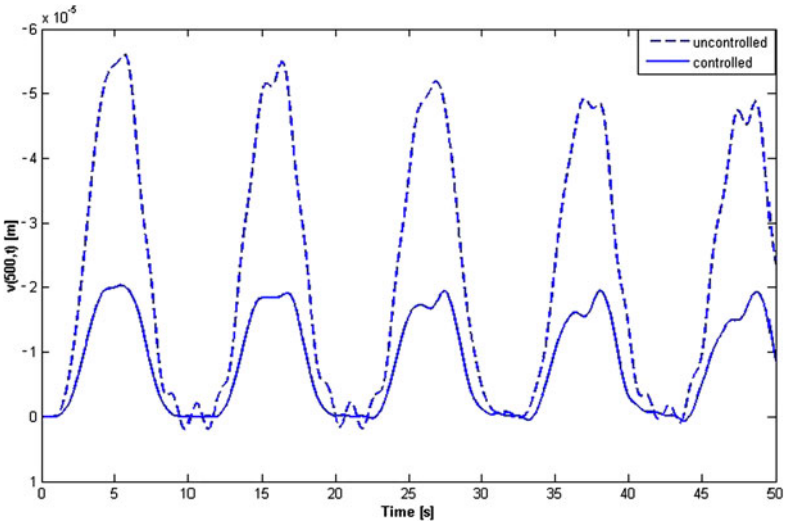

(a)

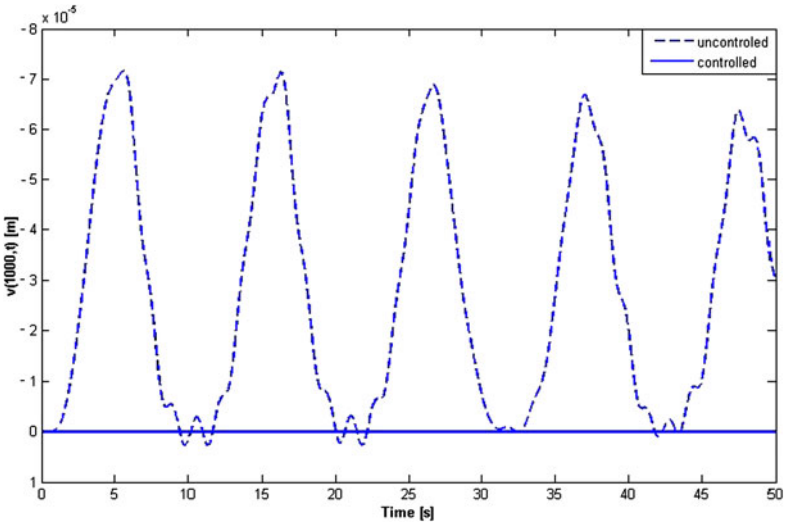

(b)

Fig. 7.9 Longitudinal displacements: (**a**) longitudinal displacement at $x = 500$ m, $v(500, t)$ for controlled (*solid*) and uncontrolled (*dashed*) and (**b**) longitudinal displacement at $x = 1000$ m, $v(1000, t)$ for controlled (*solid*) and uncontrolled (*dashed*)

gations are needed to explore the characteristics of such three-dimensional models with available control techniques to mitigate the effects of couplings while satisfying the basic requirements for the concerned system.

Chapter 8
Flexible Marine Riser with Vessel Dynamics

8.1 Introduction

With the increased focus on offshore oil and gas development in deeper and harsher environments, vibration control of the flexible marine risers has gained increasing attention. The marine riser is used as a fluid-conveyed curved pipe drilling crude oil, natural gas, hydrocarbon, petroleum materials, mud, and other undersea economic resources, and then transporting those resources in the ocean floor to the production vessel or platform in the ocean surface [3]. A drilling riser is used for drilling pipe protection and transportation of the drilling mud, while a production riser is a pipe used for oil transportation [4]. Vibration and deformation of the riser due to the ocean current disturbance and tension exerted at the top can produce premature fatigue problems, which require inspections and costly repairs.

For the purpose of dynamic analysis, the riser is modeled as an Euler–Bernoulli beam structure with PDEs since the diameter-to-length ratio of the riser is small. Based on the distributed-parameter model, various kinds of control methods integrating computer software and hardware with sensors and actuators have been investigated to suppress the riser's vibration. In [48], boundary control for the flexible marine riser with actuator dynamics is designed based on the Lyapunov direct method and the backstepping technique. In [4], a torque actuator is introduced at the top boundary of the riser to reduce the angle and transverse vibration of the riser with guaranteed closed-loop stability. In [49], boundary control for a coupled nonlinear flexible marine riser with two actuators in transverse and longitudinal directions has been designed to suppress the riser's vibration. However, in these works, only the riser dynamics is considered, and the coupling between riser and vessel is neglected, which can influence the dynamic response of the riser system and lead to an imprecise model.

Mathematically, the flexible marine riser with vessel dynamics is represented by a set of infinite-dimensional equations (i.e., PDEs describing the dynamics of the flexible riser) coupled with a set of finite-dimensional equations (i.e., ODEs describing the vessel dynamics). The dynamics of the flexible mechanical system modeled by a set of PDEs is difficult to control due to the infinite dimensionality

W. He et al., *Dynamics and Control of Mechanical Systems in Offshore Engineering*, Advances in Industrial Control, DOI 10.1007/978-1-4471-5337-5_8,

of the system. The modal control method for the control design of PDE is based on truncated finite-dimensional modes of the system, which are derived from the finite element method, Galerkin's method, or assumed-modes method [53, 54, 57–60]. The truncated models are obtained via the model analysis or spatial discretization, in which the flexibility is represented by a finite number of modes by neglecting the higher-frequency modes. The problems from the truncation procedure in the modeling need to be carefully treated in practical applications. A potential drawback in the above control design approaches is that the control can cause the actual system to become unstable due to excitation of the unmodeled, high-frequency vibration modes (i.e., spillover effects) [67]. Spillover effects that result in instability of the system have been investigated in [68, 69] when the control of the truncated system is restricted to a few critical modes. The control order needs to be increased with the number of flexible modes considered to achieve high accuracy of performance, and the control may also be difficult to implement from the engineering point of view since full-state measurements or observers are often required. In an attempt to overcome the above shortcomings of the truncated model-based control, control methodologies, such as method based on bifurcation theory and the application of Poincaré maps [258], variable structure control [70], sliding-mode control [71], energy-based robust control [72, 73], model-free control [74], and boundary control [8, 80, 81, 93, 97, 110, 111, 114, 116, 120], have been developed. In these approaches, system dynamics analysis and control design are carried out directly based on PDEs of the system. In contrast, boundary control where the actuation and sensing are applied only through the boundary of the system utilizes the distributed-parameter model with PDEs to avoid control spillover instabilities.

Boundary control is considered to be more practical in a number of research fields including vibration control of flexible structures, fluid dynamics, and heat transfer, which requires relatively few sensors and actuators. The relevant applications for this approach in mechanical flexible structures consist of second-order structures (strings and cables) and fourth-order structures (beams and plates) [88]. In [98], robust and adaptive boundary control laws based on the Lyapunov synthesis are developed to reduce the vibration of a stretched string on a moving transporter. In [80], adaptive boundary control is designed for an axially moving string with a spatiotemporally varying tension, where the system is proved to be asymptotically stable. In [105], a boundary control law based on the Lyapunov method with sliding mode is employed to guarantee the asymptotic and exponential stability of an axially moving string. In [101], boundary control for a linear gantry crane model with a flexible cable is developed and experimentally implemented. In [114, 140], backstepping boundary controller and observer are designed to stabilize the string and beam model, respectively. In [128], boundary control is presented to stabilize beams by using active constrained layer damping. In [107], nonlinear boundary control is constructed to exponentially stabilize a free transversely vibrating beam.

The rest of the chapter is organized as follows. The governing equation (PDE) and boundary conditions (ODEs) of the flexible riser system are introduced by use of Hamilton's principle in Sect. 8.2. The boundary control design via the Lyapunov direct method is discussed separately for both exact model case and system parametric uncertainty case in Sect. 8.3, where it is shown that the uniform boundedness

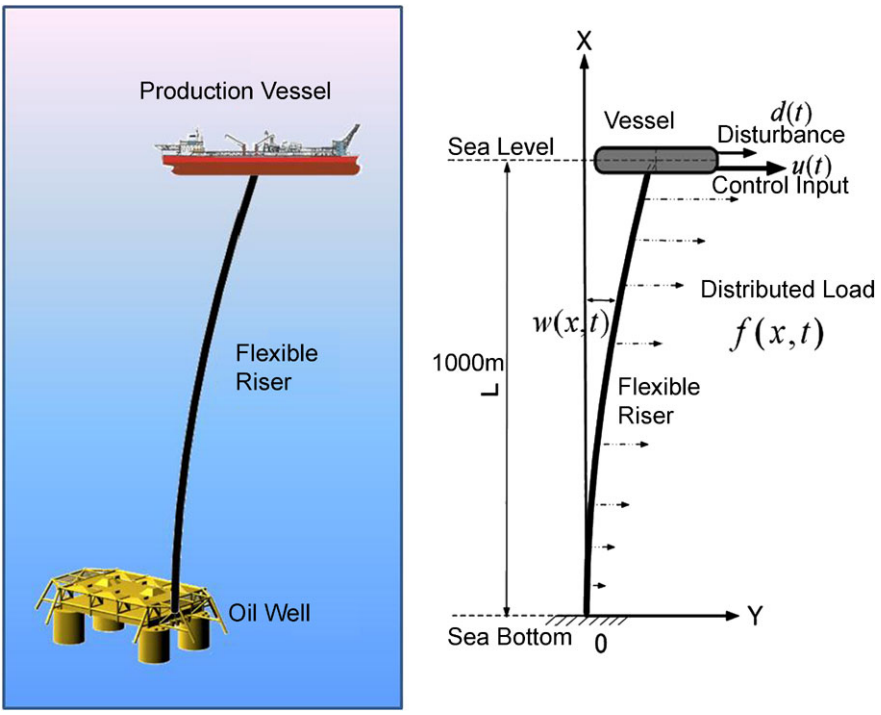

Fig. 8.1 A typical flexible marine riser system

of the closed-loop system can be achieved by the proposed control. Simulations are carried out to illustrate the performance of the proposed control in Sect. 8.4. The conclusion of this chapter is given Sect. 8.5.

8.2 Problem Formulation

A typical marine riser system for crude oil transportation depicted in Fig. 8.1 is the connection between a production vessel on the ocean surface and a well head on the ocean floor. As shown in Fig. 8.1, the control is implemented from the actuator in the vessel, i.e., the top boundary of the riser. In this chapter, we assume that the original position of the vessel is directly above the subsea well head with no horizontal offset and the riser is filled with seawater.

The kinetic energy of the riser system E_k can be represented as

$$E_k = \frac{1}{2}M_s\left[\dot{w}(L,t)\right]^2 + \frac{1}{2}\rho\int_0^L \left[\dot{w}(x,t)\right]^2 dx, \tag{8.1}$$

where x and t represent the independent spatial and time variables, respectively, M_s denotes the mass of the surface vessel, $w(L,t)$ and $\dot{w}(L,t)$ are the position and

velocity of the vessel, respectively, $w(x,t)$ is the displacement of the riser at the position x for time t, $\rho > 0$ is the uniform mass per unit length of the riser, and L is the length of the riser.

The potential energy E_p of the riser system can be obtained from the equality

$$E_p = \frac{1}{2}EI\int_0^L \left[w''(x,t)\right]^2 dx + \frac{1}{2}T\int_0^L \left[w'(x,t)\right]^2 dx, \tag{8.2}$$

where EI is the bending stiffness of the riser, and T is the tension of the riser. The first term of Eq. (7.2) is due to the bending, and the second term is due to the strain energy of the riser.

The virtual work done by the ocean current disturbance on the riser and the vessel is given by

$$\delta W_f = \int_0^L f(x,t)\delta w(x,t)\,dx + d(t)\delta w(L,t), \tag{8.3}$$

where $f(x,t)$ is the distributed transverse load on the riser due to the hydrodynamic effects of the ocean current, and $d(t)$ denotes the environmental disturbance on the vessel. The virtual work done by damping on the riser and the vessel is represented by

$$\delta W_d = -\int_0^L c\dot{w}(x,t)\delta w(x,t)\,dx - d_s\dot{w}(L,t)\delta w(L,t), \tag{8.4}$$

where c is the damping coefficient of the riser, and d_s denotes the damping coefficient of the vessel. We introduce the boundary control u from the actuator in the vessel, i.e., the top boundary of the riser, to produce a transverse force for vibration suppression. The virtual work done by the boundary control is written as

$$\delta W_m = u(t)\delta w(L,t). \tag{8.5}$$

Then, we have the total virtual work done on the system as

$$\begin{aligned}\delta W &= \delta W_f + \delta W_d + \delta W_m \\ &= \int_0^L \left[f(x,t) - c\dot{w}(x,t)\right]\delta w(x,t)\,dx \\ &\quad + \left[u(t) + d(t) - d_s\dot{w}(L,t)\right]\delta w(L,t).\end{aligned} \tag{8.6}$$

Subsequently, we obtain the governing equations of the system as

$$\rho\ddot{w}(x,t) + EIw''''(x,t) - Tw''(x,t) - f(x,t) + c\dot{w}(x,t) = 0 \tag{8.7}$$

for $(x,t) \in (0,L)\times[0,\infty)$ and the boundary conditions of the system as

$$w'(0,t) = 0, \tag{8.8}$$

$$w''(L,t) = 0, \tag{8.9}$$

$$w(0,t) = 0, \tag{8.10}$$

$$-EIw'''(L,t) + Tw'(L,t) = u(t) + d(t) - d_s\dot{w}(L,t) - M_s\ddot{w}(L,t), \tag{8.11}$$

for $t \in [0, \infty)$.

Assumption 8.1 For the distributed load $f(x,t)$ on the riser and the environmental disturbance $d(t)$ on the vessel, we assume that there exist constants $\bar{f} \in \mathbb{R}^+$ and $\bar{d} \in \mathbb{R}^+$ such that $|f(x,t)| \leq \bar{f}$ for all $(x,t) \in [0, L] \times [0, \infty)$ and $|d(t)| \leq \bar{d}$ for all $t \in [0, \infty)$. This is a reasonable assumption as the time-varying disturbances $f(x,t)$ and $d(t)$ have finite energy and hence are bounded, i.e., $f(x,t) \in \mathcal{L}_\infty([0, L])$ and $d(t) \in \mathcal{L}_\infty$.

Remark 8.2 For control design in Sect. 8.3, only the assertion that there exist an upper bound on the disturbance in Assumption 8.1, $|f(x,t)| < \bar{f}$ and $|d(t)| \leq \bar{d}$, is necessary. The knowledge of the exact values for $f(x,t)$ and $d(t)$ is not required. As such, different distributed load models up to various levels of fidelity, such as those found in [195, 196, 227–229], can be applied without affecting the control design or analysis.

Property 8.3 [237] If the kinetic energy of system (8.7)–(8.11), given by Eq. (8.1), is bounded for all $t \in [0, \infty)$, then $\dot{w}(x,t)$, $\dot{w}'(x,t)$, $\dot{w}''(x,t)$, and $\dot{w}'''(x,t)$ are bounded for all $(x,t) \in [0, L] \times [0, \infty)$.

Property 8.4 [237] If the potential energy of system (8.7)–(8.11), given by Eq. (8.2), is bounded for all $t \in [0, \infty)$, then $w''(x,t)$, $w'''(x,t)$, and $w''''(x,t)$ are bounded for all $(x,t) \in [0, L] \times [0, \infty)$.

8.3 Control Design

The control objective is to suppress the vibration of the riser and stabilize the riser at the small neighborhood of its original position in the presence of the time-varying distributed load $f(x,t)$ and the disturbance $d(t)$ due to the ocean current. In this section, the Lyapunov direct method is used to construct a boundary control law $u(t)$ at the top boundary of the riser and to analyze the closed-loop stability of the system.

In this chapter, we analyze two cases for the riser system: (i) exact model-based control, i.e., EI, T, M_s, and d_s are all known; and (ii) adaptive control for the system parametric uncertainty, i.e., EI, T, M_s, and d_s are unknown. For the first case, robust boundary control is introduced for the exact model of the riser system subject to the ocean disturbance. For second case where the system parameters cannot be directly measured, the adaptive control is designed to compensate the system parametric uncertainty.

8.3.1 Exact Model-Based Boundary Control of the Riser System

To stabilize the system given by governing Eq. (8.7) and the boundary conditions (8.8)–(8.11), we propose the following control law:

$$u = -EIw'''(L,t) + Tw'(L,t) - \mathrm{sgn}(u_a)\bar{d} + d_s\dot{w}(L,t) - k_1M_s\dot{w}'(L,t) + k_2M_s\dot{w}'''(L,t) - ku_a, \tag{8.12}$$

where $\mathrm{sgn}(\cdot)$ denotes the signum function, k, k_1, k_2 are the control gains, and the auxiliary signal u_a is defined as

$$u_a = \dot{w}(L,t) + k_1w'(L,t) - k_2w'''(L,t). \tag{8.13}$$

After differentiating the auxiliary signal Eq. (8.13), multiplying the resulting equation by M_s, and substituting Eq. (8.11), we obtain

$$M_s\dot{u}_a = EIw'''(L,t) - Tw'(L,t) + d - d_s\dot{w}(L,t) + k_1M_s\dot{w}'(L,t) - k_2M_s\dot{w}'''(L,t) + u. \tag{8.14}$$

Substituting Eq. (8.12) into Eq. (8.14), we have

$$M_s\dot{u}_a = -ku_a + d - \mathrm{sgn}(u_a)\bar{d}. \tag{8.15}$$

Remark 8.5 All the signals in the boundary control can be measured by sensors or obtained by a backward difference algorithm. $w(L,t)$ can be sensed by a laser displacement sensor at the top boundary of the riser, $w'(L,t)$ can be measured by an inclinometer, and $w'''(L,t)$ can be obtained by a shear force sensor. In practice, the effect of measurement noise from sensors is unavoidable, which will affect the control implementation, especially when the high-order differentiating terms with respect to time exist. In our proposed control (8.12), $\dot{w}(L,t)$, $\dot{w}'(L,t)$, and $\dot{w}'''(L,t)$ with only one time differentiating with respect to time can be calculated with a backward difference algorithm. It is noted that differentiating twice and three times the position $w(L,t)$ with respect to time to get $\ddot{w}(L,t)$ and $\dddot{w}(L,t)$, respectively, is undesirable in practice due to noise amplification. For these cases, observers need to design estimation of the states values according to the boundary conditions.

Remark 8.6 The control design is based on the distributed-parameter model, Eqs. (8.7)–(8.11), and the spillover problems associated with traditional truncated model-based approaches caused by ignoring high-frequency modes in controller and observer design are avoided. For results on model-based control of distributed-parameter system, which is helpful in avoiding spillover effects, the readers can refer to [57, 58].

Consider the Lyapunov function candidate

$$V = V_1 + V_2 + V_3, \tag{8.16}$$

where the energy term V_1, an auxiliary term V_2, and a small crossing term V_3 are defined as

$$V_1 = \frac{\beta k_2}{2}\rho \int_0^L [\dot{w}]^2 dx + \frac{\beta k_2}{2} EI \int_0^L [w'']^2 dx + \frac{\beta k_2}{2} T \int_0^L [w']^2 dx, \quad (8.17)$$

$$V_2 = \frac{1}{2} M_s u_a^2, \quad (8.18)$$

$$V_3 = \alpha\rho \int_0^L x\dot{w}w' dx, \quad (8.19)$$

where k_2 is the control gain, and α and β are positive weighting constants.

Lemma 8.7 *The Lyapunov function candidate given by* (8.16) *is upper and lower bounded as*

$$0 \le \lambda_1(V_1 + V_2) \le V \le \lambda_2(V_1 + V_2), \quad (8.20)$$

where λ_1 *and* λ_2 *are positive constants defined as*

$$\lambda_1 = 1 - \frac{2\alpha\rho L}{\min(\beta\rho k_2, \beta T k_2)} \quad \text{and} \quad \lambda_2 = 1 + \frac{2\alpha\rho L}{\min(\beta\rho k_2, \beta T k_2)}. \quad (8.21)$$

Proof Applying inequality (2.11) to Eq. (8.19) yields

$$\begin{aligned} |V_3| &\le \alpha\rho L \int_0^L \left([w']^2 + [\dot{w}]^2\right) dx \\ &\le \alpha_1 V_1, \end{aligned} \quad (8.22)$$

where

$$\alpha_1 = \frac{2\alpha\rho L}{\min(\beta\rho k_2, \beta T k_2)}. \quad (8.23)$$

Then, we obtain

$$-\alpha_1 V_1 \le V_3 \le \alpha_1 V_1. \quad (8.24)$$

Considering α as a small positive weighting constant satisfying

$$0 < \alpha < \frac{\min(\beta\rho k_2, \beta T k_2)}{2\rho L},$$

we can obtain

$$\alpha_2 = 1 - \alpha_1 = 1 - \frac{2\alpha\rho L}{\min(\beta\rho k_2, \beta T k_2)} > 0, \quad (8.25)$$

$$\alpha_3 = 1 + \alpha_1 = 1 + \frac{2\alpha\rho L}{\min(\beta\rho k_2, \beta T k_2)} > 1. \tag{8.26}$$

Then, we further have

$$0 \le \alpha_2 V_1 \le V_1 + V_3 \le \alpha_3 V_1. \tag{8.27}$$

Given the Lyapunov function candidate in Eq. (8.16), we obtain

$$0 \le \lambda_1(V_1 + V_2) \le V \le \lambda_2(V_1 + V_2), \tag{8.28}$$

where $\lambda_1 = \min(\alpha_2, 1) = \alpha_2$ and $\lambda_2 = \max(\alpha_3, 1) = \alpha_3$ are positive constants. □

Lemma 8.8 *The time derivative of the Lyapunov function candidate* (8.16) *is upper bounded with*

$$\dot{V} \le -\lambda V + \varepsilon, \tag{8.29}$$

where λ *and* ε *are positive constants.*

Proof Differentiating Eq. (8.16) with respect to time leads to

$$\dot{V} = \dot{V}_1 + \dot{V}_2 + \dot{V}_3. \tag{8.30}$$

The first term of Eq. (8.30)

$$\dot{V}_1 = A_1 + A_2 + A_3, \tag{8.31}$$

where

$$A_1 = \beta\rho k_2 \int_0^L \dot{w}\ddot{w}\, dx, \tag{8.32}$$

$$A_2 = \beta EI k_2 \int_0^L w''\dot{w}''\, dx, \tag{8.33}$$

$$A_3 = \beta T k_2 \int_0^L w'\dot{w}'\, dx. \tag{8.34}$$

Substituting the governing equation (8.7) into A_1, we obtain

$$A_1 = \beta k_2 \int_0^L \dot{w}\left(-EIw'''' + Tw'' + f - c\dot{w}\right) dx. \tag{8.35}$$

Using the boundary conditions and integrating Eq. (8.33) by parts, we obtain

$$A_2 = -\beta EI k_2 w'''(L,t)\dot{w}(L,t) + \beta EI k_2 \int_0^L \dot{w}w''''\, dx. \tag{8.36}$$

Using the boundary conditions and integrating Eq. (8.34) by parts, we obtain

$$\begin{aligned} A_3 &= \beta T k_2 \int_0^L w' d(\dot{w}) \\ &= \beta T k_2 w'(L,t)\dot{w}(L,t) - \beta T k_2 \int_0^L \dot{w} w'' dx. \end{aligned} \tag{8.37}$$

Using inequality (2.12), we obtain

$$\begin{aligned} \dot{V}_1 \leq & -\frac{\beta EI}{2}\left[\left[\dot{w}(L,t)\right]^2 + k_2^2\left[w'''(L,t)\right]^2 + k_1^2\left[w'(L,t)\right]^2\right] + \frac{\beta EI}{2}u_a^2 \\ & + \beta|Tk_2 - EIk_1|\delta_1\left[w'(L,t)\right]^2 + \frac{\beta}{\delta_1}|Tk_2 - EIk_1|\left[\dot{w}(L,t)\right]^2 \\ & + \beta EIk_1k_2 w'''(L,t)w'(L,t) \\ & - \beta(c-\delta_2)k_2\int_0^L [\dot{w}]^2 dx + \frac{\beta k_2}{\delta_2}\int_0^L f^2 dx, \end{aligned} \tag{8.38}$$

where δ_1 and δ_2 are positive constants.

The second term of Eq. (8.30)

$$\begin{aligned} \dot{V}_2 &= M_s u_a \dot{u}_a, \\ &= -ku_a^2 + du_a - \operatorname{sgn}(u_a)u_a\bar{d} \\ &\leq -ku_a^2. \end{aligned} \tag{8.39}$$

The third term of Eq. (8.30)

$$\begin{aligned} \dot{V}_3 &= \alpha\rho\int_0^L \left(x\ddot{w}w' + x\dot{w}\dot{w}'\right)dx \\ &= \alpha\int_0^L xw'\left[-EIw'''' + Tw'' + f - c\dot{w}\right]dx + \alpha\rho\int_0^L x\dot{w}\dot{w}'dx. \end{aligned} \tag{8.40}$$

After integrating Eq. (8.40) by parts and using the boundary conditions, we obtain

$$\begin{aligned} \dot{V}_3 \leq & -\alpha EILw'(L,t)w'''(L,t) - \frac{3\alpha EI}{2}\int_0^L \left[w''\right]^2 dx + \frac{\alpha TL}{2}\left[w'(L,t)\right]^2 \\ & - \frac{\alpha T}{2}\int_0^L \left[w'\right]^2 dx + \frac{\alpha L}{\delta_3}\int_0^L f^2 dx + \alpha L\delta_3\int_0^L \left[w'\right]^2 dx \\ & + \frac{\alpha cL}{\delta_4}\int_0^L [\dot{w}]^2 dx + \alpha cL\delta_4\int_0^L \left[w'\right]^2 dx \\ & + \frac{\alpha\rho L}{2}\left[\dot{w}(L,t)\right]^2 - \frac{\alpha\rho}{2}\int_0^L [\dot{w}]^2 dx, \end{aligned} \tag{8.41}$$

where δ_3 and δ_4 are positive constants. Applying inequalities (8.38), (8.39), and (8.41) to Eq. (8.16) and utilizing inequality (2.12), we obtain

$$\begin{aligned}
\dot{V} \leq & -\left(\beta c k_2 + \frac{\alpha\rho}{2} - \beta\delta_2 k_2 - \frac{\alpha c L}{\delta_4}\right)\int_0^L [\dot{w}]^2\,dx \\
& -\left(\frac{\alpha T}{2} - \alpha L\delta_3 - \alpha c L\delta_4\right)\int_0^L \left[w'\right]^2 dx \\
& -\frac{3\alpha EI}{2}\int_0^L \left[w''\right]^2 dx - \left(\frac{\beta EI}{2} - \frac{\beta}{\delta_1}|Tk_2 - EIk_1| - \frac{\alpha\rho L}{2}\right)\left[\dot{w}(L,t)\right]^2 \\
& -\left(\frac{\beta EIk_1^2}{2} - \frac{\alpha TL}{2} - \beta|Tk_2 - EIk_1|\delta_1 - |\beta EIk_1k_2 - \alpha EIL|\delta_5\right) \\
& \times \left[w'(L,t)\right]^2 - \left(\frac{\beta EIk_2^2}{2} - \frac{|\beta EIk_1k_2 - \alpha EIL|}{\delta_5}\right)\left[w'''(L,t)\right]^2 \\
& -\left(k - \frac{\beta EI}{2}\right)u_a^2 + \left(\frac{\beta k_2}{\delta_2} + \frac{\alpha L}{\delta_3}\right)\int_0^L \bar{f}^2\,dx \\
\leq & -\lambda_3(V_1 + V_2) + \varepsilon, \qquad (8.42)
\end{aligned}$$

where $\varepsilon = (\frac{\beta k_2}{\delta_2} + \frac{\alpha L}{\delta_3})\int_0^L \bar{f}^2\,dx = (\frac{\beta k_2}{\delta_2} + \frac{\alpha L}{\delta_3})L\bar{f}^2$, and the constants k, k_1, k_2, α, β, δ_1, δ_2, δ_3, δ_4, and δ_5 are chosen to satisfy the following conditions:

$$\alpha < \frac{\min(\beta\rho k_2, \beta T k_2)}{2\rho L}, \qquad (8.43)$$

$$\frac{\beta EIk_1^2}{2} - \frac{\alpha TL}{2} - \beta|Tk_2 - EIk_1|\delta_1 - |\beta EIk_1k_2 - \alpha EIL|\delta_5 \geq 0, \qquad (8.44)$$

$$\frac{\beta EI}{2} - \frac{\beta}{\delta_1}|Tk_2 - EIk_1| - \frac{\alpha\rho L}{2} \geq 0, \qquad (8.45)$$

$$\frac{\beta EIk_2^2}{2} - \frac{|\beta EIk_1k_2 - \alpha EIL|}{\delta_5} \geq 0, \qquad (8.46)$$

$$\sigma_1 = \beta c k_2 + \frac{\alpha\rho}{2} - \beta\delta_2 k_2 - \frac{\alpha c L}{\delta_4} > 0, \qquad (8.47)$$

$$\sigma_2 = \frac{3\alpha EI}{2} > 0, \qquad (8.48)$$

$$\sigma_3 = \frac{\alpha T}{2} - \alpha L\delta_3 - \alpha c L\delta_4 > 0, \qquad (8.49)$$

$$\sigma_4 = k - \frac{\beta EI}{2} > 0, \qquad (8.50)$$

$$\lambda_3 = \min\left(\frac{2\sigma_1}{\beta\rho}, \frac{2\sigma_2}{\beta EI}, \frac{2\sigma_3}{\beta T}, \frac{2\sigma_4}{M_s}\right) > 0. \qquad (8.51)$$

From inequalities (8.28) and (8.42) we have

$$\dot{V} \leq -\lambda V + \varepsilon, \tag{8.52}$$

where $\lambda = \lambda_3/\lambda_2$ and ε are positive constants. □

With the above lemmas, the exact model-based control design for riser system subjected to the ocean current disturbance can be summarized in the following theorem.

Theorem 8.9 *For the system dynamics described by* (8.7) *and boundary conditions* (8.8)–(8.11), *under Assumption* 8.1 *and the control law* (8.12), *given that the initial conditions are bounded, we can conclude the uniform boundedness* (*UB*): *the state of the closed-loop system* $w(x,t)$ *will remain in the compact set* Ω *defined by*

$$\Omega := \left\{ w(x,t) \in \mathbb{R} \mid \left| w(x,t) \right| \leq H_1 \ \forall (x,t) \in [0,L] \times [0,\infty) \right\}, \tag{8.53}$$

where constant $H_1 = \sqrt{\frac{2L}{\beta T \lambda_1 k_2}(V(0) + \frac{\varepsilon}{\lambda})}$.

Proof Multiplying Eq. (8.29) by $e^{\lambda t}$ yields

$$\frac{\partial}{\partial t}\left(V e^{\lambda t}\right) \leq \varepsilon e^{\lambda t}. \tag{8.54}$$

Integrating the above inequality, we obtain

$$V \leq \left(V(0) - \frac{\varepsilon}{\lambda}\right)e^{-\lambda t} + \frac{\varepsilon}{\lambda} \leq V(0)e^{-\lambda t} + \frac{\varepsilon}{\lambda} \in \mathcal{L}_\infty, \tag{8.55}$$

which implies that V is bounded. Utilizing inequality (2.15) and Eq. (8.17), we have

$$\begin{aligned} \frac{\beta k_2}{2L} T w^2(x,t) \leq \frac{\beta k_2}{2} T \int_0^L \left[w'(x,t)\right]^2 dx \leq V_1 \leq V_1 + V_2 \\ \leq \frac{1}{\lambda_1} V \in \mathcal{L}_\infty. \end{aligned} \tag{8.56}$$

Appropriately rearranging the terms of the above inequality, we obtain that $w(x,t)$ is uniformly bounded as follows:

$$\begin{aligned} \left| w(x,t) \right| \leq \sqrt{\frac{2L}{\beta T \lambda_1 k_2}\left(V(0)e^{-\lambda t} + \frac{\varepsilon}{\lambda}\right)} \leq \sqrt{\frac{2L}{\beta T \lambda_1 k_2}\left(V(0) + \frac{\varepsilon}{\lambda}\right)} \\ \forall (x,t) \in [0,L] \times [0,\infty). \quad \square \end{aligned} \tag{8.57}$$

Remark 8.10 By choosing proper values of α and β, it is shown that the increase in the control gain k will result in a larger σ_4, which will lead to a greater λ_3. Then

the value of λ will increase, which will reduce the size of Ω and produce a better vibration suppression performance. We can conclude that the bound of the system state $w(x,t)$ can be made smaller, provided that the design control parameters are appropriately selected. However, increasing k will bring a high-gain control problem. Therefore, in practical applications, the design parameters should be adjusted carefully for achieving suitable transient performance and control action.

Remark 8.11 From Eq. (8.56) we can state that V_1 is bounded for all $t \in [0,\infty)$. Since V_1 is bounded, $\dot{w}(x,t)$, $w''(x,t)$, and $w'(x,t)$ are bounded for all $(x,t) \in [0,L]\times[0,\infty)$. From Eq. (8.1), the kinetic energy of the system is bounded, and by Property 8.3, $\dot{w}'(x,t)$ and $\dot{w}'''(x,t)$ are also bounded for all $(x,t)\in[0,L]\times[0,\infty)$. From the boundedness of the potential energy given by Eq. (8.2), we can use Property 8.4 to obtain that $w'''(x,t)$ and $w''''(x,t)$ are bounded. Using Assumption 8.1, Eq. (8.7), and the above statements, we can state that $\ddot{w}(x,t)$ is also bounded for all $(x,t)\in[0,L]\times[0,\infty)$. From the above information it is shown that the proposed control (8.12) ensures that all internal system signals, including $w(x,t)$, $w'(x,t)$, $\dot{w}(x,t)$, $\dot{w}'(x,t)$, $\ddot{w}(x,t)$, $w'''(x,t)$, $\dot{w}'''(x,t)$, and $w''''(x,t)$, are uniformly bounded. Since $\dot{w}(x,t)$, $w'(x,t)$, $\dot{w}'(x,t)$, $w'''(x,t)$, and $\dot{w}'''(x,t)$ are all bounded for all $(x,t)\in[0,L]\times[0,\infty)$, we can conclude that the boundary control (8.12) is also bounded for all $t\in[0,\infty)$.

Remark 8.12 For the system dynamics described by Eq. (8.7) and boundary conditions (8.8)–(8.11), if $f(x,t)=0$, the exponential stability can be achieved with the proposed boundary control (8.12) as follows:

$$\left|w(x,t)\right| \le \sqrt{\frac{2L}{\beta T \lambda_1 k_2} V(0) e^{-\lambda t}} \quad \forall (x,t)\in[0,L]\times[0,\infty). \tag{8.58}$$

8.3.2 Robust Adaptive Boundary Control for System Parametric Uncertainty

In Sect. 8.3.1, the exact model-based boundary control (8.12) requires the exact knowledge of the riser system. Adaptive boundary control is designed to improve the performance of the system via parameter estimation when there are some unknown parameters. The exact model-based boundary control provides a stepping stone toward the adaptive control, which is designed to deal with the system parametric uncertainty. In this section, the boundary control (8.12) is redesigned by using the adaptive control since the EI, T, d_s, and M_s are unknown. We rewrite Eq. (8.14) in the form

$$M_s \dot{u}_a = P\Phi + d + u, \tag{8.59}$$

where vectors P and Φ are defined as

$$P = \begin{bmatrix} w'''(L,t) & -w'(L,t) & -\dot{w}(L,t) & k_1\dot{w}'(L,t) - k_2\dot{w}'''(L,t) \end{bmatrix}, \tag{8.60}$$

$$\Phi = [EI \quad T \quad d_s \quad M_s]^T. \tag{8.61}$$

We propose the following adaptive boundary control law for the system:

$$u = -P\hat{\Phi} - ku_a - \text{sgn}(u_a)\bar{d}, \tag{8.62}$$

where the parameter estimate vector $\hat{\Phi}$ is defined as

$$\hat{\Phi} = [\widehat{EI} \quad \hat{T} \quad \hat{d}_s \quad \hat{M}_s]^T. \tag{8.63}$$

The adaptation law is designed as

$$\dot{\hat{\Phi}} = \Gamma P^T u_a - r\Gamma\hat{\Phi}, \tag{8.64}$$

where $\Gamma \in \mathbb{R}^{4\times4}$ is a diagonal positive-definite matrix, and r is a positive constant. We denote the maximum and minimum eigenvalues of the matrix Γ as $\lambda_{\max}$ and $\lambda_{\min}$, respectively. The parameter estimate error vector $\tilde{\Phi} \in \mathbb{R}^4$ is defined as

$$\tilde{\Phi} = \Phi - \hat{\Phi}. \tag{8.65}$$

Substituting Eq. (8.62) into Eq. (8.59) and using Eq. (8.65) in Eq. (8.64), we have

$$M_s\dot{u}_a = P\tilde{\Phi} - ku_a + d - \text{sgn}(u_a)\bar{d}, \tag{8.66}$$

$$\dot{\tilde{\Phi}} = -\Gamma P^T u_a + r\Gamma\hat{\Phi}. \tag{8.67}$$

Consider the Lyapunov function candidate

$$V_a = V + \frac{1}{2}\tilde{\Phi}^T\Gamma^{-1}\tilde{\Phi}, \tag{8.68}$$

where V is defined by Eq. (8.16).

Lemma 8.13 *The Lyapunov function candidate given by* (8.68) *is upper and lower bounded as*

$$0 \le \lambda_{1a}\big(V_1 + V_2 + \|\tilde{\Phi}\|^2\big) \le V_a \le \lambda_{2a}\big(V_1 + V_2 + \|\tilde{\Phi}\|^2\big), \tag{8.69}$$

where λ_{1a} *and* λ_{2a} *are positive constants defined as*

$$\lambda_{1a} = \min\left(1 - \frac{2\alpha\rho L}{\min(\beta\rho k_2, \beta T k_2)}, \frac{1}{2\lambda_{\max}}\right), \tag{8.70}$$

$$\lambda_{2a} = \max\left(1 + \frac{2\alpha\rho L}{\min(\beta\rho k_2, \beta T k_2)}, \frac{1}{2\lambda_{\min}}\right). \tag{8.71}$$

Proof From inequality (8.20) we have

$$\lambda_1(V_1 + V_2) \le V \le \lambda_2(V_1 + V_2), \tag{8.72}$$

where λ_1 and λ_2 are positive constants defined in Eq. (8.21). From the properties of the matrix Γ we have

$$\frac{1}{2\lambda_{\max}}\|\tilde{\Phi}\|^2 \leq \frac{1}{2}\tilde{\Phi}^T\Gamma^{-1}\tilde{\Phi} \leq \frac{1}{2\lambda_{\min}}\|\tilde{\Phi}\|^2. \tag{8.73}$$

Combining inequalities (8.72) and (8.73), we have

$$0 \leq \lambda_{1a}\big(V_1 + V_2 + \|\tilde{\Phi}\|^2\big) \leq V_a \leq \lambda_{2a}\big(V_1 + V_2 + \|\tilde{\Phi}\|^2\big), \tag{8.74}$$

where $\lambda_{1a} = \min(\lambda_1, \frac{1}{2\lambda_{\max}})$ and $\lambda_{2a} = \max(\lambda_2, \frac{1}{2\lambda_{\min}})$ are positive constants. □

Lemma 8.14 *The time derivative of the Lyapunov function candidate* (8.68) *is upper bounded with*

$$\dot{V}_a \leq -\lambda_a V_a + \psi, \tag{8.75}$$

where λ_a *and* ψ *are positive constants.*

Proof We obtain the time derivative of the Lyapunov function candidate Eq. (8.68) as

$$\dot{V}_a = \dot{V} + \tilde{\Phi}^T\Gamma^{-1}\dot{\tilde{\Phi}}. \tag{8.76}$$

Substituting Eq. (8.66) into the second term of Eq. (8.30), we have

$$\begin{aligned}\dot{V}_2 &= M_s u_a \dot{u}_a \\ &= -ku_a^2 + du_a - \operatorname{sgn}(u_a)\bar{d}u_a + P\tilde{\Phi}u_a \\ &\leq -ku_a^2 + P\tilde{\Phi}u_a.\end{aligned} \tag{8.77}$$

Applying the results of Lemma 8.7 and utilizing inequalities (8.38), (8.77), and (8.41) in $\dot{V}$, we obtain

$$\dot{V} \leq -\lambda_3(V_1 + V_2) + P\tilde{\Phi}u_a + \varepsilon, \tag{8.78}$$

where λ_3 is defined in Eq. (8.51), and ε is a positive constant. Application of inequality (8.78) to Eq. (8.76) yields

$$\dot{V}_a \leq -\lambda_3(V_1 + V_2) + \tilde{\Phi}^T\big(P^T u_a + \Gamma^{-1}\dot{\tilde{\Phi}}\big) + \varepsilon. \tag{8.79}$$

Substituting Eq. (8.67) into inequality (8.79), we have

$$\begin{aligned}\dot{V}_a &\leq -\lambda_3(V_1 + V_2) + r\tilde{\Phi}^T\hat{\Phi} + \varepsilon \\ &\leq -\lambda_3(V_1 + V_2) - \frac{r}{2}\|\tilde{\Phi}\|^2 + \frac{r}{2}\|\Phi\|^2 + \varepsilon \\ &\leq -\lambda_{3a}\big(V_1 + V_2 + \|\tilde{\Phi}\|^2\big) + \frac{r}{2}\|\Phi\|^2 + \varepsilon,\end{aligned} \tag{8.80}$$

where $\lambda_{3a} = \min(\lambda_3, \frac{r}{2})$ is a positive constant. From inequalities (8.74) and (8.80) we have

$$\dot{V}_a \leq -\lambda_a V_a + \psi, \tag{8.81}$$

where $\lambda_a = \lambda_{3a}/\lambda_{2a}$ and $\psi = \frac{r}{2}\|\Phi\|^2 + \varepsilon > 0$. □

With the above lemmas, the adaptive control design for the riser system subjected to the ocean current disturbance can be summarized in the following theorem.

Theorem 8.15 *For the system dynamics described by* (8.7) *and boundary conditions* (8.8)–(8.11), *under Assumption* 8.1 *and the control law* (8.62), *given that the initial conditions are bounded, we can conclude the uniform boundedness* (*UB*): *the state of the closed-loop system* $w(x,t)$ *will remain in the compact set* Ω_a *defined by*

$$\Omega_a := \left\{ w(x,t) \in \mathbb{R} \mid \left| w(x,t) \right| \leq H_2 \ \forall (x,t) \in [0, L] \times [0, \infty) \right\}, \tag{8.82}$$

where the constant $H_2 = \sqrt{\frac{2L}{\beta T \lambda_{1a} k_2}(V_a(0) + \frac{\psi}{\lambda_a})}$.

Proof Multiplying Eq. (8.75) by $e^{\lambda_a t}$ yields

$$\frac{\partial}{\partial t}\left(V_a e^{\lambda_a t}\right) \leq \psi e^{\lambda_a t}. \tag{8.83}$$

Integrating the above inequality, we obtain

$$V_a \leq \left(V_a(0) - \frac{\psi}{\lambda_a}\right)e^{-\lambda_a t} + \frac{\psi}{\lambda_a} \leq V_a(0)e^{-\lambda_a t} + \frac{\psi}{\lambda_a} \in \mathcal{L}_\infty, \tag{8.84}$$

which implies that V_a is bounded. Utilizing inequality (2.15) and Eq. (8.17), we have

$$\frac{\beta k_2}{2L} T w^2(x,t) \leq \frac{\beta k_2}{2} T \int_0^L \left[w'(x,t)\right]^2 dx \leq V_1 \leq V_1 + V_2 \leq \frac{1}{\lambda_{1a}} V_a \in \mathcal{L}_\infty.$$

Appropriately rearranging the terms of the above inequality, we obtain that $w(x,t)$ is uniformly bounded as follows:

$$\left| w(x,t) \right| \leq \sqrt{\frac{2L}{\beta T \lambda_{1a} k_2}\left(V_a(0)e^{-\lambda_a t} + \frac{\psi}{\lambda_a}\right)} \leq \sqrt{\frac{2L}{\beta T \lambda_{1a} k_2}\left(V_a(0) + \frac{\psi}{\lambda_a}\right)}$$
$$\forall (x,t) \in [0, L] \times [0, \infty). \quad \square \tag{8.85}$$

Remark 8.16 From the similar analysis of Remark 8.10 we can conclude that the system state $w(x,t)$ with the proposed robust adaptive boundary control can be made smaller by choosing control gain k in Eq. (8.62) appropriately.

Remark 8.17 From Eq. (8.84) we can obtain that the parameter estimate error $\tilde{\Phi}$ is bounded for all $t \in [0, \infty)$. Using the derivation similar to those employed in Remark 8.11, we can state that the proposed control (8.62) ensures that all internal system signals, including $w(x,t)$, $w'(x,t)$, $\dot{w}(x,t)$, $\dot{w}'(x,t)$, $\ddot{w}(x,t)$, $w'''(x,t)$, $\dot{w}'''(x,t)$, and $w''''(x,t)$, are uniformly bounded. Since $\hat{\Phi}$, $w'(x,t)$, $\dot{w}(x,t)$, $w'''(x,t)$, and $\dot{w}'''(x,t)$ are all bounded for all $(x,t) \in [0,L] \times [0,\infty)$, we can conclude that the boundary adaptive control (8.62) is also bounded for all $t \in [0,\infty)$.

Remark 8.18 For the system dynamics described by Eq. (8.7) and boundary conditions (8.8)–(8.11), if there is no distributed disturbance for the riser system, i.e., $f(x,t) = 0$, the boundedness stability can be achieved with the proposed boundary control (8.62) as follows:

$$|w(x,t)| \leq \sqrt{\frac{2L}{\beta T \lambda_{1a} k_2}\left(V_a(0)e^{-\lambda_a t} + \frac{r\|\Phi\|^2}{2\lambda_a}\right)}$$
$$\forall (x,t) \in [0,L] \times [0,\infty). \tag{8.86}$$

8.4 Numerical Simulations

Simulations for a riser of length 1000 m under the ocean current disturbance are carried out to demonstrate the effectiveness of the proposed boundary control defined in Eq. (8.12) and Eq. (8.62).

The riser, initially at rest, is excited by a distributed transverse disturbance due to the ocean current. The corresponding initial conditions of the riser system are given as

$$w(x,0) = 0, \tag{8.87}$$
$$\dot{w}(x,0) = 0. \tag{8.88}$$

The system parameters are given in Table 8.1.

In the simulation, the ocean surface current velocity $U(t)$ is generated by Eq. (4.94). The full current load is applied from $x = 1000$ m to $x = 0$ m and thereafter linearly declines to zero at the ocean floor, $x = 0$, to obtain a depth-dependent ocean current profile $U(x,t)$ as in Chap. 3. The distributed load $f(x,t)$ is generated by Eq. (2.5) with $C_D = 1$, $\theta = 0$, $S_t = 0.2$, and $f_v = 2.625$. The disturbance $d(t)$ on the vessel generated by the following equation is shown in Fig. 8.2:

$$d(t) = \left[3 + 0.8\sin(0.7t) + 0.2\sin(0.5t) + 0.2\sin(0.9t)\right] \times 10^6. \tag{8.89}$$

Displacement of the riser system for free vibration, i.e., $u(t) = 0$, under the ocean disturbance is shown in Fig. 8.3. Displacement of the riser system with exact model-based control Eq. (7.12), by choosing $k = 1 \times 10^7$, under the ocean disturbance is

Table 8.1 Parameters of the riser system

Parameter	Description	Value
L	Riser length	1000.00 m
D	Riser external diameter	152.40 mm
EI	Riser stiffness	1.5×10^7 N m^2
M_s	Vessel mass	9.60×10^6 kg
d_s	Vessel damping	1×10^3 N s m^{-1}
T	Riser tension	8.11×10^7 N
ρ	Riser mass per unit	500.00 kg m^{-1}
ρ_s	Sea water density	1024.00 kg m^{-3}
c	Riser damping	2.00 N s m^{-2}

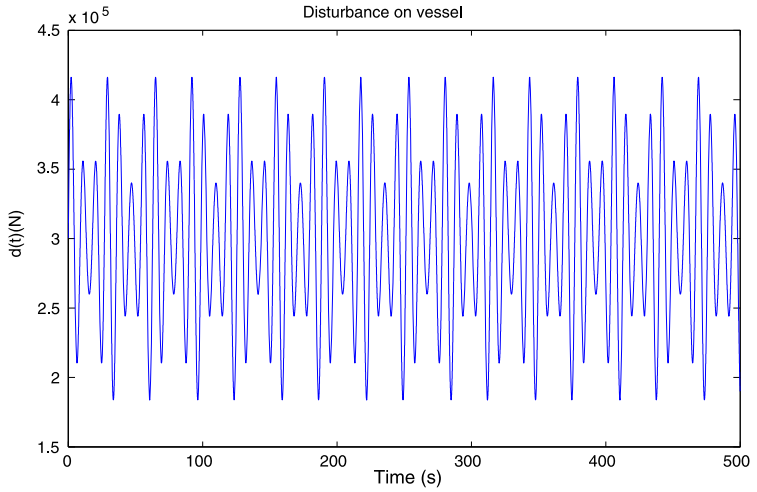

Fig. 8.2 Disturbance on the vessel $d(t)$

shown in Fig. 8.4. When the system parameters EI, T, d_s, and M_s are unknown, the displacement of the riser system with adaptive control (8.62), by choosing $k = 1 \times 10^7$, $r = 0.0001$, and $\Gamma = \text{diag}\{1, 1, 1, 1\}$, under the ocean disturbance is shown in Fig. 8.5. Figures 8.4 and 8.5 illustrate that the proposed boundary controls (8.12) and (8.62) are able to stabilize the riser at the small neighborhood of zero by appropriately choosing design parameters. The corresponding boundary control inputs for the exact model-based control and the adaptive control are shown in Fig. 8.6. Both two control inputs vary between 0 and 5×10^4 N, which are implementable in practice.

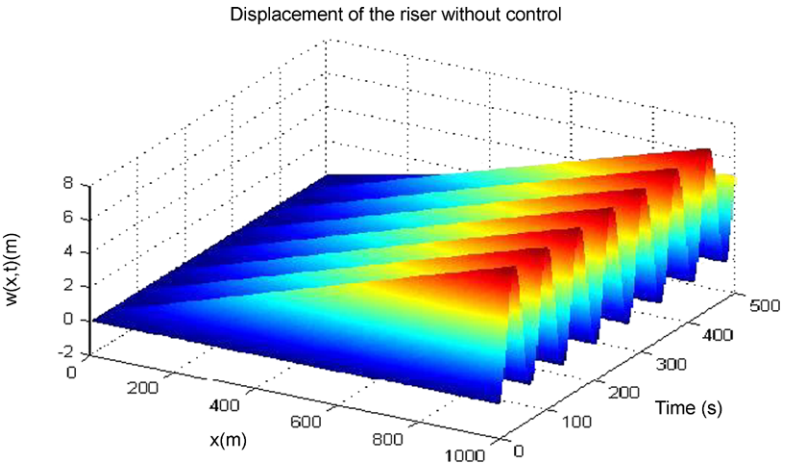

Fig. 8.3 Displacement of the riser without control

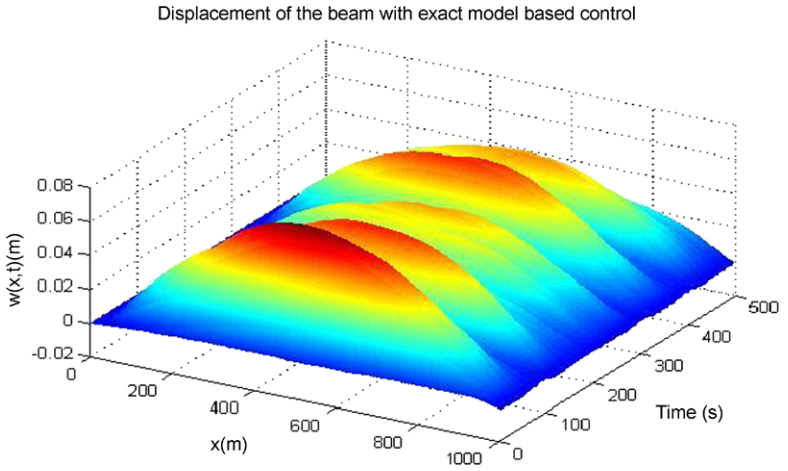

Fig. 8.4 Displacement of the riser with exact model-based control

8.5 Conclusion

Vibration suppression for a flexible marine riser system subjected to the ocean current disturbance has been presented in this chapter. Two cases have been investigated: (i) exact model-based control and (ii) robust adaptive control for the system parametric uncertainty. Robust boundary control has been proposed based on the exact model of the riser system, and adaptive control has been designed to compensate for the system parametric uncertainty. With the proposed control, closed-looped stability under the external disturbance has been proven by using the Lyapunov direct method. The proposed control has been designed based on the original infinite-

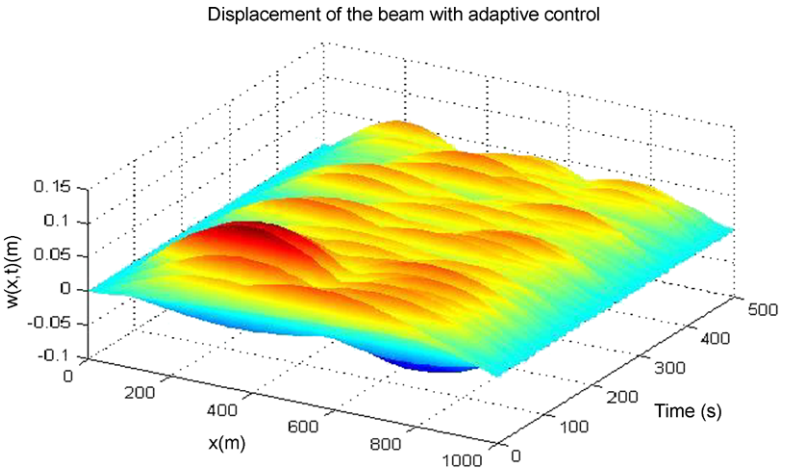

Fig. 8.5 Displacement of the riser with adaptive control

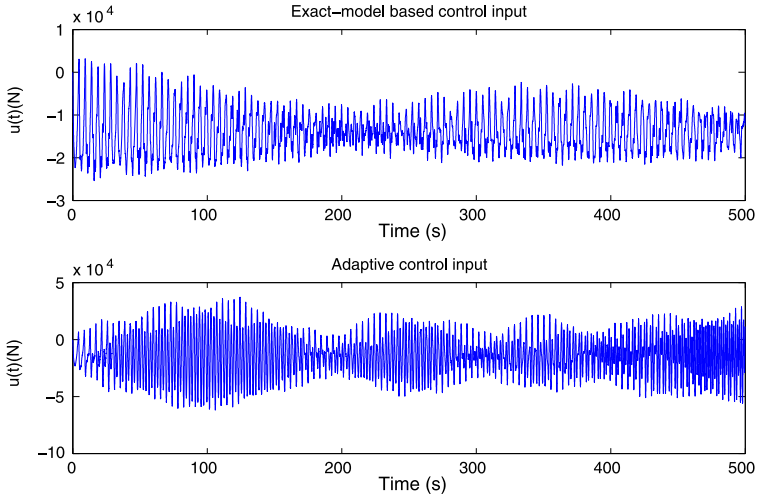

Fig. 8.6 Control input $u(t)$

dimensional model (PDE), and the spillover instability phenomenon has been eliminated. The control is implementable since all the required signals in the control can be measured by sensors or obtained by a backward difference algorithm. Numerical simulations have been provided to illustrate the effectiveness of the proposed boundary control.

In our control design, there is no term introduced to cope with the effect of the time-varying distributed disturbance $f(x,t)$. When the upper bound of the time-varying distributed disturbance is large, the control performance will be affected. For example, in the mooring system, H_1 and H_2 can receive a large value when the

upper bound of the time-varying distributed disturbance increases. Even though the sizes of H_1 and H_2 can be reduced by choosing the control gains k_p, k_v, and k_s appropriately, it may bring a high-gain control scheme. Observer for the time-varying distributed disturbance may be regarded as one solution for such problem. State observers for distributed parameter systems have been investigated in [154, 155, 259–265], which could be used to deal with the time-varying distributed disturbance $f(x,t)$. In the marine environment, the observer and control design is more challenging due to the complicated flexible system models coupled with the vessel's motion. Boundary control of flexible systems is currently an active research area, and how to take into account the time-varying distributed disturbance in the control design becomes an important and challenging problem.

Chapter 9
Structural Analysis and Riser Operations (Geoff Lyons and Minoo Patel)

9.1 Introduction

Marine risers are slender ocean structures subjected to a wide range of internal and external forces. Examples of internal forces are those due to self weight, internal hydrostatic pressures, and the momentum and Coriolis forces induced by internal flow. External forces arise from the action of hydrostatic pressures in the surrounding fluid and forces exerted by surface vessel motions, waves, and currents. This chapter describes the analysis of vertical marine risers under the influence of these forces and the subsequent application of the analysis to marine riser design. More than this, the incorporation of the analysis techniques within sophisticated Riser Management Systems enables improved operability, increased riser service lives, and better safety. In this chapter, we introduce an example. The approach adopted in this chapter is to start with the simplest of static models for a marine riser and to guide the reader toward more complex dynamic models. This approach mirrors the successive application of more complex analysis models with the progressive development of a marine riser design.

The operation of fixed and floating offshore structures requires the use of pipe connections between surface facilities and the seabed as well as pipes laying on or below the seabed for the transportation of oil and gas. Pipes bridging the vertical separation between surface vessel and seabed are called marine risers and are of two fundamental types. Since the 1950s, drilling operations from fixed and floating offshore structures have been carried out by using jointed steel pipes of between 0.204 m (8 in) to 0.762 m (30 in) external diameter to act as a conduit for the drill pipe penetrating the seabed. Such drilling risers connect a surface platform to a subsea wellhead. Drilling fluid (mud) at high pressure is transported to the drill face through the hollow drill pipe and returns up to the surface vessel through the annulus between the drill pipe and drilling riser. Marine risers are also used to transport oil and gas from producing fields for processing up to a surface platform and back for export through a subsea pipeline or a tanker loading system. Vertical steel marine risers used for drilling or production can be split into two categories. Fixed offshore structures tend to use risers that are clamped at intervals to structural members of

W. He et al., *Dynamics and Control of Mechanical Systems in Offshore Engineering*, Advances in Industrial Control, DOI 10.1007/978-1-4471-5337-5_9,

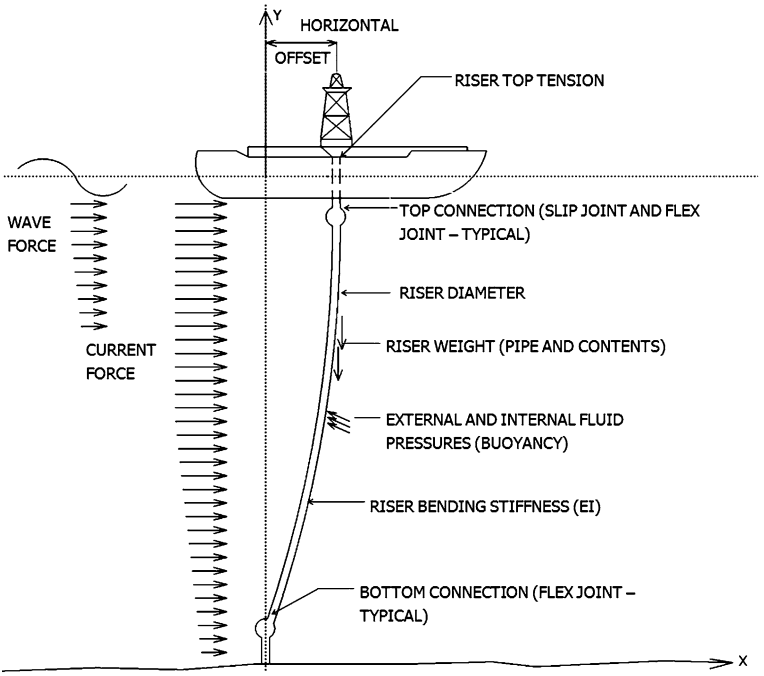

Fig. 9.1 Riser and surface vessel configuration showing the basic parameters

the platform along their vertical run up to the surface. On the other hand, floating or compliant offshore structures (such as drillships, semisubmersibles, tension leg platforms, SPARS, buoys) tend to use freely strung risers that are only connected at the surface and seabed. Such risers have to be held up with a sufficiently high tension at their top to prevent buckling due to self weight of their very slender geometry. These risers may also need to have heave compensating slip joints at their top end to take up relative motions between the moving surface vessel and stationary seabed.

For several decades, the offshore industry has used pipes of composite steel and elastomer construction for use as marine risers. These so called "flexible" risers are strung in nonvertical catenary shapes from the surface platform and are often supported by an intermediate buoy or string of buoyancy modules. More recently entirely composite (GRP and carbon fiber) risers have been introduced into service. Flexible risers are able to operate with much larger surface platform offset (from above the subsea wellhead) than is permissible with more rigid top-tensioned steel (and occasionally aluminium) risers, which are generally limited to offsets of between 7 % to 10 % of water depth. In some cases, a combined vertical steel riser with flexible pipe connections at the surface offers a worthwhile design option; see Fig. 9.2 for an example.

Both top-tensioned steel and flexible risers need to be carefully analyzed during design to ensure that the pipes have acceptable levels of deformations, stresses, and fatigue lives due to forces induced by currents, waves, and surface vessel motions.

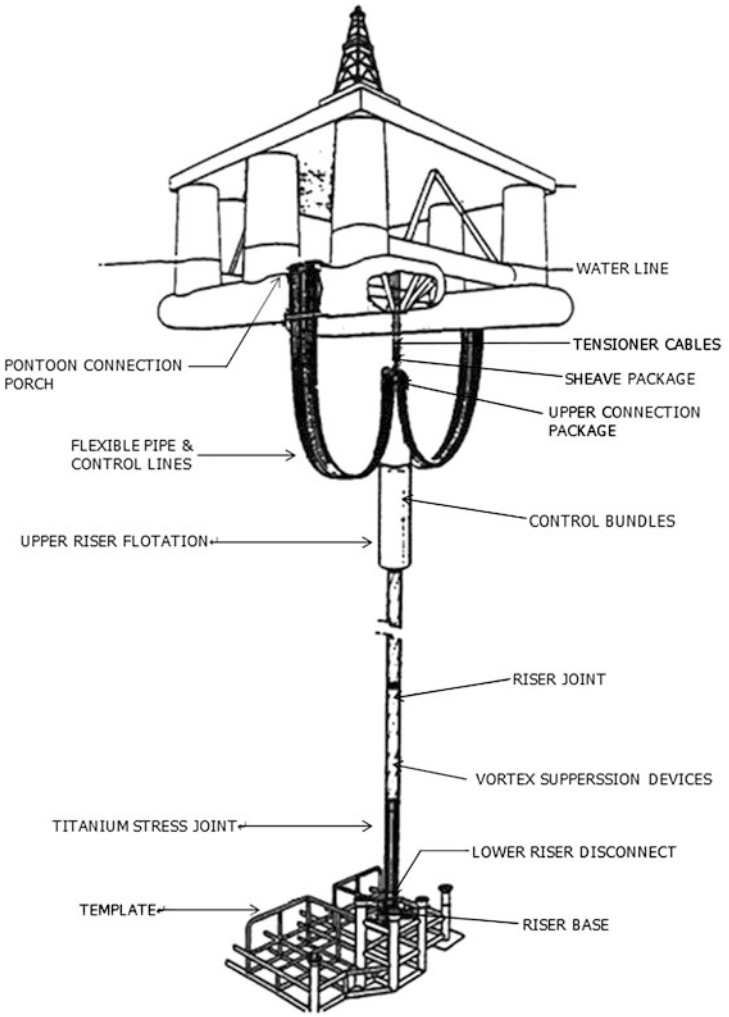

Fig. 9.2 Floating production vessel with rigid riser

The presence of internal hydrostatic pressure and external sea water pressure has a fundamental effect on the governing equations for these tubular structures as does the influence of current and wave flow around the pipe.

The marine riser is a critical component of offshore drilling and production operations. Careful maintenance, inspection, and monitoring of the riser is required in order to minimize the likelihood of failure. The following sections address these issues.

Here, we mainly focus our attention on the top-tensioned risers of compliant systems. The reader is directed to [266] for further information.

9.2 Riser Loadings

A schematic view of a marine riser connected to a surface vessel is illustrated in Fig. 9.1. Tension is applied to the top of the riser in order to prevent buckling collapse of the structure under its own self weight. The correct magnitude of the applied top tension is important in order to prevent overstressing on the one hand or buckling and collapsing of the riser pipe on the other.

The top connection of the riser to the surface vessel is normally in the form of a slip joint, which accommodates vertical motions of the surface vessel. This connection, together with the relatively high axial stiffness of the riser, results in low axial strain. In contrast, risers are characterized by relatively low bending stiffnesses and long lengths. Therefore, only lateral displacements of riser in shallow and moderate water depths are of concern. As the riser deployment water depth increases, axial vibrations become increasingly more significant particularly for water depths greater than 1000 m.

Internal forces within the riser consist of bending moments, shear forces, axial tensions and body weight. Riser lateral accelerations result in inertial loads. Forces also arise from the hydrostatic pressures of the internal riser fluid and the external sea water. The dynamics of the internal riser fluid flow can also contribute to the loading on the riser. Hydrodynamic forces are imposed on the riser as a result of waves, current, and vessel motions.

The unsteady flow around a riser is complex and is not totally understood. However, a simple model for the hydrodynamic loading on a vertical circular cylinder has been proposed by Morison et al. [267]. Morison's equation was first proposed for the hydrodynamic loading on a fixed vertical cylinder in shallow water. The equation has been extended and experimentally verified to model the hydrodynamic loading on arbitrarily orientated slender cylinders in all water depths [268]. Morison's equation states that the wave force df acting on a moving cylinder element of length ds is given by

$$df = \left[\rho\pi r^2 \frac{dv_n}{dt} + \rho\pi r^2 C_m \left(\frac{dv_n}{dt} - \frac{d^2x_n}{dt^2}\right) + \rho r C_D \left(v_n - \frac{dx_n}{dt}\right)\left|v_n - \frac{dx_n}{dt}\right|\right] ds, \tag{9.1}$$

where v_n is the water particle velocity normal to the cylinder longitudinal axis, x_n is the cylinder displacement normal to its longitudinal axis, C_m and C_D are the added mass and drag coefficients of the cylinder, respectively, ρ is the fluid density, and r is the cylinder's radius.

The added mass and drag coefficients are functions of the Reynolds number, R, and the Keulegan Carpenter number, K. R and K are given by

$$R = \frac{2rU_m}{\nu}, \tag{9.2}$$

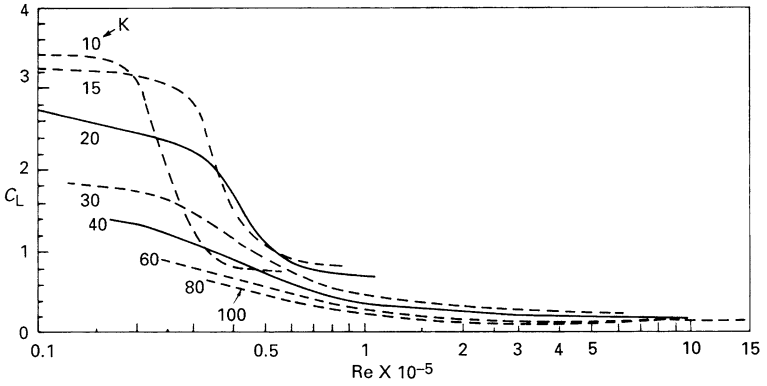

Fig. 9.3 Lift coefficient against Reynolds number for various values of Keulegan–Carpenter number, K [268]

$$K = \frac{U_m T}{2r}, \tag{9.3}$$

where U_m is the peak flow velocity, ν is the kinematic viscosity, and T is the period of flow oscillation.

The added-mass coefficient C_m is sometimes written in terms of an added-inertia coefficient $C_M = 1 + C_m$.

Morison's equation (9.1) is used to model the in-plane hydrodynamic loading on a marine riser. Out-of-plane forces also exist due to the formation of vortices that induce an oscillating transverse lift force. This lift force, dL, for a segment of length, ds, on a cylinder of radius r can be written as

$$dL = C_L \rho r U_m^2 \, ds, \tag{9.4}$$

where ρ is the fluid density, and C_L is the lift coefficient determined from experimental data in planar oscillatory flow. Figure 9.3 presents values of C_L against the Reynolds number at a range of Keulegan–Carpenter numbers for smooth cylinders from Sarpkaya and Isaacson [268].

The force oscillation can be taken to occur at the Strouhal frequency given by taking a Strouhal number of 0.2. The Strouhal number, S, is given by

$$S = 2rf/U, \tag{9.5}$$

where f is the frequency of vortex shedding, and U is the steady fluid velocity.

For smooth cylinders with Reynolds numbers greater than 1.5×10^6, a value of $C_L = 0.20$ may be used. Figure 9.4 (also from Sarpkaya and Isaacson) [268] gives equivalent data for roughened cylinders with C_L taken to be 0.25 for large K and R together with a Strouhal number of 0.22.

The oscillatory nature of the lift force can induce dynamic excitation of the loaded member. It is known that as the vortex shedding period of the cylinder approaches its natural period, this lift force increases considerably due to cylinder

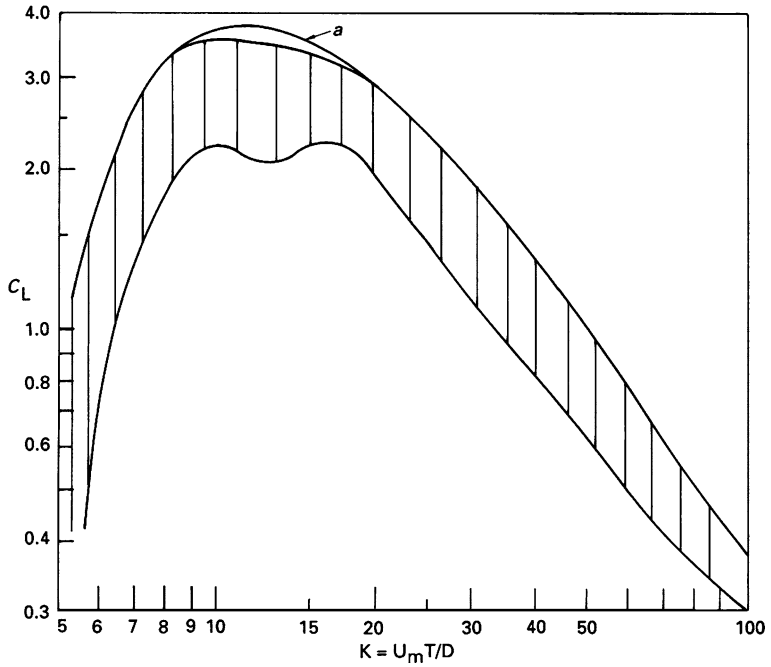

Fig. 9.4 Lift coefficient for rough cylinders as a function of Keulegan–Carpenter number for various roughness heights. *Line* a denotes smooth cylinder data for β from 1,000 to 2,000. *Cross hatched region* denotes occurrence of C_D data for rough cylinders with $L/D = 1/200$ [268]

motion, and a dynamic instability can result. In many practical situations, structural failure has been known to occur in this fashion.

The steady drag force, f_c, on a unit length of riser due to current is given by

$$f_c = \rho r C_D U^2, \tag{9.6}$$

where U is the current velocity. This force can contribute a significant proportion of the static lateral loading on a riser.

The value of drag coefficient, C_D, to be inserted into Morison's equation can only be obtained experimentally. In theory, the value of the inertia coefficient, C_m, can be calculated (it is, for example, 2.0 for a smooth cylinder in an ideal fluid). However, measured values are used in practice, particularly when drag is the dominant force. For irregular shapes, the inertia coefficient can be calculated using potential flow diffraction theory.

Many experiments have been designed to measure values of drag and inertia coefficients in steady or planar oscillatory flows, but their results can only be used with caution for wave force prediction. The most useful experimental measurements have been made in circumstances that model full-scale conditions within the ocean environment. Measurements made offshore on large test structures in real seaways are especially valuable.

Table 9.1 Wave loading regimes

D/λ	<0.20	>0.20
$K < 25$	Drag dominated flow regime. Morison's equation with C_m and C_D values required for computing wave forces. Drag coefficient is a function of Reynolds number. For $R > 1.5 \times 10^6$, $C_m = 1.8$, $C_D = 0.62$. For $10^5 < R < 1.5 \times 10^6$, $C_m = 1.0$, and C_D varies from 1.0 to 0.6	
$5 < K < 25$	Intermediate regime between drag and inertia domination. Morison's equation applicable, but published C_m and C_D values exhibit wide scatter. Flow behavior and consequent loading complex and uncertain. For $R < 1.5 \times 10^6$, $C_m = 1.8$, $C_D = 0.62$	
$K < 5$	Inertia dominated regime. Morison's equation or diffraction theory for computing wave forces. $C_m = 2.0$ Effect of C_D is negligible.	Morison's equation unsuitable for computing wave forces. Diffraction theory required.

One problem with the application of Morison's equation is the large scatter in values of the inertia and drag coefficients. However, there is a useful degree of correlation between the coefficients and two flow parameters, Keulegan–Carpenter number K and Reynolds number R. Nevertheless, the scatter and hence some uncertainty remain. Table 9.1 gives a summary of generally accepted added inertia and drag coefficients for flow around circular cylinders in unconfined flow remote from solid boundaries such as the seabed.

Sarpkaya [269] carried out many systematic studies of the variations of inertia and drag forces for circular cylinders in planar oscillatory flow. Figures 9.5 and 9.6 present plots of C_m and C_D against the Reynolds number and Keulegan–Carpenter number for smooth cylinders from data prepared by Sarpkaya and Isaacson [268]. Figures 9.7 and 9.8 also present this data plotted as a function of the Keulegan–Carpenter number with parameter β being the ratio of the Reynolds number to the Keulegan–Carpenter number. It can be seen that the C_m and C_D data show consistent and physically meaningful correlations with the Keulegan–Carpenter number.

The surface finish of the cylinder influences its drag coefficient. Figure 9.9 shows the effects of roughness on the steady flow drag coefficient. For planar oscillatory flow, Sarpkaya and Isaacson [268] present recommended data for inertia and drag coefficients as functions of roughness, Reynolds number and for Keulegan Carpenter range of from 20 and 100.

Riser configurations often consist of a main conduit surrounded by smaller diameter pipes. There is very little design information available at present on the effects of flow interference in waves between groups of closely spaced cylinders, although the physics of such phenomena are being researched at present. Recent work has shown that planar oscillatory wave flow about circular cylinders induces motion of vortex pairs that can induce substantial velocity magnifications in the flow around

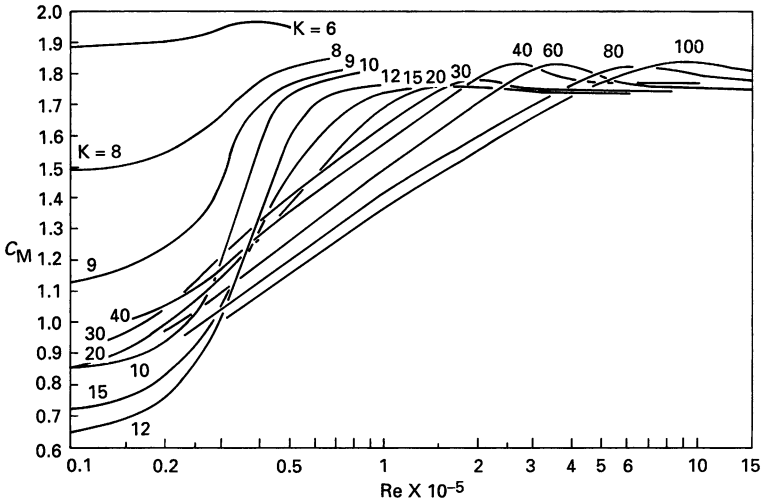

Fig. 9.5 Added inertia coefficient against Reynolds number for various values of Keulegan–Carpenter number, K [268]

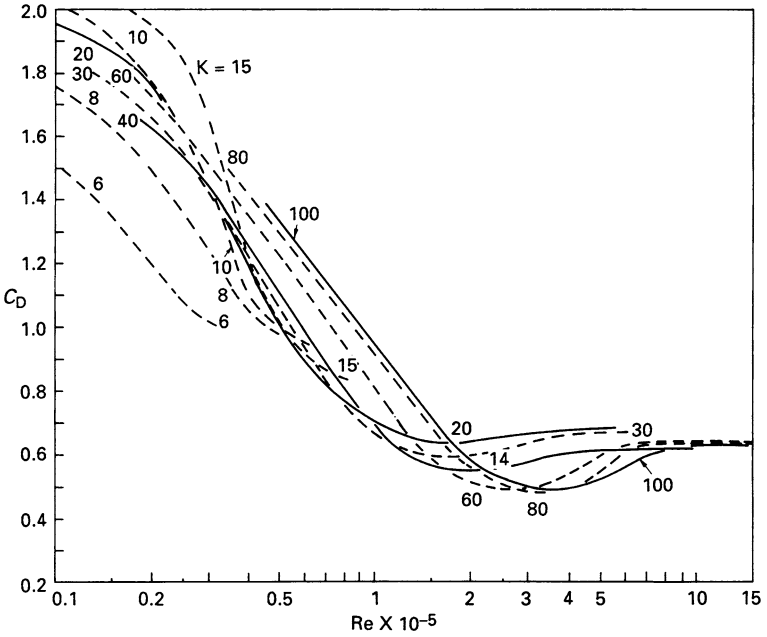

Fig. 9.6 Drag coefficient against Reynolds number for various values of Keulegan–Carpenter number, K [268]

the cylinder. The presence of smaller cylinders around a larger-diameter cylinder can interact with these velocity magnifications to give rise to significant interference effects. Grass et al. [270] present research work in this area.

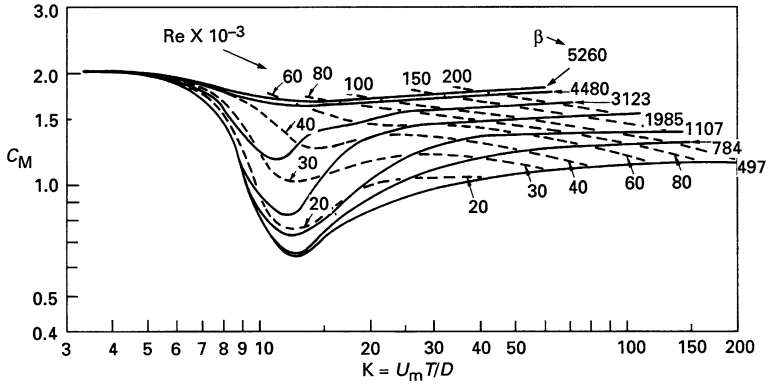

Fig. 9.7 Added inertia coefficient plotted against Keulegan–Carpenter number for various values of Reynolds number R and frequency parameter β [268]

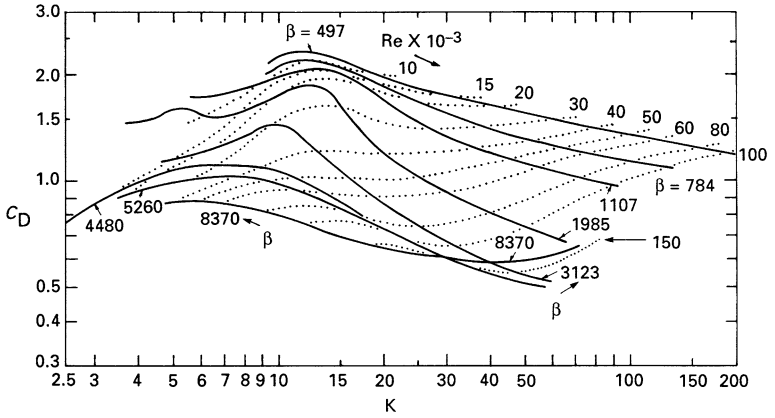

Fig. 9.8 Drag coefficient against Keulegan–Carpenter number for various values of Reynolds number R and frequency parameter β [268]

The influence of surface vessel motions on a marine riser may be decomposed into two parts. The first component is the steady displacement of the vessel from above the wellhead as a result of steady environmental forces being applied to the vessel. This displacement is known as the static vessel offset. Superimposed on the static offset are the vessel's dynamic motions in response to waves. The motion of the surface vessel represents a dynamic boundary condition that defines the horizontal displacement of the top of the riser.

The riser is constrained laterally at the wellhead. The remaining rotational boundary conditions applied to the riser depend on the riser base and top end equipment. A flex or ball joint is often used at the riser base, which ensures free rotation and hence no bending moments at the lower end. In practice, there is some rotational stiffness associated with the riser end rotations, and this needs to be measured or

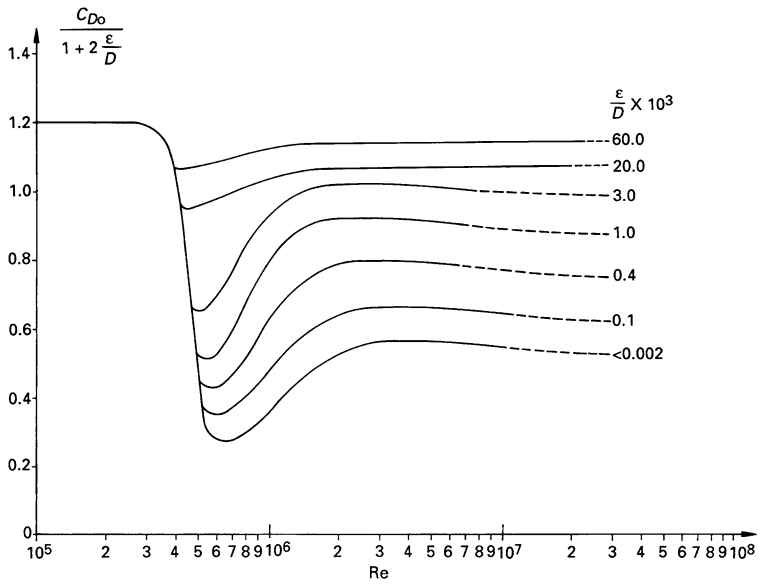

Fig. 9.9 Variation of $\frac{C_{D_o}}{1+2\frac{\varepsilon}{D}}$ with Reynolds number, R (from ESDU, 1986)

estimated for the purposes of riser analysis. Different riser boundary conditions are illustrated in Fig. 9.10.

9.3 Governing Equations

A vertical marine riser may be regarded as a hollow "beam column." The difference between a column subjected to lateral loading and a marine riser is that the riser is subjected to both internal and external hydrostatic pressures as well as to axial and lateral loadings. The development presented here first considers the static loading of a beam column and then extends the equations to apply to the static loading of a marine riser. Finally, the full dynamic equation of motion for a marine riser is presented.

If the riser is simply considered as a beam column, then the governing differential equation used for lateral static deflection is

$$\underbrace{\frac{d^2}{dy^2}\left(EI\frac{d^2x}{dy^2}\right)}_{A} - \underbrace{T(y)\frac{d^2x}{dy^2}}_{B} - \underbrace{W\frac{dx}{dy}}_{C} = f, \tag{9.7}$$

where EI is the riser bending stiffness, T is the axial tension in the riser pipe wall, W is the weight per unit length of riser, and f is the lateral force per unit length.

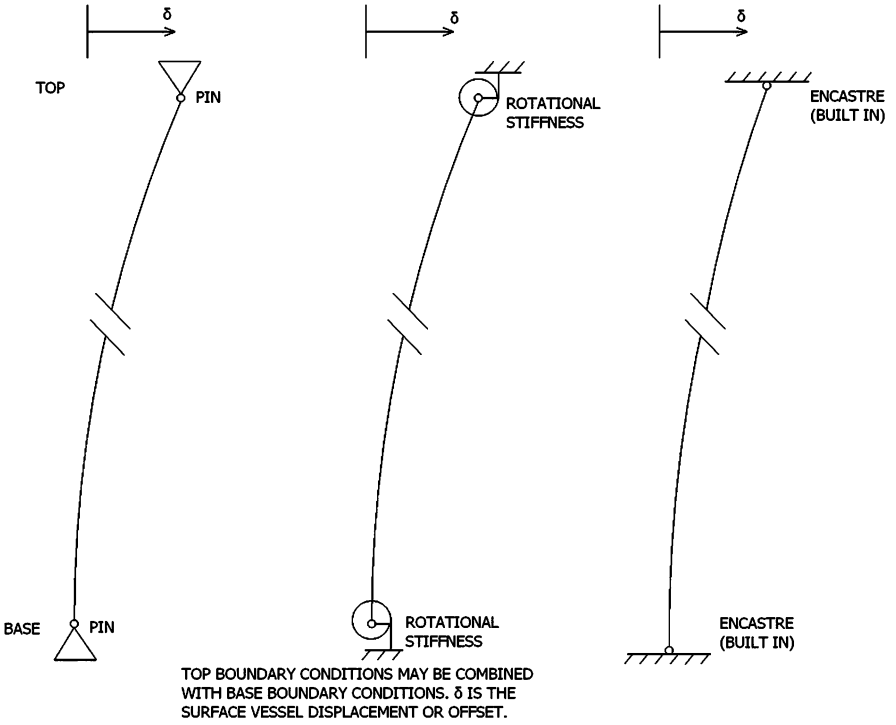

Fig. 9.10 Riser end boundary conditions

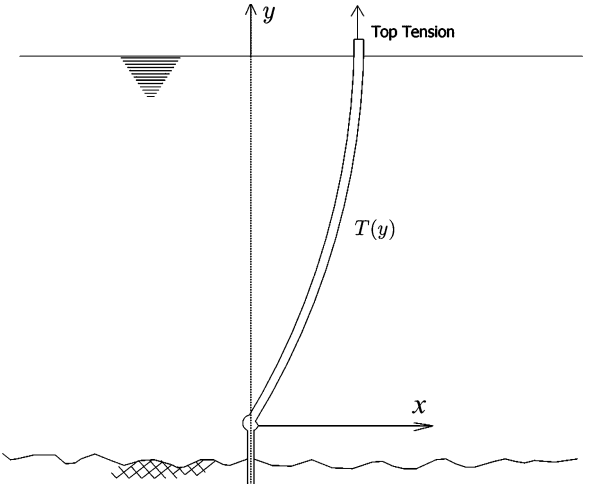

Fig. 9.11 Conventional vertical riser notation

The coordinate system used is shown in Fig. 9.11 with y measured from the bottom of the riser and positive upward, while x denotes the horizontal riser deflection from a vertical through the riser base.

The first term (A) of Eq. (9.7) is the resistance to lateral loading resulting from the riser's flexural rigidity. The second term (B) is the lateral loading due to the axial tension. The third term (C) is the lateral component of the riser's weight as a result of the riser's slope.

If the riser contains drill pipe or external control lines, then, for the purposes of analysis, these are usually incorporated into the physical properties of the riser.

If, however, the hydrostatic pressure of the riser's internal and external fluid is included in the analysis, a slightly different form of Eq. (9.7) is derived. The force due to the hydrostatic external pressure distribution, which exists around the riser, and also the force due to internal pressure (which is related to wellhead pressure) are resolved into horizontal and vertical force components and incorporated into the governing equation for static deflection to give

$$\underbrace{\frac{d^2}{dy^2}\left(EI\frac{d^2x}{dy^2}\right)}_{A} - \Big[\underbrace{T(y)}_{B} + \underbrace{A_o P_o(y) - A_i P_i(y)}_{C}\Big]\frac{d^2x}{dy^2}$$

$$- \underbrace{(\gamma_s A_s - \gamma_o A_o + \gamma_i A_i)}_{D}\frac{dx}{dy} = f, \tag{9.8}$$

where the additional terms are the external hydrostatic pressure around the riser, P_o, the internal hydrostatic pressure, P_i, with A_o being the cross-sectional area of riser bore and wall, A_i, the cross sectional area of riser bore only, and A_s, the cross-sectional area of riser wall. γ_i is the specific weight of fluid in the riser bore, γ_o is the specific weight of fluid surrounding the riser tube (sea water), and γ_s is the specific weight of riser pipe wall material. Note that the hydrostatic pressures vary linearly with position along the y axis.

Equation (9.8) will be derived later but is valid for small deflections only, that is, for offset angles less than 10° from the vertical. Therefore the error in applying this equation to a vertical steel riser is usually negligible. Some interesting points concerning the effects of pressure on the riser may be deduced by further consideration of the third term C in Eq. (9.8). The $A_o P_o(y) - A_i P_i(y)$ term comes from the lateral effect of external and internal hydrostatic pressure. Its effect is similar to that of the actual tension in the riser wall since this term also multiplies the second derivative of displacement x. The pressure term does not modify the actual riser axial tension or the resultant direct stress in the riser wall. For this reason, the collection of parameters that multiply the second derivative is sometimes called the "effective tension", T_e, given by

$$T_e = T + A_o P_o - A_i P_i. \tag{9.9}$$

The concept of effective tension is a convenient mathematical grouping of parameters that have a similar effect. Equation (9.9) demonstrates that the effect of external hydrostatic pressure is similar to that of a tensile axial force, while the internal pressure influences riser behavior as would a compressive force. The term $(\gamma_s A_s - \tau_o A_o + \gamma_i A_i)$ is equivalent to the corresponding term W in Eq. (9.7).

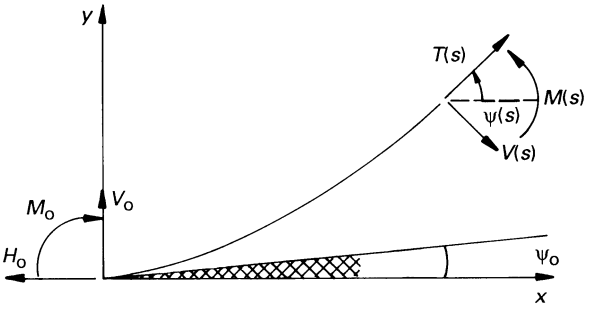

Fig. 9.12 Notation for a riser of arbitrary geometry

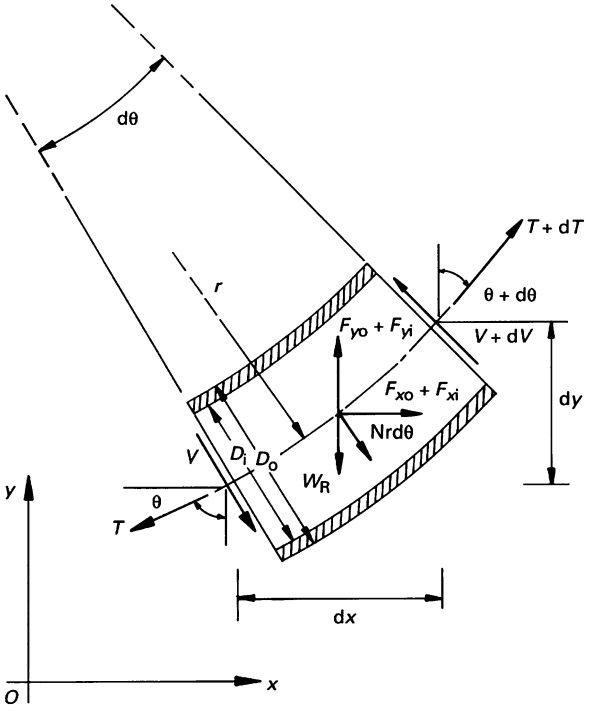

Fig. 9.13 Riser element

Now, the differential equation describing the static behavior of a marine riser of arbitrary geometry is derived using the notation of Fig. 9.12 and the element of Fig. 9.13. The analysis is restricted to two dimensions for simplicity. The static forces acting on the pipe element of Fig. 9.13 can be listed as follows:

(a) An axial tension and shear force within the pipe wall material.
(b) A horizontal force due to the resultant of external and internal hydrostatic pressures, $(F_{xo} + F_{xi})$
(c) A vertical force due to the resultant of external and internal hydrostatic pressures, $(F_{yo} + F_{yi})$

(d) A drag force due to steady current. The velocity vector is resolved into components normal and tangential to the element, with only the normal component assumed to exert a distributed force of N per unit length.
(e) The weight of the element W_R, acting vertically downward.

Summing the components of force in the y direction for the element in Fig. 9.13 yields the equation

$$(T + dT)\sin(\theta + d\theta) - T\sin\theta - (V + dV)\cos(\theta + d\theta) + V\cos\theta + (F_{yo} + F_{yi}) - W_R - N\cos\theta r\, d\theta = 0. \tag{9.10}$$

Similarly, summing forces in the x direction yields

$$(T + dT)\cos(\theta + d\theta) - T\cos\theta + (V + dV)\sin(\theta + d\theta) - V\sin\theta + (F_{yo} + F_{yi}) + N\sin\theta r\, d\theta = 0. \tag{9.11}$$

These equations can be simplified for small $d\theta$ to

$$(T + dT)\cos(\theta + d\theta) - T\cos\theta + (V + dV)\sin(\theta + d\theta) - W_R - N\cos\theta r\, d\theta = 0 \tag{9.12}$$

and

$$-(T\sin\theta - V\cos\theta)\, d\theta + dT\cos\theta + dV\sin(\theta) + (F_{yo} + F_{yi})\sin\theta - Nr\, d\theta = 0. \tag{9.13}$$

Combining these expressions gives

$$T\, d\theta - dV + (F_{yo} + F_{yi} - W_R)\cos\theta - (F_{xo} + F_{xi})\sin\theta - Nr\, d\theta = 0. \tag{9.14}$$

Continuing with the above analysis requires the forces on a cylindrical element due to internal and external hydrostatic pressure (F_{xo}, F_{xi}, F_{yo}, F_{yi}) to be defined. This is done using the derivation presented below.

A hollow cylindrical member submerged in a fluid and containing a fluid within itself will experience a force due to the external and internal hydrostatic pressures of both fluids acting on the surfaces of the cylinder. An element of the cylinder is shown in Fig. 9.14. The resultant force is obtained by finding the force on an arbitrary section of the element (shaded portion of Fig. 9.14) and resolving it into components before integrating to obtain the total force on the element. Note that only the force on the curved walls of the cylinder due to hydrostatic pressure is evaluated. The force on the end cross-sections is not considered here since the cylinder is taken to be very long and the end cross-section will usually terminate to a coupling such that hydrostatic pressure will not act on the cylinder cross sections. Furthermore, the axis system used in Fig. 9.14 is such that the hydrostatic pressure is taken to increase linearly along the vertical axis.

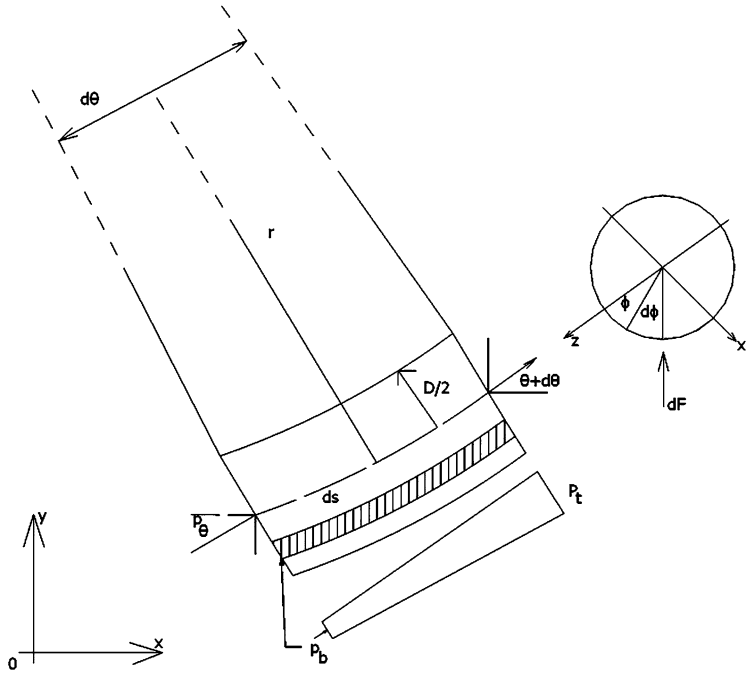

Fig. 9.14 Cylinder element

The angle ϕ is used to describe the position on the circumference of the element to be analyzed. Initially, only the external pressure is considered in the derivation. The forces due to the internal pressure can be readily deduced from those due to the external pressure by a simple reversal of signs and change of diameter.

As shown in Fig. 9.14, the length, ds, of any strip on the cylinder circumference parallel to its axis is given by

$$ds = \left(r + \frac{1}{2} D \cos\phi\right) d\theta, \tag{9.15}$$

where r is the element radius of curvature, D is the diameter of the pressure bearing surface, and θ and ϕ are defined in Fig. 9.14. If the hydrostatic pressure on the centreline of the element at its lower end is p, then the pressure, P_b, at various levels along the bottom surface is given by

$$P_b = p - \frac{1}{2} \gamma D \cos\theta \sin\phi, \tag{9.16}$$

where γ is the weight per unit volume of the fluid medium. Also, the corresponding pressure P_t at the top of the element is hydrostatic and given by the equation

$$P_t = P_b - \gamma \cos\theta \, ds \tag{9.17}$$

since

$$\cos\theta = \frac{dy}{ds}. \tag{9.18}$$

The area of the section of element described by arc $d\phi$ is given by

$$dA = \frac{1}{2} D\, ds\, d\phi. \tag{9.19}$$

The force that acts on this section of the element is then

$$dF = \frac{1}{2}(P_b + P_t)\, dA. \tag{9.20}$$

Substituting the expressions derived for dA, P_b, P_t into (9.20) gives

$$dF = \frac{1}{2}(P_b + P_t - \gamma\, ds \cos\theta)\left(\frac{1}{2} D\, ds\, d\phi\right), \tag{9.21}$$

$$dF = \left(p - \frac{1}{2}\gamma D \cos\theta \sin\phi - \frac{1}{2}\gamma\, ds \sin\theta\right)\left(\frac{1}{2} D\, ds\, d\phi\right). \tag{9.22}$$

Replacing Eq. (9.15) for ds leads to

$$\begin{aligned} dF = &\left\{p - \frac{1}{2}\gamma D \cos\theta \sin\phi - \frac{1}{2}\gamma\left(r + \frac{1}{2} - D\cos\phi\right) d\theta \sin\theta\right\} \\ &\times \left(\frac{1}{2} r + \frac{1}{4} D\cos\phi\right) D\, d\theta\, d\phi. \end{aligned} \tag{9.23}$$

Expanding the individual terms gives

$$\begin{aligned} dF = &\left[\frac{1}{2} pDr\, d\theta - \frac{1}{4}\gamma Dr^2 \sin\theta (d\theta)^2\right] d\phi \\ &+ \left[\frac{1}{4} pD^2\, d\theta + \frac{1}{4}\gamma D^2 r \cos\theta\, d\theta - \frac{1}{4} D^2 r \sin\theta (d\theta)^2\right] + \sin\phi\, d\phi \\ &+ \left[\frac{1}{8}\gamma D^2 \cos\theta\, d\theta - \frac{1}{8}\gamma D^3 \sin\theta (d\theta)^2\right] \sin^2\phi\, d\phi. \end{aligned} \tag{9.24}$$

The differential force may be resolved into its three directional components $-F_x$, F_y, and F_z along the x, y, and z axes, respectively. In this case, the analysis is restricted to two dimensions, and since there is no deformation out of the x–y plane, the resultant force in the z direction is taken as zero, i.e., $F_z = 0$.

$$dF_x = \int_{\phi=0}^{\phi=2\pi} -dF \sin\theta \sin\phi \tag{9.25}$$

$$dF_y = \int_{\phi=0}^{\phi=2\pi} dF \cos\theta \sin\phi. \tag{9.26}$$

Therefore,

$$\begin{aligned} F_x = &-\left[\frac{1}{2}pDr\sin\theta\,d\theta - \frac{1}{4}\gamma r^2 D\sin^2\theta(d\theta)^2\right]\int_0^{2\pi}\sin\phi\,d\phi \\ &-\left[\frac{1}{4}pD^2\sin\theta\,d\theta + \frac{1}{4}\gamma D^2 r\sin\theta\cos\theta\,d\theta - \frac{1}{4}\gamma D^2 r\sin^2\theta(d\theta)^2\right] \\ &\times\int_0^{2\pi}\sin^2\phi(d\phi) \\ &-\left[\frac{1}{8}\gamma D^3\cos\theta\sin\theta\,d\theta - \frac{1}{16}\gamma D^3\sin\theta(d\theta)^2\right]\int_0^{2\pi}\sin^3\phi\,d\phi, \end{aligned} \tag{9.27}$$

using

$$\begin{aligned} &\int_0^{2\pi}\sin\phi\,d\phi = 0, \\ &\int_0^{2\pi}\sin^2\phi\,d\phi = \pi, \\ &\int_0^{2\pi}\sin^3\phi\,d\phi = 0, \\ &A = \frac{\pi D^2}{4} \end{aligned} \tag{9.28}$$

gives the force in the x direction on a curved beam as

$$F_x = -\left[pA + r\gamma A(\cos\theta - \sin\theta\,d\theta)\right]\sin\theta\,d\theta. \tag{9.29}$$

When the force due to internal pressure is considered, its form will be the same but of opposite sign. Combining the effects of internal and external pressure for the most general case gives

$$(F_{xo}+F_{xi}) = \left[(P_iA_i - P_oA_o) + r(\gamma_iA_i - \gamma_oA_o)(\cos\theta - \sin\theta d\theta)\right]\sin\theta\,d\theta, \tag{9.30}$$

where P_o, P_i are the external and internal pressures, respectively, at the level of the bottom of the element centreline.

The vertical force F_y is obtained in a similar way. Before the integration is performed, the expression for the force in the vertical direction appears as

$$\begin{aligned} F_y = &-\left[\frac{1}{2}pDr\,d\theta - \frac{1}{4}\gamma r^2 D\sin\theta(d\theta)^2\right]\cos\theta\int_0^{2\pi}\sin\phi\,d\phi \\ &+\left[\frac{1}{4}pD^2\,d\theta + \frac{1}{4}\gamma D^2 r\cos\theta\,d\theta - \frac{1}{4}\gamma D^2 r\sin\theta(d\theta)^2\right]\cos\theta\int_0^{2\pi}\sin^2\phi(d\phi) \\ &+\left[\frac{1}{8}\gamma D^3\cos\theta\,d\theta - \frac{1}{8}\gamma D^3\sin\theta(d\theta)^2\right]\cos\theta\int_0^{2\pi}\sin^3\phi\,d\phi. \end{aligned} \tag{9.31}$$

In evaluating this integral, the following results are used:

$$\int_0^{2\pi} \sin\phi \, d\phi = 0,$$
$$\int_0^{2\pi} \sin^2\phi \, d\phi = \pi, \tag{9.32}$$
$$\int_0^{2\pi} \sin^3\phi \, d\phi = 0.$$

Thus, Eq. (9.31) becomes

$$F_y = \left[pA + r\gamma A(\cos\theta - \sin\theta \, d\theta)\right]\cos\theta \, d\theta. \tag{9.33}$$

As before, the effect of including the internal pressure acting on the element can be done quite easily. The final expression for the vertical force on a curved inclined element due to both internal and external pressures is given by

$$F_{yo} + F_{yi} = \left[(P_o A_o - P_i A_i) + r(\gamma_o A_o - \gamma_i A_i)(\cos\theta - \sin\theta \, d\theta)\right]\cos\theta \, d\theta. \tag{9.34}$$

Substituting the above expressions (9.30) and (9.34) for the resultant horizontal forces, $(F_{xo} + F_{xi})$ and vertical forces, $(F_{yo} + F_{yi})$ due to internal and external hydrostatic pressure, together with equations for the element weight and drag force, into Eq. (9.9) yields

$$\begin{aligned} &T \, d\theta - dV - \left[(P_i A_i - P_o A_o) + r(\gamma_i A_i - \gamma_o A_o)(\cos\theta - \sin\theta \, d\theta)\right]\cos^2\theta \, d\theta \\ &\quad - W_R \cos\theta - \left[(P_i A_i - P_o A_o) + r(\gamma_i A_i - \gamma_o A_o)(\cos\theta - \sin\theta \, d\theta)\right]\sin^2\theta \, d\theta \\ &\quad - Nr \, d\theta \\ &= 0, \end{aligned} \tag{9.35}$$

and after simplification this becomes

$$\begin{aligned} &[T - P_i A_i + P_o A_o] d\theta - dV \\ &\quad + \left\{(\cos\theta - \sin\theta \, d\theta)(\gamma_o A_o - \gamma_i A_i) - \gamma_s A_s \cos\theta - N\right\} r \, d\theta = 0 \end{aligned} \tag{9.36}$$

with $W_R = \gamma_s A_s r \, d\theta$, where γ_s is the weight per unit volume of the pipe material, and A_s is the pipe wall area of cross-section. It is of interest at this stage to rewrite Eq. (9.36) for a nearly vertical pipe. This can be done by using ψ as the angle between the pipe element and the vertical such that $\psi = \pi/2 - \theta$ and $dy = -d\theta$. Then, Eq. (9.36) can be rewritten in terms of ψ as

$$\begin{aligned} &-[T - P_i A_i + P_o A_o] d\psi - dV \\ &\quad - \left\{(\sin\psi - \cos\psi \, d\psi)(\gamma_o A_o - \gamma_i A_i) - \gamma_s A_s \sin\psi - N\right\} r \, d\psi = 0. \end{aligned} \tag{9.37}$$

Now, for small ψ, the expressions $\cos\psi = 1$, $r d\psi = -dy$, $\sin\psi = -\frac{dx}{dy}$, and $\frac{d\psi}{dy} = -\frac{d^2x}{dy^2}$ are substituted into Eq. (9.37). After neglecting products of differentials, dividing by dy, and using the small deflection equation

$$\frac{dV}{dy} = \frac{d^2}{dy^2}\left(EI\frac{d^2x}{dy^2}\right), \tag{9.38}$$

the equation becomes

$$\frac{d^2}{dy^2}\left\{EI\frac{d^2x}{dy^2}\right\} - (T + \underbrace{P_oA_o - P_iA_i}_{A})\underbrace{\left\{\left(1+\left(\frac{dx}{dy}\right)^2\right)\right\}^{-1}}_{B}\frac{d^2x}{dy^2}$$

$$\underbrace{-(\gamma_sA_s - \gamma_oA_o + \gamma_iA_i)\frac{dx}{dy}}_{C} = N\underbrace{\left\{\left(1+\left(\frac{dx}{dy}\right)^2\right\}^{\frac{1}{2}}\right.}_{D}. \tag{9.39}$$

Note that the term A in the above equation arises from the lateral effects of internal and external pressure and is the source of the concept of effective tension outlined earlier. The terms B and D, on the other hand, are due to the effects of riser orientation. Now, because small deflections are assumed in vertical riser analysis, terms B and D in Eq. (9.39) may be equated to unity to give

$$\frac{d^2}{dy^2}\left\{EI\frac{d^2x}{dy^2}\right\} - (T + P_oA_o - P_iA_i)\frac{d^2x}{dy^2} - (\gamma_sA_s - \gamma_oA_o + \gamma_iA_i)\frac{dx}{dy} = N, \tag{9.40}$$

which is of a form similar to Eq. (9.8). The equation of equilibrium for the static deflection of a marine riser Eq. (9.8) is readily extended to include riser dynamics. The equation of horizontal motion for a marine riser is given by

$$m\frac{d^2x}{dt^2} + c\frac{dx}{dt} + \frac{d^2x}{dy^2}\left[EI\frac{d^2x}{dy}\right] - \left[T(y) + A_oP_o(y) - A_iP_i(y)\right]\frac{d^2x}{dy^2}$$

$$-(\gamma_sA_s - \gamma_oA_o + \gamma_iA_i)\frac{dx}{dy} = f(t). \tag{9.41}$$

The horizontal deflection, x, of the riser is now a function of both position, y, and time, t, and hence partial derivatives are used. m is the physical mass per unit length of riser and contents, and c is the equivalent linear structural damping coefficient. The two new terms in Eq. (9.41) are the inertia force $m(d^2x/dt^2)$, which is a result of the lateral acceleration of the riser, and the equivalent linear structural damping $c\,dx/dt$. The lateral hydrodynamic force per unit length, $f(t)$, is now a function of time. This lateral force may be modeled by Morison's equation.

Thus,

$$f(t) = \rho\pi r^2(1+C_m)\frac{dw}{dt} + \pi r^2C_m\frac{d^2x}{dt^2} + \rho rC_D\left(w - \frac{dx}{dt}\right)\left|w - \frac{dx}{dt}\right|, \tag{9.42}$$

where w is the horizontal external fluid particle velocity, ρ is the density of the external fluid (sea water), ρ is the riser's radius, and C_m and C_D are the riser's added mass and drag coefficients, respectively.

Substituting Eq. (9.42) into Eq. (9.41) gives

$$(m+m_a)\frac{d^2x}{dt^2}+c\frac{dx}{dt}+\frac{d^2}{dy^2}\left[EI\frac{d^2x}{dy^2}\right]-\left[T(y)+A_oP_o(y)-A_iP_i(y)\right]\frac{d^2x}{dy^2}$$
$$-(\gamma_sA_s-\gamma_oA_o+\gamma_iA_i)\frac{dx}{dy}$$
$$=\rho\pi r^2(1+C_m)\frac{dw}{dt}+\rho rC_D\left(w-\frac{dx}{dt}\right)\left|w-\frac{dx}{dt}\right|, \tag{9.43}$$

where $m_a=\rho\pi r^2C_m$.

m_a is the added mass per unit length of the riser and is now combined with the physical mass of the riser to form the inertial term on the left-hand side of Eq. (9.43). The quadratic drag term on the right-hand side of Eq. (9.43) provides a formidable analysis problem as a result of its nonlinear dependency on the relative velocity.

Analytical solutions of Eq. (9.43) do not exist, and some form of numerical solution is necessary. One popular method of solution is the finite element method, which is described in further detail in the following section.

9.4 Finite Element Analysis

This section describes a representative finite element analysis for the analysis of vertical marine risers. In the context of vertical marine risers, there are special features that must be accounted for in the analysis. These are briefly discussed first.

It is important to identify which elements of the contents of the riser influence the tension. Since the marine riser is a long slender structure with relatively small bending stiffness, it needs to be kept in tension to prevent buckling collapse. Tension is applied to the top of the riser, and it is the weight in air of the riser pipe, associated choke and kill lines, and the vertical force due to the internal and external hydrostatic pressures on a nonvertical pipe segment or buoyancy module, which cause a variation in tension along the riser's length. The weight of the separately tensioned drill pipe and the riser fluid contents do not directly affect the tension variation.

However, the nontension contributing elements in a riser cross-section must be accounted for when computing an effective lateral force component term C in Eq. (9.39).

For deep water risers, the top tension requirement to prevent buckling collapse can become excessive. In order to reduce top tension, one option is to attach buoyancy modules along the length of the riser. The distribution of buoyancy modules influences the tension variation in the riser; thus, altering its structural response and internal stresses. The increase in diameter of a riser cross-section due to buoyancy

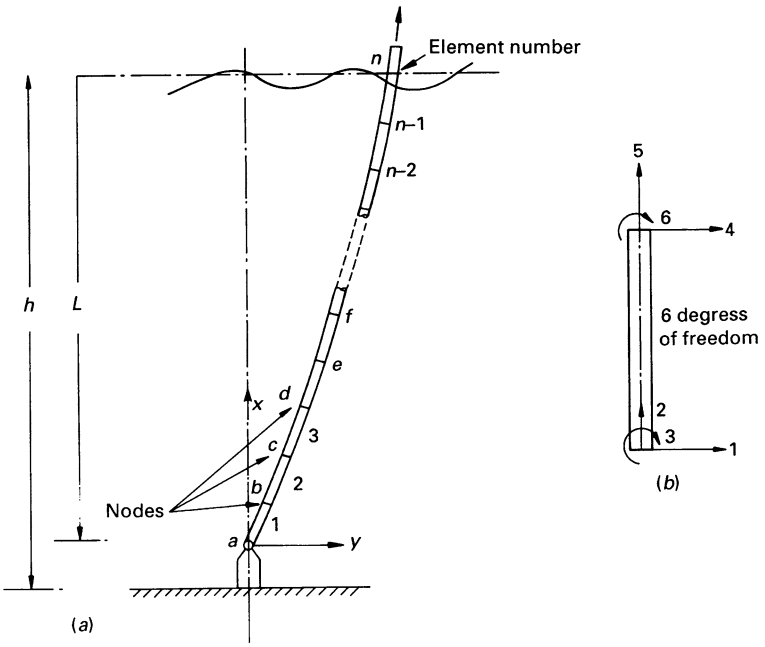

Fig. 9.15 Element and global node description for a finite element idealization of a vertical riser. (**a**) Risers element nodes; (**b**) Single beam element

modules also increases current and wave forces. This introduces considerable scope for optimizing the intensity and distribution of buoyancy modules in deep water applications.

9.4.1 Static Analysis

The static finite element analysis presented here is based on a governing equation of the form given by Eq. (9.39). The description of the analysis is also restricted to two dimensions for simplicity. The vertical riser pipe is idealized as an assembly of beam elements as shown in Fig. 9.15. Each element possesses six degrees of freedom, two translations, and one rotation at each end. The degrees of freedom for each beam element are illustrated in Fig. 9.15. Consequently, the numerical computation is two-dimensional with all external forces on the riser, including forces due to current and waves acting in one plane.

The current loading q per unit length along the riser due to a lateral drag force is

$$q = \frac{1}{2}\rho_o C_D d|U_c|U_c, \tag{9.44}$$

where ρ_o is the density of sea water, C_D is a drag coefficient, d is an effective riser external diameter, and U_c is the vector of current velocity. The variation of current velocity with depth needs to be known.

A static analysis can also be used to relate riser deflections and stresses to current and wave loadings in a quasi-static manner. For a known regular wave height and period, the current velocity U_c can be superimposed onto the horizontal component of the wave particle velocity U_w at any instant. The quasi-static hydrodynamic loading can then be written as

$$q = \frac{1}{2}\rho_o C_D d|U_c + U_w|(U_c + U_w) + \frac{1}{4}\rho_o \pi d^2 C_M \dot{U}_w, \tag{9.45}$$

where $\dot{U}_w$ is the horizontal local component of wave particle acceleration, and C_M is an applicable inertia coefficient.

The total stiffness matrix, S_m, for each beam element is derived as the sum of the standard elastic stiffness matrix, S_e, and a geometric stiffness matrix, S_g, which is a function of deflected element geometry and axial force on the element. Thus,

$$S_m = S_e + S_g. \tag{9.46}$$

For an element of length L and an "effective" axial tension T_e, S_e, and S_g in member axes are given by

$$S_e = \frac{EI}{L^3}\begin{bmatrix} AL^2/I & & & & & \\ 0 & 12 & & & & \\ 0 & 6L & 4L^2 & & & \\ -AL^2/I & 0 & 0 & AL^2/I & & \\ 0 & -12 & -6L & 0 & 12 & \\ 0 & 6L & 2L^2 & 0 & -6L & 4L^2 \end{bmatrix} \tag{9.47}$$

and

$$S_g = \frac{T_e}{L}\begin{bmatrix} 0 & & & & & \\ 0 & 6/5 & & & & \\ 0 & L/10 & 2L^2/15 & & & \\ 0 & 0 & 0 & 0 & & \\ 0 & -6/5 & -L/10 & 0 & 6/5 & \\ 0 & L/10 & -L^2/30 & 0 & -L/10 & 2L^2/15 \end{bmatrix}, \tag{9.48}$$

where A is the area of steel cross-section, E is Young's modulus, and I is the appropriate second moment of area. The local effective axial tension, T_e, is calculated by accounting for the modification due to hydrostatic pressures in the surrounding fluid, as described earlier in Eq. (9.9).

The fixed end action vectors $A_m L$ are obtained by using an assumed shape function $N(y)$ in conjunction with a total lateral load distribution $W(y)$. This load is due to both the hydrodynamic loading q and an effective lateral load derived from

term C in governing Eq. (9.39) with dx/dy obtained from an initially assumed undeflected riser configuration. Thus,

$$A_{mL} = -\int_0^{l_r} W(y)N(y)\,dy, \tag{9.49}$$

where y is the vertical distance from the bottom ball or flex joint, and l_r is the total riser length. The final static member end actions A_m are then obtained from

$$A_m = A_{ml} + S_m D_m, \tag{9.50}$$

where D_m is the nodal displacement vector. These combined end actions are applied incrementally in order to account for the changes in term C of Eq. (9.39) and the nonlinear behavior caused by large deflections of the riser pipe. Thus, A_m is divided into a specified number of equal increments ΔA_m, which are applied progressively to obtain the incremental displacements ΔD through the equation

$$\Delta D = S^{-1}\Delta A_m, \tag{9.51}$$

where D is the overall displacement vector, and S is the overall stiffness matrix. Both D and S are in global coordinates. The overall stiffness matrix is reevaluated after each load increment to account for the change in geometry due to large deflections.

9.4.2 Dynamic Analysis

The differential equation of motion for a system with many degrees of freedom and having a mass matrix M_T can be written as

$$M_T\ddot{D} + C\dot{D} + SD = F, \tag{9.52}$$

where D is the vector of nodal displacements, F is the vector of external forces, and C and S are the structural damping matrix and overall stiffness matrix, respectively. All the above vectors and matrices are defined in global riser axes.

The external force vector F due to wave action on the system is obtained from a modified form of Morison's Eq. (9.1),

$$F = \rho_{oT} V\dot{U} + M_a(\dot{U} - \ddot{D}) + B|U - \dot{D}|(U - \dot{D}), \tag{9.53}$$

where V the diagonal matrix of elemental volumes, M_a is the added mass matrix, B is the matrix of hydrodynamic drag coefficients, and U and $\dot{U}$ are the horizontal components of wave particle velocities and accelerations. It is assumed here that the fluid-induced forces on a structure are given by the linear superposition of a drag force and an inertia force. The first two terms of Eq. (9.53) signify the Froude–Krylov and added mass forces, respectively, while the last term describes the drag force.

By substituting Eq. (9.53) into (9.52) with $M_T = M + M_a$ and rearranging we get

$$M_T\ddot{D} + C\dot{D} + SD = M_a\dot{U} + B|U - \dot{D}|(U - \dot{D}). \tag{9.54}$$

The above matrix equation cannot be used directly for incorporating the boundary condition at the surface vessel, which requires that the riser top end must follow the horizontal motion of the surface platform. This known horizontal riser nodal translation at the surface (denoted by suffix B) can be separated from all other unknown degrees of freedom (denoted by suffix A) through the following matrix partitioning:

$$\begin{bmatrix} M_{TAA} & M_{TAB} \\ M_{TBA} & M_{TBB} \end{bmatrix} \begin{bmatrix} \ddot{D}_A \\ \ddot{D}_B \end{bmatrix} + \begin{bmatrix} C_{AA} & C_{AB} \\ C_{BA} & C_{BB} \end{bmatrix} \begin{bmatrix} \dot{D}_A \\ \dot{D}_B \end{bmatrix} + \begin{bmatrix} S_{AA} & S_{AB} \\ S_{BA} & S_{BB} \end{bmatrix} \begin{bmatrix} D_A \\ D_B \end{bmatrix}$$
$$= \begin{bmatrix} M_{HAA} & M_{HAB} \\ M_{HBA} & M_{HBB} \end{bmatrix} \begin{bmatrix} \dot{U}_A \\ \dot{U}_B \end{bmatrix} + \begin{bmatrix} B_{AA} & B_{AB} \\ B_{BA} & B_{BB} \end{bmatrix} \begin{bmatrix} |U_A - \dot{D}_A|.(U_A - \dot{D}_A) \\ |U_B - \dot{D}_B|.(U_B - \dot{D}_B) \end{bmatrix}$$
$$+ \begin{bmatrix} 0 \\ F_B \end{bmatrix}. \tag{9.55}$$

Here, F_B is a force required to cause the specified horizontal motion at the surface. The dynamic response of the riser structure in terms of the remaining degrees of freedom can be obtained solely from the upper set of equations from (9.55), which do not contain F_B.

9.4.3 Element Property Formulation

In the formulation of the beam element mass matrix, the lumped mass or the consistent mass approach may be used. With the former approach, the entire mass is assumed to be concentrated at nodes where the translational degrees of freedom are defined. For such a system, the mass matrix has a diagonal form. Off-diagonal terms disappear since the acceleration of any nodal point mass would only produce an inertia force at that point. The consistent mass formulation, however, makes use of the finite element concept and requires the mass matrix to be computed from the same shape functions that are used in deriving the stiffness matrix. Coupling due to off-diagonal terms exists, and rotational and translational degrees of freedom need to be considered.

In theory, this consistent mass approach can lead to a greater accuracy, although this improvement is believed to be small. On the other hand, the lumped mass formulation is easier to apply because fewer degrees of freedom are involved, leading to a simpler definition of element properties. The lumped mass formulation is chosen for this analysis because the advantages of a small improvement in accuracy for the consistent mass approach are outweighed by the additional computational effort entailed in its implementation.

Noting that off-diagonal terms of M_a, M_T, and B are zero for the lumped mass formulation, the following equations are obtained from (9.55):

$$\begin{aligned} &M_{TAA}\ddot{D}_A + C_{AA}\dot{D}_A + S_{AA}D_A \\ &\quad = M_{aAA}\dot{U}_A + B_{AA}\big|(U_A - \dot{D}_A)\big|(U_A - \dot{D}_A) \\ &\qquad - C_{AB}\dot{D}_B - S_{AB}D_B. \end{aligned} \tag{9.56}$$

At the end of the static analysis, the stiffness matrix of the structure in its deformed position is available. In modeling the dynamic response about this mean statically deflected shape, the stiffness matrix is assumed to remain constant throughout the dynamic analysis.

In the lumped mass approach, all the rotational degrees of freedom need to be substructured out. Since vertical wave forces are not significant for the riser system, the vertical translation degrees of freedom can also be eliminated. This feature can lead to a substantial reduction in computer time and storage in the dynamic analysis. The horizontal degrees of freedom having been segregated, the force-deflection equations can be written in partitioned form as

$$\begin{bmatrix} S_{HH} & S_{HN} \\ S_{NH} & S_{NN} \end{bmatrix} \begin{bmatrix} D_H \\ D_N \end{bmatrix} = \begin{bmatrix} F_H \\ 0 \end{bmatrix}, \tag{9.57}$$

where the subscript H denotes the horizontal degrees of freedom, and N denotes the remaining vertical and rotational degrees of freedom.

From Eq. (9.57) we have

$$D_N = -S_{NN}^{-1} S_{NH} D_H. \tag{9.58}$$

The condensed stiffness matrix suitable for use in the equations of motion is then

$$S_{HH}^{*} = S_{HH} - S_{HN} S_{NN}^{-1} S_{NH}. \tag{9.59}$$

The matrix is further partitioned to separate out the top horizontal degree of freedom:

$$S_{HH}^{*} = \begin{bmatrix} S_{AA} & S_{AB} \\ S_{BA} & S_{BB} \end{bmatrix}, \tag{9.60}$$

where the subscript B denotes the vessel motion as before.

The mass matrix for each element is built up by concentrating half of the total mass of mud, pipes, and buoyancy material at each end of the element. For a fully submerged vertical element of volume V, the added mass associated with unit horizontal body acceleration is $\rho_0 C_m V$, where C_m is an added mass coefficient. Taking half the added mass to be lumped at each node, the added mass submatrix for each element is

$$\begin{bmatrix} \frac{1}{2}\rho_0 C_m V & 0 \\ 0 & \frac{1}{2}\rho_0 C_m V \end{bmatrix}. \tag{9.61}$$

This added mass matrix and the real mass matrix are summed together to give the total mass matrix M_{TAA}.

The manner in which the partially submerged element at the water surface is idealized depends on the amount by which the element is wetted at the mean sea level. If the wetted length L_s is less than half the element length, all the added mass is lumped at the lower node, and the element submatrix becomes

$$\begin{bmatrix} \rho_0 C_m A_x L_s & 0 \\ 0 & 0 \end{bmatrix}, \tag{9.62}$$

where A_x is the total cross-sectional area of the riser element, including buoyancy elements when present. Should L_s be greater than half the element length L, the added mass associated with the lower half of the element is concentrated at the lower node, while the rest of the hydrodynamic effects are taken to act on the top node. The element submatrix for such a situation is

$$\begin{bmatrix} \frac{1}{2}\rho_o C_m A_x L_s & 0 \\ 0 & \rho_o C_m A_x (L_s - \frac{L}{2}) \end{bmatrix}. \tag{9.63}$$

For the riser structure, this appears to be a simple and logical way to treat the element at the water surface in the lumped mass formulation. The hydrodynamic mass matrix M_{aAA}, which includes the Froude–Krylov forces, is built up from element submatrices in a similar manner. The submatrices corresponding to Eqs. (9.62) and (9.63) respectively are:

$$\begin{bmatrix} \rho_o (C_m + 1) A_x L_s & 0 \\ 0 & 0 \end{bmatrix}, \tag{9.64}$$

$$\begin{bmatrix} \rho_o C_m A_x L_s & 0 \\ 0 & \rho_o (C_m + 1) A_x (L_s - \frac{L}{2}) \end{bmatrix}. \tag{9.65}$$

Due to the unit relative horizontal velocity $(U - \dot{D})$, the horizontal drag force on a fully submerged element is $\frac{1}{2}\rho_o C_D L d$, where d is the diameter of the element. The hydrodynamic damping submatrix for such an element is

$$\begin{bmatrix} \frac{1}{4}\rho_o C_D L d & 0 \\ 0 & \frac{1}{4}\rho_o C_d L d \end{bmatrix}. \tag{9.66}$$

The corresponding submatrices for a partially immersed element are

$$\begin{bmatrix} \frac{1}{2}\rho_o C_D L_s d & 0 \\ 0 & 0 \end{bmatrix} \quad \text{for } L_s \leq \frac{L}{2} \tag{9.67}$$

and

$$\begin{bmatrix} \frac{1}{4}\rho_o C_D L d & 0 \\ 0 & \frac{1}{2}\rho_o C_d (L_s - \frac{L}{2}) d \end{bmatrix} \quad \text{for } L_s > \frac{L}{2}. \tag{9.68}$$

The structural damping matrix may be explicitly defined as

$$C = \alpha_0 M_T + \alpha_1 S. \tag{9.69}$$

To obtain the coefficients α_o and α_1, the damping ratios, ζ_1 and ζ_2, in any two modes need to be specified. An eigenvalue analysis is carried out to find the natural frequencies corresponding to the two modes chosen. Bathe and Wilson [271] give further details of this approach.

For Rayleigh damping,

$$\begin{bmatrix} \zeta_1 \\ \zeta_2 \end{bmatrix} = \frac{1}{2} \begin{bmatrix} \frac{1}{\omega_1} & \omega_1 \\ \frac{1}{\omega_2} & \omega_2 \end{bmatrix} \begin{bmatrix} \alpha_0 \\ \alpha_1 \end{bmatrix}. \tag{9.70}$$

From Eq. (9.70) we have

$$\begin{aligned} \alpha_0 &= 2\big(\zeta_1 \omega_1 - \alpha_1 \omega_1^2\big), \\ \alpha_1 &= \frac{2(\zeta_1 \omega_1 - \zeta_2 \omega_2)}{\omega_1^2 - \omega_2^2}. \end{aligned} \tag{9.71}$$

A damping ratio of 5 % in the first two modes is usually chosen for all the analyses carried out in this work. The actual level of structural damping that should be specified is rather unclear in current literature.

9.4.4 Frequency Domain Solution

A linearized form of the equation of motion may be obtained by replacing the drag term in Eq. (9.56) with a suitable equivalent linear damping term, which is proportional to the relative velocity $U_A - \dot{D}_A$. For such a linear system,

$$\begin{aligned} &M_{TAA}\ddot{D}_A + (C_{AA} + B_{eqAA})\dot{D}_A + S_{AA} D_A \\ &\quad = M_{aAA}\dot{U}_A + B_{eqAA} U - C_{AB}\dot{D}_B - S_{AB} D_B. \end{aligned} \tag{9.72}$$

Since the current velocity imposed is not sinusoidal, only the wave particle velocity U_A and the structure velocity $\dot{D}_A$ can be included in the fluid interaction term. The stiffness matrix in the frequency analysis will therefore be obtained from the final statically deformed shape caused by current and riser internal forces.

From linear wave theory, the elevation of a single wave train may be represented by

$$\xi = a \cos(kx - \omega t), \tag{9.73}$$

where a is the wave amplitude, k is the wave number, and ω is the wave frequency.

The corresponding horizontal wave particle velocities, U_w, and accelerations, $\dot{U}_w$, are given by

$$U_w = \omega a \frac{\cosh k(y - l_r + h)}{\sinh kh} \cos(kx - \omega t), \tag{9.74}$$

$$\dot{U}_w = \frac{\omega^2 a \cosh k(y - l_r + h)}{\sinh kh} \sin(kx - \omega t), \tag{9.75}$$

where h is the water depth.

Rewriting Eq. (9.74) in complex form gives

$$U_w = \mathrm{Re}\left[\frac{\cosh k(y - l_r + h)}{\sinh kh} e^{ikx} e^{-i\omega t}\right] \tag{9.76}$$

or

$$\mathrm{Re}\left(U'_\omega\right) e^{i\omega t}, \tag{9.77}$$

where U'_w is a complex amplitude. Similarly,

$$\dot{U_\omega} = \mathrm{Re}\left(-i\omega U'_w\right) e^{i\omega t}. \tag{9.78}$$

The steady-state response of the system represented by Eq. (9.72) to a sinusoidal wave will also be proportional to $e^{-i\omega t}$. Thus,

$$D_A = \mathrm{Re}\left(D'_A e^{-i\omega t}\right), \tag{9.79}$$

where $(D')_A$ is the complex amplitude vector.

Differentiating Eq. (9.79) and substituting Eqs. (9.77) and (9.78) into (9.72) gives

$$\begin{aligned}&\left[S_{AA} - \omega^2 M_{TAA} - i\omega(C_{AA} + B_{\mathrm{eq}AA})\right] D'_A \\ &\quad = M_{aAA}\left(-i\omega U'_W\right) + B_{\mathrm{eq}AA} U'_W = F',\end{aligned} \tag{9.80}$$

where F' is the complex forcing amplitude vector, and B_{eq} is an equivalent linear damping matrix. The linearization of the damping is described later.

Since the matrix B_{eq} contains a term in A, available only from the final solution, an iterative calculation scheme needs to be derived. Starting from a trial solution for the displacement D_A, B_{eq} is estimated, and the set of complex algebraic equations (9.80) are solved for a new set of displacements, $(D')_A$. These displacements are compared with the previous set of values, and the whole calculation is repeated with a better estimate of B_{eq} until the real and imaginary parts of D_A differ by a small specified tolerance.

Since damping forces are responsible for the dissipation of energy in a vibratory system, the obvious, and most common, way of obtaining B_{eq} is to equate the work done by the linearized and the nonlinear forces such that

$$B_{\mathrm{eq}}(U - \dot{D}) \equiv B|U - \dot{D}|(U - \dot{D}). \tag{9.81}$$

For the purpose of illustration, a convenient node where x is assumed to be zero is chosen. By Eq. (9.74) the wave particle velocity is

$$U = R\cos\omega t, \tag{9.82}$$

where

$$R = \frac{\omega a \cosh k(y - l_r + h)}{\sinh kh}. \tag{9.83}$$

Let the corresponding riser nodal velocity be defined by

$$\dot{D} = Q\cos(\omega t - \phi), \tag{9.84}$$

where Q is the amplitude of vibration velocity, and ϕ is an arbitrary phase difference. The relative velocity is

$$(U - \dot{D}) = R\cos\omega t - Q\cos(\omega t - \phi) = R_T\cos(\omega t - \psi), \tag{9.85}$$

where

$$\begin{aligned} R_T &= \left(R^2 - 2RQ\cos\phi + Q^2\right)^{1/2}, \\ \tan\psi &= \frac{-Q\sin\phi}{R - Q\cos\phi}. \end{aligned} \tag{9.86}$$

The work done by the damping force $B|U - \dot{D}|(U - \dot{D})$ over an elemental displacement dD may be written as

$$dW = B\left|R_T\cos(\omega t - \psi)\right|R_T\cos(\omega t - \psi)Q\cos(\omega t - \phi)d(\omega t). \tag{9.87}$$

Using the substitutions $\beta = \omega t - \psi$ and $\gamma = \omega t - \phi$, we can express the work done over a complete wave period by this nonlinear term as

$$W = \int_{-\psi}^{2\pi-\psi} B|R_T\cos\beta|R_T\cos\beta Q\cos(\beta + \gamma)\,dB = \frac{8}{3}QBR_T^2\cos\gamma \tag{9.88}$$

by splitting up the limits of integration to account for the modulus sign, and assuming that $\gamma = \omega t - \phi$ is time independent.

The work done by an equivalent linearized damping force $B_{\text{eq}}(U - \dot{D})$ over a wave cycle is readily obtained from

$$\begin{aligned} W &= \int B_{\text{eq}}R_T\cos(\omega t - \psi)Q\cos(\omega t - \phi)\,d\big(\omega(t)\big) \\ &= \pi QB_{\text{eq}}R_T\cos\gamma. \end{aligned} \tag{9.89}$$

Finally, equating the work done by the two damping terms gives

$$B_{\text{eq}} = \frac{8}{3\pi}BR_T. \tag{9.90}$$

Hence, the equivalent linear damping matrix in Eq. (9.80) is given by

$$B_{\text{eq}} = \frac{8}{3\pi} B \left| (U - \dot{D})_{\max} \right|. \tag{9.91}$$

The other issue remaining in the iterative solution of Eq. (9.80) is the choice of the initial estimate of the displacement vector, D'_A.

To ensure that Eq. (9.80) converges rapidly to the final solution, a reasonably accurate initial estimate of the displacements D'_A and thus of the velocities $\dot{D}_A$ is required for evaluating the equivalent damping matrix from the total mass matrix and the diagonal terms of the stiffness matrix. Then, assuming a damping ratio of 10 %, the initial estimate of B_{eq} is taken to be

$$B_{\text{eq}} \begin{bmatrix} (M^{11}_{TAA} S^{11}_{AA})^{1/2} & 0 & 0 \\ 0 & (M^{22}_{TAA} S^{22}_{AA})^{1/2} & 0 \\ & & (M^{NN}_{TAA} S^{NN}_{AA})^{1/2} \end{bmatrix}. \tag{9.92}$$

This matrix is substituted into Eq. (9.80), which is subsequently solved for the initial trial solution. This method leads to rapid convergence with only two or three iterations required for forcing frequencies away from the structure's resonant frequencies. Up to 10 iterations may be necessary in the region of resonance frequencies.

9.4.5 Time Domain Solution

The basic method of analysis here involves integrating Eq. (9.52) through discrete steps in time and accounting for the nonlinear drag loading without a linearization approximation.

In the equation of motion, Eq. (9.54), the generalized fluid velocity can be decomposed into the static current velocity U_c and a wave particle velocity U_w. Thus, Eq. (9.54) becomes

$$M_T \ddot{D} + C\dot{D} + SD = M_a \dot{U}_w + B|U_w + U_C - \dot{D}|(U_w + U_c - \dot{D}), \tag{9.93}$$

where U_c is taken to be zero for the current velocity. The requirement to sum the current and wave velocities before applying the resultant loading through the square-law relationship requires the current velocity to be ignored in the static analysis that precedes this time-domain calculation.

The time step integration of the equation of motion also allows irregular wave sequences (and the corresponding surface vessel surge responses) to generate random dynamic excitation forces on the riser. This wave sequence can be specified in two ways. A wave elevation spectrum of the incident irregular waves with random phase can be used to generate the Fourier transform of the wave elevation.

The Fourier transform of the subsurface wave velocities and accelerations and surface vessel surge motions may be obtained using the appropriate transfer functions. These Fourier transforms are inverse Fourier transformed to generate corresponding time series of these quantities for use in the dynamic analysis. However, this procedure can be cumbersome and computationally time-consuming. Therefore, a simple alternative method is usually employed. The incident wave elevation is specified as a "frequency comb" sum of individual sinusoidal components with randomly distributed phase angles. The subsurface wave kinematics and surface vessel surge response are then readily computed by summing the effects of all the sinusoidal components in the wave spectrum.

The numerical time step integration technique proposed by Newmark is used with the following relations:

$$\dot{D}_{t+\Delta t} = \dot{D}_t + \left[(1-\delta)\ddot{D}_t + \delta \ddot{D}_{t+\Delta t}\right]\Delta t, \tag{9.94}$$

$$\dot{D}_{t+\Delta t} = \dot{D}_t + \dot{D}_t \Delta t + \left[\left(\frac{1}{2} - \beta'\right)\ddot{D}_t + \beta' \ddot{D}_{t+\Delta t}\right]\Delta t^2, \tag{9.95}$$

where β' and D are parameters that can be varied to achieve acceptable integration accuracy and stability. The subscript t denotes the variable at the beginning of the time interval Δt.

The direct integration analysis does rely on selection of an appropriate time step which must be small enough to obtain sufficient accuracy, although a time step smaller than necessary would reflect on the cost of the solution. Bathe and Wilson [271] have analyzed the stability and accuracy of various numerical integration schemes and suggested that, for reasonable accuracy, the time step-to-period ratio be not greater than $1/6$ for the highest significant mode. In its standard form, the Newmark technique is unconditionally stable.

The two parameters D and β' introduced in Eq. (9.95) indicate how the acceleration is modeled over the time interval. The parameters $D = 1/2$ and $\beta' = 1/6$ correspond to a linearly varying acceleration. Newmark's original scheme, which is pursued here, uses $D = 1/2$ and $\beta' = 1/4$ and gives a constant-average acceleration-based integration scheme. Using the latter values in Eq. (9.95) and rearranging gives:

$$\dot{D}_{t+\Delta t} = \frac{4}{(\Delta t)^2}\left[\ddot{D}_{t+\Delta t} - D_t - (\Delta t)\dot{D}_t\right] - \ddot{D}_t, \tag{9.96}$$

$$\dot{D}_{t+\Delta t} = \frac{2}{(\Delta t)}[\ddot{D}_{t+\Delta t} - \ddot{D}_t] - \dot{D}_t. \tag{9.97}$$

Then expressing Eq. (9.93) explicitly at instant $t + \Delta t$ and using the lumped-mass approach with the top vessel surge motion duly separated as in Eq. (9.56), we get

$$M_{TAA}\ddot{D}_{A,t+\Delta t} + C_{AA}\dot{D}_{A,t+\Delta t} + S_{AA}D_{A,t+\Delta t}$$
$$= M_{aAA}\dot{U}_{WA,t+\Delta t}$$

$$+ B_{AA}\left|(U_{WA} + U_{CA} - \dot{D}_A)\right|_{t+\Delta t}(U_{WA} + U_{CA} - \dot{D}_A)_{t+\Delta t}$$
$$- C_{AB}\dot{D}_{B,t+\Delta t} - S_{AB}D_{B,t+\Delta t}. \tag{9.98}$$

Substituting Eq. (9.96) into Eq. (9.98) and rearranging gives

$$\left[\frac{4M_{TAA}}{\Delta t^2} + \frac{2C_{AA}}{\Delta t} + S_{AA}\right]D_{A,t+\Delta t}$$
$$= M_{aAA}\dot{U}_{WA,,t+\delta t}$$
$$+ B_{AA}\left|(U_{WA} + U_{CA} - \dot{D}_A)\right|_{t+\Delta t}$$
$$- C_{AB}\dot{D}_{B,t+\Delta t} - S_{AB}D_{B,t+\Delta t}\left[\frac{4}{\Delta t}M_{TAA} + D_{AA}\right]\dot{D}_{A,t}$$
$$+ \left[\frac{4M_{TAA}}{\Delta t^2} + \frac{2C_{AA}}{\Delta t}\right]D_{A,t} + M_{TAA}\ddot{D}_{A,t} = F_{t+\Delta t}. \tag{9.99}$$

This is the basic equation used in the time step integration scheme.

The solution scheme assumes that displacement, velocity, and acceleration vectors at time zero are known and the solution is required from time zero to time t. The given time span τ is subdivided into equal time intervals $\Delta t = \tau/n$, where n is the number of time intervals. The algorithm calculates the solution at the next required time step from the information known at the previous time steps. The process is repeated until the solution at all discrete time points is known.

To initialize the numerical solution, the acceleration corresponding to zero time is derived from the reduced form of Eq. (9.99) giving

$$\ddot{D}_A|_{t=0} = M_{TAA}^{-1}\left[M_{aAA}\dot{U}_{WA,0} + B_{AA}\left|(U_{WA} + U_{CA})_0\right|(U_{WA} + U_{CA})_0\right.$$
$$\left. - C_{AB}\dot{D}_{B,0} - S_{AB}D_{B,0}\right]\Big|_{t=0}. \tag{9.100}$$

Arriving at Eq. (9.100), the unknown value of velocity $\dot{D}_{A,t+\Delta t}$ of the forcing vector of Eq. (9.99) has been approximated to $\dot{D}_{A,t}$. The approximation gives an acceptable degree of accuracy, provided that the time step chosen is sufficiently small. An alternative approach to this would require an elaborate iterative scheme with a significantly greater computation effort.

By the simultaneous equation (9.99) the displacements are simply obtained from

$$\dot{D}_{A,t+\Delta t} = \mathcal{J}^{-1}F_{t+\Delta t}, \tag{9.101}$$

where

$$\mathcal{J} = \frac{4}{\Delta t^2}M_{TAA} + \frac{2}{\Delta t}C_{AA} + S_{AA}. \tag{9.102}$$

The inversion of matrix $\mathcal{J}$ in the above equation can be made more efficient by the use of banded equation solvers as suggested by Bathe and Wilson [271]. However, $\mathcal{J}$ is independent of time and needs to be inverted once only. When $\dot{D}_{A,t+\Delta t}$ is

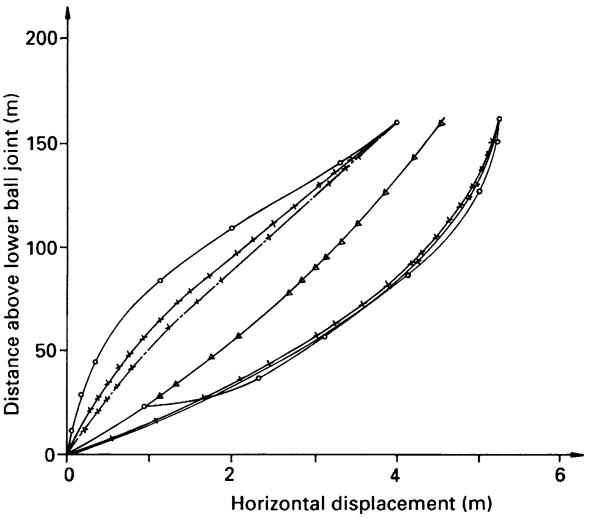

Fig. 9.16 Displacement for a marine riser compared with API case 500-20-ID

known, the accelerations and velocities at time $t + \Delta t$ are derived from Eqs. (9.96) and (9.97).

9.4.6 Typical Results

Finite element calculations of the type presented here can be validated by a number of methods.

For the static analysis, the finite element formulation can be checked by comparison with the analytic result for an idealized weightless tensioned beam. Such comparisons can confirm the validity of the computational procedure and indicate the number of finite elements required for an acceptable level of accuracy.

The American Petroleum Institute Committee on the Standardization of Offshore Structures defined a set of test risers as a basis for comparing the performance of riser analysis methods for both static and dynamic loadings. Nine anonymous participants in this study submitted solutions for the various test cases, and API Bulletin 2J [272] gives the overall comparisons. These are displayed in terms of maximum bending stress value and position, maximum total stress (axial plus peak bending), as well as upper and lower riser angles from the vertical.

The frequency domain and time domain dynamic analyses presented here have also been compared with the dynamic analyses in the API bulletin. Figures 9.16 and 9.17 show typical results for one of the API test risers; the plotted API values are the maximum and minimum of the combined results from the nine calculations compiled in the bulletin. The frequency domain analysis is computed conventionally using a regular wave period of 9 s and wave height of 6.096 m. The time domain analysis uses a single frequency "comb" to produce equivalent data but with the nonlinear drag force due to current and wave velocities included in the calculations.

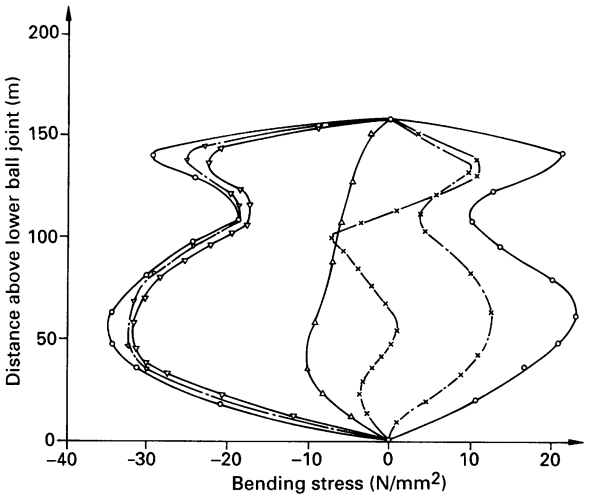

Fig. 9.17 Stresses for a marine riser compared with API case 500-20-ID

It should be emphasized that none of the results published in the API bulletin has, to our knowledge, been directly validated by measurements on full-scale risers. Nevertheless, this comparison gives an indication of agreement between the other methods and the analysis presented here.

A comparison of the time domain and frequency domain analyses presented in Figs. 9.16 and 9.17 gives an indication of the effects of nonlinear fluid loading on the riser structural response. A static current profile is included, and so the time domain and frequency domain results differ markedly owing to the effect of the square law drag force with and without linearization. However, the frequency domain results are at lower values for the induced stresses.

The finite element analysis and the frequency domain and time domain solutions outlined in this section attempt to balance the small computing cost advantages of linearization against the additional accuracy available from the nonlinear time domain calculation. The frequency domain analysis uses the linearization approximation of equal energy dissipation between nonlinear damping and equivalent linear damping in the solution. An alternative linearization technique for frequency domain analysis has been tested by Krolikowski and Gray [273]. It is based on a statistical minimization of mean squared error between the nonlinear damping force and its linear representation used in the analysis. The statistical approach uses linearization at the discrete frequency components of a wave spectrum to arrive at a global linearized damping force with a least squares minimized error. This technique allows a frequency domain method to be applied over a wider frequency range, in contrast to the linearization method used in the analysis presented here, which is used for regular waves only.

The technique of linearization by least squares minimization is not followed up in the frequency domain analysis presented here. This is because both riser methods developed here have been aimed at computing riser motions and stresses, the latter for feeding into fatigue calculations based on linear elastic theory or fracture

mechanics. The fracture mechanics approach demands the representative stress time histories for a marine riser in waves to be known in detail, particularly in terms of the sequences of stress cycles that are likely to occur. A computationally efficient time domain analysis is capable of producing this information, whereas frequency domain analyses, whatever their level of sophistication in linearization, operate in the frequency domain where the phase information which governs wave sequencing is lost.

A further feature, which has promoted the use of an efficient time domain analysis for riser calculations, is based on the comparative performance of the frequency domain and time domain analyses, which shows that there are substantial differences in peak stresses between the two analyses. These discrepancies may be reduced by a more sophisticated linearization technique in the frequency domain analyses, but the discrepancies do highlight the importance of modeling the nonlinear fluid loading on the riser cross-section in a physically representative manner.

An additional problem associated with marine risers occurs in the analysis of multitube production risers of complex cross-sectional geometries. These may be made up of a central structural riser with a number of large diameter satellite flow lines or as a bundle or array of flow lines. The beam finite element analysis techniques described in this chapter need to be extended to these production risers. Patel and Sarohia [274] suggest one solution by equivalencing a production riser of complex cross-section to a simpler single-tube marine riser, which is then used for the finite element analysis. This approach is sufficient for a global riser analysis, but it needs to be used with care when localized riser fluid forces or member stresses are required. Krolikowski [275] presents an alternative frequency domain approach.

9.5 Principles of Operation

Whether the riser is required for drilling or production duty, the fitness for purpose of the design is determined by the estimates of its likely loading conditions. These conditions include environmental forces and, if applicable, surface support motions. Confident estimates of these are essential. They are not limited to static behavior, but should include dynamic response. For rigid risers, the likely causes of failure are local material yielding and Euler column buckling.

The design of all types of tensioned risers is affected by:

(i) static and dynamic motions of the surface vessel;
(ii) tensioner stroke limits and response rates;
(iii) bottom connection angle limits;
(iv) distribution of buoyancy modules.

Additionally, drilling risers are particularly affected by:

(i) mud weight;
(ii) drill string tension;
(iii) possible abnormal gas pressure.

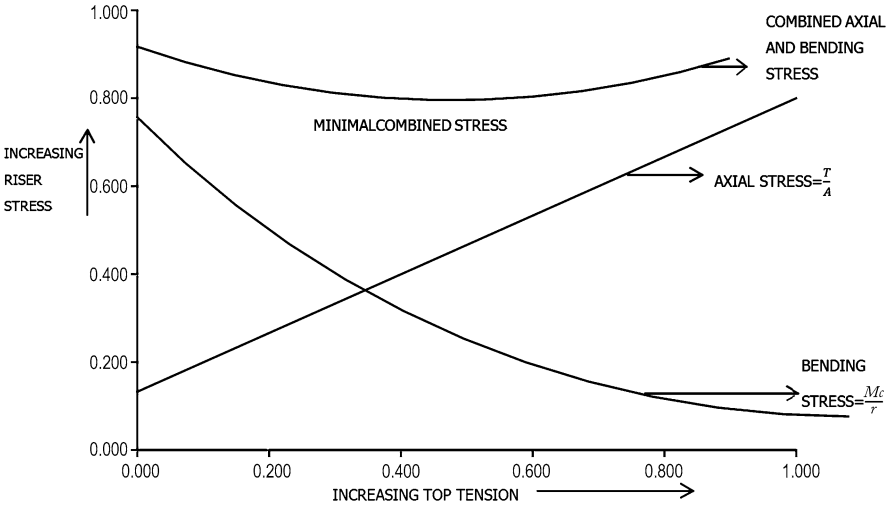

Fig. 9.18 Aid to optimizing riser top tension

Whilst production risers are particularly affected by:

(i) buoyancy modules for the free-standing mode
(ii) drag of multiple piping;
(iii) rigidity of multiple piping;
(iv) installation, repair and maintenance procedures.

9.5.1 Riser Top Tension and Supplementary Buoyancy

Currently (2013), there is increasing need to develop fields in the region of 3000 m water depth. The tensioning requirements for risers in these water depths are substantial. A truly vertical riser connected at the seabed has no buoyancy force. This is because buoyancy is the resultant net force acting vertically on a body, and if there is no horizontal surface on which the hydrostatic pressures may act, the resultant force is zero. However, disconnection on the riser from the seabed or its inclination will exhibit a buoyancy force. Generally, for risers, the combined effects of self-weight and buoyancy yields a net negative force, which is destabilizing in that the riser will continue to move away from the vertical unless restrained. This restraint is provided by means of top tensioning, which may be aided by the use of supplementary buoyancy modules along the riser length.

A nearly optimum choice of top tension can be arrived at by calculating the sum of the reduction in bending stress and the increase in axial stress with increase in top tension shown in Fig. 9.18.

Care must be taken to ensure that the lateral component of top tension does not result in excessive horizontal deflection of the bottom BOP stack, Fig. 9.19. The

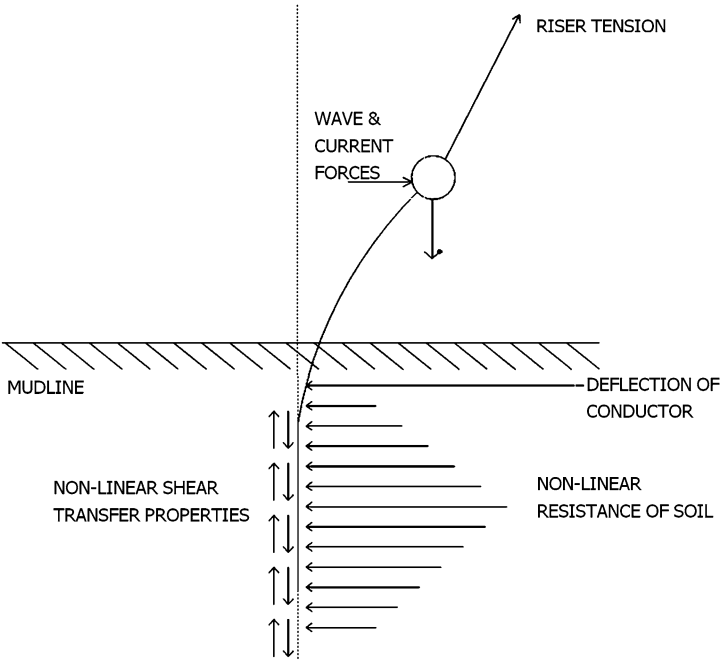

Fig. 9.19 BOP eccentricity resulting in bending of the conductor column

moment due to the BOP weight and its eccentricity may lead to bending failure of the seabed conductor column. Reduction in top tension requirement is particularly advantageous in very deep water. Care must be taken to ensure that such reductions do not lead to local compression, which is more likely to occur near the seabed.

Buoyancy modules in use include air-filled cans in which the volume of air may be controlled from the surface and so alter the buoyancy available. Other forms do not offer this control but have cost advantages in certain cases. Materials for these include cellular polystyrene, syntactic foams which may contain spheres of various materials, and foamed aluminium. Some of these materials can deteriorate with time resulting in a change in buoyancy. Manufacturers should be consulted for suitability of depth ratings.

Addition of buoyancy modules beneficially reduces the bending stresses by "straightening" the riser by tension and also adversely increases the lateral hydrodynamic loading and bending stresses on the riser. Careful design and usage is required to ensure the desired benefit.

9.5.2 Drilling Riser Configurations

Whilst drilling risers are essentially of one form, during their operational life, they will be used in several configurations. These are:

(i) Free-hanging mode

This situation will occur in the early stages of drilling and possibly during the drilling program. An associated free-hanging configuration occurs initially as the hole is spudded-in during running of the 36-inch hole opener and 26-inch hole bit, as well as the running of 30-inch and 20-inch conductors and 18.75-inch wellhead. These operations are performed without a riser connecting the surface vessel to the sea bed, with the free-hanging conductor's guidance aided by a utility guide frame and guidelines, although guidelineless systems also have applications.

This free-hanging riser mode is important operationally since current action can have adverse effects on it. However, the conditions for lowering the riser itself with its blowout preventor stack at its free end present greater difficulties. Careful control of this operation is critical since the BOP stack may weigh up to 200 tonnes in air and is an expensive item. BOP stacks may be landed with the aid of guidelines or without. If no guidelines are used, then recourse to acoustic positioning transponders and underwater television cameras is made.

As the stack nears the wellhead, it can be liable to damage by a heavy landing or impact, since the surface vessel will be heaving to some extent whatever the sea-state. As the final joints of the riser are added, the riser tensioner wires are added below the slip joint enabling part of the load to be transferred to them, and so a proportion of the total load is taken by the rig's surface motion compensator. The remainder is taken by the riser's tensioning wires. Hence, the stack may be landed with minimum jarring.

The riser, once connected to the wellhead, will inevitably enter the free-hanging configuration at least once more in its life. That is when it is retrieved along with the BOP stack on completion of the drilling programme. It is possible, however, especially when drilling in particularly hostile environments that the riser will be pulled, that is, retrieved to prevent damage to it. Depending upon the water depth and weather severity, among other factors, the riser may be disconnected and hung-off, that is, not fully retrieved. In this configuration, only the lower riser package part of the BOP stack remains attached to the lower end of the riser.

(ii) Connected modes

It is in this mode that the riser will spend the majority of its working life. In this condition, the primary operational concerns are the riser's static and dynamic performance induced by the rig's horizontal motions as it maintains station over the wellhead. These motions will have steady components from mooring offset and oscillating motions due to wave action.

The connected mode may be further divided into two separate conditions:

(a) Operational

The flex joint angle must be less than 4 degrees in this mode.

(b) Nonoperational but connected

For flex joint angles greater than 4 degrees, normal drilling operations cannot continue. but the riser can remain connected.

(iii) Operational Mode

The maximum 4-degree flex joint angle for this mode arises so as not to damage the riser bore (by internal drill pipe) or the BOP during drilling operations. The 4-degree angle criterion is derived from combination of experience and experimental data. In actual service, this flex joint angle will coincide with vessel offsets of between 3 to 4 % of water depth. Furthermore, it is normally impossible to maintain an operable flex joint angle (that is below 4 degrees) with the surface vessel offset to over 6 % of water depth). This corresponds to the 3.3-degree angle of offset (from the vertical) of the line connecting the vessel to the BOP. Thus, the desirable maximum vessel offset is normally 3 to 4 % of water depth when drilling or running large tools, although the offset needs to be much less when running casing and other special-purpose operations. These, however, only occur for a relatively short proportion of the total drilling time.

For particular riser systems, graphs or tables for determining optimum top tension under prescribed operating conditions should be prepared. These recommended tensions only offer a starting point and may be in error because the recommendations are based on site estimates of current and waves that may also be in error. For example, underestimating the current acting on the lower part of the riser will lead to a low estimate for optimum riser tension, and this will be reflected in the flex joint angle.

The flex joint angle does give a reasonable indication of riser stresses. In particular, the flex joint angle will give an indication of riser problems, usually, low tension or large offset, but it alone cannot give a complete analysis of the situation.

Use of a sophisticated Riser Management System operating with real-time environmental data to provide a more representative analysis. See Sect. 9.7.

(iv) Nonoperational but Connected Mode

Figure 9.20 is a typical example of maximum/minimum stress behavior in a riser when the flex joint is on or near its angular motion stop. When on its stop, maximum and minimum stresses will occur at or near the connection between the riser and flex joint. When the flex joint is off its stop, maximum stresses will occur at another position in the riser. In Fig. 9.20, the flex joint is just off the stop when the maximum and minimum stresses at the ball joint become coincidental. For this case, the flex joint disengages at about 100 kips. Increasing the tension to 150 or 190 kips has little effect on the riser stress, but decreasing the tension to 50 kips could lead to riser failure. The minimum tension to be allowed for the conditions stated in the figure is 100 kips.

In practice, riser tension cannot be held precisely constant during floating drilling operations, and the actual tension will fluctuate about a mean value. The magnitude of fluctuation is believed to be about 15 % of the mean tension. Thus, as an example, if 100 kips is the minimum permissible tension for a riser, then the recommended setting should be 100/0.85 or 118 kips in order to make an allowance for the fluctuation. The actual tension will then be in the range 100 to 136 kips. According to Fig. 9.20, this is the calculated tension setting to minimize the riser stress for 10 %

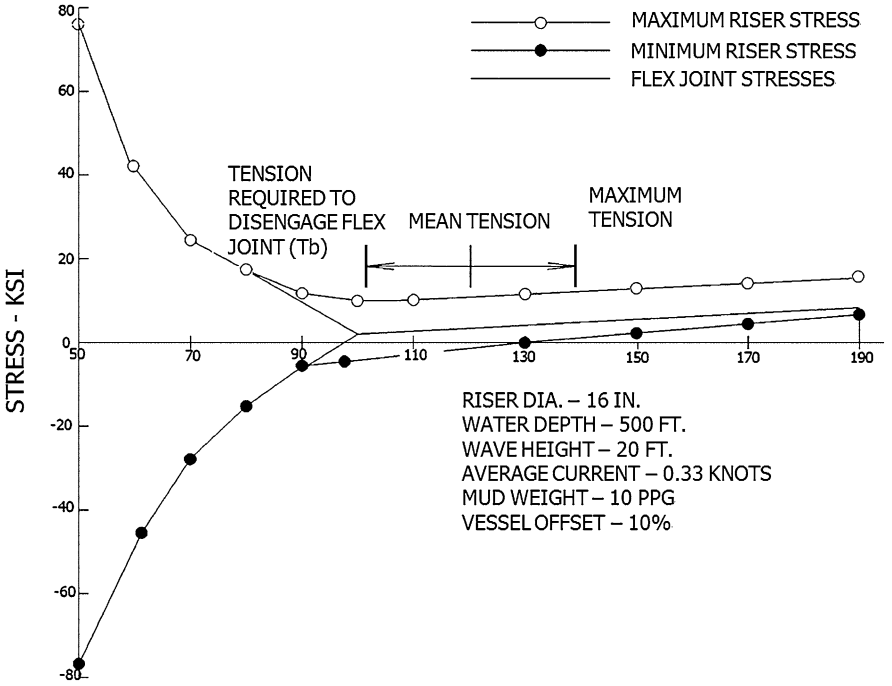

Fig. 9.20 Typical curve of stress vs applied tension of riser—nonoperational mode

offset. Lower offsets will require lower tensions using the same criterion. When setting tensions, the possibility of a partial tensioner failure can be accommodated by increases in recommended settings.

9.5.2.1 Operating Factors

Since a marine riser is sensitive to vessel offset, the influence of mooring capability and reliability plays a key part in system performance. In operating conditions, vessel offset must be such as to maintain flex joint angle below 4 degrees. In the non-operational but connected case, care must be taken to ensure that a too low tension and excessive vessel offset do not cause riser yield and permanent deformation. Figure 9.21 gives an example of the stress increase due to increasing vessel offset at constant tension. It can be seen that at 225 kips tension, the maximum riser stress increases from 11 ksi at 6 % vessel offset to 34 ksi at 10 % vessel offset. In this instance, the riser would be damaged if its material yield stresses was below 34 ksi. However, for all offsets from 3 to 10 %, the yield stress would not be exceeded if the recommended tension of 296 kips for 10 % offset is used.

The above considerations lead to three conditions that must be followed to maintain riser integrity under nonoperational but connected conditions:

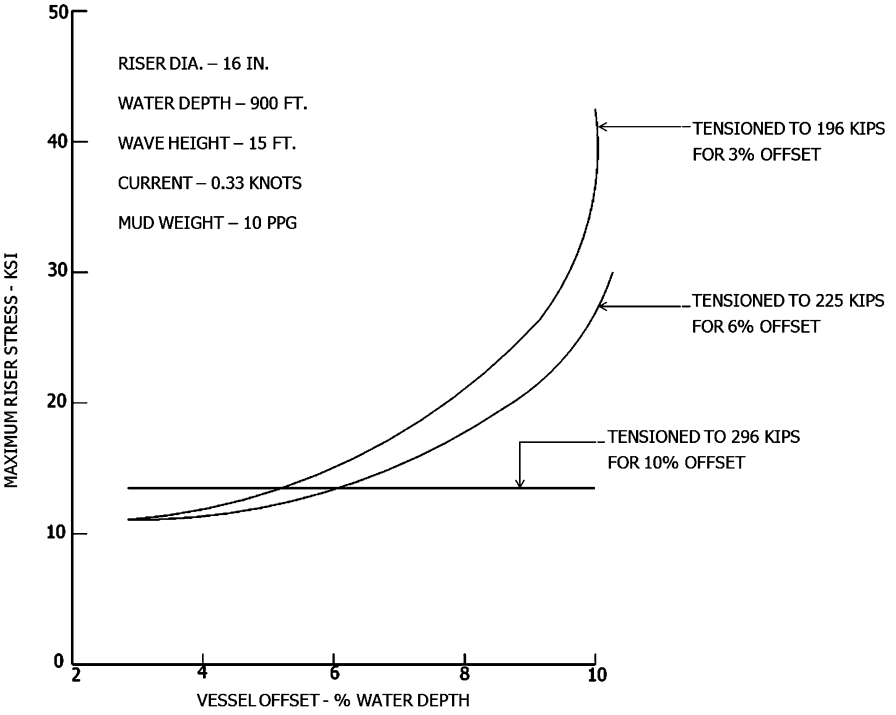

Fig. 9.21 An example of the effect of vessel offset on stress at a constant tension

(i) Setting the tension to that suitable for maximum possible offset minimizes the risk of overstressing the riser.
(ii) The capability of the vessel mooring system to limit vessel excursions under the worst anticipated conditions should be fully known.
(iii) Procedures should be devised to monitor vessel position and to manipulate the moorings so that the vessel will be held within the design offset value and such that the riser will be released prior to the design offset value being exceeded.

9.5.2.2 Operating Procedures

A marine riser can be maintained in an operable condition by ensuring that the lower flex joint angle remains below about 4 degrees. Increase of the flex joint angle above this value is often an indicator of a riser structural problem either due to a too high vessel offset or a too low top tension. The latter could arise if the current and wave forces on the riser string have been underestimated.

If the flex joint angle does go above 4 degrees, when the riser is operational, the following procedure is useful in bringing the angle down.

(i) Check vessel offset, and if it is greater than 4 %, reduce the offset by adjustment of the vessel mooring system. It may be possible to move a moored vessel (by slackening mooring lines) using the riser angle itself in water depths less than 76.20 m (250 ft).
(ii) If the flex joint angle remains above 4 degrees with vessel offset of less than 4 % of water depth, then increase the top tension from being equal to riser weight in water to a point where it exceeds the riser weight in water by 10 %. This should decrease the flex joint angle by more than 0.5 degree.
(iii) Continue to increase tension in increments of 5 to 10 % of the riser weight in water until the resultant change in lower flex joint angle is less than 10 degrees. Note that the flex joint angle will help with increasing the top tension to minimize riser stresses but it does not yield the levels of these stresses. The flex joint angle should not be used to minimize riser tension because a relatively small change in vessel offset can require significantly higher tension settings.

A sophisticated Riser Management System will advise the operator of the recommended top tension. See Sect. 9.7.

Modern work-over and production risers also employ so-called stress joints to replace the lower flex joint. The stress joint is a rigid riser section tapering from a large cross-sectional area at the riser base to the cross-section of the riser pipe at some height above the base. Stress joints are designed to take the high bending moments applied by lateral forces on the riser and its own weight and respond only by structural deflection. They, therefore, eliminate the problems of high curvature experienced in the internal bore of a flex joint but at the expense of higher local moments. The bending moment that can be applied at stress joints is usually limited by the moment that can be applied on the BOP stack. Some stress joints are made out of titanium to improve their strength to weight ratio.

9.5.3 Riser Failure Modes

The principal failure modes for risers include local material yielding and Euler column buckling (elastic instability). The probability of occurrence of these failure modes may be minimized by using analysis methods to select the appropriate riser top tension and arrangement of buoyancy modules for the prevailing operating conditions. Use of a too high tension on the riser may be indicated by excessive wear of the tensioning equipment. Insufficient tensioning leading to the onset of buckling may be indicated by large angles of rotation at the lower flex joint. Large angles of rotation at the lower flex joint may also be due to large vessel offsets.

It is important to understand the likely causes of riser failure when designing and operating a riser system. Almost inevitably, this understanding of failure causes comes from past experience. Listed below are the main failure modes for tensioned risers:

Response	Cause
1. Buckling	Failure to predict multiple curvature Failure to predict high curvature Inadequate top tension available Inadequate tensioner rate Excessive bending in free-hanging condition Failure of buoyancy modules
2. Flex Joint Damage Drill String Fatigue BOP Fatigue Damage Blowout Risk	Drill bit, collars, casing causing mechanical damage as a result of excessive flex joint angle
3. Riser/Conductor Failure	Excessive bending moment due to vessel excursion and BOP weight
4. Emergency Disconnect Failure	Excessive bending causing binding
5. Riser to Supplementary Buoy Overstressing	Out of phase dynamics of system elements
6. Conductor Pipe Failure and BOP Stack Collapse	Resonant excitation of BOP

9.6 In Service Monitoring

The minimum monitoring information required for marine riser operations comprises:

(i) surface platform heave motion;
(ii) surface platform horizontal position with respect to the wellhead; and
(iii) angle from the vertical of the riser at the lower flex joint.

This information must be continuously available to operating personnel as it warns of the possibility of riser failure. The heave motion indicator warns of excessive vertical motions that require disconnection of the riser from the wellhead. The surface vessel's position is normally indicated by an acoustic or satellite positioning system and is used to warn of excessive vessel offsets. Typically, connected risers can sustain a maximum offset of approximately 10 % of the water depth. Operations such as drilling will often require a smaller maximum offset of around 5 %. Similarly, the maximum permitted lower flex joint angle from the vertical during operations is 4 degrees. Exceedance of the lower flex joint limits on the maximum offset limit will result in failure of the riser.

It is desirable in the case of production risers (for which long-term fatigue assessment should be available) to install a comprehensive surface vessel and marine riser monitoring system. In the case of drilling risers, the use of Riser Management Systems becomes increasingly important for greater water depths.

Typical monitoring systems may acquire over 100 channels of data, which are usually analyzed and reduced to a more manageable size on site before being returned (via the internet if desired) to the design office for possible further analysis and review. These data provide valuable information on the actual behavior of the

platform and the marine riser and comparisons can be made with results predicted from calculation methods including the projected fatigue life of the riser.

In the context of monitoring a marine riser, measurements of the environmental conditions, vessel position and motions, and marine riser parameters are required.

These parameters are now explained in more detail.

(i) Environmental Conditions:

(a) Wave elevation at three points around the surface platform or a measure of wave elevation and directionality.
(b) Wind speed and direction at two locations on the surface platform.
(c) Current velocity components in two directions either relative to the vessel or in absolute terms.

(ii) Vessel Motions:

(a) Vessel mean horizontal position relative to a subsea reference point such as the wellhead.
(b) Surface platform wave-induced motions in heave, surge, sway, roll, pitch, and yaw.
(c) Surface platform mean inclination in roll and pitch together with orientation (heading).

(iii) Marine riser parameters:

(a) Riser tension.
(b) Lower flex joint angles in orthogonal directions.
(c) Subsurface motions, velocities, and accelerations of one or more segments of riser pipe.
(d) Fluid particle velocity components relative to the riser pipe at one or more pipe segments.
(e) Strains (and hence stresses) in one or more segments of the riser pipe.
(f) Wellhead fluid pressures and flow rates.
(g) Curvature of one or more segments of riser pipe.

Full-scale structural monitoring provides a means by which in-service behavior and structure maintenance programmes can be planned more effectively. There is an increasing acceptance of the fact that the initial capital cost of a structural monitoring system is likely to be small compared to the savings in maintenance cost that can be achieved by effective use of the data arising from the system.

9.7 Riser Management Systems

The simplest (and most common) approach to determine the safe operation of a riser is to conduct analysis prior to carrying out drilling operations based on expected environmental conditions (wind, wave, current), vessel and riser physical form and properties (for quasi-static and dynamic responses). Typically, this will

determine for specified riser tension safe operating envelopes of vessel lateral motion (restrained by the DP capability of the vessel), the limits of which are set by undesirable stresses, bending moments, and deflections of the riser.

This is not the optimal way of proceeding since the limits as set will generally be overly conservative because of unrealistic assumptions of the way in which the environmental forces act (for example, collinear assumed for wind, wave, and current, which is generally not so). Also there are difficulties in perfectly accurately modeling the dynamic behavior of the vessel (for example, response in a random sea).

However, by measuring environmental conditions, vessel motions, and riser motions along with tensions, mud weight, etc. it is possible to use this information within a computer model that is part of a Riser Management System (RMS) on the vessel to estimate the static and dynamic response of the riser. These estimates enable more reliable limits to be set than the former (shore-based) analysis, and as a consequence, the operability of the riser may be improved.

9.7.1 Riser Inclination and Current Profile

The quality of operational RMS calculated stress, bending moments, and deflection analysis improves with improving quality of input data. It is of course possible to measure stress directly, and such approaches are used for stress joints in workover riser arrangements. Flex joints used in drilling risers significantly remove the bending stresses where they are located.

However, there are bending stresses within the main body of the riser that can be readily inferred from the knowledge of the riser inclination. As a minimum, inclination measurements at the top and bottom are required to provide a reasonable representation.

For very deep riser applications, the influence of currents is most important. These currents can have shear in both speed and direction along the length of the riser. Just monitoring the riser angles at top and bottom, with an assumption of uniform current from the surface, will provide less accurate estimates of riser stresses than when an accurate knowledge of the current profile is available to be fed into the RMS riser analysis model, or the riser profile is available by some other form of instrumentation. Hence, the provision of Acoustic Doppler Current Profiling (ADCP) is highly recommended.

If none of the above is available, the RMS will function as intended but with a lower level of accuracy than can otherwise be achieved.

9.7.2 BPP-RMS

BPP-RMS [276] is an example of a comprehensive Riser Management System that provides for the requirements mentioned in the foregoing and provides additional capabilities.

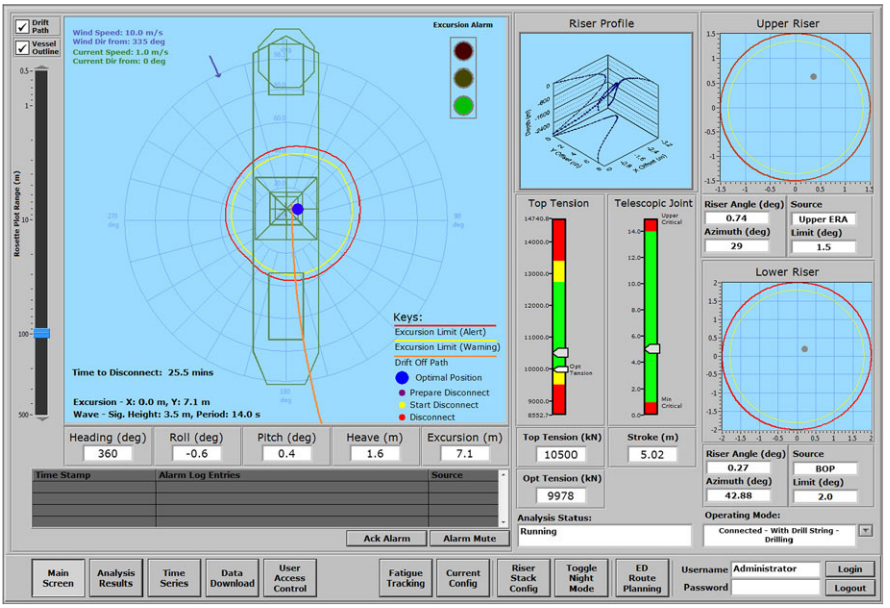

Fig. 9.22 Typical main display of BPP-RMS (Drillship)

It provides optimum position advice for the vessel, limiting the flex-joint angles and wellhead loads within preset limits. This ensures less wear of the riser and helps the operator to maximize the time available for emergency disconnect operations.

It provides real-time guidance for carrying out connected and disconnected mode drilling riser operations on board a vessel. The system combines a simple, intuitive operator's interface with a state-of-the-art numerical 3D finite element model of the riser system that is used to predict the behavior of the riser in the prevailing conditions. The main display of BPP-RMS (Drillship) is illustrated in Fig. 9.22. Its main functions are as follows:

- Integrate and display riser-related data from existing vessel systems in a consistent and operator-oriented manner;
- Compute and display the rig envelope of operation and optimum rig location in the prevailing metocean conditions;
- Compute the minimum and maximum top tension limits and the optimum top tension;
- Automatically acquire data from other relevant vessel systems where available;
- Computed data may be streamed to any desired networked system.

BPP-RMS calculates and displays the following operational guidance parameters:

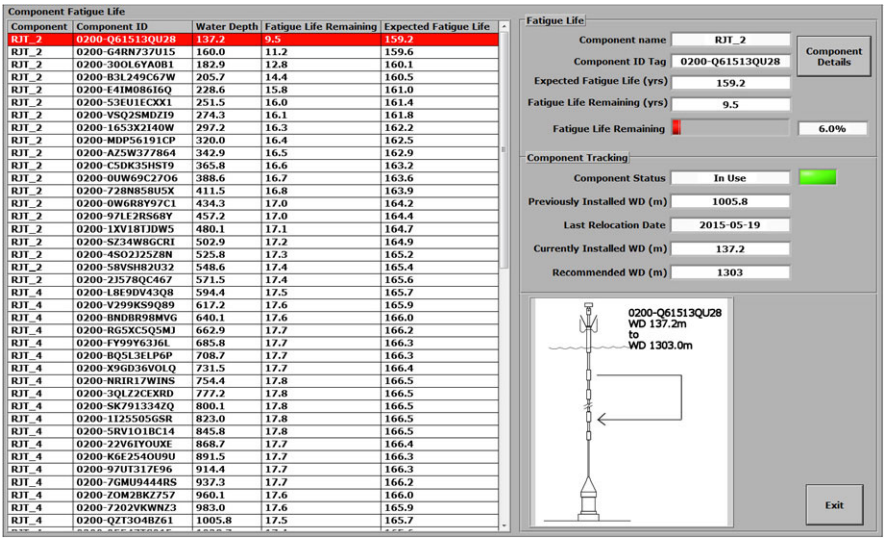

Fig. 9.23 Joint tracking page with fatigue advice (BPP-RMS)

Operational Guidance Parameters
Operating envelope for riser and vessel under prevailing metocean conditions and riser loads (top tension and internal fluid density) for connected (drilling) and connected (standby) modes of operation
Minimum stability tension (as per API-RP16Q)
Maximum tension limit under prevailing metocean conditions
Recommended total top tension under prevailing metocean conditions
Recommended vessel position under prevailing metocean conditions (based on multiple criteria)
Estimated required time to disconnect (drift off dependent)

BPP-RMS also automatically generates a detailed report file containing relevant results at regular intervals. Based on the data from the DP system and environmental sensors, the RMS provides information on the "time to go" margin before the emergency disconnect sequence has to be initiated.

9.7.3 Joint Tracking

As shown in Fig. 9.23, the primary function of the riser joint tracker is as a database containing the joint sequence for each well and the time in operation for each particular joint identified by its serial number or equivalent. These data will be exported by means of a file to the unit's maintenance system after each drilling operation. Keeping track of where in the riser string the joints have been used enables to some extent rotation of joints from well to well to avoid joints staying repeatedly in the

most loaded areas. The information can also be used in the process of inspection planning, i.e., selecting the most loaded joints as candidates for inspection.

The riser joint deployment sequence is input by the operation and stored in the database for each well in order to keep track of where the joints have been used. Joints close to the surface will experience the most fatigue loading due to direct wave loading, whereas joints in the lower part of the riser may be more prone to fatigue loading due to vortex shedding. By rotating the positioning of joints within each rating class, the wear will be distributed between the joints.

Some basic means of tracking the riser components with visual ID enables the service lives of the sections to be tracked and managed. A more sophisticated system is to use RFID tracking.

9.7.4 Wave-Induced Motion Fatigue

The wave/vessel induced motions of the riser cause stresses that contribute to fatigue damage. For each component within the riser, it is possible to estimate the fatigue damage accumulated (and hence the remaining fatigue life). This may be estimated from the dynamic model of the riser in BPP-RMS that is continuously running. This provides a constant update on fatigue lives of all joints and aids in choice of section location when running the riser (from a fatigue perspective). This is more useful than hind-casting of the fatigue that is possible by reviewing the data on shore.

The contributions of vortex-induced vibrations (VIV) to fatigue damage [277–280] can be similarly assessed running suitable VIV analytical software such as BPP-VIVALL [281–283] within the RMS. This can be supplemented by suitable instrumentation (strain or inertial based) located along the riser. The choice is dependent on operational possibilities to run connecting cables (for real-time high-rate VIV data) or to use lower-rate acoustic data transfer.

9.8 Riser Maintenance and Inspection

Each riser component, especially riser joints, must receive frequent periodic inspection and maintenance. This requires labeling and keeping records of each riser component. Visual inspections should be made each time the riser is run. Resilient seals should be inspected and replaced when necessary. Each entire joint should be inspected, particularly at the sealing areas. Damaged joints should be sent ashore for additional inspection and repair.

Annual inspections should be performed on all riser components, especially the riser joints. It is preferable, but not essential, to inspect the joints on land, under more controlled conditions than are available on a drilling vessel. Prior to inspection, the joint must be cleaned thoroughly, and it is advisable to sand blast the joints at the welds to remove the paint. All seals should be removed, and the joint visually inspected.

Welds should be inspected using a combination of the following techniques:

DYES will detect only cracks that penetrate the surface. These are low-viscosity oil-base dyes that thoroughly wet the metal and penetrate any cracks on the surface. To use dyes, the paint must be removed from the joints.

MAGNETIC PARTICLE INSPECTION will detect cracks at or near the surface. Magnetic flux density increases at discontinuities in a steel medium. The riser is magnetized, and magnetic particles are used for detection since they collect at the cracks. It is advisable to sand blast the areas around the welds prior to magnetic particle inspection.

ULTRASONIC inspection may detect cracks below the surface but may miss cracks that are isolated near the surface. Acoustic signals are very sensitive to density changes in a transmitting medium and are reflected readily by high-density discontinuities such as steel and air or steel and water. The transmitter and receiver are both run inside of the riser; thus paint, flotation material, or air cans do not have to be removed for inspection.

X-RAY inspections are for internal cracks and may miss cracks at the surface. X-ray techniques depend on radiation absorption and must be used on the bare riser only.

ACPD (alternating current potential difference) inspection devices detect the increased drop in electrical potential associated with the increased surface path length as a result of a crack.

No single-inspection technique will find all the cracks that may exist, however, dyes and magnetic particle inspections are the most popular. The decrease in catastrophic failures of risers can be attributed in part to improved riser inspection techniques. After the welds have been thoroughly inspected, the riser should be repaired, and the seals replaced.

Proper handling techniques for tubular goods apply to risers. The connector pin should be protected when not in use. Only lift subs that are designed for the riser should be used. Hard banding on drill pipe will cause unnecessary wear to the riser and BOPs and should not be used on a drilling vessel.

High standards of material quality and construction are used in the manufacture of risers. Under no circumstances should field welding on the riser be permitted.

The position of riser joints along the length of the riser should be rotated periodically. This ensures that the service conditions for each joint are evenly distributed and that no individual riser joint is continuously subjected to a highly loaded part of the riser.

9.9 Conclusion

In this chapter, we have investigated vertical riser operations from principally floating offshore structures. For these the pipe connections (the riser) between surface facilities and seabed are for transportation of oil and gas, as well as drilling and workover operations. Analysis methods for vertical marine risers under the influences of both internal and external forces have been described. Sophisticated riser

analysis tools have been developed which enable operations in ultra-deep waters, often with complex and difficult currents. Operators are increasingly appreciating the benefits that Riser Management Systems offer for improved operability, increased service lives of risers, and importantly as an aid for improving safety. Four modes of operation that marine risers may experience have been introduced, namely free-hanging, connected, operational, and non-operational but connected modes. It has been considered that typically a marine drilling riser can be maintained in an operable condition by ensuring that the lower flex joint angle remains below about 4 degrees (depending on particular flex joint design). Three operating procedures are described which may be used to reduce this angle. Marine riser monitoring systems provide information on the behaviors of the platform, and the marine riser. By additionally using a suitable analytical model of the riser dynamics within these it is possible to estimate the expended fatigue life of the riser. BPP-RMS, an example of such a comprehensive Riser Management System (RMS) for riser maintenance and inspection, has been presented. It is a state-of-the-art on-board riser operation management system that provides real-time guidance for carrying out connected and disconnected mode riser operations on board drilling and workover vessels.

Chapter 10
Conclusions

The book has been dedicated to the modeling and control design of the marine mechanical systems subjected to the environmental disturbances. The results of the research work conducted in this book are summarized in each chapter, and the contributions made are reviewed. The key results are listed as follows.

In Chap. 3, stable adaptive neural-based positioning control has been designed for installation of subsea structure with attached thrusters in the presence of time-varying environmental disturbances and parametric uncertainties. The main contributions are: (i) the full-state and output feedback adaptive neural control design to generate surge, sway, and yaw control commands for subsea positioning in presence of parametric uncertainties and disturbances, (ii) the rigorous stability analysis via backstepping and Lyapunov synthesis to demonstrate the semiglobal uniform boundedness of the tracking error, and (iii) the investigation on the effects of a time-varying current on the proposed control in comparison with different control methods that do not compensate the current explicitly or generally assume ocean currents to be constant. Simulation results have demonstrated that the adaptive neural control is robust and effective in reducing the tracking error for the subsea installation operation.

In Chap. 4, the model of the coupled vessel, crane, cable, and payload with uniform and nonuniform parameters has been presented. The contributions in the study of the coupled system are (i) the coupled modeling of the vessel, crane, flexible cable, and subsea payload where nonuniformity, parametric uncertainties, and distributed disturbances are admissible in the PDE model of the cable. The cable under consideration need not be uniform, and the tension can be a function of both transverse gradient and axial coordinate, (ii) the design of positioning control using symmetric barrier Lyapunov functions (SBLFs) and stability analysis of the coupled system. Through Lyapunov synthesis, we have ensured that the coupled system is stable, the physical safety limits are not transgressed, and simultaneous positioning of the crane and payload is achieved, and (iii) design of the stabilizing boundary control via Lyapunov synthesis when nonuniformity in the flexible cable is considered. Through rigorous stability analysis, the uniform boundedness of the coupled system

W. He et al., *Dynamics and Control of Mechanical Systems in Offshore Engineering*, Advances in Industrial Control, DOI 10.1007/978-1-4471-5337-5_10,

is demonstrated when excited by the distributed environment load. The performance of the proposed control has been illustrated through numerical simulations.

In Chap. 5, both position control and vibration suppression have been considered for a flexible marine installation system. Two cases for the flexible marine installation system are studied: (i) exact model-based control and (ii) adaptive control for the system parametric uncertainty. For the first case, a boundary controller has been introduced for the exact model of the installation system. For second case where the system parameters cannot be directly measured, to fully compensate the effect of unknown system parameters, a signum term and an auxiliary signal term have been introduced to develop a robust adaptive boundary control law. Both types of boundary control have been designed based on the original infinite-dimensional model (PDE), and thus the spillover instability phenomenon has been eliminated. All the signals of the closed-loop system have been proved to be uniformly bounded by using the Lyapunov direct method. The proposed schemes have offered implementable design procedures for the control of marine installation systems since all the signals in the control can be measured by sensors or calculated by a backward difference algorithm. The main contributions include: (i) the mathematical model of the marine installation system has been described as a nonhomogeneous hyperbolic PDE; and (ii) two implementable boundary controllers at the top and bottom boundary of the cable have been designed to position the subsea payload to the desired set-point and suppress the cable's vibration.

In Chap. 6, both state feedback and output feedback control have been designed for thruster-assisted single-point mooring systems with unknown backlash-like hysteresis in thruster dynamics. The backlash-like hysteresis has been transformed into a liner term plus a bounded nonlinear term, and then an effective full-state feedback control has been proposed via backstepping design. The main contributions of this chapter can be summarized as follows: (i) in the presence of both uncertainties and unknown backlash-like hysteresis nonlinearities, robust adaptive full-state feedback has been presented via backstepping design, and all signals of the closed-loop system are semiglobally uniformly ultimately bounded; (ii) an observer has been constructed to estimate the unmeasurable velocity vector of the single-point mooring system, where high-order neural network (HONN) is employed to approximate the unknown nonlinear functions; and (iii) by using the previous HONN-based observer, adaptive output feedback control has been proposed via backstepping design for the case where the velocity vector of a single-point mooring system is unmeasurable.

In Chap. 7, we have studied the vibration problems of a coupled nonlinear marine flexible riser subjected to the ocean disturbances. The riser system is modeled as a nonlinear PDE system via the Hamilton principle. The difficulty of the control of the nonlinear PDE system lies in the couplings between the transverse and longitudinal vibrations. To overcome this difficulty, we have developed the boundary control with two actuators in transverse and longitudinal directions based on the distributed-parameter system model, and the problems associated with traditional truncated-model-based design are overcome. With the proposed control, uniform boundedness under the ocean current disturbances and exponential stability under free vibration

condition have been theoretically proved based on the Lyapunov direct method. The control is easy to implement since it is independent of the system parameters and only two sensors and actuators are required. The main contributions are: (i) the coupled nonlinear dynamic model of the marine flexible riser for transverse and longitudinal vibrations reduction has been formulated; and (ii) the implementable boundary control with two actuators in transverse and longitudinal directions has been designed to reduce both transverse and longitudinal vibrations of the marine flexible riser.

In Chap. 8, robust adaptive boundary control for a flexible marine riser with vessel dynamics has been designed to suppress the riser's vibration. To provide an accurate and concise representation of the riser's dynamic behavior, the flexible marine riser with vessel dynamics has been described by a distributed parameter system with a partial differential equation (PDE) and four ordinary differential equations (ODEs). Two cases have been investigated: (i) exact model-based control and (ii) robust adaptive control for the system parametric uncertainty. Robust boundary control has been proposed based on the exact model of the riser system, and adaptive control has been designed to compensate the system parametric uncertainty. With the proposed control, closed-looped stability under the external disturbances has been proven by using the Lyapunov direct method. The state of the system is proven to converge to a small neighborhood of zero by appropriately choosing design parameters. The main contributions are: (i) the model of the marine flexible riser with vessel dynamics has been formulated; and (ii) robust adaptive boundary control at the top boundary of the riser has been developed to suppress the riser's vibration.

In Chap. 9, we have investigated riser structural analysis, riser operations, and riser management systems. The main contributions are summarized as (i) the analysis of vertical marine risers under the influences of both internal and external forces have been described; (ii) four configurations of the marine risers have been introduced; (iii) three operating procedures have been given to bring the angle down; and (iv) BPP-RMS, an example of the comprehensive Riser Management System (RMS) for riser maintenance and inspection, has been presented.

References

1. Rowe S, Mackenzie B, Snell R (2001) Deep water installation of subsea hardware. In: Proceedings of the 10th offshore symposium
2. Eastaugh P (2005) Wideband wins the day at Ormen Lange, subsea special offshore engineer, pp 32–34
3. Kaewunruen S, Chiravatchradj J, Chucheepsakul S (2005) Nonlinear free vibrations of marine risers/pipes transport fluid. Ocean Eng 32(3–4):417–440
4. How BVE, Ge SS, Choo YS (2009) Active control of flexible marine risers. J Sound Vib 320:758–776
5. Rustad AM (2007) Modeling and control of top tensioned risers. PhD thesis, Norwegian University of Science and Technology
6. Huse E (1993) Interaction in deep-sea riser arrays. In: The 25th annual offshore technology conference, Houston, TX, pp 313–322
7. How BVE, Ge SS, Choo YS (2010) Dynamic load positioning for subsea installation via adaptive neural control. IEEE J Ocean Eng 35(2):366–375
8. How BVE, Ge SS, Choo YS (2011) Control of coupled vessel, crane, cable, and payload dynamics for subsea installation operations. IEEE Trans Control Syst Technol 19(1):208–220
9. He W, Ge SS, Zhang S (2011) Adaptive boundary control of a flexible marine installation system. Automatica 47(12):2728–2734
10. Van Amerongen J (1984) Adaptive steering of ships—a model reference approach. Automatica 20(1):3–14
11. Sorensen A, Sagatun S, Fossen T (1996) Design of a dynamic positioning system using model-based control. Control Eng Pract 4(3):359–368
12. Fossen T, Grovlen A (1998) Nonlinear output feedback control of dynamically positioned ships using vectorial observer backstepping. IEEE Trans Control Syst Technol 6(1):121–128
13. Ghommam J, Mnif F, Benali A, Derbel N (2006) Asymptotic backstepping stabilization of an underactuated surface vessel. IEEE Trans Control Syst Technol 14(6):1150–1157
14. Tee KP, Ge SS (2006) Control of fully actuated ocean surface vessels using a class of feedforward approximators. IEEE Trans Control Syst Technol 14:750–756
15. Nguyen T, Sorensen A, Tong Quek S (2007) Design of hybrid controller for dynamic positioning from calm to extreme sea conditions. Automatica 43(5):768–785
16. Suzuki H, Tao Q, Yoshida K (2002) Automatic installation of underwater elastic structures under unknown currents. In: Proceedings of 1998 international symposium on underwater technology. IEEE, New York, pp 274–281
17. Watanabe K, Suzuki H, Qi T, Toshida K (1998) Basic research on underwater docking of flexible structures. In: Proceedings of IEEE international conference on robotics and automation, vol 1. IEEE, New York, pp 458–463

W. He et al., *Dynamics and Control of Mechanical Systems in Offshore Engineering*, Advances in Industrial Control, DOI 10.1007/978-1-4471-5337-5,

18. How BVE (2009) Modeling and control of subsea installation. PhD thesis, National University of Singapore
19. Ge SS, He W, Ren B, Choo YS (2010) Boundary control of a flexible marine installation system. In: Proceedings of the 49th IEEE conference on decision and control, Atlanta, GA, vol 1, pp 2590–2595
20. He W (2011) Modeling and control of marine flexible systems. PhD thesis, National University of Singapore
21. Fung P, Grimble M (1983) Dynamic ship positioning using a self-tuning Kalman filter. IEEE Trans Autom Control 28(3):339–350
22. Saelid S, Jenssen N, Balchen J (1983) Design and analysis of a dynamic positioning system based on Kalman filtering and optimal control. IEEE Trans Autom Control 28(3):331–339
23. Robertsson A, Johansson R (1998) Comments on "Nonlinear output feedback control of dynamically positioned ships using vectorial observer backstepping". IEEE Trans Control Syst Technol 6(3):439–441
24. Fossen TI, Strand JP (1999) Passive nonlinear observer design for ships using Lyapunov methods: full-scale experiments with as supply vessel. Automatica 35(1):3–16
25. Fossen TI, Strand JP (2001) Nonlinear passive weather optimal positioning control (WOPC) system for ships and rigs: experimental results. Automatica 37(5):701–715
26. Do KD, Jiang ZP, Pan J (2005) Global partial-state feedback and output-feedback tracking controllers for underactuated ships. Syst Control Lett 54(10):1015–1036
27. Do KD, Pan J (2006) Underactuated ships follow smooth paths with integral actions and without velocity measurements for feedback: theory and experiments. IEEE Trans Control Syst Technol 14(2):308–322
28. Do KD, Pan J (2009) Control of ships and underwater vehicles: design for underactuated and nonlinear marine systems. Springer, New York
29. Leira BJ, Sorensen AJ, Larsen CM (2004) A reliability-based control algorithm for dynamic positioning of floating vessels. Struct Saf 26(1):1–28
30. Aamo O, Fossen T (1999) Controlling line tension in thruster assisted mooring systems. In: Proceedings of the IEEE international conference on control applications, Hawaii, US, vol 2, pp 1009–1104
31. Berntsen P, Aamo O, Leira B (2009) Ensuring mooring line integrity by dynamic positioning: controller design and experimental tests. Automatica 45(5):1285–1290
32. Nguyen DT, Sorensen AJ (2009) Switching control for thruster-assisted position mooring. Control Eng Pract 17(9):985–994
33. Nguyen DT, Sorensen AJ (2009) Setpoint chasing for thruster-assisted position mooring. IEEE J Ocean Eng 34(4):548–558
34. Nguyen DH, Nguyen DT, Quek S, Sorensen A (2010) Control of marine riser end angles by position mooring. Control Eng Pract 18(9):1013–1021
35. Aamo O, Fossen T (2001) Finite element modelling of moored vessels. Math Comput Model Dyn Syst 7(1):47–75
36. Sorensen AJ, Strand JP, Fossen TI (1999) Thruster assisted position mooring system for turret-anchored FPSOs. In: Proceedings of the 1999 IEEE international conference on control applications, vol 2
37. Dai S-L, Wang C, Luo F (2012) Identification and learning control of ocean surface ship using neural networks. IEEE Trans Ind Inform 8(34):801–810
38. Cui R, Ge SS, How VEB, Choo YS (2010) Leader-follower formation control of underactuated autonomous underwater vehicles. Ocean Eng 37(17):1491–1502
39. Berntsen PIB, Aamo OM, Leira BJ, Sørensen AJ (2008) Structural reliability-based control of moored interconnected structures. Control Eng Pract 16(4):495–504
40. Chen M, Ge SS, How BVE, Choo YS (2012) Robust adaptive position mooring control for marine vessels. IEEE Trans Control Syst Technol 99:1–15
41. Huang T, Chucheepsakul S (1985) Large displacement analysis of a marine riser. J Energy Resour Technol 107:54

42. Bernitsas M, Kokarakis J, Imron A (1985) Large deformation three-dimensional static analysis of deep water marine risers. Appl Ocean Res 7(4):178–187
43. Huang T, Kang Q (1991) Three dimensional analysis of a marine riser with large displacements. Int J Offshore Polar Eng 1(4):300–306
44. Patel M, Jesudasen A (1987) Theory and model tests for the dynamic response of free hanging risers. J Sound Vib 112(1):149–166
45. Young RD, Fowler JR, Fisher EA, Luke RR (1978) Dynamic analysis as an aid to the design of marine risers. J Press Vessel Technol 100:200–205
46. Aldraihem O, Wetherhold R, Singh T (1997) Distributed control of laminated beams: Timoshenko theory vs Euler–Bernoulli theory. J Intell Mater Syst Struct 8(2):149
47. Do K, Pan J (2009) Boundary control of three-dimensional inextensible marine risers. J Sound Vib 327(3–5):299–321
48. Do K, Pan J (2008) Boundary control of transverse motion of marine risers with actuator dynamics. J Sound Vib 318(4–5):768–791
49. Ge SS, He W, How BVE, Choo YS (2010) Boundary control of a coupled nonlinear flexible marine riser. IEEE Trans Control Syst Technol 18(5):1080–1091
50. He W, Ge SS, How BVE, Choo YS, Hong K-S (2011) Robust adaptive boundary control of a flexible marine riser with vessel dynamics. Automatica 47(4):722–732
51. He W, How BVE, Ge SS, Choo YS (2010) Boundary control of a flexible marine riser with vessel dynamics. In: Proceedings of the American control conference, Baltimore, MD, pp 1532–1537
52. Logan JD (2006) Applied mathematics, 3rd edn. Wiley, New York
53. Balas MJ (1978) Feedback control of flexible systems. IEEE Trans Autom Control 23:673–679
54. Vandegrift MW, Lewis FL, Zhu SQ (1994) Flexible-link robot arm control by a feedback linearization/singular perturbation approach. J Robot Syst 11(7):591–603
55. Lin J, Lewis FL (1994) Enhanced measurement and estimation methodology for flexible link arm control. J Robot Syst 11(5):367–385
56. Lin J, Lewis FL (1994) A symbolic formulation of dynamic equations for a manipulator with rigid and flexible links. Int J Robot Res 13(5):454
57. Armaou A, Christofides P (2000) Wave suppression by nonlinear finite-dimensional control. Chem Eng Sci 55(14):2627–2640
58. Christofides P, Armaou A (2000) Global stabilization of the Kuramoto–Sivashinsky equation via distributed output feedback control. Syst Control Lett 39(4):283–294
59. Sakawa Y, Matsuno F, Fukushima S (1985) Modeling and feedback control of a flexible arm. J Robot Syst 2(4):453–472
60. Ge SS, Lee TH, Zhu G (1997) A nonlinear feedback controller for a single-link flexible manipulator based on a finite element model. J Robot Syst 14(3):165–178
61. Ge SS, Lee TH, Zhu G (1997) Non-model-based position control of a planar multi-link flexible robot. Mech Syst Signal Process 11(5):707–724
62. Slotine J, Li W (1991) Applied nonlinear control. Prentice Hall, Englewood Cliffs
63. Krstic M, Kanellakopoulos I, Kokotovic P (1995) Nonlinear and adaptive control design. Wiley, New York
64. Ge SS, Lee TH, Harris CJ (1998) Adaptive neural network control of robotic manipulators. World Scientific, London
65. Ge SS, Hang CC, Lee TH, Zhang T (2001) Stable adaptive neural network control. Kluwer Academic, Boston
66. Khalil HK (2002) Nonlinear systems. Prentice Hall, New Jersey
67. Ge SS, Lee TH, Zhu G (1998) Improving regulation of a single-link flexible manipulator with strain feedback. IEEE Trans Robot Autom 14(1):179–185
68. Balas MJ (1978) Active control of flexible systems. J Optim Theory Appl 25:415–436
69. Meirovitch L, Baruh H (1983) On the problem of observation spillover in self-adjoint distributed systems. J Optim Theory Appl 30(2):269–291

70. Ge SS, Lee TH, Zhu G, Hong F (2001) Variable structure control of a distributed parameter flexible beam. J Robot Syst 18:17–27
71. Zhu G, Ge SS (1998) A quasi-tracking approach for finite-time control of a mass-beam system. Automatica 34(7):881–888
72. Ge SS, Lee TH, Zhu G (1996) Energy-based robust controller design for multi-link flexible robots. Mechatronics 6(7):779–798
73. Lee TH, Ge SS, Wang Z (2001) Adaptive robust controller design for multi-link flexible robots. Mechatronics 11(8):951–967
74. Ge SS, Lee TH, Wang Z (2001) Model-free regulation of multi-link smart materials robots. IEEE/ASME Trans Mechatron 6(3):346–351
75. Bentsman J, Hong K-S (1991) Vibrational stabilization of nonlinear parabolic systems with Neumann boundary conditions. IEEE Trans Autom Control 36(4):501–507
76. Bentsman J, Hong K-S, Fakhfakh J (1991) Vibrational control of nonlinear time lag systems: vibrational stabilization and transient behavior. Automatica 27(3):491–500
77. Bentsman J, Hong K-S (1993) Transient behavior analysis of vibrationally controlled nonlinear parabolic systems with Neumann boundary conditions. IEEE Trans Autom Control 38(10):1603–1607
78. Hong K-S, Bentsman J (1994) Direct adaptive control of parabolic systems: algorithm synthesis and convergence and stability analysis. IEEE Trans Autom Control 39(10):2018–2033
79. Hong K-S, Bentsman J (1994) Application of averaging method for integro-differential equations to model reference adaptive control of parabolic systems. Automatica 30(9):1415–1419
80. Yang K-J, Hong K-S, Matsuno F (2004) Robust adaptive boundary control of an axially moving string under a spatiotemporally varying tension. J Sound Vib 273(4–5):1007–1029
81. Nguyen QC, Hong K-S (2010) Asymptotic stabilization of a nonlinear axially moving string by adaptive boundary control. J Sound Vib 329(22):4588–4603
82. Nguyen QC, Hong K-S (2012) Simultaneous control of longitudinal and transverse vibrations of an axially moving string with velocity tracking. J Sound Vib 331(13):3006–3019
83. Bamieh B, Paganini F, Dahleh M (2002) Distributed control of spatially invariant systems. IEEE Trans Autom Control 47(7):1091–1107
84. Wu F (2003) Distributed control for interconnected linear parameter-dependent systems. IEE Proc, Control Theory Appl 150:518
85. Banks H, Smith R, Wang Y (1997) Smart material structures: modeling, estimation, and control. Wiley, New York
86. Ge SS, Lee TH, Gong J, Wang Z (2000) Model-free controller design for a single-link flexible smart materials robot. Int J Control 73(6):531–544
87. Ge SS, Lee TH, Gong JQ (1999) A robust distributed controller of a single-link SCARA/Cartesian smart materials robot. Mechatronics 9(1):65–93
88. Rahn CD (2001) Mechatronic control of distributed noise and vibration. Springer, New York
89. Ge SS, Lee TH, Zhu G (1996) Genetic algorithm tuning of Lyapunov-based controllers: an application to a single-link flexible robot system. IEEE Trans Ind Electron 43(5):567–574
90. Ge SS, Lee TH, Zhu G (1998) Asymptotically stable end-point regulation of a flexible SCARA/Cartesian robot. IEEE/ASME Trans Mechatron 3(2):138–144
91. Morgul O (1990) Control and stabilization of a flexible beam attached to a rigid body. Int J Control 51(1):11–31
92. Morgul O (1991) Orientation and stabilization of a flexible beam attached to a rigid body: planar motion. IEEE Trans Autom Control 36(8):953–962
93. Morgul O (1992) Dynamic boundary control of a Euler–Bernoulli beam. IEEE Trans Autom Control 37(5):639–642
94. Morgul O, Rao B, Conrad F (2002) On the stabilization of a cable with a tip mass. IEEE Trans Autom Control 39(10):2140–2145
95. Morgul O (1994) A dynamic control law for the wave equation. Automatica 30(11):1785–1792
96. Morgul O (1994) Control and stabilization of a rotating flexible structure. Automatica 30(2):351–356

97. Geniele H, Patel R, Khorasani K (1997) End-point control of a flexible-link manipulator: theory and experiments. IEEE Trans Control Syst Technol 5(6):556–570
98. Qu Z (2001) Robust and adaptive boundary control of a stretched string on a moving transporter. IEEE Trans Autom Control 46(3):470–476
99. Qu Z (2002) An iterative learning algorithm for boundary control of a stretched moving string. Automatica 38(5):821–827
100. Qu Z, Xu J (2002) Model-based learning controls and their comparisons using Lyapunov direct method. Asian J Control 4(1):99–110
101. Rahn C, Zhang F, Joshi S, Dawson D (1999) Asymptotically stabilizing angle feedback for a flexible cable gantry crane. J Dyn Syst Meas Control 121:563–565
102. Baicu CF, Rahn CD, Nibali BD (1996) Active boundary control of elastic cables: theory and experiment. J Sound Vib 198:17–26
103. Shahruz SM, Krishna LG (1996) Boundary control of a nonlinear string. J Sound Vib 195:169–174
104. Hu J (1999) Active impedance control of linear one-dimensional wave equations. Int J Control 72(3):247–257
105. Fung RF, Tseng CC (1999) Boundary control of an axially moving string via Lyapunov method. J Dyn Syst Meas Control 121:105–110
106. Fard M, Sagatun S (2001) Exponential stabilization of a transversely vibrating beam via boundary control. J Sound Vib 240(4):613–622
107. Fard M, Sagatun S (2001) Exponential stabilization of a transversely vibrating beam by boundary control via Lyapunov's direct method. J Dyn Syst Meas Control 123:195–200
108. Choi J-Y, Hong K-S, Yang K-J (2004) Exponential stabilization of an axially moving tensioned strip by passive damping and boundary control. J Vib Control 10(5):661
109. Yang K-J, Hong K-S, Matsuno F (2005) Boundary control of a translating tensioned beam with varying speed. IEEE/ASME Trans Mechatron 10(5):594–597
110. Yang K-J, Hong K-S, Matsuno F (2005) Robust boundary control of an axially moving string by using a PR transfer function. IEEE Trans Autom Control 50(12):2053–2058
111. Yang K-J, Hong K-S, Matsuno F (2005) Energy-based control of axially translating beams: varying tension, varying speed, and disturbance adaptation. IEEE Trans Control Syst Technol 13(6):1045–1054
112. Kim C-S, Hong K-S (2009) Boundary control of container cranes from the perspective of controlling an axially moving string system. Int J Control Autom Syst 7(3):437–445
113. Ngo QH, Hong K-S (2009) Skew control of a quay container crane. J Mech Sci Technol 23(12):3332–3339
114. Krstic M, Smyshlyaev A (2008) Boundary control of PDEs: a course on backstepping designs. SIAM, Philadelphia
115. Li T, Hou Z (2006) Exponential stabilization of an axially moving string with geometrical nonlinearity by linear boundary feedback. J Sound Vib 296(4–5):861–870
116. Li T, Hou Z, Li J (2008) Stabilization analysis of a generalized nonlinear axially moving string by boundary velocity feedback. Automatica 44(2):498–503
117. Mahmood IA, Moheimani SOR, Bhikkaji B (2008) Precise tip positioning of a flexible manipulator using resonant control. IEEE/ASME Trans Mechatron 13(2):180–186
118. Pereira E, Aphale SS, Feliu V, Moheimani SOR (2010) Integral resonant control for vibration damping and precise tip-positioning of a single-link flexible manipulator. IEEE/ASME Trans Mechatron 99:1–9
119. Halim D, Moheimani SOR (2001) Spatial resonant control of flexible structures-application to a piezoelectric laminate beam. IEEE Trans Control Syst Technol 9(1):37–53
120. Endo K, Matsuno F, Kawasaki H (2009) Simple boundary cooperative control of two one-link flexible arms for grasping. IEEE Trans Autom Control 54(10):2470–2476
121. He W, Ge SS (2012) Robust adaptive boundary control of a vibrating string under unknown time-varying disturbance. IEEE Trans Control Syst Technol 20(1):48–58
122. He W, Ge SS, Hang CC, Hong K-S (2010) Boundary control of a vibrating string under unknown time-varying disturbance. In: The 49th IEEE conference on decision and control, Atlanta, GA, pp 2584–2589

123. Zhang S, Ge SS, He W, Hong K-S (2011) Modeling and control of a nonuniform vibrating string under spatiotemporally varying tension and disturbance. In: Proceedings of the IFAC world congress, Milano, Italy, pp 7678–7683
124. Ge SS, He W, Zhang S (2012) Modeling and control of a flexible riser with application to marine installation. In: Proceedings of the 2012 American control conference, Montreal, Canada, pp 664–669
125. He W, Zhang S, Ge SS (2012) Boundary output-feedback stabilization of a Timoshenko beam using disturbance observer. IEEE Trans Ind Electron 60(11):5186–5194
126. Ge SS, Zhang S, He W (2011) Vibration control of a coupled nonlinear string system in transverse and longitudinal directions. In: Proceedings of the 50th IEEE conference on decision and control and European control conference (CDC-ECC), Orlando, FL, vol 1, pp 3742–3747
127. de Queiroz MS, Rahn CD (2002) Boundary control of vibration and noise in distributed parameter systems: an overview. Mech Syst Signal Process 16:19–38
128. Baz A (1997) Dynamic boundary control of beams using active constrained layer damping. Mech Syst Signal Process 11(6):811–825
129. Tanaka N, Iwamoto H (2007) Active boundary control of an Euler–Bernoulli beam for generating vibration-free state. J Sound Vib 304:570–586
130. Zhang S, He W, Ge SS (2012) Modeling and control of a nonuniform vibrating string under spatiotemporally varying tension and disturbance. IEEE/ASME Trans Mechatron 17(6):1196–1203
131. Ge SS, Zhang S, He W (2011) Vibration control of an Euler–Bernoulli beam under unknown spatiotemporally varying disturbance. Int J Control 84(5):947–960
132. He W, Ge SS, Zhang S (2012) Modeling and control design for a multi-cable mooring system. In: Proceedings of the Chinese control conference, Hefei, China, pp 1285–1290
133. Krstic M (2009) Delay compensation for nonlinear, adaptive, and PDE systems. Birkhauser, Boston
134. Smyshlyaev A, Krstic M (2010) Adaptive control of parabolic PDEs. Princeton University Press, New Jersey
135. Vazquez R, Krstic M (2008) Control of 1-d parabolic PDEs with Volterra nonlinearities, part I: design. Automatica 44(11):2778–2790
136. Vazquez R, Krstic M (2008) Control of 1D parabolic PDEs with Volterra nonlinearities, part II: analysis. Automatica 44(11):2791–2803
137. Krstic M, Siranosian A, Balogh A, Guo B (2007) Control of strings and flexible beams by backstepping boundary control. In: Proceedings of the 2007 American control conference, pp 882–887
138. Krstic M (2008) Optimal adaptive control-contradiction in terms or a matter of choosing the right cost functional? IEEE Trans Autom Control 53(8):1942–1947
139. Krstic M, Smyshlyaev A (2008) Backstepping boundary control for first-order hyperbolic PDEs and application to systems with actuator and sensor delays. Syst Control Lett 57(9):750–758
140. Smyshlyaev A, Guo B, Krstic M (2009) Arbitrary decay rate for Euler-Bernoulli beam by backstepping boundary feedback. IEEE Trans Autom Control 54(5):1135
141. Krstic M, Smyshlyaev A (2008) Adaptive control of PDEs. Annu Rev Control 32(2):149–160
142. Krstic M, Smyshlyaev A (2008) Adaptive boundary control for unstable parabolic PDEs, part I: Lyapunov design. IEEE Trans Autom Control 53(7):1575
143. Smyshlyaev A, Krstic M (2007) Adaptive boundary control for unstable parabolic PDEs, part II: estimation-based designs. Automatica 43(9):1543–1556
144. Smyshlyaev A, Krstic M (2007) Adaptive boundary control for unstable parabolic PDEs, part III: output feedback examples with swapping identifiers. Automatica 43(9):1557–1564

145. Guo B, Guo W (2009) The strong stabilization of a one-dimensional wave equation by non-collocated dynamic boundary feedback control. Automatica 45(3):790–797
146. Huang D, Xu J-X (2011) Steady-state iterative learning control for a class of nonlinear pde processes. J Process Control 21(8):1155–1163
147. Luo Z, Guo B-Z, Morgul O (1999) Stability and stabilization of infinite dimensional systems with applications. Springer, London
148. Sakawa Y, Luo Z (1989) Modeling and control of coupled bending and torsional vibrations of flexible beams. IEEE Trans Autom Control 34(9):970–977
149. Luo Z (1993) Direct strain feedback control of flexible robot arms: new theoretical and experimental results. IEEE Trans Autom Control 38(11):1610–1622
150. Luo Z, Guo B-Z (1995) Further theoretical results on direct strain feedback control of flexible robot arms. IEEE Trans Autom Control 40(4):747–751
151. Luo Z, Kitamura N, Guo B-Z (1995) Shear force feedback control of flexible robot arms. IEEE Trans Robot Autom 11(5):760–765
152. Guo B-Z, Shao Z-C (2009) Stabilization of an abstract second order system with application to wave equations under non-collocated control and observations. Syst Control Lett 58(5):334–341
153. Guo B-Z, Xu C-Z (2007) The stabilization of a one-dimensional wave equation by boundary feedback with noncollocated observation. IEEE Trans Autom Control 52(2):371–377
154. Nguyen TD (2008) Second-order observers for second-order distributed parameter systems in R^2. Syst Control Lett 57(10):787–795
155. Nguyen TD (2009) Boundary output feedback of second-order distributed parameter systems. Syst Control Lett 58(7):519–528
156. Curtain R, Zwart H (1995) An introduction to infinite-dimensional linear systems theory. Springer, New York
157. Pazy A (1983) Semigroups of linear operators and applications to partial differential equations. Springer, New York
158. Bensoussan A, Prato G, Delfour M, Mitter S (2007) Representation and control of infinite dimensional systems
159. Guo B-Z, Jin F-F (2010) Arbitrary decay rate for two connected strings with joint anti-damping by boundary output feedback. Automatica 46(7):1203–1209
160. Suzuki H, Tao Q, Yoshida K (1998) Automatic installation of underwater elastic structures under unknown currents. In: Proceedings of the international symposium on underwater technology, vol 14, pp 274–281
161. Watanabe K, Suzuki H, Tao Q, Yoshida K (1998) Basis research on underwater docking of flexible structures. In: IEEE international conference on robotics and automation, pp 458–463
162. Hover F (1993) Experiments in dynamic positioning of a towed pipe. In: Proceedings of engineering in harmony with the ocean. IEEE, New York, pp 484–490
163. Cybenko G (1989) Approximation by superpositions of a sigmoidal function. Math Control Signals Syst 2(4):303–314
164. Khanna T (1990) Foundations of neural networks
165. Funahashi K (1989) On the approximate realization of continuous mappings by neural networks. Neural Netw 2(3):183–192
166. Hornik K, Stinchcombe M, White H (1989) Multilayer feedforward networks are universal approximators. Neural Netw 2:359–366
167. Cherkassky V, Gehring D, Mulier F (1996) Comparison of adaptive methods for function estimation from samples. IEEE Trans Neural Netw 7(4):969–984
168. Wang C, Ge S (2001) Adaptive backstepping control of uncertain Lorenz system. Int J Bifurc Chaos Appl Sci Eng 11(4):1115–1120
169. Moraal P, Grizzle J (1995) Observer design for nonlinear systems with discrete-time measurements. IEEE Trans Autom Control 40(3):395–404
170. Dabroom A, Khalil H (2001) Output feedback sampled-data control of nonlinear systems using high-gain observers. IEEE Trans Autom Control 46(11):1712–1725

171. Lewis FL, Jagannathan S, Yeşildirek A (1999) Neural network control of robot manipulators and nonlinear systems. CRC, Boca Raton
172. Vemuri A, Polycarpou M (1997) Neural-network-based robust fault diagnosis in robotic systems. IEEE Trans Neural Netw 8(6):1410–1420
173. Vemuri A, Polycarpou M, Diakourtis S (1998) Neural network based fault detection in robotic manipulators. IEEE Trans Robot Autom 14(2):342–348
174. Chen FC, Liu CC (1994) Adaptively controlling nonlinear continuous-time systems using multilayer neural networks. IEEE Trans Autom Control 39(6):1206–1310
175. Ge SS, Lee TH, Ren SX (2001) Adaptive friction compensation of servo mechanisms. Fuzzy Sets Syst 32(4):523–532
176. Tan KK, Huang SN, Lee TH (2004) Adaptive backstepping control for a class of nonlinear systems using neural network approximations. Int J Robust Nonlinear Control 14:643–664
177. Narendra KS, Parthasarathy K (1990) Identification and control of dynamic systems using neural networks. IEEE Trans Neural Netw 1(1):4–27
178. Levin AU, Narendra KS (1996) Control of nonlinear dynamical systems using neural networks, part II: observability, identification, and control. IEEE Trans Neural Netw 7(1):30–42
179. Lewis FL, Jagannathan S, Yeildirek A (1999) Neural network control of robot manipulators and nonlinear systems
180. Ge SS, Hang CC, Zhang T (1998) Nonlinear adaptive control using neural network and its application to CSTR systems. J Process Control 9:313–323
181. Zhang T, Ge SS, Hang CC (1999) Design and performance analysis of a direct adaptive controller for nonlinear systems. Automatica 35:1809–1817
182. Tee KP, Ge SS (2006) Control of fully actuated ocean surface vessels using a class of feedforward approximators. IEEE Trans Control Syst Technol 14(4):750–756
183. Chen M, Ge SS, Ren B (2011) Adaptive tracking control of uncertain mimo nonlinear systems with input constraints. Automatica 47(3):452–465
184. Ren B, Ge SS, Tee KP, Lee TH (2010) Adaptive neural control for output feedback nonlinear systems using a barrier Lyapunov function. IEEE Trans Neural Netw 21(8):1339–1345
185. Wang M, Liu X, Shi P (2011) Adaptive neural control of pure-feedback nonlinear time-delay systems via dynamic surface technique. IEEE Trans Syst Man Cybern, Part B, Cybern 41(6):1681
186. Wang C, Hill D (2006) Learning from neural control. IEEE Trans Neural Netw 17(1):130–146
187. Ge SS, Wang C (2002) Direct adaptive nn control of a class of nonlinear systems. IEEE Trans Neural Netw 13(1):214–221
188. Ge SS, Wang C (2004) Adaptive neural control of uncertain mimo nonlinear systems. IEEE Trans Neural Netw 15(3):674–692
189. Zhang T, Ge SS (2007) Adaptive neural control of mimo nonlinear state time-varying delay systems with unknown dead-zones and gain signs. Automatica 43(6):1021–1033
190. Yang C, Ge SS, Xiang C, Chai T, Lee TH (2008) Output feedback nn control for two classes of discrete-time systems with unknown control directions in a unified approach. IEEE Trans Neural Netw 19(11):1873–1886
191. Li Y, Qiang S, Zhuang X, Kaynak O (2004) Robust and adaptive backstepping control for nonlinear systems using RBF neural networks. IEEE Trans Neural Netw 15(3):693–701
192. Kayacan E, Cigdem O, Kaynak O (2012) Sliding mode control approach for online learning as applied to type-2 fuzzy neural networks and its experimental evaluation. IEEE Trans Ind Electron 59(9):3510–3520
193. Goldstein H (1951) Classical mechanics. Addison-Wesley, Massachusetts
194. Meirovitch L (1967) Analytical methods in vibration. Macmillan, New York
195. Wanderley J, Levi C (2005) Vortex induced loads on marine risers. Ocean Eng 32(11–12):1281–1295
196. Blevins R (1977) Flow-induced vibration. Van Nostrand Reinhold, New York
197. Faltinsen OM (1990) Sea loads on ships and offshore structures. Cambridge University Press, Cambridge

198. Sanner RM, Slotine JE (1992) Gaussian networks for direct adaptive control. IEEE Trans Neural Netw 3(6):837–863
199. Pedersen M (2000) Functional analysis in applied mathematics and engineering. CRC Press, New York
200. Hardy GH, Littlewood JE, Polya G (1959) Inequalities. Cambridge University Press, Cambridge
201. Horn R, Johnson C (1990) Matrix analysis. Cambridge University Press, Cambridge
202. Dawson D, Qu Z, Lewis F, Dorsey J (1990) Robust control for the tracking of robot motion. Int J Control 52(3):581–595
203. Ge SS, Wang C (2004) Adaptive neural network control of uncertain MIMO non-linear systems. IEEE Trans Neural Netw 15(3):674–692
204. Lin W, Qian C (2002) Adaptive control of nonlinearly parameterized systems: the smooth feedback case. IEEE Trans Autom Control 47(8):1249–1266
205. Ge SS, Hang CC, Zhang T (1999) Adaptive neural network control of nonlinear systems by state and output feedback. IEEE Trans Syst Man Cybern 29(6):818–828
206. Behtash S (1990) Robust output tracking for nonlinear system. Int J Control 51(6):931–933
207. Tee KP, Ge SS, Tay EH (2009) Barrier Lyapunov functions for the control of output-constrained nonlinear systems. Automatica 45(4):918–927
208. Rowe S, Mackenzie B, Snell R (2001) Deepwater installation of subsea hardware. In: Proceedings of the 10th offshore symposium, pp 1–9
209. How BVE, Ge SS, Choo YS (2007) Load positioning for subsea installation via approximation based adaptive control. In: IEEE international conference on control applications (CCA 2007). , pp 723–728
210. Fossen TI (2002) Marine control systems: guidance, navigation and control of ships, rigs and underwater vehicles. Marine Cybernetics, Trondheim
211. Yittervik R, Reinholdtsen SA, Larsen CM, Furnes GK (2003) Marine operations in deep water and a variable current flow environment. In: 3rd international conference on hydroelasticity in marine technology
212. Morison JR, O'Brien MP, Johnson JW, Schaaf SA (1950) The force exerted by surface waves on piles. Pet Trans 189:149–154
213. Narendra KS, Annaswamy AM (1989) Stable adaptive systems. Prentice Hall, New York
214. Whitcomb L, Yoerger D (1999) Development, comparison and preliminary experimental validation of nonlinear dynamic thruster models. IEEE J Ocean Eng 24(4)
215. Bachmayer R, Whitcomb LL, Grosenbaugh MA (2000) An accurate four-quadrant nonlinear dynamical model for marine thrusters: theory and experimental validation. IEEE J Ocean Eng 25(1):146–159
216. Smallwood DA, Whitcomb LL (2004) Model-based dynamic positioning of underwater robotic vehicles: theory and experiment. IEEE Journal of Oceanic Engineering 29(1)
217. Antonelli G, Caccavale F, Chiaverini S, Fusco G (2003) A novel adaptive control law for underwater vehicles. IEEE Trans Control Syst Technol 11:221–232
218. Feezor M, Sorrell F, Blankinship P, Bellingham J (2001) Autonomous underwater vehicle homing/docking via electromagnetic guidance. IEEE J Ocean Eng 26(4):515–521
219. Lasalle JP, Lefschetz S (1961) Stability by Lyapunov's direct method with applications. Academic Press, New York
220. Arimoto S, Miyazaki F (1984) Stability and robustness of PID feedback control for robot manipulators of sensory capability. Int J Robot Res 21:78–83
221. Ngo K, Mahony R, Jiang Z (2005) Integrator backstepping using barrier functions for systems with multiple state constraints. In: 44th IEEE conference on decision and control, 2005 and 2005 European control conference (CDC-ECC '05), pp 8306–8312
222. Tee KP, Ge SS, Tay EH (2009) Barrier Lyapunov functions for the control of output-constrained nonlinear systems. Automatica 45:918–927
223. Tee KP, Ge SS, Tay EH (2009) Adaptive control of electrostatic microactuators with bidirectional drive. IEEE Trans Control Syst Technol 17(2):340–352

224. Sane KP, Bernstein DS, Corning-IntelliSense W (2002) Robust nonlinear control of the electromagnetically controlled oscillator. In: American control conference, pp. 809–814
225. Benaroya H (2004) Mechanical vibration, analysis, uncertainties and control. Marcel Dekker, New York
226. Lee EW (1957) Non-linear forced vibration of a stretched string. Br J Appl Phys 8:411–413
227. Chakrabarti SK, Frampton RE (1982) Review of riser analysis techniques. Appl Ocean Res 4:73–90
228. Yamamoto C, Meneghini J, Saltara F, Fregonesi R, Ferrari J (2004) Numerical simulations of vortex-induced vibration on flexible cylinders. J Fluids Struct 19(4):467–489
229. Meneghini J, Saltara F, Fregonesi R, Yamamoto C, Casaprima E, Ferrari J (2004) Numerical simulations of VIV on long flexible cylinders immersed in complex flow fields. Eur J Mech B, Fluids 23(1):51–63
230. Slotine JJ, Li W, Coetsee JA (1986) Adaptive sliding controller synthesis for non-linear systems. Taylor Francis, New York
231. Xu JX, Hashimoto H, Slotine JJ, Arai Y, Harashima F (1989) Implementation of VSS control to robotic manipulators-smoothing modification. IEEE Trans Ind Electron 36:321–329
232. Polycarpou MM, Ioannou PA (1993) A robust adaptive non-linear control design. In: Proceedings of the American control conference, pp 1365–1369
233. Ledoux A, Molin B, Delhommeau G, Remy F (2006) Controlling line tension in thruster assisted mooring systems. In: Proceedings of the 21st international workshop water waves and floating bodies
234. Fossen T (2002) Marine control systems: guidance, navigation and control of ships, rigs and underwater vehicles. Marine Cybernetics, Trondheim
235. Lee S, Mote C Jr (1996) Vibration control of an axially moving string by boundary control. J Dyn Syst Meas Control 118:66
236. Hover FS, Grosenbaugh MA, Triantafyllou MS (1994) Calculation of dynamic motions and tensions in towed underwater cables. IEEE J Ocean Eng 19(3):449–457
237. Queiroz MS, Dawson DM, Nagarkatti SP, Zhang F (2000) Lyapunov based control of mechanical systems. Birkhauser, Boston
238. Tao G, Kokotovic PV (1996) Adaptive control of systems with actuator and sensor nonlinearities. Wiley, New York
239. Tao G, Kokotovic PV (1995) Adaptive control of plants with unknown hysteresis. IEEE Trans Autom Control 40(2):212–220
240. Tan X, Baras JS (2004) Modeling and control of hysteresis in magnetostrictive actuators. Automatica 40(9):1469–1480
241. Su CY, Stepanenko Y, Svoboda J, Leung TP (2000) Robust adaptive control of a class of nonlinear systems with unknown backlash-like hysteresis. IEEE Trans Autom Control 45(12):2427–2432
242. Zhou J, Wen CY, Zhang Y (2004) Adaptive backstepping control design of a class of uncertain nonlinear systems with unknown backlash-like hysteresis. IEEE Trans Autom Control 49(10):1751–1757
243. Wen CY, Zhou J (2007) Decentralized adaptive stabilization in the presence of unknown backlash-like hysteresis. Automatica 43(3):426–440
244. Su CY, Wang Q, Chen X, Rakheja S (2005) Adaptive variable structure control of a class of nonlinear systems with unknown Prandtl–Shlinskii hysteresis. IEEE Trans Autom Control 50(12):2069–2074
245. Ren B, Ge SS, Su C-Y, Lee TH (2009) Adaptive neural control for a class of uncertain nonlinear systems in pure-feedback form with hysteresis input. IEEE Trans Syst Man Cybern, Part B, Cybern 39(2):431–443
246. Ren B, Ge SS, Lee TH, Su CY (2009) Adaptive neural control for a class of nonlinear systems with uncertain hysteresis inputs and time-varying state delays. IEEE Trans Neural Netw 20(7):1148–1164
247. Bernitsas MM, Garza-Rios LO (1996) Effect of mooring line arrangement on the dynamics of spread mooring systems. J Offshore Mech Arct Eng 118(1):7–20

248. Garza-Rios LO, Bernitsas MM, Nishimoto K, Matsuura JPJ (2000) Dynamics of spread mooring systems with hybrid mooring lines. J Offshore Mech Arct Eng 122(4):274–281
249. Bernitsas MM, Papoulias FA (1986) Stability of single point mooring systems. J Appl Ocean Res 8(1):49–58
250. Garza-Rios LO, Bernitsas MM (1999) Slow motion dynamics of turret mooring and its approximation as single point mooring. Appl Ocean Res 21(1):27–39
251. Strand JP, Sørensen AJ, Fossen TI (1998) Design of automatic thruster assisted position mooring systems for ships. Model Identif Control 19(2):61–75
252. Kosmatopoulos EB, Polycarpou MM, Christodoulou MA, Ioannou PA (1995) High-order neural network structures for identification of dynamical systems. IEEE Trans Neural Netw 6(2):422–431
253. Polycarpou MM, Ioannou PA (1996) A robust adaptive nonlinear control design. Automatica 32(3):423–427
254. Skjetne R, Fossen T, Kokotović P (2005) Adaptive maneuvering, with experiments, for a model ship in a marine control laboratory. Automatica 41(2):289–298
255. Skjetne R (2005) The maneuvering problem. PhD thesis, Norwegian University of Science and Technology, Trondheim, Norway
256. Chen YH, Lin FM (1989) General drag-force linerization for nonlinear analysis of marine risers. Ocean Eng 16:265–280
257. Narasimha R (1968) Non-linear vibration of an elastic string. J Sound Vib 8(1):134–146
258. Karafyllis I, Christofides P, Daoutidis P (1999) Dynamics of a reaction-diffusion system with brusselator kinetics under feedback control. Phys Rev B 59:372–380
259. Nguyen T, Egeland O (2008) Infinite dimensional observer for a flexible robot arm with a tip load. Asian J Control 10(4):456–461
260. Demetriou M, Fahroo F (2006) Model reference adaptive control of structurally perturbed second-order distributed parameter systems. Int J Robust Nonlinear Control 16(16):773–799
261. Demetriou M (2004) Natural second-order observers for second-order distributed parameter systems. Syst Control Lett 51(3–4):225–234
262. Smyshlyaev A, Krstic M (2005) Backstepping observers for a class of parabolic PDEs. Syst Control Lett 54(7):613–625
263. Bounit H, Hammouri H (1997) Observers for infinite dimensional bilinear systems. Eur J Control 3(4):325–339
264. Balas M (1999) Do all linear flexible structures have convergent second-order observers? J Guid Control Dyn 22(6):905–908
265. Xu C, Deguenon J, Sallet G (2006) Infinite dimensional observers for vibrating systems. In: Proceedings of the 45th IEEE conference on decision and control, pp 3979–3983
266. Lyons GJ, Patel MH, Witz JA (1994) Vertical riser design manual. Bentham, New York
267. Morison JR, O'Brien MP, Johnson JW, Schaaf SA (1950) The forces exerted by surface waves on piles. Pet Trans 189(2846):149
268. Sarpkaya T, Isaacson M (1981) Mechanics of wave forces on offshore structures. Van Nostrand Reinhold, New York
269. Sarpkaya T (1976) In line and transverse forces on smooth and sand roughened cylinders in oscillatory flow at high Reynolds numbers
270. Grass AJ, Simons RR, Cavanagh NJ (1987) Vortex induced velocity enhancements in the wave flow field around cylinders. In: Proceedings of the offshore mechanics and Arctic engineering symposium. American Society of Mechanical Engineers, New York, pp 155–164
271. Bathe KJ, Wilson EL (1976) Numerical methods in finite element analysis. Int J Numer Anal Methods Geomech 1:319
272. Comparison of marine drilling riser analysis (1977) In: API bulletin 2J
273. Krolikowski LP, Gray TA (1980) An improved linearisation technique for frequency domain riser analysis. In: Proceedings of the 1980 offshore technology conference, Houston, vol OTC 3777
274. Patel MH, Sarohia S (1982) On the dynamics of production risers. In: Proceedings of the third international conference on behaviour of offshore structures, vol 1, p 599

275. Krolikowski LP (1981) Modern production risers, Pt 9: the frequency domain method for production riser analysis. Pet Eng Int 88
276. www.bpp-tech.com/riser-management-system
277. Trarieux F, Lyons GJ (2005) Fatigue damage assessment using a bandwidth parameter for VIV applied to the Foinaven dynamic umbilical. In: Proceedings of the 24th international conference on offshore mechanics and Arctic engineering
278. Lyons G, Trarieux F, Patel M, Garnham S (2006) Developments in assessment of fluid-loading regime contributions to fatigue for deepwater flexibles. In: Proceedings of the 26th offshore technology conference
279. Trarieux F, Lyons GJ, Vaz M, Patel MH, Garnham S (2006) Investigation of the influence of waves and vessel motions on the VIV response of flexible risers and umbilicals from a fatigue damage perspective. In: Proceedings of the 25th international conference on offshore mechanics and Arctic engineering
280. Trarieux F, Lyons GJ, Patel MH (2006) Investigations with a bandwidth measure for fatigue assessment of the Foinaven dynamic umbilical including VIV. Eng Struct 28(12):1671–1690
281. Lyons GJ, Patel MH (1986) A prediction technique for vortex induced transverse response of marine risers and tethers. J Sound Vib 111(3):467–487
282. Lyons GJ, Patel MH (1989) Application of a general technique for prediction of riser vortex-induced response in waves and current. J Offshore Mech Arct Eng 111(2):82–91
283. Lyons GJ, Fang J (1991) Vortex induced vibrations of tensioned and catenary marine risers. In: Proceedings of the international conference on flow induced vibrations, pp 75–86

Index

W. He et al., *Dynamics and Control of Mechanical Systems in Offshore Engineering*, Advances in Industrial Control, DOI 10.1007/978-1-4471-5337-5,